Top Quark Physics in the Standard Model Effective Field Theory

Liam Ronald Moore

Particle Physics Theory Group

School of Physics and Astronomy
University of Glasgow

Submitted in fulfilment of the requirements for the Degree of Doctor of Philosophy

Abstract

We explore some applications of the Standard Model (SM) Effective Field Theory (EFT) as a tool with which to describe generic non-resonant new physics (NP) at hadron colliders. A global fit of the dimension-six Wilson Coefficients relevant to top quark production is presented, utilizing diverse experimental datasets from both the Large Hadron Collider (LHC) Runs I and II and the TeVatron, with current results in good agreement with the SM. Machinery is developed to systematically treat redundancies between higher-dimensional operators in the automated model-building and phenomenology toolkit FeynRules, and a general SMEFT model implementation for event generators detailed. We then investigate the importance of high momentum transfer final states in $t\bar{t}$ production to the EFT fit, taking advantage of boosted reconstruction techniques. We find sensitivity is typically driven by fully resolved analyses in several benchmark scenarios for total integrated luminosity and experimental systematic uncertainties.

Declaration

This thesis is the result of my own work, except where explicit reference is made to the work of others, and has not been submitted for another qualification to this or any other university.

In Chapter 4 my unique contributions extended from the writing of the FeynRules model file described and the verification thereof through the event generation and writing of the analysis presented. I also supplied the illustrative matching calculations. I worked together with my colleagues in the interpretation of the results obtained and in the direction of the project.

In Chapter 5 the model provided is a result of my own work. I collaborated in the phenomenological analysis and in interpretation of the results.

Work in Chapters 3, 4 and 5 appear in the publications:

- "A global fit of top quark effective theory to data" [1]
- "Constraining top quark effective theory in the LHC Run II era" [2]
- "Giving top quark effective operators a boost" [3]

Liam Moore

Acknowledgements

I'd like to thank friends and colleagues at Glasgow. My supervisor David Miller, for his invaluable support, counsel and good humour throughout. Christoph Englert for being an example to me - his knowledge, insight and drive have been key to my own development in our subject. Chris White for impressively defying categorization, and with whom my interactions have been either intellectually stimulating or hilarious. Andy and James, for giving me the opportunity to work with excellent experimentalists.

In PPT I'd especially like to thank Michael Russell for his own tireless work on TopFitter, which elevated my esoteric games with effective operators and Mathematica into one part of an ambitious and practical project from which I have learned immeasurably much. Karl Nordström, for sharing with me his keen perspective, pragmatism and broad knowledge of particle phenomenology. Lies Melville, together with whom I started my journey into research, for her friendship and mutual support throughout. Also my friends Andrés, John, Euan and Andrew, and the new additions Dan and Dan for helping to make Glasgow PPT continue to be a uniquely wonderful place. Chris Bouchard for being such a great new addition to our group, and Christine Davies for giving me the opportunity to be part of something special.

My friends in PPE, particularly Stephen Ogilvy, Will Breaden-Madden and Cameron Dean, for unique and rewarding friendships throughout, and Sarah and Chris for outstanding patter.

At CERN I'd like to thank Claude Duhr for taking me into the fold with FeynRules and for many an excellent conversation, the self-annihilation working group, particularly Tim Evans, Ellis Kay, Xanthe Hoad, Bijan Haney and Harry Moss for providing stimulating extracurricular activities, and my office mates Anna, Sam and Michael.

Finally, my parents Michele and Ron and my aunt Rosslyn for everything they have done for me, and my grandparents Billy and Mabel for being the very best examples one could ask for.

Contents

Chapter 1

Introduction

The Standard Model of particle physics is the crowning contrivance with which we are entrapped in an abusive relationship built on equal-parts respect and resentment. Frustratingly impressive, with an immense empirical vindication - while also sporting glaring inadequacies - with one hand it bats away the experimental tests we thrust at it in the hope of glimpsing one of our more fanciful constructions beneath its surface, and with the other peels back layers of itself which challenge us into humility. The industry of continuous war against our creation has driven our own betterment, and a history of bogus discovery claims and premature excitement has taught us repeatedly to always first suspect our current understanding. Despite its tremendous successes both in the discovery of the Higgs [4], extraordinary machine performance [5], and theoretical arguments suggesting the existence of physics beyond the Standard Model (BSM), the Large Hadron Collider (LHC) at CERN, the current frontline on the high-energy frontier, is yet to produce any definitive experimental evidence for New Physics (NP) at the TeV scale.

Constructing testable ultraviolet (UV) completions which address both the SM's theoretical afflictions and the experimentally observed phenomena on which it remains silent is a primary responsibility of the high-energy theoretical community. While the combined action of 'top-down' BSM model-building with continuous experimental testing is our bread-and-butter machinery for confronting conjecture with reality, by itself this system relies on having clever ideas in the first place. Being able to make quantitative statements independent of guesses at the structure of new physics requires that we complement our swathe of competing hypotheses with a UV-agnostic theoretical framework built for maximal breadth of descriptive power. Effective Field Theory (EFT) is the name given to a natural language for expressing this problem (among others) which

arises whenever a Quantum Field Theory (QFT) - like the SM - contains well-separated mass scales.

With its modern roots in Fermi's phenomenological description of weak decays in 1933, EFT flowered with advances in our understanding of how the behaviour of a given QFT changes for measurements at different distance scales. The central principle - that in a given physical process, the details of the dynamics of degrees of freedom acting at disparately shorter or longer distances are not important - has seen widespread application.

Appealing only to power-counting and symmetry arguments, it has a successful track record of enabling the construction of power series which exploit ratios of length scales as useful expansion parameters, rendering previously intractable computations attackable. Since coming into its own right in the 1970s, the power and simplicity of this approach has led to its adoption as a ubiquitous tool across particle physics.

EFT has long found successful application in facilitating calculations in which a hierarchy is present in the dimensionful parameters (in QFT, usually particle masses) associated with known degrees of freedom. For example, in flavour physics, the QCD corrections to weak decays (for a review, see e.g. [6]) at low energies were first calculated by exploiting the comparatively large W boson mass m_W relative to those of the light quarks. In nonperturbative QCD, Chiral Perturbation Theory (ChPT) [7] utilizes the hierarchy between the pion masses and the scale of chiral symmetry breaking to perform limited analytic calculations in the strongly interacting regime. The methods of Soft Collinear Effective Theory (SCET) [8] ease the description of soft and collinear radiation by factorizing scattering amplitudes into regimes which exploit the disparity between the relevant momentum transfer and the QCD scale parameter Λ_{QCD}. Heavy Quark Effective Theory (HQET) [9] similarly facilitates calculations of hadronic flavour changing transitions by appealing to the small ratio of heavy flavoured quarks' typical momentum within a hadron to their masses.

The second use of EFT - that which will be the subject of this thesis - is as a parametrization of the *possible* physical effects originating from processes whose character is unknown, but which are known to arise from the action of degrees of freedom sufficiently heavier than those of which we are aware. We can then appeal to the same power-counting and symmetry arguments to construct a family of generic new contributions, *higher-dimensional operators*, in this case with an unknown NP scale to be inferred from experimental measurement. This family of operators form a dictionary of

the possible residual influences of UV physics at each order in the expansion in mass scales, and thus represent a 'bottom-up' approach to describing the phenomenology of BSM physics intrinsically free from the presence of particular new particle species.

The Standard Model Effective Field Theory (SMEFT) is the generalization of the Standard Model to an EFT that follows from the assertion that NP is present at some energy scale above that which current experiments probe. The immediate consequence of this - the presence of operators which mediate novel interactions amongst the SM particle species - provides a structure in which to interpret any experimental measurements which conflict with the SM hypothesis while falling short of inferring the presence of new resonant states. Besides providing a theoretical framework in which to model non-resonant BSM effects, the common language of the SMEFT also facilitates the unambiguous comparison of model-independent experimental constraints and the mapping thereof to the predictions of UV models made possible by matching calculations.

Given the lack of evidence for new resonant states, it is well-motivated to examine the phenomenology of the SM particles at the Electroweak scale through the lens of the SMEFT, taking advantage of the abundant statistics provided by the LHC. The top quark - the heaviest SM fermion whose $\mathcal{O}(1)$ Yukawa coupling ties its properties intimately to those of the Higgs - stands out immediately as such a candidate, being both extremely well measured and providing opportunities for measurements unique among the quarks. We will focus our attention on its interactions, and describe steps in the development of a framework to extract constraints on the Wilson Coefficients governing its novel behaviour in the SMEFT.

The layout of this work is as follows: Chapter 2 provides a short background of the SM as a relativistic QFT, summarizing its particle content and interactions. The foundations of EFT are then outlined and related to the the renormalizability and scaling behaviour of QFTs. We conclude with an illustrative historical example of an EFT calculation to provide context for subsequent chapters.

In Chapter 3 the SMEFT is described in some detail, along the way describing its implementation as a general input model file for event generators using the FeynRules [10] package and UFO format [11]. We explore in particular the treatment of the effects of dimension-six operators on the definitions of measured 'SM' parameters, and detail subtleties related to redundancies between operators in the SMEFT which demand care be taken in its use. The prevalence of these redundancies in higher-order

perturbative calculations sets the stage for discussing a continuing project to automate the procedure of operator basis reduction.

Chapter 4 is devoted to the construction of the TopFitter [2,3] framework, wherein collected LHC and TeVatron datasets were used in a global fit to place constraints on the SMEFT Wilson Coefficients contributing to the top pair, single top and $t\bar{t}Z/t\bar{t}\gamma$ associated production channels.

Chapter 5 describes phenomenological analyses aiming to improve and expand upon the EFT fit. Boosted reconstruction techniques are employed to identify top quarks produced at large momentum transfers, and the sensitivity gain of targeting this phase space region investigated in comparison with a resolved analysis.

Chapter 6 concludes with a summary of this thesis.

Chapter 2

Foundations

2.1 The Standard Model of Particle Physics

2.1.1 Overview

The Standard Model of particle physics is the relativistic Quantum Field Theory (see e.g. [12] for a pedagogical introduction) which successfully describes the behaviour of three of the four fundamental forces of nature within a unified framework. Representing the fruit of theoretical efforts spanning several decades, it is astonishingly accurate at every distance scale at which it has been experimentally tested. This is particularly staggering considering its full predictive power can - in the right hands - be extracted from an expression spanning two lines. The Lagrangian at its core is:

$$\begin{aligned}\mathcal{L}^{(4)}_{\mathrm{SM}} = &-\frac{1}{4}G^{A}_{\mu\nu}G^{A\mu\nu} - \frac{1}{4}W^{I}_{\mu\nu}W^{I\mu\nu} - \frac{1}{4}B_{\mu\nu}B^{\mu\nu} + \left(D_\mu\varphi\right)^\dagger\left(D^\mu\varphi\right) + \mu^2\varphi^\dagger\varphi - \lambda\left(\varphi^\dagger\varphi\right)^2 \\ &+ i\left(\bar{l}\not{D}l + \bar{e}\not{D}e + \bar{q}\not{D}q + \bar{u}\not{D}u + \bar{d}\not{D}d\right) - \left(\bar{l}\,Y_e e\varphi + \bar{q}\,Y_u u\widetilde{\varphi} + \bar{q}\,Y_d d\varphi + \mathrm{h.c.}\right) \quad (2.1.1)\end{aligned}$$

The objects from which it is constructed are local quantum fields, operator valued functions of spacetime which act on the vaccuum to create states which we associate with particles. These are deliberately arranged to be consistent with (special) relativity, so that physical predictions are independent of the frame of reference of a given observer. $\mathcal{L}^{(4)}_{\mathrm{SM}}$ is said to be manifestly Lorentz invariant, or invariant under the action of the (proper, orthochronous) Lorentz group $SO(1,3)$.

We have distinguished four distinct sectors. Highlighted in red is the gauge sector, the gauge bosons of which mediate the strong and electroweak interactions. Each of

these corresponds to the realization in nature of a local gauge symmetry. We say that the Lagrangian is locally invariant under the action of the Standard Model gauge group, which is the unitary product group $\boldsymbol{\mathcal{G}}_{SM} \equiv SU(3)_C \otimes SU(2)_L \otimes U(1)_Y$. The former establishes the structure of the theory of Quantum Chromodynamics (QCD), with which we associate colour charge, while the associated gauge boson is named the gluon. The latter two collectively give rise to the theory of the weak interaction and the quantum theory of electromagnetism, Quantum Electrodynamics (QED). These dictate the dynamics of the W and Z bosons and the photon.

Next is the Higgs sector, depicted in blue. The Higgs field interacts directly with the electroweak gauge bosons, and not with gluons. We say that the Higgs is charged under the electroweak gauge group. This is required for Electroweak Symmetry Breaking (EWSB), the phenomenon through which fundamental particles will acquire mass. The associated physical state is the Higgs boson, which is unique in being the only fundamental scalar particle observed in nature.

The section in purple encodes the dynamics of the fundamental fermions which we associate with matter. These are the quarks and leptons, which are distinguished by the fact that only the former carry colour charge, while both participate in the electroweak interaction. The matter sector is furthermore formulated in terms of *chiral* fermions which are distinguished as being either left- or right-handed. Loosely speaking, this refers to their possessing opposite orientations of their intrinsic angular momenta. Because the left- and right- chiral fermions carry different charges under the Electroweak gauge group, it is said to be a chiral theory, or that the discrete symmetry Parity ($\mathcal{P}$) is violated.

Lastly is the Yukawa sector, which described the interaction of the fermions with the Higgs field. When the latter triggers electroweak symmetry breaking, these interactions will cause the quarks and leptons to acquire mass. It is also the only structure* which permits violation of $\mathcal{CP}$-symmetry, through which the preferential production of fermions over antifermions can arise.

2.1.2 Structure of the Lagrangian

The statement of Lorentz invariance is made precise by examining the irreducible representations of the Lorentz group $SO(1,3)$. These are typically categorized by first noting that the Lie algebra of $SO(1,3)$ exhibits an isomorphism $SO(1,3) \simeq SU(2) \otimes SU(2)$,

*The strong $\mathcal{CP}$ problem [13] aside.

such that it can be decomposed into a direct product of two $SU(2)$ subalgebras which are exchanged by hermitian conjugation. Objects with definite transformation properaties in Minkowski spacetime can then be enumerated by specifying two integers $(\boldsymbol{m}, \boldsymbol{n})$ corresponding to the dimensions of their embeddings in each inequivalent $SU(2)$.

The first of these is the singlet (or one-dimensional) representation. This transforms trivially, and we denote it as $(\mathbf{1}, \mathbf{1})$. This means that it carries no indices to accommodate how its form changes under Lorentz transformations. An object with these properties is identified with a scalar field. In $\mathcal{L}_{\mathrm{SM}}$, the Higgs field φ alone has this property.

From standard quantum mechanics we know a basis for the fundamental representation, which we denote by $\mathbf{2}$. These were two-component complex vectors which we indexed by their σ^z eigenvalues $j = \pm\frac{1}{2}$. When we used this in the context of the angular momentum operator, we identified this eigenvalue with the spin, and called these spinors. Since we have two copies of $SU(2)$, we call the $(\mathbf{2}, \mathbf{1})$ and $(\mathbf{1}, \mathbf{2})$ representations left-chiral and right-chiral spinor fields respectively. The Standard Model contains two left-chiral spinors which are denoted q and l, and three right-chiral spinors which are denoted u, d and e. These are normally allocated dotted and undotted indices to represent their two components respectively.

We also at some point constructed the remaining finite dimensional represenations - for a given half-integer spin j, these were $(2j+1)$ dimensional vectors, with eigenvalues $j, j-1, \ldots, -j$. The representation $(\mathbf{2}, \mathbf{2})$ recovers the familiar four component vector field. In the Standard Model, the gauge bosons which are denoted G, W and B have this form.

Each of the fundamental fields belongs to one of these four categories. The Lorentz invariance of the Lagrangian can then be ensured by writing down only those terms which correspond to a direct product representation of these four objects which transforms as an overall singlet. Any number of scalar fields satisfy this requirement, as $(\mathbf{1}, \mathbf{1}) \otimes (\mathbf{1}, \mathbf{1}) \otimes \ldots = (\mathbf{1}, \mathbf{1})$.

Two spinors can be arranged in a Lorentz scalar since, in $SU(2)$ we have the decomposition $\mathbf{2} \otimes \mathbf{2} = \mathbf{1} \oplus \mathbf{3}$. We can then form a singlet from left-chiral spinor and right-chiral antispinor as $(\mathbf{2}, \mathbf{1}) \otimes (\mathbf{2}, \mathbf{1}) = (\mathbf{1}, \mathbf{1}) \oplus (\mathbf{3}, \mathbf{1})$, or vice versa.

The combination of two Lorentz vectors into a scalar follows from the same decomposition; $(\mathbf{2}, \mathbf{2}) \otimes (\mathbf{2}, \mathbf{2}) = (\mathbf{1}, \mathbf{1}) \oplus (\mathbf{1}, \mathbf{3}) \oplus (\mathbf{3}, \mathbf{1}) \oplus (\mathbf{3}, \mathbf{3})$.

Since the Lagrangian appears as an ingredient in the action functional $\mathcal{S} = \int d^4x\, \mathcal{L}$, we can use this information to determine the dimension carried by the fields. This imposes the requirement that $[\mathcal{L}] = -[d^4x]$, thus in natural units where $[\bar{h}] = [c] = 1$ we have $[x] = [E^{-1}] = [M^{-1}]$, so that each term in $\mathcal{L}$ must carry mass dimension four.

From the scalar field kinetic term we can extract* $2[\varphi] + 2 = 4$, so that $[\varphi] = 1$. Gauge bosons are constructed to transform in the same representation as ∂_μ, so these each have $[G] = [W] = [B] = 1$. The additional constraint that each operator respect gauge symmetry means the Lorentz scalar formed by two chiral fermions can only appear together with φ. The first such possible arrangement is embodied by the Yukawa sector, which gives us $[\bar{\psi}]_L[\psi]_R = [\bar{\psi}]_R[\psi]_L = 4 - 1$, so that each chiral spinor has $[\psi] = \frac{3}{2}$.

We can now check that - with the exception of the quadratic term $\mu^2\varphi^\dagger\varphi$ in the Higgs sector - each term in $\mathcal{L}^{(4)}_{\mathrm{SM}}$ carries four powers of mass *associated with its field content alone*. There is in principle nothing forbidding the inclusion of *higher-dimensional* operators satisfying $[\mathcal{O}] = d$, which carry coefficients with dimensions $[C] = 4 - d < 0$. The operators appearing in the Standard Model Lagrangian are then the subset of those possible which carry four or fewer powers of mass, hence the superscript (4). In general, a generic operator $\mathcal{O}$ is distinguished by its mass dimension by being classified as either:

- Relevant: $[\mathcal{O}] = d < 4 \quad \Longleftrightarrow \quad [\mu^{4-d}] > 0.$
- Marginal: $[\mathcal{O}] = d = 4 \quad \Longleftrightarrow \quad [\lambda] = 0.$
- Irrelevant: $[\mathcal{O}] = d > 4 \quad \Longleftrightarrow \quad [C^{4-d}] < 0.$ Not to be taken literally.

where μ, λ and C are the associated coefficients. Using this terminology, the Standard Model contains only relevant and marginal operators. This is an additional restriction baked into its construction, and is a necessary condition for the *renormalizability* of the theory. Since possible higher-dimensional operators carry powers of inverse mass - $C \propto \Lambda^{-n}$, where Λ is some mass scale - writing down the renormalizable Lagrangian $\mathcal{L}^{(4)}_{\mathrm{SM}}$ alone amounts to making the implicit assumption $\Lambda \to \infty \quad \Longleftrightarrow \quad C \to 0$. The Standard Model is then a special case of an *Effective Field Theory* in which Λ is finite, and higher-dimensional operators appear.

With this requirement, the explicit form of $\mathcal{L}^{(4)}_{\mathrm{SM}}$ is fully fixed by specifying the gauge symmetry group and the representations of the field content therein. In an analogous fashion to enumerating objects with distinct behaviours under Lorentz transformations, each field is understood as belonging to a finite dimensional irreducible representation

*Since ($[\partial_\mu] \equiv -[x]$)

of the Lie groups $SU(3)_C$, $SU(2)_L$ and $U(1)_Y$ simultaneously. These can be categorized systematically from the commutation relations of the respective Lie algebras. When written in an explicit form, indices are allocated to each field which span the dimension of the representation to which it belongs. In Table 2.1 we collect this information for the Standard Model. The operators which appear are then an exhaustive list of those which are invariant under the collective action of a local (i.e. spacetime dependent) unitary rotation acting on each of the constituent fields.

Class		**Object**	Rep($\boldsymbol{\mathcal{G}}_{SM}$)	Rep($\boldsymbol{\mathcal{G}}_{Lorentz}$)	$[\boldsymbol{D}]$	B	L
X		$G^A_{\mu\nu}$	$(\mathbf{8},\mathbf{1},0)$	$(\mathbf{3},\mathbf{1})\oplus(\mathbf{1},\mathbf{3})$ Antisymmetric Tensor	2	0	0
		$W^I_{\mu\nu}$	$(\mathbf{1},\mathbf{3},0)$				
		$B_{\mu\nu}$	$(\mathbf{1},\mathbf{1},0)$				
φ		φ^j	$(\mathbf{1},\mathbf{2},1/2)$	$(\mathbf{1},\mathbf{1})$ Lorentz Scalar	1	0	0
ψ	L	$q^{\alpha j}_{Lp}$	$(\mathbf{3},\mathbf{2},1/6)$	$(\mathbf{2},\mathbf{1})$ Left-Handed Spinor	3/2	1/3	0
		l^j_{Lp}	$(\mathbf{1},\mathbf{2},-1/2)$			0	1
	R	u^α_{Rp}	$(\mathbf{3},\mathbf{1},2/3)$	$(\mathbf{1},\mathbf{2})$ Right-Handed Spinor		1/3	0
		d^α_{Rp}	$(\mathbf{3},\mathbf{1},-1/3)$				
		e_{Rp}	$(\mathbf{1},\mathbf{1},-1)$			0	1
D		D_μ	$(\mathbf{1},\mathbf{1},0)$	$(\mathbf{2},\mathbf{2})$ Lorentz Vector	1	0	0

Table 2.1: *The Standard Model field content and the embeddings thereof as representations of the gauge and spacetime symmetry groups* $\boldsymbol{\mathcal{G}_{SM}} \equiv SU(3)_C \otimes SU(2)_L \otimes U(1)_Y$ *and* $\boldsymbol{\mathcal{G}_{Lorentz}} \equiv SO(1,3) \simeq SU(2) \otimes SU(2)$ *respectively. We introduce the classifications* $\{X, \varphi, L, R, D\}$ *as defined in [14] to establish general building blocks with fixed mass dimension and transformation properties under the Lorentz group.* $[\boldsymbol{D}]$*,* B*,* L *denote mass dimension, baryon and lepton numbers respectively.*

Gauge Bosons

The existence of the gauge fields follows from the generalization that each symmetry is preserved under spacetime dependent unitary transformations. This distinguishes a gauge symmetry from a global symmetry (such as Lorentz invariance). In order to

respect local gauge symmetry, the partial derivative is generalized to the gauge-covariant derivative, in which the vector gauge bosons arise to accommodate for the infinitesimal difference in the rotations acting on the matter fields between points in spacetime. In the Standard Model, this takes the form:

$$(D_\mu q)^{\alpha j} = \left(\partial_\mu + i g_s T^A_{\alpha\beta} G^A_\mu + i g_2 \tau^I_{jk} W^I_\mu + i g_1 Y_q B_\mu\right) q^{\beta k}. \tag{2.1.2}$$

Where we have used the example of the left-chiral q doublet which is charged under each of the gauge groups. Here, $T^A = \frac{1}{2}\lambda^A$ and $\tau^I = \frac{1}{2}\sigma^I$ denote the generators of the fundamental representation of $SU(3)_C$ and $SU(2)_L$ respectively, and the greek and latin indices carried by q represent the corresponding colour and weak isospin degrees of freedom on which they act respectively. A and I index the adjoint representations to which the G and W bosons respectively belong. g_s, g_2 and g_1 are the gauge coupling constants which are free parameters of the theory. Fermion- (and Higgs) gauge boson interactions are then understood as a consequence of local gauge invariance.

Much of the richness in phenomenology in the SM follows from the non-Abelian structure of the colour and weak isospin gauge groups, whose Lie algebras are defined respectively by the commutation relations:

$$[T^A, T^B] = i f^{ABC} T^C \tag{2.1.3}$$

$$[\tau^I, \tau^J] = i \epsilon^{IJK} \tau^C \,, \tag{2.1.4}$$

Where f^{ABC} and ϵ^{IJK} are the totally antisymmetric structure constants of $SU(3)$ and $SU(2)$. The $U(1)_Y$ Hypercharge group is Abelian, since it describes multiplication by a complex phase factor, and its single generator is just a (commuting, obviously) real number Y. Written in explicit index notation, the gauge field strength tensors and their covariant derivatives then read:

$$\begin{aligned}
G^A_{\mu\nu} &= \partial_\mu G^A_\nu - \partial_\nu G^A_\mu - g_s f^{ABC} G^B_\mu G^C_\nu, & (D_\rho G_{\mu\nu})^A &= \partial_\rho G^A_{\mu\nu} - g_s f^{ABC} G^B_\rho G^C_{\mu\nu}, \\
W^I_{\mu\nu} &= \partial_\mu W^I_\nu - \partial_\nu W^I_\mu - g_2 \varepsilon^{IJK} W^J_\mu W^K_\nu, & (D_\rho W_{\mu\nu})^I &= \partial_\rho W^I_{\mu\nu} - g_2 \varepsilon^{IJK} W^J_\rho W^K_{\mu\nu}, \\
B_{\mu\nu} &= \partial_\mu B_\nu - \partial_\nu B_\mu, & D_\rho B_{\mu\nu} &= \partial_\rho B_{\mu\nu} \,,
\end{aligned} \tag{2.1.5}$$

Where terms quadratic in the non-Abelian gauge fields bestow them with self interactions. These fundamentally change the behaviour of the strong and weak forces relative to the familiar Abelian behaviour exhibited by QED. This is most notably responsible for

confinement, whereby the effective QCD coupling constant experienced by the coloured quarks becomes larger at lower energies, leading to their becoming strongly coupled. This heralds a fundamental change in the degrees of freedom of the theory, from coloured quarks to colour-neutral hadrons.

The gauge bosons are endowed with a transverse structure which can be observed directly from the antisymmetry of the gauge Lagrangian*. This causes problems when quantizing the theory in that - most intuitively seen in the path integral formulation - we sum the probability amplitudes for all possible field configurations, including the redundant longitudinal modes which do not contribute to the action. This problem is typically accounted for using the Faddeev-Popov method [15], whereby a term is introduced at the Lagrangian level $\mathcal{L}_{\text{g.f.}}$ to 'fix the gauge', removing the integration over the redundant modes for each gauge field A_μ.

$$\mathcal{L}_{\text{g.f.}} = -\frac{1}{2\xi}(\partial^\mu A^A_\mu)^2 \tag{2.1.6}$$

Here the gauge-fixing parameter ξ is arbitrary, and guaranteed to cancel in the sum over all contributions of the gauge field in the calculation of a given correlation function. For the non-Abelian gauge fields the staging of this argument is complicated by their self-interactions, and a solution necessitates the inclusion of an additional set of anticommuting complex scalar fields to guarantee the transverse polarization of physical gauge boson states. These are the so-called Faddeev-Popov ghosts, embedded in the adjoint representations of the non-Abelian $SU(N)$ gauge groups, introduced as:

$$\mathcal{L}_{\text{ghost}} = \partial_\mu \bar{c}^A \partial^\mu c^A + g f^{ABC}(\partial^\mu \bar{c}^A) A^B_\mu c^C \,, \tag{2.1.7}$$

Where it is understood that g, A and f^{ABC} represent the coupling constants, gauge bosons and structure constants associated with each $SU(N)$. These then interact with the respective gauge bosons to cancel the net contributions of their longitudinal degrees of freedom to a given observable by construction.

*For each gauge group X, these are defined by $-ig_X F^A_{\mu\nu} T^A \equiv [D_\mu, D_\nu]$.

Electroweak Symmetry Breaking

The Brout-Englert-Higgs mechanism [16,17] is the simplest means through which gauge bosons can acquire mass while preserving the gauge symmetry of the Lagrangian*. In the SM, this is resolved by introducing a scalar field charged under $SU(2)_L \otimes U(1)_Y$ which acquires a vacuum expectation value†. This follows from observing that there exist two minima of the quartic Higgs potential:

$$V(\varphi) \equiv \mu^2 \varphi^\dagger \varphi + \lambda \left(\varphi^\dagger \varphi\right)^2 \tag{2.1.8}$$

corresponding to the scenarios $\mu^2 < 0, \mu^2 > 0$. The vacuum solution $\langle \varphi_0 \rangle \neq 0$ for the (complex) two component Higgs field (in the $(\bar{\mathbf{2}}, \frac{1}{2})$ representation of $SU(2)_L \otimes U(1)_Y$), then does not respect a transformation under the Electroweak gauge group, and the Electroweak symmetry is said to be spontaneously broken. By selecting a basis for the generators of $SU(2)_L$ such that the (real) vacuum expectation value $v \simeq 246\text{GeV}$ is aligned along one direction of the Higgs doublet we can parametrize this as:

$$\langle \varphi_0 \rangle = \frac{1}{\sqrt{2}}(0, v)^T \quad v = \sqrt{\frac{-\mu^2}{\lambda}}\,, \tag{2.1.9}$$

and observe that there is a manifestly unbroken Abelian subgroup corresponding to the linear combination of the generators $Q \equiv \tau^3 + \frac{1}{2} Y\, \mathbb{I}$‡. The would-be massless Goldstone bosons associated with the three broken symmetry directions [18] become the longitudinal degrees of freedom of linear combinations of the four original gauge bosons (W^I_μ, B_μ) given by:

$$Z_\mu = \frac{1}{\sqrt{g_1^2 + g_2^2}} \left(g_2 W^3_\mu - g_1 B_\mu\right) \tag{2.1.10}$$

$$W^\pm_\mu = \frac{1}{2}(W^1_\mu \mp W^2_\mu) \tag{2.1.11}$$

$$A_\mu = \frac{1}{\sqrt{g_1^2 + g_2^2}} \left(g_1 W^3_\mu + g_2 B_\mu\right) \tag{2.1.12}$$

Which have corresponding masses:

$$m_W^2 = \frac{1}{4} v^2 g_2^2\,, \quad m_Z^2 = \frac{1}{2} v^2 \sqrt{g_2^2 + g_1^2}\,, \quad m_A^2 = 0 \tag{2.1.13}$$

*$SU(N)$ gauge bosons transform in the adjoint representation as $A^A_\mu \to A^A_\mu + \partial_\mu \alpha^A + g_X f^{ABC} A^B_\mu \alpha^C$, so that explicit terms of the form $m_A^2 A^A_\mu A^{A\,\mu}$ are not invariant under a gauge transformation.

†A scalar is the only possibility which doesn't violate Lorentz invariance.

‡This is just $diag(1, 0)$.

The massless vector boson A_μ is identified with the photon of QED, which respects a residual $U(1)_{\text{EM}}$ gauge symmetry with the Abelian generator $Q = T^3 + \frac{1}{2}Y$, which is identified with the electric charge. The remaining scalar degree of freedom is identified with the Higgs boson H, i.e. the excitations of the Higgs field about the vacuum direction; $\varphi = \frac{1}{\sqrt{2}}(0, v + H)$. The two components of the left handed quark and lepton doublets q and l respectively are then distinguished as the left-handed and right-handed (u_L, d_L) and (ν_L, e_L) fields which carry distinct charges under $U(1)_{\text{EM}}$.

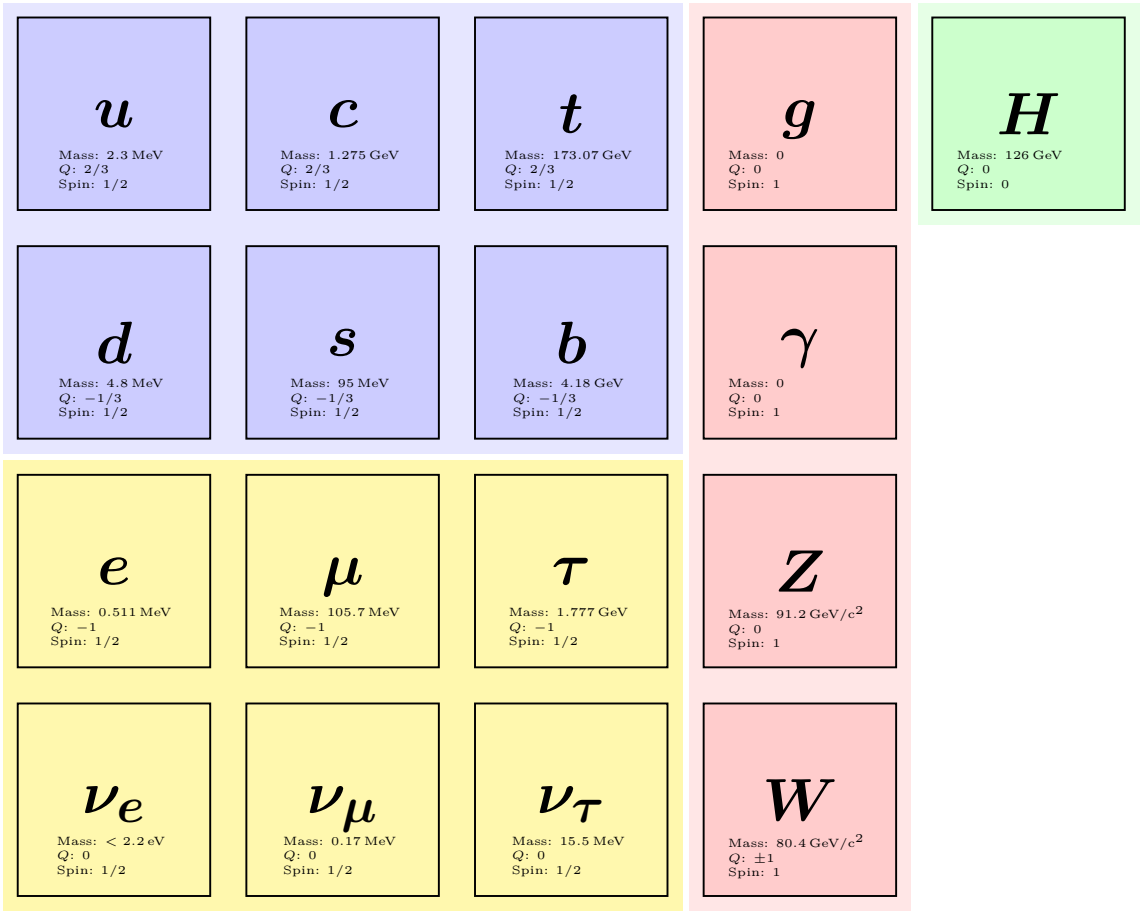

Figure 2.1: *Elementary particles of The Standard Model in their mass eigenstates, with matter generations distinguished by column.*

Fermion Masses

In the Yukawa sector, the left- and right- handed chiral fermions' couplings to the Higgs field then include a constant contribution proportional to its vacuum expectation value.

The associated couplings Y_ψ are unfixed by the gauge structure of the theory, and are thus parametrized generally by 3×3 complex matrices acting between fermions in the three observed states of flavour, which carry the same gauge quantum numbers. These matrices can be simplified by choosing an appropriate orientation of the left- and right-handed fermion fields in flavour space to select a diagonal form for each $Y_{u,d,e}$*. The fermion mass terms are identified as those which mix the left- and right-handed chiral spinors as:

$$\mathcal{L}_{mass} = \frac{v}{\sqrt{2}} \overline{d}_{L,p}\, Y^d_{pr}\, d_{R,r} + \frac{v}{\sqrt{2}} \overline{u}_{Lr}\, Y^u_{pr}\, u_{R,s} + \frac{v}{\sqrt{2}} \overline{e}_{L,p}\, Y^e_{pr}\, e_{R,s} + \text{h.c.} \tag{2.1.14}$$

$$Y^d = \text{diag}(y_d, y_s, y_b),\; Y^u = \text{diag}(y_u, y_c, y_t),\; Y^e = \text{diag}(y_e, y_\mu, y_\tau)\,, \tag{2.1.15}$$

So that each fermion acquires a mass term proportional to its coupling to the Higgs field; $m_\psi \equiv \frac{v}{\sqrt{2}} y_\psi$.

Since there are five chiral fermion fields $\{q, l, u, d, e\}$ and three complex matrices, a residual unitary matrix of free parameters $V_{CKM} \equiv L_u^\dagger L_d$ remains, which is customarily chosen to define a rotation of the down quark mass eigenstates in the Yukawa sector with respect to those appearing in the fermion gauge-covariant derivative. This is the Cabibbo-Kobayashi-Maskawa (CKM) matrix [19]:

$$V_{\text{CKM}} = \begin{bmatrix} V_{ud} & V_{us} & V_{ub} \\ V_{cd} & V_{cs} & V_{cb} \\ V_{td} & V_{ts} & V_{tb} \end{bmatrix} \tag{2.1.16}$$

This is typically parametrized by three angles and one complex phase, which is the only source of $\mathcal{CP}$-violation in the SM. The left handed quark doublet to which the W-boson couples is then:

$$q = \begin{pmatrix} u \\ d' \end{pmatrix}_L, \qquad d' = V_{ud} d + V_{us} s + V_{ub} b \tag{2.1.17}$$

*A complex matrix can be written using a singular value decomposition; $C = LDR^\dagger$, where L and R are unitary matrices, and D is a real, diagonal matrix. One can then perform an appropriate unitary rotation on each fermion flavour vector separately, e.g. $q_p \to L_{pr} q_r\,, d_p \to R_{pr} d_r$ which leaves $\mathcal{L}_{\text{SM}}$ invariant. p and r are flavour indices.

Where the unprimed quarks are mass eigenstates, and we've used the example of the charged current to the up quark. Massive quark fields are typically accommodated by arranging the corresponding left- and right-chiral fermions into the familiar, four component Dirac spinors by defining:

$$\Psi \equiv \begin{pmatrix} \psi_L \\ \psi_R \end{pmatrix}, \quad \gamma^\mu \equiv \begin{pmatrix} 0 & \sigma^\mu \\ \bar{\sigma}^\mu & 0 \end{pmatrix} \tag{2.1.18}$$

Where ψ_L and ψ_R are two component left- and right- chiral Weyl spinors respectively, and $\sigma^\mu \equiv (\mathbb{I}, \sigma^I), \bar{\sigma^\mu} \equiv (\mathbb{I}, -\sigma^I)$. Chiral spinors can then be recovered using the projection operators $P_{L/R} = \frac{1}{2}(\mathbb{I} \pm \gamma_5)$, with $\gamma_5 \equiv \frac{i}{4!}\epsilon_{\mu\nu\alpha\beta}\gamma^\mu\gamma^\nu\gamma^\alpha\gamma^\beta$.

2.1.3 Quantization and Scale Dependence

In the so-called 'second quantization', the fields in the Lagrangian are interpreted as operators which act on the vacuum to create particle states. While this 'canonical' formulation of QFT offers an immediate interpretation of the notion of particles in this sense, ease-of-use and a manifest realization of symmetries mean that in practice it is typically formulated in the Feynman path integral formalism (see e.g. [20]), which can be considered a generalization of the classical principle of least action. Herein particle trajectories are assigned probability amplitudes weighted by the action $\mathcal{S} = \int d^4x\, \mathcal{L}$ in a functional integral over all possible field configurations. n-point correlation functions are then obtained by taking n functional derivatives of a partition function with respect to a source term J for each field:

$$Z(J) = \exp(iW(J)) = \int \mathcal{D}\varphi\mathcal{D}\psi\mathcal{D}\bar{\psi}\mathcal{D}A \exp\left(i\int d^4x\, \mathcal{L}_{\text{SM}}\right) \tag{2.1.19}$$

Where φ, ψ, $\bar{\psi}$ and A schematically represent the scalar, fermion, antifermion and gauge fields respectively. This lends itself neatly to the formulation of the perturbative expansion in the coupling constants, from which the classical behaviour of the theory (i.e. the particle trajectories which minimize the action $\delta\mathcal{S} = 0$) is recovered in the leading order approximation. In the perturbative regime for which the coupling constants $g < 1$, $W(J)$ is then given an intuitive interpretation as the sum of connected Feynman diagrams.

From the generating functional for $\mathcal{L}_{\text{SM}}$ a set of Feynman rules can be extracted straightforwardly [12]. n-point correlation functions can be systematically constructed

by connecting propagators, determined for each field by the corresponding quadratic terms in the free action with vertices, whose structure is dictated by the interaction terms. Physical scattering amplitudes then follow from the S-matrix, evaluating correlation functions between 'asymptotic' on-shell initial and final particle states identified with those in the free theory, as enshrined by the Lehmann-Symanzik-Zimmermann (LSZ) reduction formula [12]. Some sample Feynman rules for the Standard Model are provided for illustration. The momentum space gluon, ghost, electroweak boson and fermion propagators respectively take the forms:

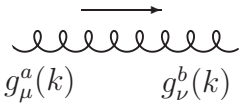

$$= \frac{-ig_{\mu\nu}\delta^{ab}}{k^2}\,, \tag{2.1.20}$$

$$= \frac{i\delta_{ab}}{k^2}\,, \tag{2.1.21}$$

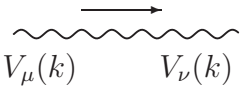

$$= \frac{-i}{k^2 - m_V^2 + im_V\Gamma_V}\left(g_{\mu\nu} - \frac{k_\mu k_\nu}{m_V^2 - im_V\Gamma_V}\right)\,, \tag{2.1.22}$$

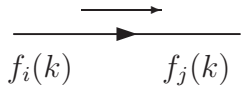

$$= \frac{i\delta^{ij}k_\mu\gamma^\mu}{k^2} = \frac{i\delta^{ij}\not{k}}{k^2}\,, \tag{2.1.23}$$

Where the raised arrows distinguish the direction of the flow of momentum from the flow of electric charge. The width Γ_V accommodates the finite lifetime of the massive weak bosons. The Feynman Gauge $\xi = 1$ is chosen for QCD, and each δ symbol in the fermion propagator collectively represents each quantum number carried by the particular fermion species f.

The form of the fermions' couplings to the gauge bosons follows from the structure of the covariant derivative, for $SU(3)_C$ these are:

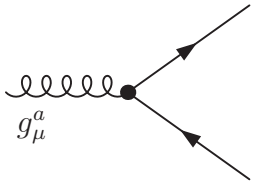

$$= ig_s T^A_{ij}\gamma^\mu\,,$$

where T^A are the generators of $SU(3)$, and i and j index the colour indices of the quarks. The $SU(N)$ gauge bosons' non-Abelian nature manifests in self interactions, exemplified

here by the gluon trilinear coupling;

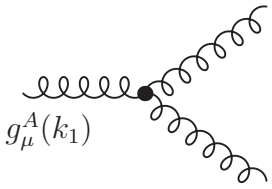

$$= g_s f^{ABC}\left[g_{\mu\nu}(k_1-k_2)_\rho + g_{\nu\rho}(k_2-k_3)_\mu + g_{\rho\mu}(k_3-k_1)_\nu\right],$$

while the chiral interactions of quarks and leptons with the massive weak gauge bosons inherits a more complex pattern as a consequence of Electroweak symmetry breaking:

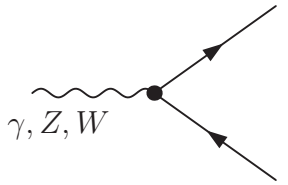

$$= ie\gamma_\mu\left(C_L P_L + C_R P_R\right)$$

	$\gamma\bar{f}_i f_j$	$Z\bar{f}_i f_j$	$W^+\bar{u}_i d_j$	$W^-\bar{d}_i u_j$	$W^+\bar{\nu}_i \ell_j$	$W^-\bar{\ell}_i \nu_j$
C_L	$-Q_f\delta_{ij}$	$g_f^-\delta_{ij}$	$\frac{1}{\sqrt{2}s_w}V_{ij}$	$\frac{1}{\sqrt{2}s_w}(V_{ij})^\dagger$	$\frac{1}{\sqrt{2}s_w}\delta_{ij}$	$\frac{1}{\sqrt{2}s_w}\delta_{ij}$
C_R	$-Q_f\delta_{ij}$	$g_f^+\delta_{ij}$	0	0	0	0

Table 2.2: *Couplings of the electroweak gauge bosons to the fermions. i and j represent flavour indices.*

where the electric charges of each fermion Q_f appears are assembled in Fig. 2.2, C_L and C_R are defined in Table. 2.2, $s_w = \sin\theta_w \equiv \frac{g_1}{g_1^2+g_2^2}$ defines the sine of the weak mixing angle, and we have introduced

$$g_f^+ = -\tan\theta_w\, Q_f\,, \quad g_f^- = \frac{T_f^3 - \sin^2\theta_w\, Q_f}{\sin\theta_w\cos\theta_w}\,, \tag{2.1.24a}$$

and $T_f^3 = \sigma^3/2$ is the weak isospin of the fermions. The genuinely quantum behaviour of the theory arises from the inclusion of higher-order terms in the expansion, corresponding to Feynman diagrams with closed loops of virtual particle states. These qualitatively change the behaviour relative to the classical theory, and their dynamical generation of scales is responsible for the most striking features exhibited by QCD of *asymptotic*

freedom and *confinement*. For QCD where the coupling constant $\alpha_s(m_Z) \sim 0.1185$ is large enough to render the leading order approximation insufficient in comparison with the experimental accuracy, the inclusion thereof is essential.

Renormalization and Scale Dependence

In evaluating loop diagrams we encounter Ultraviolet (UV) divergences associated with integrations over virtual states with arbitrarily high momenta. While long thought to render QFT mathematically inconsistent, these are now naturally understood by distinguishing the fundamental parameters written down in the Lagrangian from those determined by experiment. The latter are associated with measurements conducted with reference to a particular distance scale, or equivalently, momentum transfer, while the former (in the classical Lagrangian) are fixed constants defining the theory. The journey toward a physically sound reasoning to justify the removal of ultraviolet divergences is closely related to the concept of an Effective Field Theory, and with the mass dimension of the operators appearing in the Lagrangian.

The condition that divergences can be removed at all orders in perturbation theory by adjusting the definitions of a finite number of parameters distinguishes a theory as renormalizable. It is thus an essential requirement for the predictivity of the theory. These are typically brought under control by introducing a regularization scheme whereby they are extracted as the limits of well-defined quantities. Although the most immediately intuitive picture associates these with the limit of infinite loop momentum, these are usually pinned down in a more abstract way to preserve gauge invariance. This is achieved using Dimensional Regularization (DR) where it is recognized that the infinities are also unique to four spacetime dimensions. The infinite contributions to matrix elements can then be extracted by working instead in $d = 4 - 2\epsilon$ dimensions, and obtaining isolated poles $\frac{1}{\epsilon}$ in the limit $\epsilon \to 0$. Schematically, a divergent amplitude for a one-loop scattering amplitude in QCD would take the form:

$$\mathcal{M}^{\text{1-loop}}_{\text{div}} = g_s^2 \int \frac{d^4 l}{(2\pi)^4} f(l^2, \Delta) \to g_s^2 \mu^{4-d} \int \frac{d^d l}{(2\pi)^d} f(l^2, \Delta) \propto g_s^2 \mu^{2\epsilon} \frac{\Gamma(\epsilon)}{(4\pi)^{2-\epsilon}} \left(\frac{1}{\Delta}\right)^{\epsilon} \times (\ldots)$$

Where $f(l^2, \Delta)$ represents a generic integrand corresponding to a combination of propagator and numerator factors specified by the particular divergent Feynman graph. Ellipses represent finite terms. Scales associated with external momenta and masses are denoted by Δ. μ is an arbitrary dimensionful mass scale introduced to keep the coupling g_s

dimensionless in d spacetime dimensions. The divergent result is then identified by the form of $\Gamma(\epsilon) = \frac{1}{\epsilon} + \ldots$ as $\epsilon \to 0$. The prediction of an infinite result for the quantum corrections is clearly contradicted by experiment. To agree with measurement, these then must be accounted for in some way.

The recovery of finite physical predictions then follows the procedure of renormalization. The fields and coupling constants in the Lagrangian are first redefined, factoring out a rescaling Z associtated with each, as:

$$G_\mu^{A\,0} = Z_G^{\frac{1}{2}} G_\mu^A \quad , \quad \psi^0 = Z_\psi^{\frac{1}{2}} \psi \quad , \quad g_s^0 \to Z_1 Z_\psi^{-1} Z_G^{-\frac{1}{2}} g_s \mu^\epsilon \equiv Z_{g_s} g_s \tag{2.1.25}$$

Where ψ represents a generic coloured fermion field, and superscripts (0) denote the quantities in the original 'bare' Lagrangian. The separate renormalization factors Z_G, Z_ψ and Z_1 are required to treat the distinct infinities associated with the gluon and quark two point functions and the qqg vertex function respectively. The quantities G_μ^A, ψ and g_s are then the renormalized fields and coupling respectively. An explicit calculation of each correlation function at one-loop accuracy will then distinguish three divergent integrals with which each of these factors will be chosen to accommodate. In order to distinguish the physical consequences for the strong coupling constant g_s, the particular form of all three divergences must then be found. In each case, an expansion of the divergent amplitudes about the limit $\epsilon \to 0$ recovers a quantity like:

$$\mathcal{M}_{\text{div}}^{\text{1-loop}} \propto g_s^2 \left(\frac{1}{\epsilon} + \log \frac{\mu^2}{\Delta^2} + (\text{finite}) \right) \tag{2.1.26}$$

with the particular coefficients determined by each correlation function. The factors Z are selected to cancel the respective poles at a given order in $\alpha_s \equiv \frac{g_s^2}{4\pi}$, corresponding to the $\overline{\text{MS}}$ *renormalization scheme*.

$$Z_i = 1 + \sum_{n=1}^{\infty} \frac{a_i(g_s)}{\epsilon^k} \equiv 1 + \delta_i^Z(g_s) + \mathcal{O}(g_s^2) \tag{2.1.27}$$

Where δ_i^Z is a *counterterm*. Thus at 1-loop, these factors are linear in the strong coupling constant. On a purely mathematical level, there is nothing to prevent making this choice of normalization in the Lagrangian. This was historically a source of discomfort - doing so restored the predictivity of perturbation theory beyond the leading order, and this was vindicated by the dramatically accurate predictions of QED [21]. Moreover, an arbitrary mass scale μ was introduced as an artefact of the regularization procedure used to isolate the divergences. Fixing its value is directly analogous to fixing a momentum

scale at which the high momentum modes propagating in the loop are cut off [12]. In either regularization scheme, the predictions of the theory should be independent of it. However, it appears (together with the coupling constant) as a logarithmic enhancement of the physical scattering amplitude if we choose it to be much larger (or smaller) than the physical factor Δ associated with the fixed process kinematics. Therefore fixing it effectively modifies the strength of the perturbative expansion parameter α_s. It's then desirable for the accuracy of the perturbative expansion if it can be chosen to match the scale Δ associated with the process kinematics.

The condition that the parameter of the original Lagrangian be independent of this choice can then be stated in the form a differential equation:

$$0 = \frac{d}{d\log\mu}\log g_s^0 = 0 \Longrightarrow \frac{d}{d\log\mu}\log(Z_1 Z_\psi Z_G^{\frac{1}{2}} g_s \mu^\epsilon) = 0 \tag{2.1.28}$$

This is a specific case of the Callan-Symanzik equation [22]. To first order we have:

$$g_s^0 = (1 + \delta_1 - \delta_\psi - \tfrac{1}{2}\delta_A) g_s \,, \tag{2.1.29}$$

giving the condition:

$$\frac{dg_s}{d\log\mu} = -\epsilon g_s + \beta(g_s) \,, \tag{2.1.30}$$

with:

$$\beta(g_s) \equiv g_s \frac{d}{d\log\mu}(\delta_1 - \delta_\psi - \tfrac{1}{2}\delta_A) \tag{2.1.31}$$

which, with the one-loop counterterms takes the form of a renormalization group equation:

$$\beta(g_s) = -\frac{g_s^3}{16\pi^2}\left(\frac{11C_A}{3} - \frac{4n_f T_r}{3}\right) \equiv -\frac{g_s^3}{16\pi^2}\beta_0 \tag{2.1.32}$$

Where $C_A = 3$ and $T_r = \frac{1}{2}$ are the quadratic Casimir invariants associated with the adjoint and fundamental representations of $SU(3)$, and n_f the number of coloured fermions. This is the celebrated Beta function for QCD [23, 24], which explicitly absorbs the logarithmic dependence on the scale μ into the renormalized, *running* coupling constant $g_s(\mu)$ in such a way that the 'bare', unobservable coupling g_s^0 which includes the effects of propagating fields with arbitrarily high momenta remains fixed. This then relates

the value of the *effective* coupling constant (that which appears as the coefficient of a scattering amplitude which explicitly incorporates the quantum fluctuations of fields up to a momentum scale $\sim\mu$) at different (but arbitrary) choices of μ. This is referred to as the 'resummation of logarithms'. Recalling that μ plays the role of an ultraviolet cutoff, different choices of this parameter then correspond to different choices of factorization of the quantum fluctuations into those explicitly included in the (finite) matrix elements (with $p \lesssim \mu$), and those averaged over and absorbed into the definition of the renormalized coupling (with with $p \gtrsim \mu$).

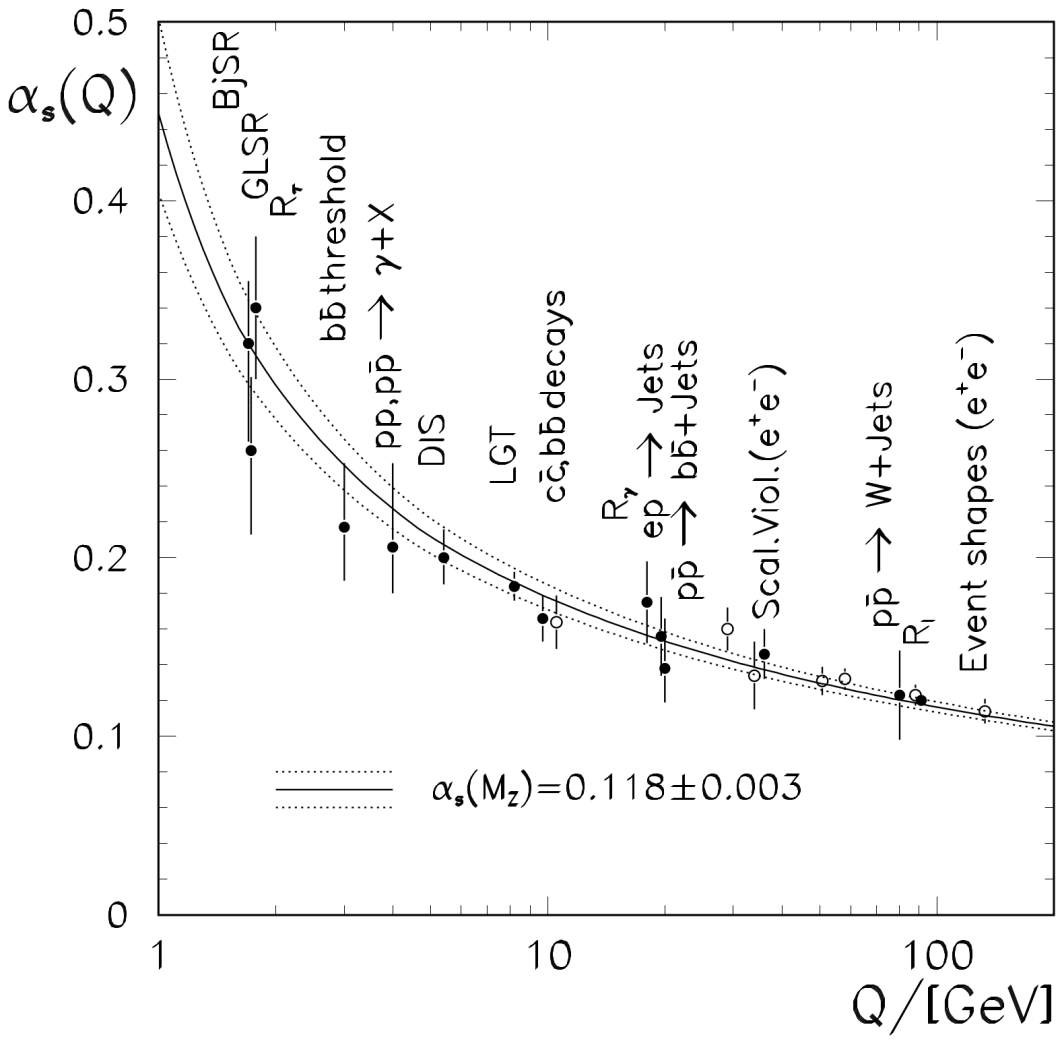

Figure 2.2: *Experimental measurements of the effective value of the strong coupling constant α_s as a function of momentum transfer Q [25].*

This argument should then also extend to heavy particle states with masses $m_H \gg \mu$, in addition to the high momentum fluctuations of the fields of which we are aware. Their dynamics should contribute only an overall rescaling of the coupling constant. This is guaranteed explicitly by the Appelquist-Carrazone decoupling theorem [26]. As a result, massive modes can be explicitly removed as dynamical degrees of freedom from the theory when calculating matrix elements to compare with experiment at momentum transfers $Q^2 \ll m_{\text{heavy}}$. For example, the inclusion of virtual top quark loops (with $m_t \simeq 173\text{GeV}$) in low energy matrix elements is not necessary, and they are said to be decoupled, or are 'integrated out'.

The solution to the beta function gives an explicit form for the running coupling $\alpha_s(\mu)$ from which the unique features of QCD emerge:

$$\alpha_s(Q^2) = \frac{4\pi\alpha_s(\mu)}{4\pi + \alpha_s(\mu)\beta_0 \log(\frac{Q^2}{\mu^2})} \tag{2.1.33}$$

The point at which the denominator becomes zero and the coupling constant diverges defines a unique scale Λ_{QCD};

$$\Lambda_{\text{QCD}} = \mu \exp\left(-\frac{2\pi}{\beta_0 \alpha_s(\mu)}\right) \tag{2.1.34}$$

This implies a unique *confinement* scale, i.e. an energy scale at which the theory is no longer perturbative and becomes strongly coupled. This relies only on the coefficients of the beta function β_0, and a measurement $\alpha_s(Q^2)$. This is an example of dimensional transmutation [27], whereby the quantum behaviour of the theory dynamically generates a mass scale absent from its classical analogue. One can then use this relation to rewrite:

$$\alpha_s(Q^2) = \frac{4\pi}{\beta_0 \log(Q^2/\Lambda^2_{\text{QCD}})} \tag{2.1.35}$$

Where all reference to the renormalization scale μ is gone. From here, the property of *asymptotic freedom* is manifest; the effective value of the strong coupling constant $\alpha_s(Q^2) \to 0$ as $Q^2/\Lambda^2_{\text{QCD}} \to \infty$. Collected experimental measurements which verify this behaviour are presented in Fig. 2.2.

The Role of Operator Mass Dimension

The connection between renormalizability and the relevant, marginal and irrelevant operators present in a Lagrangian can be illustrated by applying dimensional analysis to a simple model. Considering the action for scalar field theory with one operator falling into each category:

$$\mathcal{S}(\phi) = \int d^d x \left[\frac{1}{2}\partial_\mu\phi\partial^\mu\phi - \frac{1}{2}m^2\phi^2 - \frac{\lambda}{4!}\phi^4 - \frac{C}{6!}\phi^6 + \ldots\right] \tag{2.1.36}$$

For $\mathcal{S}$ to be dimensionless, the field ϕ and the parameters in the Lagrangian must carry mass dimensions $[\phi] = \frac{1}{2}(d-2)$, $[d^d x] = d$, $[m^2] = 2$, $[\lambda] = 4 - d$ and $[C] = 6 - 2d$. Consider one generic n-point correlation function for the scalar particles ϕ following from $\mathcal{S}$:

$$\langle\phi(x_1)\ldots\phi(x_n)\rangle_{\mathcal{S}} \tag{2.1.37}$$

and the same process in which ϕ interact over a shorter distance scale (or equivalently, at higher momentum transfer):

$$\langle\phi(x'_1)\ldots\phi(x'_n)\rangle_{S} \tag{2.1.38}$$

For fixed x', the co-ordinates x are related by some appropriate rescaling factor $x_\mu \to sx'_\mu$. In $\mathcal{S}$, this changes the normalization of the kinetic term; i.e. $\partial_\mu \to \frac{1}{s}\partial'_\mu$. To renormalize the kinetic term ϕ must be rescaled appropriately as:

$$\phi'(x') = s^{\frac{1}{2}(d-2)}\phi(x) \tag{2.1.39}$$

which is associated with a new action in which the relevant, marginal and irrelevant operators themselves carry different dependencies on s:

$$\mathcal{S}'(\phi') = \int d^d x' \left[\frac{1}{2}\partial'_\mu\phi\partial^{\mu\prime}\phi - \frac{1}{2}m^2 s^2\phi'^2 - \frac{\lambda}{4!}s^{4-d}\phi'^4 - \frac{C}{6!}s^{6-2d}\phi'^6 + \ldots\right]$$

The n-point correlation functions in terms of the original and rescaled fields are:

$$\langle\phi(sx_1)\ldots\phi(sx_n)\rangle_S = s^{\frac{1}{2}n(2-d)}\,\langle\phi'(x_1)\ldots\phi'(x_n)\rangle_{S'} \tag{2.1.40}$$

Specifying to four spacetime dimensions, in the rescaled action $\mathcal{S}'$ the mass operator carries a quadratic dependence on s which causes the two point function to grow with s^2. Meanwhile the coupling for marginal operator ϕ^4 is independent of the distance scale*, while the effective coefficient of the ϕ^6 operator falls. If we identify the long-distance correlation functions as those appropriate to describing currently observable energy scales q^2, and the short distance analogues as associated with a mass scale Λ^2 corresponding to new physics, in momentum space this means:

$$m^2 \sim \Lambda^2\,, \quad \lambda \sim 1\,, \quad C \sim \Lambda^{-2}\,, \tag{2.1.41}$$

i.e. the mass parameter at low energies is directly proportional to the heavy scale, while the coefficient of the higher-dimensional operator is suppressed by it. This is a general problem for scalar field theories †, and in the Standard Model leads to the so-called Hierarchy problem, whereby the Higgs boson mass is directly sensitive to the influence of virtual states at arbitrarily high energies. This is manifest in a momentum cut-off regularization scheme, where the one-loop Higgs mass parameter acquires contributions as:

$$m_H^2 = (m_H^0)^2 + \left(-\frac{3y_t^2}{8\pi^2}\right)\Lambda_t^2 + \left(\frac{9}{64\pi^2}g^2\right)\Lambda_{vec}^2 + \left(\frac{\lambda^2}{64\pi^2}\right)\Lambda_H^2 \tag{2.1.42}$$

where subscripts distinguish the contributions from virtual top quark, vector boson and Higgs pairs. Accommodating the observed value $m_H \sim 125\text{GeV}$ on the proviso that the SM should be valid up to arbitrarily high energies demands that the bare Higgs mass parameter m_H^0 then assume a remarkably precise value to cancel the contributions from the states running in the loop. More optimistically, this is interpreted as a signal that Λ is not too far away from presently accessible energy scales.

In the contrasting scenario, higher-dimensional operators are expected to carry *Wilson coefficients* which are accordingly suppressed; the assumption that one can write down a Lagrangian from dimension-four operators alone is valid in the scenario $q^2 \ll \Lambda^2$. A requirement for a renormalizable, predictive theory is then that it permits finitely many marginal operators, which, in the case of the Standard Model, is dictated by the symmetry requirements placed on the Lagrangian. An experimental measurement of a non-zero Wilson coefficient then heralds the proximity of the scale Λ, at which heavy states will be resolved.

*This is adjusted, as in QCD, by quantum corrections which break scale invariance by introducing a perturbative anomalous dimension.

†Fermion mass terms are protected by chiral symmetry.

Fermi Theory

To motivate the Standard Model Effective Field Theory (SMEFT) and its use as a tool with which to search for new physics, we'll look at the historical example of Fermi's theory of beta decay to establish the physical context for higher-dimensional operators.

After Electroweak symmetry breaking, the weak interaction experienced by the quarks is described by the Lagrangian:

$$\mathcal{L}_W = \frac{g_2}{\sqrt{2}} V_{ij} \bar{q}_i \gamma^\mu P_L q_j W_\mu^\pm \tag{2.1.43}$$

where P_L is the left-handed projection operator, and V_{ij} elements of the CKM matrix. In Fig. 2.3 we depict a tree-level $\Delta S = 1$ transition $u\,s \to d\,u$ mediated by the W-boson. The Standard Model matrix element is given by:

$$\mathcal{M} = (\frac{ig_2}{\sqrt{2}})^2 V_{us} V_{ud}^* (\bar{u}\gamma^\mu P_L s)(\bar{d}\gamma^\nu P_L u) \times \frac{-ig_{\mu\nu}}{q^2 - m_W^2} \tag{2.1.44}$$

Where we adopt the Feynman gauge $\xi = 1$, and q is the t-channel momentum transfer.

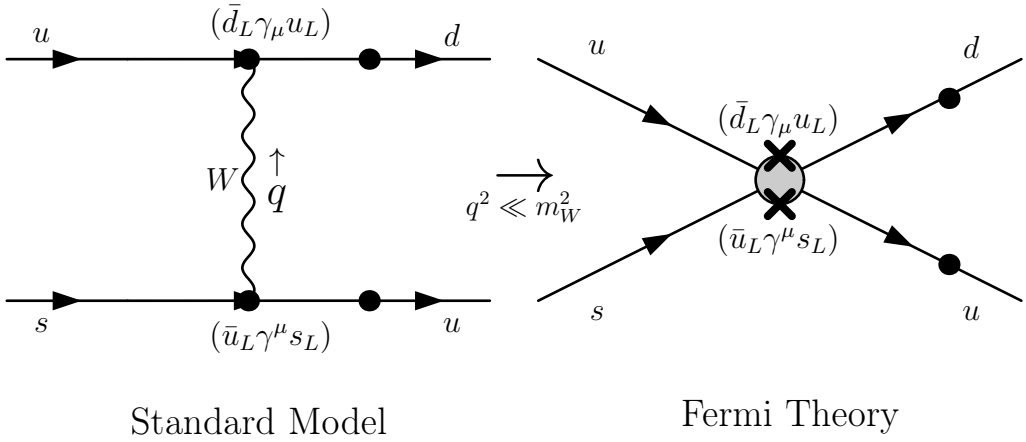

Figure 2.3: *Tree-level Feynman diagram representation of the flavour transition $us \to du$ in the full SM and in Fermi's theory. The leading behaviour of the W-boson in m_W^{-1} is encapsulated by a dimension-six operator possessing the same charged-current structure.*

It is non-local, as implied by the momentum dependence q^2 in the virtual W-boson propagator. However, in the limit $q^2 \ll m_W^2$ the matrix element permits a Taylor

expansion:

$$\frac{1}{q^2 - m_W^2} = \frac{1}{m_W^2}\left(1 + \frac{q^2}{m_W^2} + \dots\right) \tag{2.1.45}$$

so that we can write:

$$\mathcal{M} = \frac{i}{m_W^2}\left(\frac{ig_2}{\sqrt{2}}\right)^2 V_{us}V_{ud}^*(\bar{u}\gamma^\mu P_L s)(\bar{d}\gamma_\mu P_L u) + \mathcal{O}\left(\frac{1}{m_W^4}\right) \tag{2.1.46}$$

This is the same matrix element one would get if we used the dimension-six effective Lagrangian*:

$$\mathcal{L}_{D6} = -\frac{4G_F}{\sqrt{2}}V_{us}V_{ud}^*(\bar{u}\gamma^\mu P_L s)(\bar{d}\gamma^\nu P_L u) \tag{2.1.47}$$

G_F is called the Fermi constant, the value of which is fixed by applying the matching condition:

$$\frac{G_F}{\sqrt{2}} = \frac{g_2^2}{8m_W^2} \tag{2.1.48}$$

such that the effective description reproduces the behaviour of the Standard Model matrix element at $\mathcal{O}(m_W^{-2})$. The higher-order terms in the expansion in m_W^{-1} can be reintroduced order-by-order and associated with operators of higher mass dimension. The next term is:

$$\mathcal{M} = \frac{iq^2}{m_W^4}\left(\frac{ig_2}{\sqrt{2}}\right)^2 V_{us}V_{ud}^*(\bar{u}\gamma^\mu P_L s)(\bar{d}\gamma^\nu P_L u) + \mathcal{O}\left(\frac{1}{m_W^4}\right) \tag{2.1.49}$$

The presence of q^2 signals that the corresponding effective Lagrangian must contain a derivative. This can be accommodated by assembling the possible arrangements which could produce this:

$$\begin{aligned}\mathcal{L}_{D8} = {} & C_1(\bar{u}\gamma^\mu P_L D_\nu D^\nu s)(\bar{d}\gamma_\mu P_L u) \\ & + C_2(\bar{u}\gamma^\mu P_L s)(\bar{d}\gamma_\mu P_L D_\nu D^\nu u) \\ & + C_3(\bar{u}\gamma^\mu P_L D^\nu s)(\bar{d}\gamma_\nu P_L D_\nu u)\end{aligned}$$

where D_μ is the gauge covariant derivative for $SU(3)_C \otimes U(1)_{\text{EM}}$. By comparing the matrix elements order by order in m_W^{-1} of these with the Standard Model result, the

*More formally, this can be extracted directly from the generating functional $Z(J)$ in the path integral formalism, see e.g. [6]

appropriate values of the Wilson coefficients $C^{(D)} \propto m_w^{4-D}$ can be determined in terms of the underlying weak coupling constant g_2 and appropriate numerical factors. As the momentum transfer of the quarks $q \to m_W$, the convergence of the Taylor expansion in the propagator becomes poorer and poorer such that higher mass dimension operators must be included. However, since the production of an on-shell W-boson is kinematically forbidden until the threshold $q^2 = m_W^2$ is reached, the correlation functions of the effective and Standard Model descriptions remain the same. Thus until this point, the behaviour of the underlying theory can be fully described by including sufficiently many higher dimensional operators.

Crucially, the argument that a set of gauge-invariant operators can be constructed to represent the leading behaviour of massive states does not depend on their exact nature. From a position of ignorance, as in the original construction of Fermi theory, the W-boson represents an unknown degree of freedom, with its mass m_W playing the role of a new physics scale Λ. The interpretation of Wilson coefficients C however is then inherently ambiguous, as these are related in a non-trivial way by the structure possessed by the underlying theory. Nonetheless, the construction of a fully general EFT expansion in an unknown Λ^{-1} permits the description of the low-energy behaviour of a wide category of the possible agents of new physics.

In Section 3.4.1 we will detail the procedure of calculating QCD radiative corrections to Fermi Theory, after introducing operator identities pertinent to the calculation. The reader may however choose instead to explore this topic following the current discussion, as the novel aspects are minimal and are reiterated for clarity.

Chapter 3

The Standard Model Effective Field Theory

The construction of the Standard Model Effective Field Theory proceeds in accordance with a set of assumptions motivated by the predictive successes of the SM as a renormalizable gauge field theory. Following the procedure outlined in Chapter 2, by appealing to gauge and Lorentz invariance we can construct the leading set of higher-dimensional operators that could arise from integrating out physics at the as-yet undetermined high scale, Λ.

The minimal set of guiding principles adopted are as follows. Firstly, motivated by the lack of experimental evidence for light species not described by but interacting with the SM, it is assumed that any coupling of BSM states with $m < v \sim 246\text{GeV}$ to SM fields must be mediated by physics at or above Λ.

Secondly, we require that new physics respect the SM's $SU(3)_C \times SU(2)_L \times U(1)_Y$ gauge symmetry, either by the UV theory sharing it, or possessing an enlarged symmetry of which it is preserved as an unbroken subgroup.

Finally, the observed Higgs boson is assumed to be embedded in a complex scalar doublet transforming in the representation $\mathbf{2}_{1/2}$ of $SU(2)_L \times U(1)_Y$, i.e. it is identified with the Standard Model Higgs. This last requirement distinguishes the SMEFT from so-called Higgs Effective Field Theory (HEFT), a nonlinear sigma model in which the Goldstone bosons transform amongst themselves under the Electroweak symmetry under which the Higgs boson is a singlet. This is in contrast with the SM Higgs sector, in which

the Goldstone modes and observed scalar Higgs belong to a multiplet transforming linearly under the enlarged global 'Custodial' symmetry $O(4) \sim SU(2)_L \times SU(2)_R$.*.

Nonlinear realizations of Electroweak symmetry breaking are typical of models in which the observed scalar is a composite particle arising from the dynamics of a strongly interacting sector resolved at some scale $\Lambda_{Strong} \gg v$ (for a pedagogical review, see e.g. [29]). While HEFT does generalize the SMEFT to permit a larger class of operators by allowing a more arbitrary pattern of couplings between the Goldstone bosons, the composite Higgs models most consistent with experimental constraints generate operators at low energies contained within the SMEFT [30, 31]. Furthermore, since the distinction between symmetry breaking realizations determines the details of the structure of Goldstone-Higgs interactions, the phenomenological consequences will be manifest in Higgs and longitudinally polarized gauge boson scattering observables, while we will be primarily concerned with t-quark physics.

With these grounding assumptions, along with the requirement that $\mathcal{L}_{\text{eff}}$ be hermitian, we expect decoupled heavy states with masses $m \geq \Lambda$ to exert their influence through higher dimensional operators transforming as Lorentz scalars and singlets under $\mathcal{G}_{SM} \equiv SU(3)_C \times SU(2)_L \times U(1)_Y$. With the renormalizable SM Lagrangian $\mathcal{L}^{(4)}_{\text{SM}}$ in the unbroken Electroweak phase as a starting point:

$$\begin{aligned}\mathcal{L}^{(4)}_{\text{SM}} &= -\frac{1}{4}G^A_{\mu\nu}G^{A\mu\nu} - \frac{1}{4}W^I_{\mu\nu}W^{I\mu\nu} - \frac{1}{4}B_{\mu\nu}B^{\mu\nu} + \left(D_\mu\varphi\right)^\dagger\left(D^\mu\varphi\right) + \mu^2\varphi^\dagger\varphi - \frac{1}{2}\lambda\left(\varphi^\dagger\varphi\right)^2 \\ &+ \quad i\left(\bar{l}\not{D}l + \bar{e}\not{D}e + \bar{q}\not{D}q + \bar{u}\not{D}u + \bar{d}\not{D}d\right) - \left(\bar{l}\,Y_e e\varphi + \bar{q}\,Y_u u\widetilde{\varphi} + \bar{q}\,Y_d d\varphi + \text{h.c.}\right), \qquad (3.0.1)\end{aligned}$$

we anticipate the SMEFT Lagrangian to take the form:

$$\mathcal{L}_{\text{SM}} = \mathcal{L}^{(4)}_{\text{SM}} + \sum_k C^{(5)}_k Q^{(5)}_k + \sum_k C^{(6)}_k Q^{(6)}_k + \mathcal{O}\left(\frac{1}{\Lambda^3}\right), \qquad (3.0.2)$$

with:

$$Q_i = Q_i(G^a_\mu, W^I_\mu, B_\mu, \varphi, q_L, u_R, d_R, l_L, e_R). \qquad (3.0.3)$$

Here $Q^{(n)}_k$ denotes operators of mass dimension n, and $C^{(n)}_k$ are Wilson Coefficients carrying mass dimension $4-n$. As has been described, these are the leftover parameters arising from integrating out the BSM degrees of freedom which mediate the short-distance

*A geometrical interpretation of the distinction between the SMEFT and HEFT was recently formulated in terms of the properties of a curved scalar field manifold in [28].

physics above Λ*. These should be implicitly understood as being defined at the high scale Λ, and as such run and mix under the renormalization group. In the bottom-up approach, they are coupling constants to be determined by experiment, and any measurements thereof used in turn to inform guesses about the structure of the UV theory. Here and in what follows, we will adopt the notation employed in [14]†, wherein the authors approached the task of constructing a minimal set of operators systematically.

The SM field content was presented for reference in Tab. 2.1 in a form conducive to constructing higher-dimensional operators. In addition to the definitions already established, isospin, colour, and flavour indices are denoted explicitly by $j = 1, 2$, $\alpha = 1, 2, 3$, and $p = 1, 2, 3$, respectively. Dual tensors are to be defined by $\widetilde{X}_{\mu\nu} = \frac{1}{2}\varepsilon_{\mu\nu\rho\sigma}X^{\rho\sigma}$ $(\varepsilon_{0123} = +1)$, where X stands for G^A, W^I or B.

3.1 Operator Lagrangians

From our understanding that irrelevant operators Q_i with $[\boldsymbol{Q}] = n$ will contribute to observables at $\mathcal{O}(^{s^n}/_{\Lambda^n})$, we expect operators at dimensions five and six to provide the leading contributions to matrix elements. It is known in the SM that interactions mediated by operators of odd mass dimension necessarily violate conservation of B or L. That is, for an operator with Baryon number ΔB and Lepton number ΔL, its mass dimension is even (odd) if $(\Delta B - \Delta L)/2$ is even (odd) [32]. There is in fact only one L-violating dimension-five operator consistent with the SM gauge symmetry [33],

$$Q_{\nu\nu} = \varepsilon_{jk}\varepsilon_{mn}\varphi^j\varphi^m(l_p^k)^T C l_r^n \;\equiv\; (\widetilde{\varphi}^\dagger l_p)^T C(\widetilde{\varphi}^\dagger l_r). \tag{3.1.4}$$

where C is the charge conjugation matrix. In the broken Electroweak phase, $Q_{\nu\nu}$ generates neutrino masses and mixings, and constraints on these infer the dynamics responsible to exist at $\Lambda > 10^{13}$TeV. The first family of operators which could be generated by TeV scale physics are then those with mass dimension six, to which we now turn our attention. To construct the set of operators arising at $\mathcal{O}(\Lambda^{-2})$, the building blocks in 2.1 must be arranged in gauge and Lorentz invariant combinations which have total mass dimension $[\boldsymbol{Q}] = 6$. There is in general no unique prescription for populating the set

*One can equivalently choose to write these in the form $^{C^{(n)}}/_{\Lambda^n}$, whereby an explicit scale carries the mass dimension and the Wilson Coefficients C become dimensionless.

†The one exception to this is that we use the convention $\tau^I = {}^1/_2\sigma^I$, such that the Lie algebra generators τ^I and T^A have the same normalizations with respect to the Pauli and Gell-Mann matrices σ

Bosonic	Mixed	Fermionic	Empty
X^3		ψ^4	$X^2\varphi D$
$X^2\varphi^2$	$\psi^2 X D$	$\equiv$	$X\varphi^4$
$X^2 D^2$	$\psi^2\varphi^3$	$\bar{L}L\bar{L}L$	$X\varphi^3 D$
$X\varphi^2 D^2$	$\psi^2\varphi^2 D$	$\bar{R}R\bar{R}R$	$X\varphi D^3$
φ^6	$\psi^2\varphi D^2$	$\bar{L}L\bar{R}R$	$\varphi^5 D$
XD^4	$\psi^2 D^3$	$\bar{L}R\bar{L}R$	$\varphi^3 D^3$
$\varphi^4 D^2$	$\psi^2 X\varphi$	$\bar{L}R\bar{R}L$	φD^5
$\varphi^2 D^4$			D^6

Table 3.1: *Classifications of dimension-six operators by field content, obtained by generating combinations of* $\{\psi, X, \varphi, D\}$ *subject to the constraint* $3/2N_\psi + N_\varphi + 2N_X + N_D = 6$*, where* N_x *denotes the number of species* x*. The rightmost column may be discarded by inspection, lacking either sufficient Lorentz indices to form scalars, or an even number of Higgs doublets to form* $SU(2)_L$ *singlets. The remaining classification in red* XD^4 *is equivalent to* X^2D^2 *by the antisymmetry of* X *and the definition of the field strength tensors* $[D_\mu, D_\nu] \sim X_{\mu\nu}$*.*

of allowed operators at each order subject to these constraints simultaneously. A pragmatic system for approaching this problem was proposed in [14], whereby operators are first separated according to the general classifications defined in the left column of 2.1. We review and elaborate on this formalism here, the automation and generalization of which we will go on to describe in the context of an extension of the MATHEMATICA package FEYNRULES [10, 34].

The possible combinations of the generic objects $\{X, \varphi, \psi, D\}$ satisfying the constraint $[\boldsymbol{Q}] = 6$ are given in 3.1. Having catalogued these, the next task is to replace each of the proxies $\{\psi, X, \varphi\}$ with the corresponding fields $\{q_L, u_R, d_R, l_L, e_R, G^a_\mu, W^I_\mu, B_\mu, \varphi\}$ to form all possible combinations which respect gauge invariance. It is possible (at least at dimension six) to approach this problem 'by eye'. That is, for a given classification, choose a set of fields whose total Hypercharge $Y = 0$, identify which of these also constitute compatible multiplets of $SU(2)_L$ and $SU(3)_C$, and ensure that all Lorentz and spinor indices can be contracted to form an overall scalar *.

*In fact, it was very recently [32] noted that the constraint that operators are $U(1)_Y$ singlets can actually be formulated in such a way that it *contains* the analogous $SU(3)_C \times SU(2)_L$ invariance

For an example, say we want to populate the classification $\psi^2\varphi D^2$. Firstly we can appeal to Lorentz invariance. The fermion billinear must either be a tensor current $\bar{\psi}\sigma^{\mu\nu}\psi$ if it contracts with covariant derivatives carrying two different Lorentz indices D_μ and D_ν, or a Lorentz scalar $\bar{\psi}\psi$ if the covariant derivatives carry the same Lorentz index. Furthermore, because the fermions are chiral, nonzero scalar and tensor currents must contain one left- and one right-handed field.

Now appealing to gauge invariance, the fermions must together form a colour singlet: since the Higgs is itself a singlet, the only possibility comes from the $\mathbf{1}$ in the decomposition $\bar{\mathbf{3}} \otimes \mathbf{3} = \mathbf{1} \oplus \mathbf{8}$. Similarly the left-handed fermion must form a $SU(2)_L$ singlet with the Higgs, as the possibilities are $\mathbf{2} \otimes \mathbf{2} = \mathbf{1} \oplus \mathbf{3}$. Letting the left-chiral fermions appear as the barred spinors within the billinear, the $Y = 0$ Hypercharge combinations for the possible choices of $\bar{\psi}_L, \psi_R, \varphi$ can be enumerated from 2.1. Then the classification can then be filled by exhausting all arrangements of the covariant derivatives. If we let $\boldsymbol{D}^{(3)}_{(\mu\nu)}$ denote the set of all arrangements of the pair $\{D_\mu, D_\nu\}$ acting on an operator comprised of three fields, then schematically:

$$\boxed{\psi^2\varphi D^2} = \boldsymbol{D}^{(3)}_{(\mu\nu)} \left((\bar{q}\sigma^{\mu\nu}u)\widetilde{\varphi} + (\bar{q}\sigma^{\mu\nu}d)\varphi + (\bar{l}\sigma^{\mu\nu}e)\varphi \right) + h.c. \tag{3.1.5}$$

$$+ \boldsymbol{D}^{(3)}_{(\mu\mu)} \left((\bar{q}u)\widetilde{\varphi} + (\bar{q}d)\varphi + (\bar{l}e)\varphi \right) + h.c. \tag{3.1.6}$$

$$= (D_\mu\bar{q}\sigma^{\mu\nu}D_\nu u)\widetilde{\varphi} + (D_\mu\bar{q}\sigma^{\mu\nu}u)D_\nu\widetilde{\varphi} + (\bar{q}\sigma^{\mu\nu}D_\mu u)D_\nu\widetilde{\varphi}$$

$$+ \cdots + h.c. \tag{3.1.7}$$

$$+ (D_\mu\bar{q}\,D^\mu u)\widetilde{\varphi} + (D_\mu\bar{q}\,u)D^\mu\widetilde{\varphi} + (\bar{q}\,D_\mu u)D^\mu\widetilde{\varphi}$$

$$+ (D^\mu D_\mu\bar{q}\,u)\widetilde{\varphi} + (\bar{q}\,D^\mu D_\mu u)\widetilde{\varphi} + (\bar{q}\,u)D_\mu D^\mu\widetilde{\varphi} + h.c. \tag{3.1.8}$$

Here, the ellipsis represent the remaining terms making up the $3!\,2! = 12$ distinct ways of distributing two unique derivatives D_μ and D_ν over the three fields present in each tensor current operator. The $3!\,2!\,/2 = 6$ ways of distributing the two identical derivatives D_μ and D^μ over the three fields in their scalar current counterparts are shown explicitly. Individual operators are shown explicitly for the first of the three possible choices of field content in 3.1.6 and 3.1.8, with the other two following trivially.

Next, considering the tensor current operators, we notice that the presence of $\sigma^{\mu\nu}$ renders these antisymmetric in the indices μ, ν. Thus, only half of the 12 operators arising for each case are unique. Then for each choice of field content there are six opera-

constraints. This enhances the prospect of automating the generation of gauge-invariant operators at a given order in Λ^{-1} significantly.

tors; those three written explicitly in 3.1.7, and another three in which both derivatives act together on one of the fields. By the antisymmetry of $\sigma^{\mu\nu}$, each $D_\mu D_\nu \psi$ is projected onto its antisymmetric part, $[D_\mu, D_\nu]$, where here ψ stands in for any of the fields $\{u,\, q,\, d,\, e,\, \varphi\}$. Through the identity $[D_\mu, D_\nu] = -ig_X T^A X^A_{\mu\nu}$, where the right hand side is an implicit sum over each of the gauge field strength tensors for the groups under which ψ is charged, these operators are actually a linear combination of those in the $\psi^2 X \varphi$ classification. In total then, for each choice of field content, there are the three unique tensor current operators given by 3.1.7, and the six scalar currents given by 3.1.8.

Finally, we must allocate Wilson Coefficients appropriately. As was implied by the addition of *h.c.*, the $\psi^2 \varphi D$ class operators are not self-hermitian, so we must add their hermitian conjugates to them to keep the action real. Each of the independent terms in 3.1.7 and 3.1.8 carries two flavour indices, one on each of the fermion fields, which were not written explicitly. Then each operator is actually a 3×3 matrix in flavour space, each entry of which may carry a distinct Wilson Coefficient C_{pr}, where $p,\, r = 1, 2, 3$ are flavour indices. In general each C_{pr} may be complex, but must be real for self-hermitian operators to preserve the condition $\mathcal{L} = \mathcal{L}^\dagger$. For each of the three choices of field content, the $\psi^2 \varphi D^2$ class then contains nine unique operators which possess 3×3 complex Wilson Coefficients and their hermitian conjugates, for a total of 486 real parameters. The remaining operator classifications can be filled by following by the same recipe.

Clearly the number of couplings required to fully parametrize all possible gauge-invariant interactions at dimension six will quickly become intractable if no further limitations are enforced in constructing the Lagrangian. Fortunately, strong experimental constraints on processes violating the global symmetries of the SM, and identities which interrelate seemingly distinct operators will permit us to make some systematic simplifications.

3.1.1 Accommodating Global Symmetries

It is possible to place further restrictions on the operators which may appear in the SMEFT Lagrangian, most prominently to accommodate the SM's (exact and approximate) global symmetries. These are baryon and lepton numbers B and L, flavour symmetry, the custodial $SU(2)$ symmetry of the Higgs sector, and the discrete symmetry of the Lorentz group $\mathcal{CP}$. Although they play no direct role in the construction of the Lagrangian, one can distinguish higher dimensional operators by which global

symmetries they respect or break. Physics associated with the breaking of a given symmetry tends to have a corresponding distinct phenomenological signature (for example, the B-violating decay of the proton), which makes it more vulnerable to experimental detection. Bounds obtained from indirect searches targeting processes signifying the breaking of a global symmetry can then be interpreted in terms of the magnitude of the Wilson coefficients of these operators. Table 3.2 shows a summary of some experimental constraints [35–38] on Λ obtained from parametrizing the symmetry breaking by the corresponding, lowest-order operators in the SMEFT.

Broken Global Symmetry	Operators	Λ
B, L	$(qqql)/\Lambda^2$	10^{13} TeV
Flavour (1,2$^{\text{nd}}$ family), CP	$(\bar{d}s\bar{d}s)/\Lambda^2$	1000 TeV
Flavour (2,3$^{\text{rd}}$ family)	$m_b(\bar{s}\sigma_{\mu\nu}F^{\mu\nu}b)/\Lambda^2$	50 TeV
Custodial $SU(2)$	$(\varphi^\dagger D_\mu\varphi)^2/\Lambda^2$	5 TeV

Table 3.2: *Lower bounds [39] on the scale Λ associated with some select global symmetry violating higher-dimensional operators of the Standard Model.*

The stringent bounds in Tab. 3.2 suggest particularly that the symmetries B, L and flavour symmetry among the light quarks are conserved by physics well into the multi-TeV scale. This fact constrains the anatomy of models of NP accessible at LHC energies. For example, the theoretical assertion that we should reasonably expect to see NP in a window around $\mathcal{O}$(TeV) to resolve the Hierarchy Problem should be accompanied by the understanding that this physics must respect these symmetries. This can be accommodated in the EFT language by imposing conditions on the Wilson Coefficients of any operators we construct which explicitly break them. It is by this rationale, for example, that B-violating operators would be ignored (their coefficients being fixed to zero) when considering qq scattering at the LHC, where the centre-of-mass energy is 13 orders of magnitude lower than Λ.

To accommodate flavour violation constraints, one commonly adopted hypothesis is that of Minimal Flavour Violation (MFV) [37]. This is the assertion that TeV scale physics' breaking of flavour symmetry should follow the same pattern as exists in the SM Yukawa sector. In the SM, $\mathcal{L}_{\text{SM}} - \mathcal{L}_{yuk}$ is invariant under five $U(3)$ symmetries

corresponding to unitary rotations of the flavour multiplets $U_{pr}\psi_r$, where U is a unitary matrix carrying flavour indices p, r and $\psi_r = \{q_r, l_r, u_r, d_r, e_r\}$. We observe (as in 3.2) that this symmetry, with its breaking described by the Yukawa sector, is an excellent description of all flavour-changing processes up to at least $\mathcal{O}(\,50\,\text{TeV})$. One can then bake the requirement into a given BSM model that flavour violation remains the prerogative of the SM parameters V_{CKM} and $Y_{u,d,e}$.

Taking the example of flavour multiplets of the chiral quark fields $\{q, u, d\}$, each of these can be considered as vectors in the fundamental representation of appropriate copies of an $SU(3)$ flavour symmetry:

$$\begin{aligned} \boldsymbol{\mathcal{G}}_{flav} &\equiv SU(3)_q \times SU(3)_u \times SU(3)_d \\ q \in (\mathbf{3},\mathbf{1},\mathbf{1}), u \in (\mathbf{1},\mathbf{3},\mathbf{1}), d \in (\mathbf{1},\mathbf{1},\mathbf{3}). \end{aligned} \tag{3.1.9}$$

where the barred counterparts are similarly in the corresponding $\overline{\mathbf{3}}$ representations. We wish to widen the definition of the flavour symmetry of the SM to denote both terms which are invariant under unitary rotations of the quark flavours, and those which violate this symmetry through the explicit flavour space matrices $Y_{u,d,e}$. To do this, $Y_{u,d,e}$ are promoted to non-propagating, constant 'auxiliary' fields which are each taken to transform with the quark multiplets in an appropriate representation of the $SU(3)$ flavour symmetry groups [37]:

$$Y_u \sim (\mathbf{3}, \overline{\mathbf{3}}, \mathbf{1}) \ , \quad Y_d \sim (\mathbf{3}, \mathbf{1}, \overline{\mathbf{3}}). \tag{3.1.10}$$

The quark Yukawa Lagrangian now transforms as:

$$\begin{aligned} \mathcal{L}_{yuk} &= -\,\bar{q}_p\,[Y_d]_{pr}\,d_r\varphi + \overline{q}_p\,[Y_u]_{pr}\,u_r\widetilde{\varphi} + h.c. \\ &\to -\,\bar{q}_p\left[(U_q^\dagger)_{pr}(U_q)_{rs}(Y_d)_{st}(U_d^\dagger)_{tv}(U_d)_{vw}\right] d_w\varphi \\ &\quad + \overline{q}_p\left[(U_q^\dagger)_{pr}(U_q)_{rs}(Y_u)_{st}(U_u^\dagger)_{tv}(U_u)_{vw}\right] u_w\widetilde{\varphi} + h.c. \\ &= \mathcal{L}_{yuk}\,, \end{aligned} \tag{3.1.11}$$

Where $U_{\{q,u,d\}}$ are the unitary $SU(3)$ matrices acting separately on the q, u, d flavour multiplets, and Latin subscripts denote flavour indices. $\mathcal{L}_{yuk}$ now satisfies the extended definition of flavour symmetry in the SM by construction.

With these definitions in place, requiring that all higher-dimensional operators belong to representations of $\boldsymbol{\mathcal{G}}_{flav}$ built from 3.1.9 and 3.1.10 enforces the condition that flavour

transitions arise from from $Y_{u,d,e}$ alone. As with in the SM, by fixing the five unitary flavour rotations into the definitions of the fermion fields, one can choose the basis:

$$Y_d = \Gamma_d, \quad Y_l = \Gamma_l, \quad Y_u = V^\dagger \Gamma_u, \tag{3.1.12}$$

where V is the CKM matrix, and $\Gamma_{u,d,l}$ the usual diagonal matrices of fermion Yukawa couplings $\Gamma_u = \text{diag}(y_u, y_c, y_t)$, ... The permissible flavour-changing invariants are then:

$$\bar{q}_p \, (Y_u Y_u^\dagger)_{pr} \, q_r, \quad \bar{d}_p \, (Y_d^\dagger Y_u Y_u^\dagger)_{pr} \, q_r, \quad \bar{d}_p \, (Y_d^\dagger Y_u Y_u^\dagger Y_d)_{pr} \, d_r, \tag{3.1.13}$$

which, neglecting the ratio of the light quark Yukawas over that of the top identifies:

$$\bar{q} \, \lambda^{FC} \, q \quad \& \quad \bar{d} \, \lambda_d \lambda^{FC} q, \quad \lambda^{FC} \equiv (Y_u Y_u^\dagger) \simeq y_t^2 V_{3p}^* V_{3r} \quad p \neq r \tag{3.1.14}$$

as the allowed flavour non-diagonal billinears in $\mathcal{L}$. A ψ^4 class operator such as:

$$Q \equiv C_{prst} (\bar{q}_p \gamma^\mu q_r)(\bar{q}_s \gamma_\mu q_t), \tag{3.1.15}$$

which carries $n_f^4 = 81$ Wilson Coefficients C_{prst} permitting arbitrary transitions between quark flavours may now only have the structure:

$$Q \overset{MFV}{\to} C_2 (\bar{q}_p \gamma^\mu \lambda_{pr}^{FC} q_r)(\bar{q}_s \gamma_\mu \lambda_{st}^{FC} q_t) + C_1 (\bar{q}_p \gamma^\mu \lambda_{pr}^{FC} q_r)(\bar{q}_s \gamma_\mu q_s) + C_0 (\bar{q}_p \gamma^\mu q_p)(\bar{q}_r \gamma_\mu q_r). \tag{3.1.16}$$

By adopting the MFV ansatz, the number of nonzero coefficients required to describe the effective coupling have been reduced from 81 to 3, as there are only three possible structures invariant under the extended flavour symmetry group. This is a formidable simplification over the general SMEFT, for which the authors of [40] identified 2499 independent Wilson Coefficients when no such simplifications are made.

3.2 Operator Redundancies

Once an exhaustive set of candidates has been identified in each classification, there remains the task of accounting for identities which relate linear combinations of operators to each other. Operator redundancy in the SMEFT was for a long time a source of confusion in the literature, with the initial, highly cited work proposing a basis at dimension six [41] arriving at a set now known to be overcomplete by 21 terms. The

consequences of failing to conclusively identify and eliminate these interdependencies amount to the implicit over- or under-representation of distinct physical effects, and the artificial enlargement of the parameter set used to describe the contributions to observables arising at this order in Λ^{-1}. We will find that there exist a set of mappings between the valid (black) classifications summarized in 3.1, and as such, operators therein will not be independent. This follows as a consequence of the classical equations of motion for the SM fields, the Fierz identities for spin, colour and isospin, and the vanishing of total derivatives of gauge invariant objects from the action. Together these necessitate the adoption of a procedure by which these relations should be used to reduce operators to an independent basis.

3.2.1 Fierz Identities

Fierz identities [42]* are relationships which may be derived whenever a general set of orthogonal $N \times N$ real (complex) matrices $\{M\}$ span the vector space on which they are defined, $\mathbb{R}^N$ ($\mathbb{C}^N$). Practically, they exploit the completeness of $\{M\}$ over the space to re-order matrix products as:

$$(\phi_1^T M_A \phi_2)\,(\phi_3^T M_A \phi_4) = (\phi_1^T M_C \phi_4)\,(\phi_3^T M_D \phi_2) \tag{3.2.17}$$

where ϕ (ϕ^T) are generic $1 \times N$ ($N \times 1$) column (row) vectors, and the matrices M_X are some linear combinations of the orthogonal set $\{M\}$. For a pedagogical review of their derivation and applications, see e.g. [43,44], some of whose main results are summarized here.

In the SM, the objects used to form gauge and Lorentz invariant products of fields are the generators $\{\tau^I\}$ and $\{T^A\}$ of $SU(2)_L$ and $SU(3)_C$, and the set of 4×4 matrices $\{\Gamma^A\}$ which form the Dirac basis for the Lorentz group. The generators of $SU(2)$ and $SU(3)$ are equipped with an inner product through the trace billinear:

$$\begin{aligned} \mathrm{Tr}[\tau_I \tau_J] &= C\,\delta_{IJ} \quad (I, J = 1, 2, 3) \\ \mathrm{Tr}[T_A T_B] &= C\delta_{AB} \quad (A, B = 1, \ldots, 8) \end{aligned} \tag{3.2.18}$$

where the $SU(2)$ and $SU(3)$ generators are denoted in terms of the Pauli and Gell-Mann matrices σ_I and λ_A by $\tau_I = {}^1\!/_2\,\sigma_I$ and $T_A = {}^1\!/_2\,\lambda_A$. The conventional normalization for

*Originally, these referred to one specific set of relations for the Dirac algebra which allowed one to re-order spinors in products of fermion billinears.

the fundamental representation has $C = 1/2$. Since there are $N^2 - 1$ traceless, orthogonal generators for the fundamental representation of $SU(N)$, together with the respective identity matrices $\mathbb{I}_2$ and $\mathbb{I}_3$ these span the space of complex $N \times N$ matrices $M_2(\mathbb{C})$ and $M_3(\mathbb{C})$. That is, each is a set of N^2 independent basis vectors onto which a general $N \times N$ complex matrix X may be decomposed. For the fundamental representations of $SU(2)$ and $SU(3)$:

$$X = X_0 \mathbb{I} + X_I \tau^I \quad \text{and} \quad X = X_0 \mathbb{I} + X_A T^A, \tag{3.2.19}$$

where X are general, complex 2×2 and 3×3 matrices respectively, and where the subscripted X are the coefficients of each of the basis matrices $\{ \mathbb{I}_2, \tau_I \}$ and $\{ \mathbb{I}_3, T_A \}$ respectively. Using the orthogonality relations 3.2.18, these can be projected out by taking the trace of the product of X with each of the basis matrices:

$$\begin{aligned} X_0 &= \frac{1}{2}\mathrm{Tr}[X], \quad X_I = 2\,\mathrm{Tr}[X\tau_I], \\ X_0 &= \frac{1}{3}\mathrm{Tr}[X], \quad X_A = 2\,\mathrm{Tr}[XT_A]. \end{aligned} \tag{3.2.20}$$

Inserting the coefficients 3.2.20 into 3.2.19 and writing indices explicitly gives, for $N \times N$ complex matrices $X^{(N)}$:

$$\begin{aligned} (\delta_{il}\,\delta_{kj})(X^{(2)})_{lk} &= (\frac{1}{2}\,\delta_{ij}\,\delta_{kl} + 2\,(\tau_I)_{kl}\,(\tau_I)_{ij})\,(X^{(2)})_{lk} \\ (\delta_{il}\,\delta_{kj})(X^{(3)})_{lk} &= (\frac{1}{3}\,\delta_{ij}\,\delta_{kl} + 2\,(T_A)_{kl}\,(T_A)_{ij})\,(X^{(3)})_{lk}, \end{aligned} \tag{3.2.21}$$

from which the $SU(2)$ and $SU(3)$ Fierz identities can be read off:

$$\tau^I_{ij}\,\tau^I_{kl} = \frac{1}{2}\,\delta_{il}\,\delta_{kj} - \frac{1}{4}\,\delta_{ij}\,\delta_{kl} \tag{3.2.22}$$

$$T^A_{ij}\,T^A_{kl} = \frac{1}{2}\,\delta_{il}\,\delta_{kj} - \frac{1}{6}\,\delta_{ij}\,\delta_{kl} \tag{3.2.23}$$

These are completeness relations which map products of matrices in the fundamental representation of $SU(N)$ to linear combinations of themselves with their indices rearranged. In practice, this allows one to reshuffle the ordering of the $SU(N)$ vectors on which these act to form gauge-invariant quantities. These can be used in the SM to rewrite the colour (or isospin) factors in matrix elements, and are typically given a Feynman diagrammatic interpretation as depicted in 3.1.

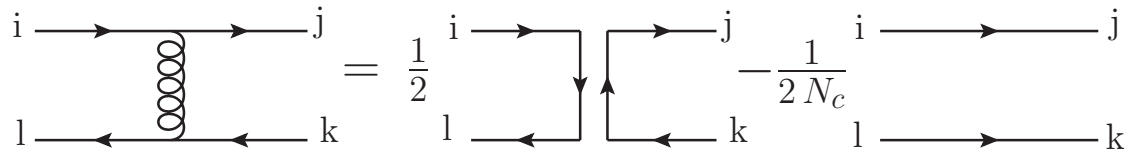

Figure 3.1: *Diagrammatic interpretation of the $SU(3)$ Fierz identity 3.2.23, with $N = N_c = 3$ in QCD. Matrix elements for the exchange of a colour-octet gluon in $q\bar{q}$ scattering can be expressed as a linear combination of contributions in which different combinations of the quarks form colour singlets.*

Since $\mathcal{L}^{(6)}$ contains the classification ψ^4 - that is: the set of local operators comprised of four fermion fields - pairs of $SU(N)$ matrices will arise in each operator which is a product of two fermion billinears carrying indices in the fundamental representations of $SU(2)_L$ or $SU(3)_C$. In the case of the Higgs field φ which carries mass dimension 1 and an index in the fundamental representation of $SU(2)_L$, operators containing up to three $SU(2)_L$ matrices will occur in the classification φ^6. The Fierz identities 3.2.22 & 3.2.23 will then relate any such operators to a linear combinations of others for which the colour or isospin matrices T^A and τ^I contract the fields in a different order. To illustrate this, let's apply the Fierz identities to a dimension six operator we write down that is a product of two $(\mathbf{1}, \mathbf{3}, 0)$ Lorentz vectors:

$$\begin{aligned}
\mathcal{O} &= (\varphi^{\dagger\, i}\, \tau^I_{ij}\, D_\mu \varphi^j)(\varphi^{\dagger\, k}\, \tau^I_{kl}\, D^\mu \varphi^l) \\
&\overset{(3.2.22)}{=} \frac{1}{2}(\varphi^{\dagger\, i}\, \delta_{il} D^\mu \varphi^l)(\varphi^{\dagger\, k}\, \delta_{kj} D_\mu \varphi^j) - \frac{1}{4}(\varphi^{\dagger\, i}\, \delta_{ij}\, D_\mu \varphi^j)(\varphi^{\dagger\, k}\, \delta_{kl}\, D^\mu \varphi^l) \\
\mathcal{O} &= \frac{1}{4}(\varphi^{\dagger\, i}\, \delta_{ij}\, D_\mu \varphi^j)(\varphi^{\dagger\, k}\, \delta_{kl}\, D^\mu \varphi^l) \equiv \frac{1}{4}\mathcal{O}', \qquad (3.2.24)
\end{aligned}$$

where weak isospin indices are denoted by i, j, k, l. In the last equality we have relabeled the indices and combined the terms, since the Higgs doublets φ are identical. We see that $\mathcal{O}$ and $\mathcal{O}'$ are actually the same operator up to a factor of $1/4$, which may not have been obvious had we not been aware of 3.2.22.

The benefit of these Fierz identities to constructing operator bases is that one need not consider all the distinct contractions of each of the colour and weak isospin matrices with the fields in a given operator. In particular, since products of fields which are colour octets or isospin triplets can be written as a linear combination of respective singlets, one can aim to form an independent set with as few of the matrices T^A and τ^I as is possible. This choice can lead to, for example, the simplification of matrix elements involving colour factors.

The same reasoning as before can be used to derive Fierz identities for the Dirac algebra, for which a set of matrices $\{\Gamma^A\}$ form a basis in which fermion billinears $\bar{\psi}\,\Gamma\,\psi$ have definite transformation properties under the Lorentz group. We adopt some simplifying notation introduced by Takahashi [45], whereby the order in which indices are contracted is encoded by the parentheses ( ) and [ ]. In this notation, the $SU(2)$ Fierz identity 3.2.22 is represented by:

$$(\tau_I)[\tau_I] = \frac{1}{2}(\ ][\ ) - \frac{1}{4}(\ )[\ ], \tag{3.2.25}$$

with the position of the indices i, j, k, l inferred by the style of parentheses, and the identity δ_{ij} denoted by the empty brackets ().

The usual set of 4×4 matrices which form the Dirac representation of the Lorentz group are:

$$\{\Gamma^A\} \equiv \{\mathbb{I}, \gamma_5, \gamma^\mu, \gamma^\mu\gamma_5, \sigma^{\mu\nu}\}, \tag{3.2.26}$$

where $A = (1, \ldots, 16)$ indexes each of the distinct matrices. These obey an orthogonality relation analogous to 3.2.18 which can be verified by appealing to the usual properties of the gamma matrices:

$$\mathrm{Tr}[\Gamma_A\Gamma^B] = 4\,\delta_A^B. \tag{3.2.27}$$

Orthogonality as expressed through the trace billinear 3.2.27 requires that the product contain one covariant and one contravariant index. This can be conveniently accounted for, following the convention in [44], by absorbing this requirement into the definition of a dual basis where spacetime indices appear lowered:

$$\{\Gamma_A\} \equiv \{\mathbb{I}, \gamma_5, \gamma_\mu, -\gamma_\mu\gamma_5, \frac{1}{2}\sigma_{\mu\nu}\}. \tag{3.2.28}$$

Here, the factor of $1/2$ corrects for overcounting redundant permutations of Lorentz indices following from the antisymmetry of $\sigma_{\mu\nu}$, and the additional minus sign accounts for the anticommutivity property $\{\gamma_\mu, \gamma_5\} = 0$. Then it is understood in 3.2.27 that the matrix product is defined for one element from the dual basis Γ_A and one from the original basis Γ^B.

The 16 matrices $\{\Gamma^A\}$ span the space of 4×4 complex matrices $M_4(\mathbb{C})$, so any $X \in M_4(\mathbb{C})$ may be decomposed as:

$$X = X_A \Gamma^A, \quad X_A = \frac{1}{4}\mathrm{Tr}[X\Gamma_A]. \tag{3.2.29}$$

The Fierz identities then follow from an identical procedure as used for the generators of the $SU(N)$ algebras. In this case however, the basis matrices aren't enumerated by a common index in the adjoint representation, but by the five (sets of) matrices making up the scalar, pseudoscalar, vector, pseudovector and tensor representations of the Lorentz group. Writing:

$$X = \frac{1}{4}(\mathrm{Tr}[X]\mathbb{I} + \mathrm{Tr}[X\gamma_5]\gamma_5 + \mathrm{Tr}[X\gamma_\mu]\gamma^\mu - \mathrm{Tr}[X\gamma_\mu\gamma_5]\gamma^\mu\gamma^5 + \frac{1}{2}\mathrm{Tr}[X\sigma_{\mu\nu}]\sigma^{\mu\nu}), \tag{3.2.30}$$

and representing indices using the notation of 3.2.25 yields the completeness relation:

$$(\ )[\ ] = \frac{1}{4}(\Gamma_A][\Gamma^A) = \frac{1}{4}(\Gamma^A][\Gamma_A). \tag{3.2.31}$$

The Fierz identities follow immediately from appropriately multiplying the identity matrices $(\ )$ and $[\ ]$ in 3.2.31 by each possible pairing of the basis matrices (Γ^A, Γ_B):

$$(\Gamma^A)[\Gamma_B] = (-)\frac{1}{4^2}\mathrm{Tr}[\Gamma^A\Gamma^C\Gamma_B\Gamma_D](\Gamma^D][\Gamma_C). \tag{3.2.32}$$

This is a 5×5 matrix mapping each pairing of the form $(\Gamma^A)[\Gamma_B]$ onto a linear combination with rearranged indices $(\Gamma^D][\Gamma_C)$, with coefficients given by gamma matrix traces. The minus sign in parentheses is to be understood as present whenever these sit between anticommuting spinor fields. We will be interested in operators comprised of fermion billinears of the form $(\bar\psi_1\,\Gamma^A\,\psi_2)(\bar\psi_3\,\Gamma_A\,\psi_4)$ which are Lorentz scalars, so only the five diagonal entries are important. These are:

$$\begin{aligned}
(\ )[\ ] &= \frac{1}{4}\left[(\gamma^5][\gamma^5) + (\gamma^\mu][\gamma^\mu) + (\ ][\ ) + \frac{1}{2}(\sigma^{\mu\nu}][\sigma^{\mu\nu}) - (\gamma^\mu\gamma^5][\gamma^\mu\gamma^5)\right] \\
(\gamma^\mu)[\gamma^\mu] &= \left[-(\gamma^5][\gamma^5) - \frac{1}{2}(\gamma^\mu][\gamma^\mu) + (\ ][\ ) - \frac{1}{2}(\gamma^\mu\gamma^5][\gamma^\mu\gamma^5)\right] \\
(\sigma^{\mu\nu})[\sigma^{\mu\nu}] &= \left[3(\gamma^5][\gamma^5) + 3(\ ][\ ) - \frac{1}{2}(\sigma^{\mu\nu}][\sigma^{\mu\nu})\right] \\
(\gamma^\mu\gamma^5)[\gamma^\mu\gamma^5] &= \left[(\gamma^5][\gamma^5) - \frac{1}{2}(\gamma^\mu][\gamma^\mu) - (\ ][\ ) - \frac{1}{2}(\gamma^\mu\gamma^5][\gamma^\mu\gamma^5)\right]
\end{aligned} \tag{3.2.33}$$

$$(\gamma^5)\,[\gamma^5] \quad = \quad \frac{1}{4}\left[(\gamma^5]\,[\gamma^5) - (\gamma^\mu]\,[\gamma^\mu) + (\ ]\,[\ ) + \frac{1}{2}(\sigma^{\mu\nu}]\,[\sigma^{\mu\nu}) + (\gamma^\mu\gamma^5]\,[\gamma^\mu\gamma^5)\right],$$

with an additional overall minus sign present when applied to rearranging anticommuting spinors.

$\mathcal{L}_{\text{SM}}$ contains only massless left- and right-handed chiral fermion fields in the unbroken electroweak phase, which are eigenvectors of γ^5 with eigenvalue -1 and $+1$ respectively. Hence, for the field content of the SMEFT, only the first three identities of 3.2.33 are relevant. Furthermore, the class ψ^4 is the only place in which two fermion billinears can appear at $\mathcal{O}(\Lambda^{-2})$, and it can be subdivided according to the chiralities L and R of the fermions appearing in a given operator. Then for the operators therein which are products of two $Y = 0$ billinears - that is, the subclassifications $(\bar{L}L)(\bar{L}L)$, $(\bar{R}R)(\bar{R}R)$, and $(\bar{L}L)(\bar{R}R)$ - the identical chiralities of the fermion fields within each billinear means that only vector currents like $(\bar{\psi}_L\gamma_\mu\psi_L)$ will be nonzero. For these operators, only the second identity is relevant.

In the cases $(\bar{L}L)(\bar{L}L)$ and $(\bar{R}R)(\bar{R}R)$, both of the L and R fermions have the same γ^5 eigenvalue. Then the axial vector term $(\gamma^\mu\gamma^5]\,[\gamma^\mu\gamma^5)$ is just $(\pm 1)^2(\gamma^\mu]\,[\gamma^\mu) = (\gamma^\mu]\,[\gamma^\mu)$, while the pseudoscalar $(\gamma^5]\,[\gamma^5)$ likewise becomes $(\pm 1)^2(\ ]\,[\ ) = (\ ]\,[\ )$. In the remaining such case $(\bar{L}L)(\bar{R}R)$, the product of γ^5 eigenvalues is always $(+1)\times(-1)$, so $(\gamma^\mu\gamma^5]\,[\gamma^\mu\gamma^5) = -(\gamma^\mu]\,[\gamma^\mu)$ and $(\gamma^5]\,[\gamma^5) = -(\ ]\,[\ )$. This second identity then implies three particularly simple relations between products of chiral currents:

$$(\bar{\psi}_L\gamma_\mu\psi_L)(\bar{\chi}_L\gamma^\mu\chi_L) = (\bar{\psi}_L\gamma_\mu\chi_L)(\bar{\chi}_L\gamma^\mu\psi_L) \tag{3.2.34}$$

$$(\bar{\psi}_R\gamma_\mu\psi_R)(\bar{\chi}_R\gamma^\mu\chi_R) = (\bar{\psi}_R\gamma_\mu\chi_R)(\bar{\chi}_R\gamma^\mu\psi_R) \tag{3.2.35}$$

$$(\bar{\psi}_L\gamma_\mu\psi_L)(\bar{\chi}_R\gamma^\mu\chi_R) = -2(\bar{\psi}_L\chi_R)(\bar{\chi}_R\psi_L). \tag{3.2.36}$$

The identities 3.2.33, together with the weak isospin and colour identities 3.2.22 and 3.2.23 respectively, are together responsible for generating redundancies between four-fermion operators. For example, suppose we write down three operators in the $(\bar{L}L)(\bar{L}L)$ class:

$$Q_{qq}^{(1)\,prst} \equiv (\bar{q}_p\gamma^\mu q_r)(\bar{q}_s\gamma_\mu q_t) \tag{3.2.37}$$

$$Q_{qq}^{(3)\,prst} \equiv (\bar{q}_p\gamma^\mu\tau^I q_r)(\bar{q}_s\gamma_\mu\tau^I q_t) \tag{3.2.38}$$

$$Q_{qq}^{(8)\,prst} \equiv (\bar{q}_p\gamma^\mu T^A q_r)(\bar{q}_s\gamma_\mu T^A q_t), \tag{3.2.39}$$

where p, t, s, r are generation indices, and the superscripts (1), (3), and (8) reflect that the quark currents are $SU(2)_L$ and $SU(3)_C$ singlets, $SU(2)_L$ triplets and $SU(3)_C$ octets respectively. These are not independent, and we can choose to eliminate one by applying the Fierz identities accordingly:

$$\begin{aligned}
(\bar{q}_p\gamma^\mu T^A q_r)(\bar{q}_s\gamma_\mu T^A q_t) &\overset{(3.2.23)}{=} \frac{1}{2}(\bar{q}_p^a\gamma^\mu q_r^b)(\bar{q}_s^c\gamma_\mu q_t^d)\delta_{ad}\delta_{cb} - \frac{1}{6}(\bar{q}_p\gamma^\mu q_r)(\bar{q}_s\gamma_\mu q_t) \\
&\overset{(3.2.34)}{=} \frac{1}{2}(\bar{q}_p^i\gamma^\mu q_t^l)(\bar{q}_s^k\gamma_\mu q_r^j)\delta_{ij}\delta_{kl} - \frac{1}{6}(\bar{q}_p\gamma^\mu q_r)(\bar{q}_s\gamma_\mu q_t) \\
&\overset{(3.2.22)}{=} \frac{1}{2}(\bar{q}_p^i\gamma^\mu q_t^l)(\bar{q}_s^k\gamma_\mu q_r^j)(2\tau_{il}^I\tau_{kj}^I + \frac{1}{2}\delta_{il}\delta_{kj})) - \frac{1}{6}Q_{qq}^{(1)\,prst} \\
\implies Q_{qq}^{(8)\,prst} &= Q_{qq}^{(3)\,ptsr} + \frac{1}{4}Q_{qq}^{(1)\,ptsr} - \frac{1}{6}Q_{qq}^{(1)\,prst}. \qquad (3.2.40)
\end{aligned}$$

Therefore the effect of including a contact interaction between two colour octet, $(\mathbf{8}, \mathbf{1}, 0)$ left-handed quark currents is already present as a particular linear combination of products of colour singlet, isospin singlet and triplet currents $(\mathbf{1}, \mathbf{1}, 0)$ and $(\mathbf{1}, \mathbf{3}, 0)$ respectively.

In reordering the fields to have colour, isospin and spinor indices contracted in the same order between the fermions in each billinear, we also have permuted generation indices. To be fully general and parametrize interactions with generic flavour configurations, Q^{prst} should be considered as a set of independent operators indexed by $p, r, s, t = \{1, 2, 3\}$. In this picture, each of these operators has Wilson coefficient C_{prst}, an element of a $3 \times 3 \times 3 \times 3$ matrix in flavour space. Allowing for different arrangements of flavour indices in a given operator is thus essential to encoding relationships such as 3.2.40. A full discussion of the flavour representations of the ψ^4 class operators and the corresponding parameter counting can be found in [40].

3.2.2 Euler-Lagrange Equations

The classical Equations of Motion (EoM) for the SM are the set of 9 Euler-Lagrange equations obtained by minimizing the action functional $\mathcal{S} = \int d^4x\, \mathcal{L}_{\text{SM}}$ with respect to each of the fields $\{G_\mu^a, W_\mu^I, B_\mu, \varphi, q, u, d, l, e\}$. For the renormalizable, dimension-four Lagrangian $\mathcal{L}_{\text{SM}}$, these are:

$$i\not{D}l - \Gamma_e e\varphi = 0 \qquad (3.2.41)$$

$$i\not{D}e - \Gamma_e^\dagger \varphi^\dagger l = 0 \qquad (3.2.42)$$

$$i\not{D}q - \Gamma_u u\widetilde{\varphi} + \Gamma_d d\varphi = 0 \quad (3.2.43)$$

$$i\not{D}u - \Gamma_u^\dagger \widetilde{\varphi}^\dagger q = 0 \quad (3.2.44)$$

$$i\not{D}d - \Gamma_d^\dagger \varphi^\dagger q = 0 \quad (3.2.45)$$

$$(D^\mu D_\mu \varphi)^j - m^2\varphi^j + \lambda\left(\varphi^\dagger\varphi\right)\varphi^j + \bar{e}\,\Gamma_e^\dagger l^j - \varepsilon_{jk}\bar{q}^k\,\Gamma_u u + \bar{d}\,\Gamma_d^\dagger q^j = 0 \quad (3.2.46)$$

$$(D^\rho G_{\rho\mu})^A - g_s\left(\bar{q}\gamma_\mu T^A q + \bar{u}\gamma_\mu T^A u + \bar{d}\gamma_\mu T^A d\right) = 0 \quad (3.2.47)$$

$$(D^\rho W_{\rho\mu})^I - \frac{g}{2}\left(\varphi^\dagger i\overleftrightarrow{D}_\mu^I \varphi + \bar{l}\gamma_\mu\tau^I l + \bar{q}\gamma_\mu\tau^I q\right) = 0 \quad (3.2.48)$$

$$\partial^\rho B_{\rho\mu} - g' Y_\varphi\,\varphi^\dagger i\overleftrightarrow{D}_\mu \varphi - g' \sum_{\psi\in\{l,e,q,u,d\}} Y_\psi\,\bar{\psi}\gamma_\mu\psi = 0, \quad (3.2.49)$$

each of which is of the form:

$$\frac{\delta}{\delta\Phi_A(x)}\left(\int d^4x'\,\mathcal{L}_{\rm SM}\right) = \frac{\partial\mathcal{L}_{\rm SM}}{\partial\Phi_A} - \partial_\mu\left(\frac{\partial\mathcal{L}_{\rm SM}}{\partial(\partial_\mu\Phi_A)}\right) = 0, \quad (3.2.50)$$

where Φ_A represents any field in $\mathcal{L}_{\rm SM}$ carrying generic indices A.

Despite describing the evolution of classical fields (i.e. those following the classical trajectories that minimize the action), it is a well-known result in Quantum Field Theory [12, 46] that at the quantum level, matrix elements of the (linear combinations of) operators on the left hand sides of 3.2.41 - 3.2.49 vanish between on-shell states. These linear combinations, which we will denote by E, are obtained from varying the gauge-invariant Lagrangian with respect to a field in some representation of $\boldsymbol{\mathcal{G}}_{SM}$, so each of the terms carries the same quantum numbers.

The appropriate generalization of the classical Euler-Lagrange equations are the Schwinger-Dyson equations, which for the special case of S-matrix elements take the form:

$$\mathcal{S}_{i\to f} \equiv \left\langle f\left|\frac{\delta}{\delta\Phi_A(x)}\left(\int d^4x'\,\mathcal{L}_{\rm SM}\right)\Phi_B\,\Phi_C\ldots\right|i\right\rangle = 0$$

This holds for a general correlation function between f and i, any on-shell final and initial states respectively, whenever generic field operators Φ appear with one of the combinations of operators obtained from minimizing the action. 3.2.41 - 3.2.49 play this role in the SM, and since they don't contribute to scattering observables, the classical equations can be taken literally.

In the full dimension-six Lagrangian $\mathcal{L}^{(6)}$, operators of interest carry coefficients proportional to Λ^{-2}. The Euler-Lagrange equations for $\mathcal{L}^{(6)}$ will then be those of $\mathcal{L}_{\rm SM}$, plus

the additional terms arising from taking functional derivatives of the higher-dimensional operators unique to $\mathcal{L}^{(6)}$. However, if we aim to use these EoM to replace products of fields in operators that are suppressed through their coefficients by the scale Λ^{-2}, the resulting terms will be $\mathcal{O}(\Lambda^{-4})$, and can be neglected when working to $\mathcal{O}(\Lambda^{-2})$. Then those EoM obtained from $\mathcal{L}_{\text{SM}}$ alone will suffice as the relations which make linear combinations of operators redundant at dimension six.

As an example of how the EoM can be used to identify redundant linear combinations, we can write down a dimension six operator:

$$Q \equiv C_Q \, (D^\mu G_{\mu\nu})^A \, (\bar{u}\gamma^\nu T^A u),$$

and take note that, according to 3.2.47:

$$\left[D^\rho G^A_{\rho\mu} - g_s(\bar{q}\gamma_\mu T^A q) \; - \; g_s(\bar{u}\gamma_\mu T^A u) \; - \; g_s(\bar{d}\gamma_\mu T^A d)\right](\bar{u}\gamma^\mu T^A u) = \mathcal{O}(\Lambda^{-4})$$

We can use this constraint to eliminate Q in favour of a linear combination of three four-fermion operators as:

$$\begin{aligned} Q &= C_Q \, (D^\mu G_{\mu\nu})^A \, (\bar{u}\gamma^\nu T^A u) \\ &= g_s \, C_Q \left((\bar{q}\gamma_\mu T^A q)(\bar{u}\gamma^\mu T^A u) + (\bar{u}\gamma_\mu T^A u)(\bar{u}\gamma^\mu T^A u) + (\bar{d}\gamma_\mu T^A d)(\bar{u}\gamma^\mu T^A u)\right) + \mathcal{O}(\Lambda^{-4}). \end{aligned} \tag{3.2.51}$$

Generally, whenever a gauge-invariant operator contains any of the terms in 3.2.41 - 3.2.49 (the products of fields which arise as the conserved currents or partial derivatives of $\mathcal{L}$ associated with minimizing $\mathcal{S}$ with respect to a field), one can use the EoM to substitute this operator for a related linear combination.

This approach has been traditionally used as a tool to reduce the number of covariant derivatives present in a given set of operators as far as possible [47]. This is an agnostic convention through which one unique prescription for eliminating terms using the EoM is decided upon. Appealing again to the language introduced in [14], this corresponds, in the example given by 3.2.51, to a mapping between operator classifications which can be denoted as:

$$\boxed{\psi^2 X D} \to \boxed{\psi^4} + \boxed{E} \tag{3.2.52}$$

where $\boxed{E}$ represents any linear combination of operators (in this case, that of 3.2.47) which vanishes by the EoM. It is customary to say that - for a fixed mass dimension

- an operator possessing fewer covariant derivatives than another belongs to a 'lower' classification. Applying the EoM identities in this way then corresponds to a *reduction* of this operator to some sum of others belonging to lower classifications.

The opportunity afforded by the EoM identities to express the same physics using different choices of operators can be taken advantage of by tailoring the set used towards a particular phenomenological application. The so-called SILH Lagrangian [48, 49], one of the commonly used dimension six operator bases for the SMEFT, is one such example. Motivated by BSM models of strongly interacting Higgs sectors, one can use the freedom of EoM redefinitions to instead maximally represent the Higgs field φ, the Electroweak gauge bosons $W_{\mu\nu}$ and $B_{\mu\nu}$, and their derivatives. By integrating out the heavy states in the hypothetical strongly interacting sector, one will obtain a particular set of higher-dimensional operators which - while equivalent to linear combinations of others by the EoM - will have a more direct interpretation in terms of the new physics model. For example, integrating out a heavy $SU(2)_L$ scalar doublet with mass m_ρ produces the $\varphi^2 D^4$ class dimension-six operator [48]:

$$Q \equiv \frac{C_Q}{m_\rho^2}(D_\mu D^\mu \varphi^\dagger)(D_\nu D^\nu \varphi), \tag{3.2.53}$$

Where the scale Λ is explicitly identified with the mass of the heavy state m_ρ. If we were to use a basis of operators in which the EoM were used to minimize the number of covariant derivatives, Q would be expressed as:

$$\begin{aligned} Q &\overset{3.2.46}{\to} \frac{C_Q}{m_\rho^2}(D_\mu D^\mu \varphi^\dagger)\left(\mu^2\varphi - \lambda(\varphi^\dagger\varphi)\varphi - \bar{e}\,\Gamma_e^\dagger l + \varepsilon_{jk}\bar{q}^k\,\Gamma_u u - \bar{d}\,\Gamma_d^\dagger q\right) + \mathcal{O}(\Lambda^{-4}) \\ &\overset{3.2.46}{\to} \frac{C_Q}{m_\rho^2}\left(\mu^2\varphi^\dagger - \lambda(\varphi^\dagger\varphi)\varphi^\dagger - \bar{l}\,\Gamma_e e - \varepsilon_{jk}\bar{u}\,\Gamma_u^\dagger q^k - \bar{q}\,\Gamma_d d\right) \\ &\qquad \times \left(\mu^2\varphi - \lambda(\varphi^\dagger\varphi)\varphi - \bar{e}\,\Gamma_e^\dagger l + \varepsilon_{jk}\bar{q}^k\,\Gamma_u u - \bar{d}\,\Gamma_d^\dagger q\right) + \mathcal{O}(\Lambda^{-4}). \end{aligned} \tag{3.2.54}$$

Through the EoM, the physical contributions of the operator 3.2.53 to S-matrix elements are identical to those of 3.2.54 - one particular linear combination of dimension-six operators belonging to the classifications $\boxed{\varphi^6}$, $\boxed{\varphi^3\psi^2}$, $\boxed{\bar{L}R\bar{L}R}$ and $\boxed{\bar{L}R\bar{R}L}$. Suppose that this heavy scalar existed, but to remain indifferent towards the probability of one BSM model being realized over another, we used a basis containing the latter operators, allocating each of them an independent Wilson Coefficient. Despite the physical effects being identical in both descriptions, measurements targeting the set of lower classifica-

tion operators would have to establish that only the single linear combination controlled by $\frac{C_Q}{m_\rho^2}$ in 3.2.54 was realized.

Without knowledge of the BSM physics, clearly it isn't possible to make a choice of basis which directly corresponds to operators generated by integrating out the heavy fields. However, if we had evidence to suggest the realization of one particular model or class thereof in nature, a prudent choice of basis could be made in which measurements of Wilson Coefficients would have a more immediate interpretation in terms of the masses and couplings of new states.

In re-expressing Q in this basis, the linear combination 3.2.54 also contained operators of the form:

$$Q \supset \frac{\mu^2 \lambda C_Q}{m_\rho^2}(\varphi^\dagger\varphi)^2\,, \quad \frac{\mu^2 C_Q}{m_\rho^2}\varphi^\dagger \bar{e}\,\Gamma_e^\dagger l\,, \quad \frac{\mu^4 \lambda C_Q}{m_\rho^2}(\varphi^\dagger\varphi)\ \ldots$$

Since the quadratic coefficient in the Higgs potential μ is itself dimensionful, using the EoM in this case has produced dimension two and four terms proportional to operators already present in $\mathcal{L}_{\text{SM}}$. These rescale the coefficients of the renormalizable SM operators by terms of $\mathcal{O}(\frac{\mu^4}{m_\rho^2})$ and $\mathcal{O}(\frac{\mu^2}{m_\rho^2})$ respectively. In this case, a global redefinition of the parameters λ, Y_e and μ should be made to restore the canonical normalization of $\mathcal{L}_{\text{SM}}$. This will be detailed in the next section.

The EoM also play an important role in perturbative calculations beyond the leading order which include higher-dimensional operators. It is a general feature that operators with mass dimension greater than four are mixed by radiative corrections. That is, their correlation functions can produce UV poles which must be absorbed in the counterterms of *other* operators. This 'additive renormalization' is in contrast to the solely 'multiplicative' renormalization characteristic of Lagrangians containing operators up to dimension four. In dimensional regularization, the general relationship between bare and renormalized $d > 4$ operators would be written as:

$$Q_0^i = Z_{ij}(\mu)\, Q^j(\mu), \tag{3.2.55}$$

where $\{Q\}$ is a set of N operators indexed by i and renormalized at the scale μ, with ultraviolet divergences contained in Z_{ij} , an $N \times N$, non-diagonal matrix.

In the context of the SM, this was first encountered when calculating the QCD corrections to the effective Fermi description of the weak interaction obtained in the

limit $s \ll m_W^2$*. In the SMEFT, QCD and Electroweak corrections can in this way generate operators belonging to the EoM vanishing combinations 3.2.41 - 3.2.49, which are redundant in the chosen basis. The EoM must then be used to reorganize the UV poles back into the coefficients of the original operator set. This procedure was detailed and applied to the 'Warsaw' operator basis for the SMEFT [14] by the authors of Refs. [40,50,51]. Hereby the one-loop counterterms for the dimension-six SMEFT are now known, provided one always expresses effective operators in this basis.

3.2.3 Integration-by-Parts Identities

Because the action functional $\mathcal{S}$ is an integral of the Lagrange density over all spacetime, we are free to add to $\mathcal{L}$ a term proportional to a total divergence:

$$\mathcal{S} \equiv \int d^4x\, \mathcal{L} = \int d^4x\, \mathcal{L} + \partial_\mu \mathcal{J}^\mu,$$

where in this notation $\mathcal{J}^\mu$ represents any local operator carrying one free Lorentz index (not to be confused, for example, with a specific Noether current). In the Lagrangian of a gauge theory, $\mathcal{J}^\mu$ must then itself be gauge-invariant, so we can identify $\partial_\mu \leftrightarrow D_\mu$.

By construction, the covariant derivative $D_\mu \mathcal{O}$ of any object $\mathcal{O}$ embedded in a representation of $\boldsymbol{\mathcal{G}}_{SM}$ transforms in the same representation as $\mathcal{O}$. Then, a gauge-invariant operator possessing one or more covariant derivatives leaves behind another gauge (but clearly no longer Lorentz) invariant piece when stripped of these. The total derivative of this leftover operator is then precisely of the form $D_\mu \mathcal{J}^\mu$, and thus doesn't contribute to scattering observables. However, through the Leibniz rule, this is equal to the sum of operators obtained from acting with D_μ on each field individually. This linear combination of operators is then redundant, as integrating any individual term by parts will produce the remaining terms occurring when expanding out $D_\mu \mathcal{J}^\mu$, plus a surface term which integrates to zero.

Consider the following operator, the presence of which introduces additional $g(gg)\bar{q}q$ couplings. This is generated (for the third generation quarks) by models in which the top quark is a composite object [52,53], with the top radius playing the role of the scale

*For a review of the original development of methods for calculating radiative corrections to effective operators in flavour physics, see e.g. [6].

Λ:

$$\mathcal{L}_Q \equiv C_{pr} Q_{pr} + h.c. = C_{pr} (\bar{q}_p \, \gamma^\mu \, T^A \, D^\nu q_r) \, G^A_{\mu\nu} + C^*_{pr} (D^\nu \bar{q}_r \, \gamma^\mu \, T^A \, q_p) \, G^A_{\mu\nu}. \tag{3.2.56}$$

Here, flavour indices p and r, and the hermitian conjugate $Q^\dagger$ (which we had to add since $Q^\dagger \neq Q$) are written explicitly to illustrate a few points. In general, upon conjugation, flavour indices in a fermion billinear are transposed. This impacts the parameter counting - that is, the allocation of real or complex Wilson Coefficients - in a way that depends on the symmetries of the operator in question. Here, we allocated the most general 3×3 matrix of complex coefficients C_{pr} (possessing 18 independent parameters), as was required by hermiticity.

If instead we had been interested in the operator:

$$\begin{aligned} \mathcal{L}'_Q \equiv C'_{pr} Q'_{pr} + h.c. &= C'_{pr} (\bar{q}_p \, \gamma^\mu \, T^A \, q_r) \, D^\nu G^A_{\mu\nu} + C'^*_{pr} (\bar{q}_r \, \gamma^\mu \, T^A \, q_p) \, D^\nu G^A_{\mu\nu} \\ &= C'_{pr} Q'_{pr} + C'^*_{pr} Q'_{rp} \\ &\implies C'^*_{pr} = C'_{rp}. \end{aligned} \tag{3.2.57}$$

we'd find that, since the left-handed quark doublets are distinguished only by their generation indices and $G^A_{\mu\nu}$ is hermitian, hermiticity is ensured simply by summing over the flavour indices p and r. C_{pr} is then hermitian in flavour space, with $1/2 \, n_f(n_f + 1) = 6$ real and $1/2 \, n_f(n_f - 1) = 3$ imaginary entries, the latter of which represent $\mathcal{CP}$-odd couplings. Put otherwise, since hermitian conjugation and flavour-transposition are equivalent, there can only be as many unique parameters as there are permutations of flavour indices. The same considerations apply generally: any symmetries associated with interchanging fields or indices can relate Wilson Coefficients associated with different flavour arrangements of the same operator. Care must then be taken to avoid over or undercounting *.

Returning to 3.2.56, the $(\bar{q} \leftrightarrow q) \equiv (p \leftrightarrow r)$ interchange symmetry is no longer present due to the covariant derivative D_ν, C_{pr} is unrestricted, and the flavour-diagonal arrangements of Q may carry imaginary Wilson Coefficients which give rise to $\mathcal{CP}$-violation. For a given choice $p \leq r$, the redundant linear combination arising from the total divergence is:

$$D^\nu \mathcal{J}_\nu = D^\nu ((\bar{q}_p \, \gamma^\mu \, T^A \, q_r) \, G^A_{\mu\nu} + h.c.) = 0$$

*This issue was tackled systematically for one choice of basis in [40].

$$\begin{aligned}
\implies & ((\bar{q}_p\,\gamma^\mu\,T^A\,D^\nu q_r)\,G^A_{\mu\nu} + (D^\nu\bar{q}_r\,\gamma^\mu\,T^A\,q_p)\,G^A_{\mu\nu}) \\
+ \quad & ((\bar{q}_r\,\gamma^\mu\,T^A\,D^\nu q_p)\,G^A_{\mu\nu} + (D^\nu\bar{q}_p\,\gamma^\mu\,T^A\,q_r)\,G^A_{\mu\nu}) \\
+ \quad & ((\bar{q}_p\,\gamma^\mu\,T^A\,q_r)\,D^\nu G^A_{\mu\nu} + (\bar{q}_r\,\gamma^\mu\,T^A\,q_p)\,D^\nu G^A_{\mu\nu}) = 0, \qquad (3.2.58)
\end{aligned}$$

where the individual hermitian (physical) combinations are collected in parentheses. Suppose that the new physics generated flavour-violating interactions related to the top's substructure, and Λ corresponded to the confinement scale of the composite dynamics. In 3.2.56, the preferential action of D_ν on one particular quark flavour would arise naturally from integrating out any dynamics which distinguished between the heavy (composite) and light quarks. Through 3.2.58, gauge symmetry then dictates that the dimension-six operators corresponding to effects with *physically distinct origins* are related, as both the configurations $D^\nu q_p$ and $D^\nu q_r$ appear in the total derivative. Any two of the three hermitian operators may then be taken as an independent pair.

To see one physical consequence of operators being related through total divergences, consider the flavour-diagonal arrangements $p = r$ in 3.2.56:

$$\begin{aligned}
\mathcal{L}^{pp}_Q = & R_p((\bar{q}_p\,\gamma^\mu\,T^A\,D^\nu q_p)\,G^A_{\mu\nu} + (D^\nu\bar{q}_p\,\gamma^\mu\,T^A\,q_p)\,G^A_{\mu\nu}) \\
& + iI_p((\bar{q}_p\,\gamma^\mu\,T^A\,D^\nu q_p)\,G^A_{\mu\nu} - (D^\nu\bar{q}_p\,\gamma^\mu\,T^A\,q_p)\,G^A_{\mu\nu}) \qquad (3.2.59)
\end{aligned}$$

where the complex Wilson Coefficients C_{pp} are written explicitly as the sum of their real and imaginary parts $R_p + iI_p$, and the terms arranged into orthogonal $\mathcal{CP}$-even and odd combinations respectively. The flavour-diagonal constraint in equation 3.2.58 implies the relationship:

$$\begin{aligned}
& ((\bar{q}_p\,\gamma^\mu\,T^A\,D^\nu q_p)\,G^A_{\mu\nu} + (D^\nu\bar{q}_p\,\gamma^\mu\,T^A\,q_p)\,G^A_{\mu\nu}) \\
= & -((\bar{q}_p\,\gamma^\mu\,T^A\,q_p)\,D^\nu G^A_{\mu\nu} + \mathcal{O}(\Lambda^{-4}) \equiv -Q_E + \mathcal{O}(\Lambda^{-4}).
\end{aligned}$$

We see that the $\mathcal{CP}$-even combination is redundant with the operator Q_E, while the $\mathcal{CP}$-odd counterpart is unconstrained. Through the equation of motion for the gluons 3.2.47, $D^\nu G^A_{\mu\nu}$ is proportional to the Noether currents associated with the $SU(3)_C$ gauge symmetry, which are the colour-octet quark billinears. By making this replacement, we are free to move to a basis in which Q_E is represented by a linear combination of four-quark operators. Then, despite the the $\mathcal{CP}$-even effective Lagrangian in 3.2.56 describing a gluon-top interaction, its contribution to S-matrix elements with external gluons vanishes, such as in $gg \to t\bar{t}$ scattering.

Equivalently, QCD amplitudes obey Ward identities resulting from the conservation of colour current. If $\mathcal{M}$ is the momentum space amplitude for a scattering process with external gluons, $k_\mu \mathcal{M}^\mu = 0$, where k_μ is the four-momentum vector of any external gluon, and $\mathcal{M}^\mu$ the amplitude with the external gluon leg removed. Since the covariant derivative D^ν and the gluon tensor $G_{\mu\nu}$ share a Lorentz index, insertions of this operator will give rise to terms proportional to k_ν, which must then cancel.

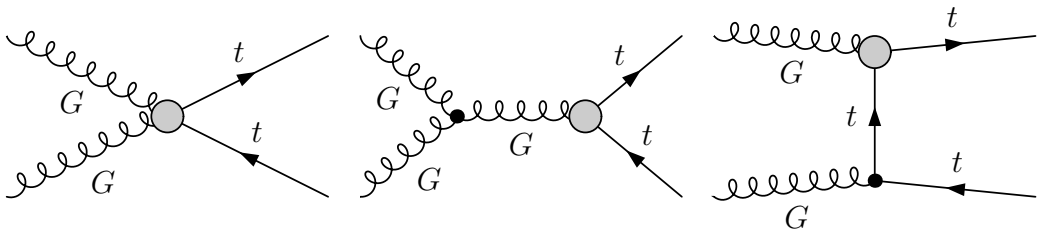

Figure 3.2: *Tree-level topologies for $gg \to \bar{t}t$ in the SMEFT. Insertions of the $\mathcal{CP}$-even operator 3.2.59 at each $(g)g\bar{t}t$ vertex (represented by shaded circles) cancel due to the Ward identity.*

By examining the structure of the redundancies affecting 3.2.56, we have revealed some properties that may not have been obvious from the outset. The presence of the additional coupling of the top to gluons is only felt in the scattering of quarks, as required by gauge symmetry. However, the $\mathcal{CP}$-odd part of the Lagrangian is not subject to this restriction, and will leave a physical footprint in suitable observables in gluon-gluon scattering.

3.3 Working with an Operator Basis in the Electroweak Broken Phase

Having explored the construction of dimension-six operators, the mechanisms by which they can become related, and some simplifying symmetry-based assumptions which can reduce the total number of terms, we should examine the complete Lagrangian at this order. We aim to implement a complete set of operators as a model which we can use, particularly to understand and search for possible footprints of non-resonant new physics in top quark production. We adopt the standard 'Warsaw' basis described in [54], wherein the independent operators are chosen to belong to the lowest possible classifications. $\mathcal{L}^{(6)}$ henceforth refers to this basis unless stated otherwise, which will be summarized here for completeness. The content of the following discussion is reflected

in a fully general FeynRules [10, 34] model for the SMEFT which was implemented in parallel. This is a Mathematica package allowing the implementation of user-defined Lagrangians for general quantum field theory models, and extracting from these corresponding input files for event generators containing the relevant coupling and parameter information. This will underpin our phenomenological applications in the subsequent chapters.

$\mathcal{L}^{(6)}$ supplements the $\mathcal{L}_{\rm SM}$ with 59 (2499) additional B-conserving terms * for one (three) generation(s) of fermions. The operators organized according to their classifications are shown in tables 3.3 and 3.4. This basis makes use of the definitions:

X^3		φ^6 and $\varphi^4 D^2$		$\psi^2\varphi^3$	
Q_G	$f^{ABC}G^{A\nu}_{\mu}G^{B\rho}_{\nu}G^{C\mu}_{\rho}$	Q_{φ}	$(\varphi^\dagger\varphi)^3$	$Q_{e\varphi}$	$(\varphi^\dagger\varphi)(\bar{l}_p e_r \varphi)$
$Q_{\widetilde{G}}$	$f^{ABC}\widetilde{G}^{A\nu}_{\mu}G^{B\rho}_{\nu}G^{C\mu}_{\rho}$	$Q_{\varphi\Box}$	$(\varphi^\dagger\varphi)\Box(\varphi^\dagger\varphi)$	$Q_{u\varphi}$	$(\varphi^\dagger\varphi)(\bar{q}_p u_r \widetilde{\varphi})$
Q_W	$\varepsilon^{IJK}W^{I\nu}_{\mu}W^{J\rho}_{\nu}W^{K\mu}_{\rho}$	$Q_{\varphi D}$	$\left(\varphi^\dagger D^\mu\varphi\right)^\star\left(\varphi^\dagger D_\mu\varphi\right)$	$Q_{d\varphi}$	$(\varphi^\dagger\varphi)(\bar{q}_p d_r \varphi)$
$Q_{\widetilde{W}}$	$\varepsilon^{IJK}\widetilde{W}^{I\nu}_{\mu}W^{J\rho}_{\nu}W^{K\mu}_{\rho}$				
$X^2\varphi^2$		$\psi^2 X\varphi$		$\psi^2\varphi^2 D$	
$Q_{\varphi G}$	$\varphi^\dagger\varphi\, G^A_{\mu\nu}G^{A\mu\nu}$	Q_{eW}	$(\bar{l}_p\sigma^{\mu\nu}e_r)\tau^I\varphi W^I_{\mu\nu}$	$Q^{(1)}_{\varphi l}$	$(\varphi^\dagger i\overleftrightarrow{D}_\mu\varphi)(\bar{l}_p\gamma^\mu l_r)$
$Q_{\varphi\widetilde{G}}$	$\varphi^\dagger\varphi\,\widetilde{G}^A_{\mu\nu}G^{A\mu\nu}$	Q_{eB}	$(\bar{l}_p\sigma^{\mu\nu}e_r)\varphi B_{\mu\nu}$	$Q^{(3)}_{\varphi l}$	$(\varphi^\dagger i\overleftrightarrow{D}^I_\mu\varphi)(\bar{l}_p\tau^I\gamma^\mu l_r)$
$Q_{\varphi W}$	$\varphi^\dagger\varphi\, W^I_{\mu\nu}W^{I\mu\nu}$	Q_{uG}	$(\bar{q}_p\sigma^{\mu\nu}T^A u_r)\widetilde{\varphi}\, G^A_{\mu\nu}$	$Q_{\varphi e}$	$(\varphi^\dagger i\overleftrightarrow{D}_\mu\varphi)(\bar{e}_p\gamma^\mu e_r)$
$Q_{\varphi\widetilde{W}}$	$\varphi^\dagger\varphi\,\widetilde{W}^I_{\mu\nu}W^{I\mu\nu}$	Q_{uW}	$(\bar{q}_p\sigma^{\mu\nu}u_r)\tau^I\widetilde{\varphi}\, W^I_{\mu\nu}$	$Q^{(1)}_{\varphi q}$	$(\varphi^\dagger i\overleftrightarrow{D}_\mu\varphi)(\bar{q}_p\gamma^\mu q_r)$
$Q_{\varphi B}$	$\varphi^\dagger\varphi\, B_{\mu\nu}B^{\mu\nu}$	Q_{uB}	$(\bar{q}_p\sigma^{\mu\nu}u_r)\widetilde{\varphi}\, B_{\mu\nu}$	$Q^{(3)}_{\varphi q}$	$(\varphi^\dagger i\overleftrightarrow{D}^I_\mu\varphi)(\bar{q}_p\tau^I\gamma^\mu q_r)$
$Q_{\varphi\widetilde{B}}$	$\varphi^\dagger\varphi\,\widetilde{B}_{\mu\nu}B^{\mu\nu}$	Q_{dG}	$(\bar{q}_p\sigma^{\mu\nu}T^A d_r)\varphi\, G^A_{\mu\nu}$	$Q_{\varphi u}$	$(\varphi^\dagger i\overleftrightarrow{D}_\mu\varphi)(\bar{u}_p\gamma^\mu u_r)$
$Q_{\varphi WB}$	$\varphi^\dagger\tau^I\varphi\, W^I_{\mu\nu}B^{\mu\nu}$	Q_{dW}	$(\bar{q}_p\sigma^{\mu\nu}d_r)\tau^I\varphi\, W^I_{\mu\nu}$	$Q_{\varphi d}$	$(\varphi^\dagger i\overleftrightarrow{D}_\mu\varphi)(\bar{d}_p\gamma^\mu d_r)$
$Q_{\varphi\widetilde{W}B}$	$\varphi^\dagger\tau^I\varphi\,\widetilde{W}^I_{\mu\nu}B^{\mu\nu}$	Q_{dB}	$(\bar{q}_p\sigma^{\mu\nu}d_r)\varphi\, B_{\mu\nu}$	$Q_{\varphi ud}$	$i(\widetilde{\varphi}^\dagger D_\mu\varphi)(\bar{u}_p\gamma^\mu d_r)$

Table 3.3: Non four fermion dimension-six operators in the Warsaw basis.

*There are five more B-violating operators.

$(\bar{L}L)(\bar{L}L)$		$(\bar{R}R)(\bar{R}R)$		$(\bar{L}L)(\bar{R}R)$	
Q_{ll}	$(\bar{l}_p\gamma_\mu l_r)(\bar{l}_s\gamma^\mu l_t)$	Q_{ee}	$(\bar{e}_p\gamma_\mu e_r)(\bar{e}_s\gamma^\mu e_t)$	Q_{le}	$(\bar{l}_p\gamma_\mu l_r)(\bar{e}_s\gamma^\mu e_t)$
$Q_{qq}^{(1)}$	$(\bar{q}_p\gamma_\mu q_r)(\bar{q}_s\gamma^\mu q_t)$	Q_{uu}	$(\bar{u}_p\gamma_\mu u_r)(\bar{u}_s\gamma^\mu u_t)$	Q_{lu}	$(\bar{l}_p\gamma_\mu l_r)(\bar{u}_s\gamma^\mu u_t)$
$Q_{qq}^{(3)}$	$(\bar{q}_p\gamma_\mu\tau^I q_r)(\bar{q}_s\gamma^\mu\tau^I q_t)$	Q_{dd}	$(\bar{d}_p\gamma_\mu d_r)(\bar{d}_s\gamma^\mu d_t)$	Q_{ld}	$(\bar{l}_p\gamma_\mu l_r)(\bar{d}_s\gamma^\mu d_t)$
$Q_{lq}^{(1)}$	$(\bar{l}_p\gamma_\mu l_r)(\bar{q}_s\gamma^\mu q_t)$	Q_{eu}	$(\bar{e}_p\gamma_\mu e_r)(\bar{u}_s\gamma^\mu u_t)$	Q_{qe}	$(\bar{q}_p\gamma_\mu q_r)(\bar{e}_s\gamma^\mu e_t)$
$Q_{lq}^{(3)}$	$(\bar{l}_p\gamma_\mu\tau^I l_r)(\bar{q}_s\gamma^\mu\tau^I q_t)$	Q_{ed}	$(\bar{e}_p\gamma_\mu e_r)(\bar{d}_s\gamma^\mu d_t)$	$Q_{qu}^{(1)}$	$(\bar{q}_p\gamma_\mu q_r)(\bar{u}_s\gamma^\mu u_t)$
		$Q_{ud}^{(1)}$	$(\bar{u}_p\gamma_\mu u_r)(\bar{d}_s\gamma^\mu d_t)$	$Q_{qu}^{(8)}$	$(\bar{q}_p\gamma_\mu T^A q_r)(\bar{u}_s\gamma^\mu T^A u_t)$
		$Q_{ud}^{(8)}$	$(\bar{u}_p\gamma_\mu T^A u_r)(\bar{d}_s\gamma^\mu T^A d_t)$	$Q_{qd}^{(1)}$	$(\bar{q}_p\gamma_\mu q_r)(\bar{d}_s\gamma^\mu d_t)$
				$Q_{qd}^{(8)}$	$(\bar{q}_p\gamma_\mu T^A q_r)(\bar{d}_s\gamma^\mu T^A d_t)$
$(\bar{L}R)(\bar{R}L)$ and $(\bar{L}R)(\bar{L}R)$		B-violating			
Q_{ledq}	$(\bar{l}_p^j e_r)(\bar{d}_s q_t^j)$	Q_{duq}	$\varepsilon^{\alpha\beta\gamma}\varepsilon_{jk}\left[(d_p^\alpha)^T C u_r^\beta\right]\left[(q_s^{\gamma j})^T C l_t^k\right]$		
$Q_{quqd}^{(1)}$	$(\bar{q}_p^j u_r)\varepsilon_{jk}(\bar{q}_s^k d_t)$	Q_{qqu}	$\varepsilon^{\alpha\beta\gamma}\varepsilon_{jk}\left[(q_p^{\alpha j})^T C q_r^{\beta k}\right]\left[(u_s^\gamma)^T C e_t\right]$		
$Q_{quqd}^{(8)}$	$(\bar{q}_p^j T^A u_r)\varepsilon_{jk}(\bar{q}_s^k T^A d_t)$	$Q_{qqq}^{(1)}$	$\varepsilon^{\alpha\beta\gamma}\varepsilon_{jk}\varepsilon_{mn}\left[(q_p^{\alpha j})^T C q_r^{\beta k}\right]\left[(q_s^{\gamma m})^T C l_t^n\right]$		
$Q_{lequ}^{(1)}$	$(\bar{l}_p^j e_r)\varepsilon_{jk}(\bar{q}_s^k u_t)$	$Q_{qqq}^{(3)}$	$\varepsilon^{\alpha\beta\gamma}(\tau^I\varepsilon)_{jk}(\tau^I\varepsilon)_{mn}\left[(q_p^{\alpha j})^T C q_r^{\beta k}\right]\left[(q_s^{\gamma m})^T C l_t^n\right]$		
$Q_{lequ}^{(3)}$	$(\bar{l}_p^j\sigma_{\mu\nu} e_r)\varepsilon_{jk}(\bar{q}_s^k\sigma^{\mu\nu} u_t)$	Q_{duu}	$\varepsilon^{\alpha\beta\gamma}\left[(d_p^\alpha)^T C u_r^\beta\right]\left[(u_s^\gamma)^T C e_t\right]$		

Table 3.4: Four-fermion operators.

$$\varphi^\dagger i\overleftrightarrow{D}_\mu\,\varphi \equiv i\varphi^\dagger\left(D_\mu - \overleftarrow{D}_\mu\right)\varphi \qquad \text{and} \qquad \varphi^\dagger i\overleftrightarrow{D}^I_\mu\,\varphi \equiv i\varphi^\dagger\left(\tau^I D_\mu - \overleftarrow{D}_\mu\tau^I\right)\varphi, \tag{3.3.60}$$

where $\varphi^\dagger\overleftarrow{D}_\mu\varphi \equiv (D_\mu\varphi)^\dagger\varphi$. This implicitly includes the hermitian conjugates in the definitions of non self-hermitian operators in which φ appears. After Electroweak symmetry breaking, and working in the unitary gauge where $\varphi = \frac{1}{\sqrt{2}}(0,\, H+v)^T$, each higher-dimensional operator involving the Higgs doublet acquires separate contributions from the dynamical Higgs boson H and the static vacuum expectation value of the Higgs field, v. This leads in $\mathcal{L}^{(6)}$ to the appearance of terms of the form $v^2 C_i Q_i^{(4)}$ in the broken Electroweak phase, where $Q_i^{(4)}$ is a dimension-four operator. The presence of such terms mixes the renormalizable operators in $\mathcal{L}_{SM}$ with dimension-six operators by terms of $\mathcal{O}(v^2/\Lambda^2)$, destroying the canonical normalization and diagonality of the kinetic and mass

terms and rescaling each coupling. This necessitates a further redefinition of the parameters of $\mathcal{L}_{SM}$ to absorb these contributions, which can be thought of as a tree-level finite renormalization of $\mathcal{L}_{SM}$. In an analogous fashion to conventional UV renormalization, this results in a dependence in the parameters of the theory such as the gauge couplings on the values of these Wilson Coefficients.

Since we work to $\mathcal{O}(\Lambda^{-2})$, we aim for a set of parameters consistent also to this order. This means in particular that field rescalings may be treated as a higher-order effect in the dimension-six sector and neglected*. The following relationships were verified explicitly in FeynRules.

3.3.1 The Higgs Sector

Potential

The operator Q_φ changes the shape of the scalar doublet potential at order v^2/Λ^2 to:

$$V(\varphi) = \lambda\left(\varphi^\dagger\varphi - \frac{1}{2}v^2\right)^2 - C_\varphi\left(\varphi^\dagger\varphi\right)^3, \tag{3.3.61}$$

With the implicit definition $\mu^2 = -v^2\lambda$. Minimizing this potential:

$$\frac{\partial V}{\partial|\varphi|} = -2|\varphi|(3C_\varphi|\varphi|^4 - 2\lambda|\varphi|^2 + \lambda v^2) = 0, \tag{3.3.62}$$

One defines the new vacuum expectation value in the usual way with $\langle\varphi^\dagger\varphi\rangle := \frac{1}{2}v_T^2$, and chooses the solution to the quadratic equation which reproduces the SM vev at $C = 0$.

$$\frac{1}{2}{v_T}^2 := \frac{1}{3C_\varphi}\left(\lambda - \lambda\sqrt{\left(1 - \frac{3C_\varphi v^2}{\lambda}\right)}\right) \tag{3.3.63}$$

Expanding this expression to second order in C in a binomial series to obtain v_T:

$$\begin{aligned}\langle\varphi^\dagger\varphi\rangle := \frac{1}{2}{v_T}^2 &= \frac{1}{3C_\varphi}(\lambda - \lambda(1 - \frac{3C_\varphi v^2}{2\lambda} - \frac{9{C_\varphi}^2 v^4}{8\lambda^2})) \\ v_T^2 &= \frac{v^2}{2}\left(1 + \frac{3C_\varphi v^2}{4\lambda}\right)\end{aligned} \tag{3.3.64}$$

*A similar procedure had been detailed previously in Higgs physics, for example for the SILH operators [49]. At the time of implementing this for the Warsaw basis, [40] published the analagous set of redefinitions for $\mathcal{L}^{(6)}$, with which these results agree up to minor differences in convention.

The shift in the vev is then proportional to $C_\varphi v^2$, which is of order v^2/Λ^2.

Kinetic Normalization

The kinetic Lagrangian is modified by the presence of the $\varphi^4 D^2$ operators and becomes:

$$\mathcal{L} = (D_\mu \varphi^\dagger)(D^\mu \varphi) + C_{\varphi\Box}\left(\varphi^\dagger\varphi\right)\Box\left(\varphi^\dagger\varphi\right) + C_{\varphi D}\left(\varphi^\dagger D^\mu\varphi\right)^*\left(\varphi^\dagger D_\mu\varphi\right), \tag{3.3.65}$$

Leaving the Higgs-Gauge Boson interaction terms for later, and transferring one derivative on $Q_{\varphi\Box}$ to the other doublet product and ignoring the implicit surface term, we first write the scalar field as:

$$\varphi = \begin{pmatrix} -i\left[1+c_\pm\right]G_+ \\ \frac{1}{\sqrt{2}}(v_T + \left[1+c_H\right]h + i\left[1+c_0\right]G_0) \end{pmatrix}, \tag{3.3.66}$$

Where c_H, c_0 and $c_\pm$ are order C terms included in each of the renormalization factors inserted whose values we may choose to restore the canonical scalar field kinetic normalization.
Expanding the kinetic pieces of the Lagrangian which is now:

$$\mathcal{L} = (\partial_\mu \varphi^\dagger)(\partial^\mu \varphi) - C_{\varphi\Box}\partial_\mu\left(\varphi^\dagger\varphi\right)\partial^\mu\left(\varphi^\dagger\varphi\right) + C_{\varphi D}\left(\varphi^\dagger\partial^\mu\varphi\right)^*\left(\varphi^\dagger\partial_\mu\varphi\right), \tag{3.3.67}$$

The coefficient of h in Eq. (3.3.66) is no longer unity, in order for the Higgs boson kinetic term to be properly normalized when the dimension-six operators are included. Collecting each of the kinetic terms one obtains:

$$\begin{aligned}
\mathcal{L}_{H,kin} &= \frac{1}{2}(1+c_H)^2\left(1+2v^2\left(\frac{C_{\varphi D}}{4} - C_{\varphi\Box}\right)\right)\partial_\mu h\partial^\mu h, \\
\mathcal{L}_{G0,kin} &= \frac{1}{2}(1+c_{G0})^2\left(1+2v^2\frac{C_{\varphi D}}{4}\right)\partial_\mu G_0\partial^\mu G_0, \\
\mathcal{L}_{G\pm,kin} &= \frac{1}{2}(1+c_G\pm)^2\partial_\mu G_+\partial^\mu G_-
\end{aligned} \tag{3.3.68}$$

Expanding the renormalization factors to first order in c and demanding that each of the prefactors then be equal to unity yields the necessary values:

$$c_H = v^2\left(C_{\varphi\Box} - \frac{C_{\varphi D}}{4}\right),$$

$$c_{G0} = -v^2 \frac{C_{\varphi D}}{4},$$
$$c_{G\pm} = 0 \tag{3.3.69}$$

In the unitary gauge, collecting the kinetic and potential parts of the Higgs Lagrangian one obtains:

$$\mathcal{L} = \frac{1}{2}(\partial_\mu h)^2 - \frac{c_H}{v_T^2}\left[h^2(\partial_\mu h)^2 + 2vh(\partial_\mu h)^2\right] - \lambda v_T^2\left(1 - \frac{3C_\varphi v^2}{2\lambda} + 2c_{H,\text{kin}}\right)h^2$$
$$- \lambda v_T\left(1 - \frac{5C_\varphi v^2}{2\lambda} + 3c_{H,\text{kin}}\right)h^3 - \frac{1}{4}\lambda\left(1 - \frac{15C_\varphi v^2}{2\lambda} + 4c_{H,\text{kin}}\right)h^4 + \frac{3}{4}C_\varphi v h^5 + \frac{1}{8}C_\varphi h^6, \tag{3.3.70}$$

for pure Higgs terms. The Higgs boson mass is modified to:

$$m_H^2 = 2\lambda v_T^2\left(1 - \frac{3C_\varphi v^2}{2\lambda} + 2c_{H,\text{kin}}\right). \tag{3.3.71}$$

3.3.2 Gauge Sector

The definition of the gauge fields and the gauge couplings are affected by the dimension-six terms. The relevant dimension-six Lagrangian terms are:

$$\mathcal{L}^{(6)}_{Gauge} = C_{\varphi G}\,(\varphi^\dagger\varphi)\,G^A_{\mu\nu}G^{A\mu\nu} + C_{\varphi W}\,(\varphi^\dagger\varphi)\,W^I_{\mu\nu}W^{I\mu\nu} + C_{\varphi B}\,(\varphi^\dagger\varphi)\,B_{\mu\nu}B^{\mu\nu}$$
$$+ C_{\varphi WB}\,(\varphi^\dagger\tau^I\varphi)\,W^I_{\mu\nu}B^{\mu\nu} + C_G\,f^{ABC}\,G^{A\nu}_\mu G^{B\rho}_\nu G^{C\mu}_\rho + C_W\,\epsilon^{IJK}\,W^{I\nu}_\mu W^{J\rho}_\nu W^{K\mu}_\rho\,.$$

In the broken theory, the $X^2\varphi^2$ operators contribute to the gauge kinetic terms,

$$\mathcal{L}_{SM} + \mathcal{L}^{(6)} = -\frac{1}{2}W^+_{\mu\nu}\,W^{\mu\nu}_- - \frac{1}{4}W^3_{\mu\nu}\,W_3^{\mu\nu} - \frac{1}{4}B_{\mu\nu}\,B^{\mu\nu} - \frac{1}{4}G_{\mu\nu}\,G^{\mu\nu} + \frac{1}{2}v_T^2\,C_{\varphi G}\,G^A_{\mu\nu}\,G^{A\mu\nu},$$
$$+ \frac{1}{2}v_T^2\,C_{\varphi W}W^I_{\mu\nu}W^{I\mu\nu} + \frac{1}{2}v_T^2\,C_{\varphi B}B_{\mu\nu}B^{\mu\nu} - \frac{1}{2}v_T^2\,C_{\varphi WB}W^3_{\mu\nu}B^{\mu\nu}. \tag{3.3.72}$$

so the gauge fields in the Lagrangian are not canonically normalized, and the last term in Eq. (3.3.73) leads to kinetic mixing between W^3 and B.

Gluons

The Gluon field can be renormalized in a similar fashion to the Higgs Boson, but with the caveat that one must also redefine the gauge coupling constant to absorb one factor

of field renormalization in the gluon self-interaction term. Collecting Gluon terms, and schematically writing the normalized field as $\mathcal{G}_\mu$ satisfying $\mathcal{G}_\mu = (1+c_G)^{\frac{1}{2}} G_\mu$, the kinetic Lagrangian is now:

$$\begin{aligned}\mathcal{L}_{Gluons} &= -\frac{1}{4}\left(1 - 2v_T^2\, C_{\varphi G}\right) G_{\mu\nu} G^{\mu\nu}. \\ &= -\frac{1}{4}\left(1 - 2v_T^2\, C_{\varphi G}\right)\left(1 + c_G\right)^{-1} \mathcal{G}_{\mu\nu}\, \mathcal{G}^{\mu\nu}, \\ &= -\frac{1}{4}\, \mathcal{G}_{\mu\nu} \mathcal{G}^{\mu\nu}. \end{aligned} \tag{3.3.73}$$

Again demanding canonical normalization by choosing a value for c_G to make this equal to one, and expanding to first order in C, one identifies the necessary gluon rescaling as:

$$G_\mu^A = \mathcal{G}_\mu^A \left(1 + C_{\varphi G} v^2\right), \tag{3.3.74}$$

With the D6 contribution to the Gluon normalizations as,

$$c_G = -2v^2\, C_{\varphi G}, \tag{3.3.75}$$

provided one makes the simultaneous redefinition of g_s:

$$\overline{g}_s = g_s \left(1 + C_{\varphi G}\, v^2\right), \tag{3.3.76}$$

so that the products $g_3 G_\mu^A = \overline{g}_s \mathcal{G}_\mu^A$, etc. are unchanged.

Electroweak Bosons

The normalization of the Electroweak terms proceeds identically to that of the Gluon terms, and yields the field redefinitions:

$$W_\mu^I = \mathcal{W}_\mu^I \left(1 + C_{\varphi W} v^2\right), \tag{3.3.77}$$

$$B_\mu = \mathcal{B}_\mu \left(1 + C_{\varphi B} v^2\right). \tag{3.3.78}$$

With the dimension six contributions being;

$$\begin{aligned} c_W &= -2v^2\, C_{\varphi W}, \\ c_B &= -2v^2\, C_{\varphi B}\,, \end{aligned} \tag{3.3.79}$$

and coupling rescalings:

$$\overline{g}_2 = g_2\left(1 + C_{\varphi W}\, v^2\right), \tag{3.3.80}$$

$$\overline{g}_1 = g_1\left(1 + C_{\varphi B}\, v^2\right). \tag{3.3.81}$$

The Electroweak kinetic terms are now,

$$\mathcal{L} = -\frac{1}{2}\mathcal{W}^+_{\mu\nu}\,\mathcal{W}^{\mu\nu}_- - \frac{1}{4}\mathcal{W}^3_{\mu\nu}\,\mathcal{W}^{\mu\nu}_3 - \frac{1}{4}\mathcal{B}_{\mu\nu}\,\mathcal{B}^{\mu\nu} - \frac{1}{2}\left(v_T^2 C_{\varphi WB}\right)\mathcal{W}^3_{\mu\nu}\mathcal{B}^{\mu\nu}. \tag{3.3.82}$$

The kinetic terms of the $\mathcal{W}^3$ and $\mathcal{B}$ bosons are now described by the quadratic form,

$$\mathcal{L}_{Kin} = -\frac{1}{4}\begin{bmatrix} \mathcal{W}^3_{\mu\nu} \\ \mathcal{B}_{\mu\nu} \end{bmatrix}^T \begin{bmatrix} 1 & v_T^2\, C_{\varphi WB} \\ v_T^2\, C_{\varphi WB} & 1 \end{bmatrix} \begin{bmatrix} \mathcal{W}^{\mu\nu}_3 \\ \mathcal{B}^{\mu\nu} \end{bmatrix} \tag{3.3.83}$$

which must be rewritten so as to absorb the off-diagonal, $\mathcal{O}(C)$ terms into redefinitions of the $\mathcal{W}^3$ and $\mathcal{B}$ fields. We can choose a matrix decomposition $K = T^T T$ where T is an upper triangular matrix which we interpret as a transformation on the vector of field strength tensors $F = \left(\mathcal{W}^3_{\mu\nu}, \mathcal{B}_{\mu\nu}\right)$. Then $F^T K F = (TF)^T I (TF)$ where we identify the new vector of field strength tensors which yields diagonal kinetic terms as TF. We perform this decomposition and find to order C:

$$K = T^T T = -\frac{1}{4}\begin{bmatrix} 1 & 0 \\ v^2\, C_{\varphi WB} & 1 \end{bmatrix}\begin{bmatrix} 1 & v^2\, C_{\varphi WB} \\ 0 & 1 \end{bmatrix} \tag{3.3.84}$$

We can immediately then redefine the basis of field strength tensors to absorb these transformation matrices. T can be taken as a second and final transformation on the vector of $\left(\mathcal{W}^3_\mu, \mathcal{B}_\mu\right)$ fields directly, so that:

$$\begin{bmatrix} \boldsymbol{\mathcal{W}}^3_\mu \\ \boldsymbol{\mathcal{B}}_\mu \end{bmatrix} = \begin{bmatrix} 1 & v_T^2\, C_{\varphi WB} \\ 0 & 1 \end{bmatrix}\begin{bmatrix} \mathcal{W}^3_\mu \\ \mathcal{B}_\mu \end{bmatrix} \tag{3.3.85}$$

The kinetic Lagrangian is now simply:

$$\mathcal{L}_{Kin} = -\frac{1}{4}\boldsymbol{\mathcal{W}}^I_{\mu\nu}\boldsymbol{\mathcal{W}}^{\mu\nu}_I - \frac{1}{4}\boldsymbol{\mathcal{B}}_{\mu\nu}\boldsymbol{\mathcal{B}}^{\mu\nu} = -\frac{1}{2}\boldsymbol{\mathcal{W}}^+_{\mu\nu}\boldsymbol{\mathcal{W}}^{\mu\nu}_- - \frac{1}{4}\boldsymbol{\mathcal{W}}^3_{\mu\nu}\boldsymbol{\mathcal{W}}^{\mu\nu}_3 - \frac{1}{4}\boldsymbol{\mathcal{B}}_{\mu\nu}\boldsymbol{\mathcal{B}}^{\mu\nu}. \tag{3.3.86}$$

where $\boldsymbol{\mathcal{W}}_\mu^{1,2} \equiv \mathcal{W}_\mu^{1,2}$. The mass terms for the gauge bosons from $\mathcal{L}_{\rm SM}$ and the $\varphi^4 D^2$ operators of $\mathcal{L}^{(6)}$ are:

$$\mathcal{L} = \frac{1}{4} g_2^2 v_T^2 W_\mu^+ W^{-\,\mu} + \frac{1}{8} v_T^2 (g_2 W_\mu^3 - g_1 B_\mu)^2 + \frac{1}{16} v_T^4 C_{\varphi D} (g_2 W_\mu^3 - g_1 B_\mu)^2 \tag{3.3.87}$$

Rewriting this using the set of identities for each vector boson $g_2 W_\mu^I = \overline{g}_2 \mathcal{W}_\mu^I$ and so on, and transforming to the basis of $(\boldsymbol{\mathcal{W}}_\mu^I,\, \boldsymbol{\mathcal{B}}_\mu)$ we can calculate the new mass matrices and coupling definitions. From the starting point:

$$\mathcal{L}_{mass} = \frac{1}{4} \overline{g}_2{}^2 v_T^2 \mathcal{W}_\mu^+ \mathcal{W}^{-\,\mu} + \frac{1}{8} v_T^2 (\overline{g}_2 \mathcal{W}_\mu^3 - \overline{g}_1 \mathcal{B}_\mu)^2 + \frac{1}{16} v_T^4 C_{\varphi D} (\overline{g}_2 \mathcal{W}_\mu^3 - \overline{g}_1 \mathcal{B}_\mu)^2. \tag{3.3.88}$$

The $\boldsymbol{\mathcal{W}}_\pm$ mass term can be read off as:

$$M_{W\pm}^2 = \frac{1}{4} \overline{g}_2{}^2 v_T^2. \tag{3.3.89}$$

The $\boldsymbol{\mathcal{W}}_3$ and $\boldsymbol{\mathcal{B}}$ terms can be rewritten:

$$\mathcal{L}_{mass} = \frac{1}{2} \left(\frac{1}{4} v_T^2 \left(1 + \frac{1}{2} v_T^2 C_{\varphi D} \right) \right) \begin{bmatrix} \mathcal{W}_\mu^3 \\ \mathcal{B}_\mu \end{bmatrix}^T \begin{bmatrix} \overline{g}_2{}^2 & -\overline{g}_1 \overline{g}_2 \\ -\overline{g}_1 \overline{g}_2 & \overline{g}_1{}^2 \end{bmatrix} \begin{bmatrix} \mathcal{W}_3^\mu \\ \mathcal{B}^\mu \end{bmatrix}.$$

Absorbing the matrices T of 3.3.85 into the mass matrix which we call $M_{\boldsymbol{\mathcal{ZA}}}$ gives:

$$M_{\boldsymbol{\mathcal{ZA}}} = \left(\frac{1}{8} v_T^2 \left(1 + \frac{1}{2} v_T^2 C_{\varphi D} \right) \right) \begin{bmatrix} \overline{g}_2{}^2 & -\overline{g}_2 (\overline{g}_1 + v_T^2 \overline{g}_2 C_{\varphi WB}) \\ -\overline{g}_2 (\overline{g}_1 + v_T^2 \overline{g}_2 C_{\varphi WB}) & (\overline{g}_1 + v_T^2 \overline{g}_2 C_{\varphi WB})^2 \end{bmatrix}.$$

This can be diagonalized in the usual way using eigendecomposition to obtain:

$$M_{\boldsymbol{\mathcal{ZA}}} = \left(\frac{1}{8} v_T^2 \left(1 + \frac{1}{2} v^2 C_{\varphi D} \right) \right) \begin{bmatrix} \overline{g}_1{}^2 + \overline{g}_2{}^2 + 2 \overline{g}_1 \overline{g}_2 v^2 C_{\varphi WB} & 0 \\ 0 & 0 \end{bmatrix} \tag{3.3.90}$$

Where the matrix of eigenvectors which rotates the fields $\boldsymbol{\mathcal{W}}_3$ and $\boldsymbol{\mathcal{B}}$ onto mass eigenstates $\boldsymbol{\mathcal{A}}$ and $\boldsymbol{\mathcal{Z}}$ is written as usual as:

$$\begin{bmatrix} \boldsymbol{\mathcal{Z}}^\mu \\ \boldsymbol{\mathcal{A}}^\mu \end{bmatrix} = \begin{bmatrix} \cos\overline{\theta} & -\sin\overline{\theta} \\ \sin\overline{\theta} & \cos\overline{\theta} \end{bmatrix} \begin{bmatrix} \boldsymbol{\mathcal{W}}_3^\mu \\ \boldsymbol{\mathcal{B}}^\mu \end{bmatrix},$$

With entries:

$$\sin\overline{\theta} = \frac{\overline{g}_1}{\sqrt{\overline{g}_1{}^2+\overline{g}_2{}^2}}\left[1+v^2\,\frac{\overline{g}_2}{\overline{g}_1}\,\frac{\overline{g}_2{}^2}{\overline{g}_2{}^2+\overline{g}_1{}^2}C_{\varphi WB}\right],$$
$$\cos\overline{\theta} = \frac{\overline{g}_2}{\sqrt{\overline{g}_1{}^2+\overline{g}_2{}^2}}\left[1-v^2\,\frac{\overline{g}_2}{\overline{g}_1}\,\frac{\overline{g}_1{}^2}{\overline{g}_2{}^2+\overline{g}_1{}^2}C_{\varphi WB}\right]. \tag{3.3.91}$$

These satisfy $\sin^2\overline{\theta}+\cos^2\overline{\theta} = 1+\mathcal{O}(C^2)$. The Z mass is:

$$M_Z^2 = \frac{v_T^2}{4}(\overline{g}_1{}^2+\overline{g}_2{}^2)+\frac{1}{8}v^4C_{HD}(\overline{g}_1{}^2+\overline{g}_2{}^2)+\frac{1}{2}v^4\overline{g}_1\overline{g}_2C_{\varphi WB}. \tag{3.3.92}$$

Inserting the new definitions for the Photon and Z into the covariant derivative gives the modifications to the electromagnetic and Z coupling constants. The covariant derivative (for $SU(2)_L\times U(1)_Y$) is now:

$$\begin{aligned}
D_\mu &= \partial_\mu + i\,\frac{\overline{g}_2}{\sqrt{2}}\left[\boldsymbol{\mathcal{W}}_\mu^+T^+ + \boldsymbol{\mathcal{W}}_\mu^-T^-\right] + i\overline{g}_2T^3\left[\boldsymbol{\mathcal{W}}_\mu^3 - v_T^2C_{\varphi WB}\boldsymbol{\mathcal{B}}_\mu\right] + i\,\overline{g}_1\,Y\,\boldsymbol{\mathcal{B}}_\mu,\\
&= \partial_\mu + i\,\frac{\overline{g}_2}{\sqrt{2}}\left[\boldsymbol{\mathcal{W}}_\mu^+T^+ + \boldsymbol{\mathcal{W}}_\mu^-T^-\right] + i\left[\overline{g}_2T_3(\cos\overline{\theta}+v_T^2C_{\varphi WB}\sin\overline{\theta}) - \overline{g}_1Y\sin\overline{\theta}\right]\boldsymbol{\mathcal{Z}}_\mu\\
&+\ i\left[\overline{g}_2(\sin\overline{\theta}-v_T^2C_{\varphi WB}\cos\overline{\theta})\,T^3 + \overline{g}_1\cos\overline{\theta}\,Y\right]\boldsymbol{\mathcal{A}}_\mu,\\
&= \partial_\mu + i\,\frac{\overline{g}_2}{\sqrt{2}}\left[\boldsymbol{\mathcal{W}}_\mu^+T^+ + \boldsymbol{\mathcal{W}}_\mu^-T^-\right] + i\,\overline{g}_Z\left[T^3-(\overline{s}^2+\kappa)\,Q\right]\boldsymbol{\mathcal{Z}}_\mu + i\,\overline{e}\,Q\,\boldsymbol{\mathcal{A}}_\mu
\end{aligned} \tag{3.3.93}$$

where the electric charge is $Q = T_3+Y$, and the effective couplings are now given by:

$$\begin{aligned}
\overline{e} &= \frac{\overline{g}_1\overline{g}_2}{\sqrt{\overline{g}_2{}^2+\overline{g}_1{}^2}}\left[1-\frac{\overline{g}_1\overline{g}_2}{\overline{g}_2{}^2+\overline{g}_1{}^2}v^2C_{\varphi WB}\right] = \overline{g}_2\,\sin\overline{\theta}-\frac{1}{2}\,\cos\overline{\theta}\,\overline{g}_2\,v^2\,C_{\varphi WB},\\
\overline{g}_Z &= \sqrt{\overline{g}_2{}^2+\overline{g}_1{}^2}+\frac{\overline{g}_1\overline{g}_2}{\sqrt{\overline{g}_2{}^2+\overline{g}_1{}^2}}v^2C_{\varphi WB} = \frac{\overline{e}}{\sin\overline{\theta}\cos\overline{\theta}}\left[1+\frac{\overline{g}_1{}^2+\overline{g}_2{}^2}{2\overline{g}_1\overline{g}_2}v^2C_{\varphi WB}\right],\\
\overline{s}^2+\kappa &= \sin^2\overline{\theta}+\kappa = \frac{\overline{g}_1{}^2}{\overline{g}_2{}^2+\overline{g}_1{}^2}+\frac{\overline{g}_1\overline{g}_2(\overline{g}_2{}^2-\overline{g}_1{}^2)}{(\overline{g}_1{}^2+\overline{g}_2{}^2)^2}v^2C_{\varphi WB}.
\end{aligned} \tag{3.3.94}$$

This differs slightly to the conventions in [40], where the authors define more symmetric $\sin\overline{\theta}$ and $\cos\overline{\theta}$ parameters, in order to retain the SM Z coupling structure of $(T^3-\sin^2\overline{\theta}\,Q)$ at the price of having the renormalized $\mathcal{W}^3$ and $\mathcal{B}$ bosons no longer related to the $\mathcal{Z}$ and $\mathcal{A}$ by a pure rotation matrix. This affects only the definitions of the mixing angles, either containing the complete information relating the $\mathcal{W}^3$ and $\mathcal{B}$ to the $\mathcal{Z}$ and $\mathcal{A}$ or being supplemented by an additional linear transformation related to the kinetic mixing matrix. The Lagrangian and hence physical predictions are unaffected.

3.3.3 Yukawa Sector

Fermion Mass Matrices

The inclusion of the $\psi^2\varphi^3$ class operators modifies the fermions' couplings to the Higgs field, necessitating a redefinition of both their mass matrices and Yukawa couplings in order to recover mass eigenstates. Furthermore, these $\mathcal{O}(v^2/\Lambda^2)$ terms break the simple proportionality relationship between the mass and Yukawa matrices that exists in the SM.

The relevant Lagrangian terms in the unbroken theory are:

$$\begin{aligned}\mathcal{L} = &-\left[\overline{q}_r\ [Y_d]_{rs}\ d_s\varphi + \overline{q}_r\ [Y_u]_{rs}\ u_s\,\widetilde{\varphi} + \overline{l}_r\ [Y_e]_{rs}\ e_s\,\varphi + \text{h.c.}\right] \\ &+ \left[C_{\substack{d\varphi\\rs}}\left(\varphi^\dagger\varphi\right)\varphi^\dagger\overline{q}_r d_s + C_{\substack{u\varphi\\rs}}\left(\varphi^\dagger\varphi\right)\tilde{\varphi}^\dagger\overline{q}_r u_s + C_{\substack{e\varphi\\rs}}\left(\varphi^\dagger\varphi\right)\varphi^\dagger\overline{l}_r e_s + \text{h.c.}\right], \end{aligned} \tag{3.3.95}$$

Rediagonalizing the mass matrices is necessary to eliminate the tree-level quark mixing two point functions induced whenever any of the Wilson Coefficients $C_{\substack{\psi\varphi\\rs}}$ are non-zero for $r \neq s$.

Collecting together the relevant terms, and demanding a real, diagonal mass matrix proceeds analagously to constructing the SM mass terms. Expanding the Higgs fields about their minimum, we write the fermion mass terms in the usual manner as:

$$\mathcal{L}_{mass} = -\left[\overline{d}_{L,r}\ [M_d]_{rs}\ d_{R,s} + \overline{u}_{Lr}\ [M_u]_{rs}\ u_{R,s} + \overline{e}_{L,r}\ [M_e]_{rs}\ e_{R,s} + \text{h.c.}\right] \tag{3.3.96}$$

Where the mass matrices are now identified as:

$$[M_\psi]_{rs} = \frac{v_T}{\sqrt{2}}\left([Y_\psi]_{rs} - \frac{1}{2}v^2 C_{\substack{\psi\varphi\\rs}}\right), \qquad \psi = u, d, e \tag{3.3.97}$$

Using a singular value decomposition of these matrices for each fermion generation, M_ψ may be rewritten as $M_\psi = UDV^\dagger$, where U and V are unitary matrices and D is a real, positive-definite diagonal matrix. As in the SM, we can then exploit the freedom to make a global unitary rotation of the left- and right-handed fermion flavours to absorb the matrices U and V, then interpreting D as the matrix of the mass eigenstates in the EFT.

Each U and V should reduce to the identity matrix in the limit that all Wilson Coefficients are zero, such that D is equal to the SM mass matrix. Then by writing each

of the matrices U, V and D as a power series in Λ:

$$U = U_0 + \Lambda^{-2}\, U_1 + \mathcal{O}(\Lambda^{-2}) \ldots$$

we can separate the zeroth order SM pieces from those dependent on the Wilson Coefficients. Working as usual at $\mathcal{O}(\Lambda^{-2})$, we can distinguish the diagonal SM mass matrix for each fermion species $M_0 \equiv D_0$ from the EFT contributions by writing $M = M_0 + M_1$ and identifying the $\mathcal{O}(\Lambda^{-2})$ coefficients:

$$M_1 = U_1\, D_0 + D_0\, V_1^\dagger + D_1.$$

The unitarity of U and V, together with the requirement that D must be real and diagonal, yield three further conditions which, when solved simultaneously, specify each U, V and D to first order in the Wilson Coefficients.

$$U_1 = -\,U_1^\dagger, \quad V_1 = -\,V_1^\dagger, \quad D_1 = \; D_1^*$$

Taking the example of the left-handed up-type quarks, the mass eigenstates are now $U^u_{rs}\, u^s_L$, where:

$$U^u = \begin{bmatrix} 1 + v_T^2 \dfrac{i\,\Im\mathfrak{m}(C^{11}_{u\varphi})}{4y_u} & v_T^2 \dfrac{(y_u\, C^{12}_{u\varphi} + y_c\, C^{21*}_{u\varphi})}{2(y_u^2 - y_c^2)} & v_T^2 \dfrac{(y_u\, C^{13}_{u\varphi} + y_t\, C^{31*}_{u\varphi})}{2(y_u^2 - y_t^2)} \\ v_T^2 \dfrac{(y_c\, C^{21}_{u\varphi} + y_u\, C^{12*}_{u\varphi})}{2(y_c^2 - y_u^2)} & 1 + v_T^2 \dfrac{i\,\Im\mathfrak{m}(C^{22}_{u\varphi})}{4y_c} & v_T^2 \dfrac{(y_t\, C^{23}_{u\varphi} + y_c\, C^{32*}_{u\varphi})}{2(y_c^2 - y_t^2)} \\ v_T^2 \dfrac{(y_t\, C^{31}_{u\varphi} + y_u\, C^{13*}_{u\varphi})}{2(y_t^2 - y_u^2)} & v_T^2 \dfrac{(y_t\, C^{32}_{u\varphi} + y_c\, C^{23*}_{u\varphi})}{2(y_t^2 - y_c^2)} & 1 + v_T^2 \dfrac{i\,\Im\mathfrak{m}(C^{33}_{u\varphi})}{4y_t} \end{bmatrix}$$

with flavour indices r and s. Meanwhile, the right-handed up-type quark mass eigenstates are $V^u_{rs}\, u^s_R$, with:

$$V^u = \begin{bmatrix} 1 - v_T^2 \dfrac{i\,\Im\mathfrak{m}(C^{11}_{u\varphi})}{4y_u} & v_T^2 \dfrac{(y_c\, C^{12}_{u\varphi} + y_u\, C^{21*}_{u\varphi})}{2(y_u^2 - y_c^2)} & v_T^2 \dfrac{(y_t\, C^{13}_{u\varphi} + y_u\, C^{31*}_{u\varphi})}{2(y_u^2 - y_t^2)} \\ v_T^2 \dfrac{(y_u\, C^{21}_{u\varphi} + y_c\, C^{12*}_{u\varphi})}{2(y_c^2 - y_u^2)} & 1 - v_T^2 \dfrac{i\,\Im\mathfrak{m}(C^{22}_{u\varphi})}{4y_c} & v_T^2 \dfrac{(y_c\, C^{23}_{u\varphi} + y_t\, C^{32*}_{u\varphi})}{2(y_c^2 - y_t^2)} \\ v_T^2 \dfrac{(y_u\, C^{31}_{u\varphi} + y_t\, C^{13*}_{u\varphi})}{2(y_t^2 - y_u^2)} & v_T^2 \dfrac{(y_c\, C^{32}_{u\varphi} + y_t\, C^{23*}_{u\varphi})}{2(y_t^2 - y_c^2)} & 1 - v_T^2 \dfrac{i\,\Im\mathfrak{m}(C^{33}_{u\varphi})}{4y_t} \end{bmatrix}$$

While the mass matrix M^u is modified accordingly to:

$$D^u = \frac{v_T}{\sqrt{2}} \begin{bmatrix} y_u - \frac{1}{2} v_T^2 \Re\mathfrak{e}\,(C^{11}_{u\varphi}) & 0 & 0 \\ 0 & y_c - \frac{1}{2} v_T^2 \Re\mathfrak{e}\,(C^{22}_{u\varphi}) & 0 \\ 0 & 0 & y_t - \frac{1}{2} v_T^2 \Re\mathfrak{e}\,(C^{33}_{u\varphi}) \end{bmatrix} \tag{3.3.98}$$

Identical expressions hold for the down-type quarks and leptons, with the SM Yukawa couplings replaced by their equivalent counterparts, and the analogous Wilson Coefficients $C_{d\varphi}\,, C_{e\varphi}$.

As in the SM, this global redefinition will cancel by virtue of the unitarity of U and V everywhere in the Lagrangian (up to terms of order Λ^{-4}, which are truncated) except for in the fermion weak-gauge boson couplings, where they will augment the definition of the CKM matrix.

The CKM Matrix

After diagonalization, and adopting the usual convention of letting the down-quarks assume the necessarily misaligned flavour and mass eigenstates, their mass term looks like:

$$\mathcal{L}^d_{mass} = -\,\overline{d}_{L,r}\; [D_d]_{rs}\; d_{R,s} + \text{h.c.}\,, \tag{3.3.99}$$

But with mass eigenstates d related to the electroweak eigenstates d' by a unitary rotation:

$$d = (U^{d\dagger}\, U^u\, V_{CKM}^\dagger d') \equiv V_{CKM}^{'\,\dagger} d'. \tag{3.3.100}$$

Here, V_{CKM} is the SM CKM matrix, into which we can absorb the matrices U^d and U^u to define an effective CKM matrix, V'_{CKM}. Writing $V'_{CKM} = V_{CKM} + V_1 + \mathcal{O}(\Lambda^{-4}) = V_{CKM}(\mathbb{I} + (U_1^d - U_1^u)) + \mathcal{O}(\Lambda^{-4})$, the explicit $\mathcal{O}(\Lambda^{-2})$ contribution is:

$$V_1 = V_{CKM}(U_1^d - U_1^u) \equiv V_{CKM} U^{du}, \tag{3.3.101}$$

where $U^{du} = -U^{du\,\dagger}$ has entries:

$$\begin{aligned}
U_{11}^{du} &= \frac{1}{2} v_T^2 \frac{i\; y_d\, \Im\mathfrak{m}\left(C_{u\varphi}^{11}\right) - \; y_u\, \Im\mathfrak{m}\left(C_{d\varphi}^{11}\right)}{2\, y_u\, y_d} \\
U_{22}^{du} &= \frac{1}{2} v_T^2 \frac{i\; y_s\, \Im\mathfrak{m}\left(C_{u\varphi}^{22}\right) - \; y_c\, \Im\mathfrak{m}\left(C_{d\varphi}^{22}\right)}{2\, y_s\, y_c} \\
U_{33}^{du} &= \frac{1}{2} v_T^2 \frac{i\; y_b\, \Im\mathfrak{m}\left(C_{u\varphi}^{33}\right) - \; y_t\, \Im\mathfrak{m}\left(C_{d\varphi}^{33}\right)}{2\, y_b\, y_t}
\end{aligned}$$

$$\begin{aligned}
U_{12}^{du} = -U_{21}^{du*} &= \frac{1}{2} v_T^2 \left(\frac{y_s C_{d\varphi}^{12} + y_d C_{d\varphi}^{21*}}{y_d^2 - y_s^2} - \frac{y_c C_{u\varphi}^{12} + y_u C_{u\varphi}^{21*}}{y_u^2 - y_c^2} \right) \\
U_{13}^{du} = -U_{31}^{du*} &= \frac{1}{2} v_T^2 \left(\frac{y_b C_{d\varphi}^{13} + y_d C_{d\varphi}^{31*}}{y_d^2 - y_b^2} - \frac{y_t C_{u\varphi}^{13} + y_u C_{u\varphi}^{31*}}{y_u^2 - y_t^2} \right) \\
U_{23}^{du} = -U_{32}^{du*} &= \frac{1}{2} v_T^2 \left(\frac{y_b C_{d\varphi}^{23} + y_s C_{d\varphi}^{32*}}{y_s^2 - y_b^2} - \frac{y_t C_{u\varphi}^{23} + y_c C_{u\varphi}^{32*}}{y_c^2 - y_t^2} \right)
\end{aligned}$$

Which mix the SM CKM elements by terms of $\mathcal{O}(v^2/\Lambda^2)$. V'_{CKM} is now unitary up to terms of $\mathcal{O}(\Lambda^{-4})$.

Yukawa Couplings

The final task is then to rewrite the Yukawa couplings in terms of the new mass eigenstates defined by U and V.

After the field redefinitions, the dimension-four fermion-higgs couplings look like:

$$\mathcal{L} = -\left[\overline{d}_{L,r}\, [\mathcal{Y}_d]_{rs}\; d_{R,s}\, h + \overline{u}_{L,r}\, [\mathcal{Y}_u]_{rs}\; u_{R,s}\, h + \overline{e}_{L,r}\, [\mathcal{Y}_e]_{rs}\; e_{R,s}\, h + \text{h.c.} \right] \tag{3.3.102}$$

With the coupling matrices now given by:

$$[\mathcal{Y}_\psi]_{rs} = \frac{1}{\sqrt{2}}\left([Y_\psi]_{rs}\,(1+c_H) - \frac{3}{2}v^2 C_{\substack{\psi\varphi\\rs}}\right), \qquad \psi = u,d,e \tag{3.3.103}$$

Separating this into a part proportional to the expression 3.3.97 for which we chose the rotation matrices U_ψ and V_ψ to diagonalize into 3.3.98 gives:

$$[\mathcal{Y}_\psi]_{rs} = \frac{1+c_H}{v_T}\,[M_\psi]_{rs} + \frac{v^2}{\sqrt{2}}\,C_{\substack{\psi\varphi\\rs}} + \text{h.c.} + \mathcal{O}(\Lambda^{-4}) \tag{3.3.104}$$

The first term is proportional to the mass matrix M rescaled by the Higgs' kinetic normalization, while the second is an additional contribution from the $\psi^2\varphi^3$ Wilson Coefficients. Since we chose the unitary rotations U and V acting on q, u and d to diagonalize M, the mass eigenstates no longer necessarily have diagonal Yukawa couplings. However, since the flavour off-diagonal term is entirely $\mathcal{O}(\Lambda^{-2})$, this expression is accurate for the rotated fields up to terms of $\mathcal{O}(\Lambda^{-4})$ (i.e. we can replace $M_{rs} \leftrightarrow D_{rs}$ above). As pointed out in Ref. [40], the loss of flavour-diagonal Higgs couplings is further exacerbated by the fact that the fermion mass and coupling parameters now also have different RGEs.

3.3.4 Input Parameter Redefinitions

The extraction of the values of the fundamental parameters in the Lagrangian from a set of measurable physical quantities is affected by the new dependence of these on the Wilson Coefficients. The set of measurable parameters $\{\alpha_{EM}, G_f, \alpha_s, m_Z, m_H, M_\psi\}$ are are sufficient to determine the underlying masses, couplings and mixing angles. The tree level relationships determining these correspondences then must be inverted to propagate this information back into $\mathcal{L}$. In particular, now:

$$\begin{aligned}
G_f &= -\frac{\sqrt{2}}{4}\left(-\frac{2}{v_T^2} + (C_{\substack{ll\\2112}} + C_{\substack{ll\\1221}}) - 2(C^{(3)}_{\substack{\varphi l\\11}} + C^{(3)}_{\substack{\varphi l\\22}})\right),\\
\alpha_{EM} &= \frac{1}{4\pi}\frac{\overline{g}_1{}^2\overline{g}_2{}^2}{\overline{g}_1{}^2+\overline{g}_2{}^2}\left(1 - 2v_T^2 C_{\varphi WB}\frac{\overline{g}_1\overline{g}_2}{\overline{g}_1{}^2+\overline{g}_2{}^2}\right),\\
m_H^2 &= 2v_T^2\left(1 - 3C_\varphi\frac{v_T^2}{2\lambda} + 2c_H\right),\\
m_Z^2 &= \frac{1}{4}v_T^2(\overline{g}_1{}^2+\overline{g}_2{}^2) + \frac{1}{8}v_T^4 C_{\varphi D}(\overline{g}_1{}^2+\overline{g}_2{}^2) + \frac{1}{2}v_T^4\overline{g}_1\overline{g}_2 C_{\varphi WB}.
\end{aligned}$$

The equations for G_f and m_H may be solved simultaneously for v_T and λ. The resulting parameter relations are, to $\mathcal{O}(\Lambda^{-2})$:

$$\lambda = \frac{3\sqrt{2}\,C_\varphi + (-2C^{(3)}_{\substack{\varphi l\\ 11}} - 2C^{(3)}_{\substack{\varphi l\\ 22}} + C_{\substack{ll\\ 1221}} + C_{\substack{ll\\ 2112}})\,G_f\,m_H^2 + 2\sqrt{2}\,G_f^2\,m_H^2\,(1-2\,c_H)}{4\,G_f}$$

$$v_T = \frac{1}{2^{1/4}\sqrt{G_f}} + \frac{C^{(3)}_{\substack{\varphi l\\ 11}} + C^{(3)}_{\substack{\varphi l\\ 22}}}{2\,2^{3/4}G_f^{3/2}} - \frac{C_{\substack{ll\\ 1221}}}{4\,2^{3/4}G_f^{3/2}} - \frac{C_{\substack{ll\\ 2112}}}{4\,2^{3/4}G_f^{3/2}}$$

Those for α_{EM} and m_Z likewise yield the couplings $\overline{g}_1$ and $\overline{g}_2$:

$$\overline{g}_1 = g_1 + \frac{v_T^2(4C_{\varphi WB}g_2 + C_{\varphi D}g_1)(-4m_Z^2 + v_T^2(g_2^2 - g_1^2 + 16\pi\alpha_{EM}))}{32(m_Z^2 - 4\pi v_T^2\alpha_{EM})}$$

$$\overline{g}_2 = g_2 - \frac{v_T^2(2(C_{\varphi D}g_2 + 4C_{\varphi WB}g_1)m_Z^2(4m_Z^4 + m_Z^2v_T^2)}{((m_Z^2 - 4\pi v_T^2\alpha_{EM}))}$$
$$\times \left[\frac{(g_2^2 - g_1^2 - 20\pi\alpha_{EM}) + \pi v_T^4\alpha_{EM}(-3g_2^2 + 3g_1^2 + 16\pi\alpha_{EM})))}{(4m_Z^2 + (g_2^2 - g_1^2)v_T^2)^2}\right]$$

Where the g_1 and g_2 are the SM couplings:

$$g_1 = \frac{\sqrt{2}}{v_T}\left(\sqrt{m_Z^2 - \sqrt{m_Z^4 - 4m_Z^2\pi v_T^2\alpha_{EM}}}\right)$$

$$g_2 = \frac{\sqrt{2}}{v_T}\left(\sqrt{m_Z^2 + \sqrt{m_Z^4 - 4m_Z^2\pi v_T^2\alpha_{EM}}}\right)$$

With these specified, all other related parameters are calculated according to the relationships established previously.

It should be noted that the renormalization of the dimension-two and four parameters of $\mathcal{L}^{(4)}_{\rm SM}$ in the presence of higher-dimensional operators follows the same procedure as in the renormalizable SM. That is, choosing a renormalization scheme to define the masses and couplings is itself not complicated by the presence of effective operators in correlation functions - their role is to supply additional divergences which are then cancelled by the appropriate counterterms as usual.

We have now reorganized the parameters of the Standard Model Lagrangian to accommodate for the presence of dimension-six operators, and incorporated this information into a model with which we can explore phenomenological applications.

3.4 Manipulating Effective Lagrangians in FeynRules

We have seen that - without imposing model-dependent restrictions (such as the MFV hypothesis) - the number of free parameters for the most general set of dimension-six operators is $\mathcal{O}(2000)$. While in practice we do (and should) focus attention on phenomenologically relevant subsets of operators to keep EFT relevant and manageable, even then it is true in general that the complexity of any calculation beyond the lowest order in both the perturbative and EFT expansions becomes formidable. In the former case, this is simply combinatorics - a jump in the number of couplings in $\mathcal{L}^{(6)}$ relative to the renormalizable $\mathcal{L}_{\rm SM}$ permits a dramatically higher number of Feynman diagrams at a given loop order. In the latter, the number of valid gauge-invariant structures also rises substantially with the larger set of possible permutations of fields applicable to operators with higher mass dimensions.

While the value of performing higher order computations in the SMEFT is presently limited by the empirical successes of $\mathcal{L}_{\rm SM}$ alone, it is prudent to develop tools which will facilitate tackling them in general. Mounting datasets, improvements in experimental systematic uncertainties and even prospects for a next-generation collider may - in the absence of discovery - necessitate the general availability of matrix elements at next-to-leading order, particularly if one or more non-resonant effects in tension with the SM does appear.

Knowledge of the effective operators arising at dimension-seven and beyond may also be useful, as the leading low-energy effects of a given model need not appear at dimension-six. This can in some cases be inferred directly from the gauge-invariance of the effective Lagrangian. For example, $\mathcal{L}^{(6)}$ does not parametrize triple neutral gauge boson couplings of the form (ZZZ, $ZZ\gamma\ldots$). UV completions which induce these interactions must then do so via dimension-eight operators [55]. Conversely, structural features of BSM scenarios can imply this directly. In models of warped extra dimensions, Kaluza-Klein gravitons and radion fields couple to the energy-momentum tensor which has mass dimension four, such that the tree-level interactions with SM fields generate operators of mass dimension eight [56]. The convergence of the expansion in Λ also depends directly on the strength of the coupling of new states to those of the SM. The effective operators generated by massive modes carrying a large coupling to SM fields will reflect this in a smaller hierarchy between the sizes of the Wilson Coefficients appearing at each order in Λ^{-1}*, rendering $D > 6$ operators numerically important.

*This will be discussed in the context of interpreting constraints on C_i in section 5.4.1.

In working with models characterized by large Lagrangians and extensive independent couplings such as the SMEFT, the availability of automated tools from which predictions can easily be extracted is a necessity. The FeynRules [10, 34] package is the predominant framework which fulfils this role, and is successful in part due to having a flexible range of interfaces to both event generators (particularly the generator-independent UFO (Universal FeynRules Output) format [11]) and further symbolic/analytic tools for manipulating scattering amplitudes such as FeynArts [57], FormCalc [58] and FeynCalc [59]. Given the scope of its applicability, and the degree of accessibility achieved by requiring only a consistent QFT Lagrangian as input, it is then an ideal candidate in which to implement EFT-specific functionality to streamline future calculations in the SMEFT.

While general-purpose Monte Carlo event generators now typically incorporate Standard Model matrix elements at NLO accuracy in QCD, the inclusion of higher-dimensional operators (even at tree-level) is a relatively recent development. The additional complexity involved in achieving the same degree of automation at this accuracy arises in part from the involved renormalization of effective operators and the role played by their associated redundancies, which - even when calculating matrix elements using a complete operator basis - reappear at loop-level*.

3.4.1 Operator Mixing in Fermi Theory

To motivate the desire for a systematic way of taking operator redundancies into account, let's pause to look at a historical example of *operator mixing*, whereby radiative corrections to effective interactions can introduce operator structures distinct from those in the tree-level Lagrangian.

Recalling (from Chapter 2) the example of Fermi Theory, the effective theory of weak interaction as experienced by light quarks with typical momenta $p^2 \ll m_W^2$. In this kinematic regime, the t-channel, tree-level W-boson exchange mediating the flavour transition $us \to du$ was approximated by a four quark operator with the Lagrangian:

$$\mathcal{L}_{us\to bd} = C_1(\bar{u}_L\gamma^\mu s_L)(\bar{d}_L\gamma_\mu u_L) \equiv C_1 Q_1,$$

*This was discussed in some detail by the authors of Refs. [40, 50, 51] in their derivation of the RGEs for the Warsaw SMEFT.

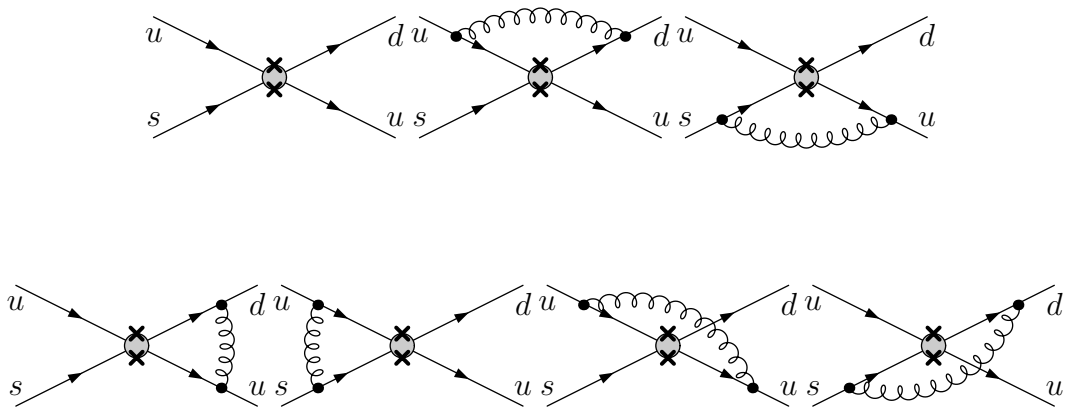

Figure 3.3: *Feynman diagrams for the quark flavour transition $us \to du$ at one loop order in QCD, and working in Fermi theory with $\sqrt{s} \ll m_W$. The shaded circles represent insertions of the dimension-six ψ^4 operator Q_1, while crosses reflect the arrangement of the quarks into a product of two weak currents. In the diagrams in the second row, the gluons linking the fermion lines 'mix' the colour indices of quarks contracted in opposite currents.*

where $\psi_L \equiv P_L\psi$. Here, the arrangement of quark billinears is structured intuitively as a product of the left-handed charged currents to which the W-boson couples. From the perspective of the Standard Model with the W-boson included, the explicit form of the Wilson coefficient is dictated by the matching condition $C_1 = \frac{4G_F}{\sqrt{2}} cos\theta_c \, sin\theta_c$, with G_F carrying the scale m_W^{-2} implicitly.

For the purposes of the present discussion, let's now forget about the W-boson and just work with the operator Q_1. We want to calculate the one-loop QCD corrections to $us \to du$ as described by the effective interaction Q_1 which carries an associated coupling C_1. In Fig. 3.3 the Feyman diagrams for this processs are shown, consisting of all possible arrangements of virtual gluons between the participating quarks. In the diagrams in the second row, the exchanged gluons link quark lines which belong to opposite bilinears in Q_1. We will be interested in how this impacts the UV-divergent piece of the loop diagram, as we anticipate that we will have to renormalize our coupling C_1. To extract this contribution, we denote the (divergent) amplitude corresponding to the first of these diagrams by $\mathcal{M}_1^{Q_1\,(0)}$, and aim to evaluate it in the limit of massless quarks, in the Feynman gauge ($\xi = 1$), and using dimensional regularization with $d = 4 - 2\epsilon$. Leaving the quark fields explicit throughout to ease a final interpretation in terms of operator counterterms (rather than e.g. replacing these with on-shell external spinors à la $u_s(p)\ldots$), and separating colour matrices from the numerator and propagator factors,

this is:

$$\begin{aligned}\mathcal{M}_1^{Q_1\,(0)} &= g_s^2(T^A_{ki}T^A_{lj})\int\frac{d^dl}{(2\pi)^d}\frac{1}{l^2(l+p_d)^2(l-p_u)^2}\left(\bar{d}_L\gamma^\nu(\not{l}+\not{p}_d)\gamma^\mu u_L\right)\left(\bar{u}_L\gamma_\nu(\not{l}-\not{p}_u)\gamma_\mu s_L\right)\\ &= g_s^2(T^A_{ki}T^A_{lj})\int_0^1 dx\int_0^{1-x}dy\int\frac{d^dl}{(2\pi)^d}\frac{1}{((l+(xp_d-yp_u))^2+2xy\,p_d.p_u)^3}\,\mathcal{N}\,,\end{aligned}$$

where we've done the usual business of combining propagators by introducing integrals over the Feynman parameters x and y, and completing the square in the loop momentum l. The numerator is abbreviated by $\mathcal{N}$. Going on to make the customary change of variable for the loop momentum $l\to l'\equiv l+(xp_d-yp_u)$, we get:

$$\mathcal{M}_1^{Q_1\,(0)} = g_s^2(T^A_{ki}T^A_{lj})\int_0^1 dx\int_0^{1-x}dy\int\frac{d^dl}{(2\pi)^d}\frac{1}{(l'^2-2xy\,p_d.p_u)^3}\,\mathcal{N}\,,$$

and we can now rewrite $\mathcal{N}$ in terms of l', discarding terms linear in the l' which will integrate to zero between positive and negative infinity:

$$\begin{aligned}\mathcal{N} &= (l'+(1-x)p_d-yp_u))^\lambda\,(l'-xp_d-(1+y)p_u)^\sigma\left(\bar{d}_L\gamma^\nu\gamma_\lambda\gamma^\mu u_L\right)(\bar{u}_L\gamma_\nu\gamma_\sigma\gamma_\mu s_L)\\ &= (l'^\lambda l'^\sigma - x(1-x)p_d^\lambda p_d^\sigma-(1-x)(1+y)p_d^\lambda p_u^\sigma+xyp_u^\lambda p_d^\sigma+y(1+y)p_u^\lambda p_u^\sigma)\\ &\times\left(\bar{d}_L\gamma^\nu\gamma_\lambda\gamma^\mu u_L\right)(\bar{u}_L\gamma_\nu\gamma_\sigma\gamma_\mu s_L)\,.\end{aligned}$$

The UV-divergent contribution from large loop momenta l' then comes from:

$$\mathcal{M}_1^{Q_1\,(0)} = g_s^2(T^A_{ki}T^A_{lj})\int_0^1 dx\int_0^{1-x}dy\int\frac{d^dl'}{(2\pi)^d}\frac{l'^\lambda l'^\sigma}{(l'^2-2xy\,p_d.p_u)^3}\,\left(\bar{d}_L\gamma^\nu\gamma_\lambda\gamma^\mu u_L\right)(\bar{u}_L\gamma_\nu\gamma_\sigma\gamma_\mu s_L)$$

Using the standard one-loop master integral:

$$\int\frac{d^dl'}{(2\pi)^d}\frac{l'^\lambda l'^\sigma}{(l'^2-\Delta)^n} = \frac{i(-1)^{n-1}}{(4\pi)^{d/2}}\frac{g^{\lambda\sigma}}{2}\frac{\Gamma(n-d/2-1)}{\Gamma(n)}\left(\frac{1}{\Delta}\right)^{n-d/2-1}\,,$$

introducing the scale μ with $g_s^2\to g_s^2\mu^{2\epsilon}$ in $d=4-2\epsilon$ dimensions, and noting that $p_d.p_u=-\frac{1}{2}t$, the integration over l' gives:

$$\mathcal{M}_1^{Q_1\,(0)} = -\frac{ig_s^2}{4(4\pi)^2}(T^A_{ki}T^A_{lj})\int_0^1 dx\int_0^{1-x}dy\left(\frac{4\pi\mu^2}{xyt}\right)^\epsilon\Gamma(\epsilon)\,(\bar{d}_L\gamma^\nu\gamma^\lambda\gamma^\mu u_L)(\bar{u}_L\gamma_\nu\gamma_\lambda\gamma_\mu s_L)\,.$$

Finally, expanding $\Gamma(\epsilon)$ about the limit $\epsilon \to 0$, performing the integral over x and y, retaining the ϵ pole and the logarithmic corrections of the form $\alpha_s \log(\ldots)$, we get:

$$\mathcal{M}_1^{Q_1\,(0)} = -\frac{i\alpha_s}{16\pi}\,(T^A_{ki}\,T^A_{lj})\,(\frac{1}{\bar{\epsilon}} + \log(\frac{\mu^2}{t}) + \ldots)\,\left\langle (\bar{d}_L\gamma^\nu\gamma^\lambda\gamma^\mu u_L)(\bar{u}_L\gamma_\nu\gamma_\lambda\gamma_\mu s_L)\right\rangle\,,$$

where $\frac{1}{\bar{\epsilon}} \equiv \frac{1}{\epsilon} - \gamma_E + \log(4\pi)$, and angled brackets have been inserted explicitly to clarify that this is the matrix element of the operator shown.

In contrast to the full SM amplitude (depicted in the left pane of Fig. 3.4), the QCD corrections to the effective vertex approximating the W-boson exchange as a pointlike interaction contain an ultraviolet divergence $1/\bar{\epsilon}$. This what we should expect for a nonrenormalizable operator. Integrating out the W-boson and re-introducing its leading contribution to matrix elements in an expansion in m_W^{-1} as a dimension-six operator amounts to making the approximation:

$$\frac{1}{q^2 - m_W^2} = \frac{-1}{m_W^2}\left(1 + \mathcal{O}\left(\frac{q^2}{m_W^2}\right)\right)\,,$$

with q is the momentum flowing in the W-boson propagator. This expansion is only justified for $q^2 \ll m_W^2$. In the one-loop matrix element in our effective description we

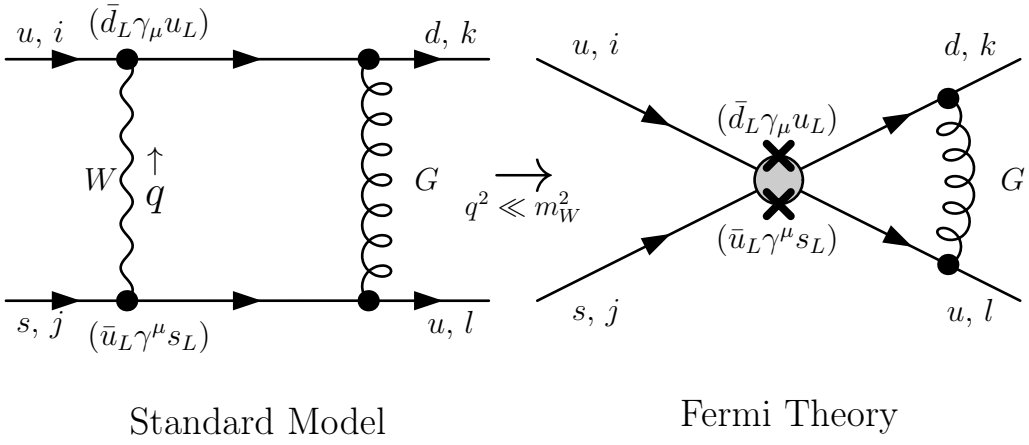

Figure 3.4: *Feynman diagram representation of $\mathcal{O}(\alpha_s)$ corrections to the flavour transition $us \to du$ in the full SM and in Fermi's theory. Integrating out the W-boson produces the local operator Q_1 in which the weak left-handed fermion currents are contracted within the same vertex. Here, i, j, k, l represent colour indices of the quarks.*

then integrate over values of the loop momentum l up to infinity, implicitly leaving the range of validity of the EFT. The ultraviolet divergences are a consequence of our assuming that we are free to do this, which can be equated with taking the limit $m_W \to \infty$. In the full matrix element in the Standard Model, the virtual W propagator is explicitly sensitive to the loop momentum, providing an additional suppression by a factor of l^{-2} which makes this integral converge again for $q > m_W^2$.

In the effective theory, we can aim to absorb this divergence into the coefficient C_1. However, the divergent amplitude is of the form:

$$\mathcal{M}_1^{Q_1\,(0)} \propto -(T^A_{ki}\,T^A_{lj})\,\left\langle (\bar{d}^k_L\gamma^\nu\gamma^\lambda\gamma^\mu u^i_L)(\bar{u}^l_L\gamma_\nu\gamma_\lambda\gamma_\mu s^j_L)\right\rangle \equiv \langle Q'\rangle\ ,$$

where the quark colour indices have been made explicit. Clearly $Q' \neq Q_1$. While the field content remains the same, the exchange of the virtual gluon between the outgoing fermions has modified the colour and Dirac algebra structure of the amplitude relative to the leading order result. This is again not surprising, as the gluon itself couples to the colours of both quarks as well as their spins, such that the $\mathcal{O}(\alpha_s)$ corrections to the amplitude reflect an exchange of information between fermions absent in the Born approximation. While the apperance of terms with different colour and spin structures is par for the course in higher-order loop amplitudes in the renormalizable SM, the distinction here is that these appear as the coefficients of ultraviolet divergences, and thus local operators with these structures *must appear at the Lagrangian level* to absorb them.

The colour and Dirac algebra factors can be simplified by applying the $SU(3)$ Fierz identity 3.2.23 and by using equation 3.2.30 to re-express the spin matrices in the basis 3.2.26. Then:

$$\begin{aligned} Q' &= -4\,(\frac{1}{2}\,\delta_{jk}\,\delta_{il} - \frac{1}{6}\,\delta_{ki}\,\delta_{lj})\,(\bar{d}^k_L\gamma^\mu u^i_L)(\bar{u}^l_L\gamma_\mu s^j_L) \\ &= -2(\bar{d}^i_L\gamma^\mu u^j_L)(\bar{u}^j_L\gamma_\mu s^i_L) + \frac{2}{3}(\bar{d}^i_L\gamma^\mu u^i_L)(\bar{u}^j_L\gamma_\mu s^j_L) \end{aligned}$$

The second term has the structure of the original operator Q_1. In the first, quarks in separate billinears form colour singlets together. The (spin) Fierz identities 3.2.33 can then be used to re-order the quarks therein such that each billinear is a colour singlet, giving:

$$Q' = \frac{2}{3}(\bar{d}_L\gamma^\mu u_L)(\bar{u}_L\gamma_\mu s_L) - 2(\bar{d}_L\gamma^\mu s_L)(\bar{u}_L\gamma_\mu u_L) \equiv \frac{2}{3}Q_1 - 2Q_2\,,$$

where the colour indices are again suppressed. We have recovered our original operator, but accompanied by a new structure Q_2. This is 'new' in the sense that we never wrote it down in our Lagrangian. But we did this based on an implicit assumption that the effective interaction was always described by the structure of a tree-level W-boson interaction, in other words by the product of two colour singlet charged currents as in Q_1. From the perspective of the effective field theory, we don't know anything about the charges that underlying state carries. Without advance knowledge of a colourless W, we would have had no bias against the configuration of the colour indices which appears in Q_2. In this case we would have written Q_2 down as a viable operator which can contribute to this process in the first place. Put otherwise, we started out by setting $C_2 = 0$ by hand as a matching condition to reflect that this colour structure does not appear in the SM at tree level, rather than this being forbidden by a structural requirement imposed on our effective field theory. Thus once we include the $\mathcal{O}(\alpha_s)$ corrections from the exchange of virtual gluons, it can appear again.

Pressing on, including the contributions from the rest of the diagrams [6] in Fig. 3.3, we would find that these supplied analogous colour factors arising from each contraction of the virtual gluon between quarks. For transparency, where the quarks carry a common off-shell momentum p (the possible kinematic invariants s, t, u appearing in the QCD logarithms are then all just $-p^2$, and we avoid infrared divergences as $p^2 \to 0$) the ultraviolet divergent portion of the overall amplitude has the structure:

$$\langle Q_1\rangle^{(0)}_{\text{1-loop}} = \left(1+\frac{8}{3}\frac{\alpha_s}{4\pi}\left(\frac{1}{\bar{\epsilon}}+\log\left(\frac{\mu^2}{-p^2}\right)\right)\right)\langle Q_1\rangle^{(0)}_{\text{tree}} \tag{3.4.105}$$
$$+\ \frac{\alpha_s}{4\pi}\left(\frac{1}{\bar{\epsilon}}+\log\left(\frac{\mu^2}{-p^2}\right)\right)\langle Q_1\rangle^{(0)}_{\text{tree}} - 3\,\frac{\alpha_s}{4\pi}\left(\frac{1}{\bar{\epsilon}}+\log\left(\frac{\mu^2}{-p^2}\right)\right)\langle Q_2\rangle^{(0)}_{\text{tree}}$$

Where the divergence on the first line is associated with diagrams in which virtual gluons are emitted and re-absorbed along the same fermion line (these are then associated with the renormalization of the quark wavefunctions, rather than our operator coefficients).

The analogous QCD corrections to Q_2 are identical up to the arrangement of colour indices to which we apply our Fierz identity, leading to an expression with the same structure with $\langle Q_1\rangle \leftrightarrow \langle Q_2\rangle$. This is an explicit example of operator mixing, whereby radiative corrections to the matrix elements of a given operator introduce local terms with the structure of other operators.

In general then, we have to renormalize both of these operators together. We can do this by following the same prescription as we would in the dimension four Lagrangian, with the caveat that our counterterms will take the form of a matrix. Our bare operator Lagrangian for our two structures is just:

$$\mathcal{L}_{us\to bd} = C_1^{(0)}Q_1^{(0)} + C_2^{(0)}Q_2^{(0)} = \delta_{ij}C_i^{(0)}Q_j^{(0)}$$

Where it is understood that $Q_i^{(0)}$ denotes an operator written in terms of bare quark fields $q^{(0)}$. Dipping into the usual renormalization bag of tricks, we can re-express these and the bare Wilson coefficients $C_i^{(0)}$ as $q^{(0)} \to Z_q^{1/2}q$ and $C_i^{(0)} \to Z_{ij}^C C_j$, where we will choose to factorize the UV divergences associated with the correlation functions of the bare operators $Q_i^{(0)}$ into the rescaling factors $Z = 1+\mathcal{O}\left(\alpha_s/\bar{\epsilon}\right)$. We anticipate the matrix form Z_{ij}^C for the rescaling of the Wilson coefficients since our bare matrix element $\langle Q_1\rangle^{(0)}_{\text{1-loop}}$ contained poles associated with Q_1 and Q_2, and distinguish this *additive* renormalization from that performed on the individual quark fields to cancel the divergences in their two-point functions by $Z_q^{1/2}$. In this form, our bare operator Lagrangian is then:

$$\mathcal{L}_{us\to bd} = \delta_{ij}C_i^{(0)}Q_j^{(0)} \equiv Z_q^2 Z_{ij}^C C_j Q_i = C_iQ_i + (Z_q^2Z_{ij}-\delta_{ij})C_jQ_i\,, \tag{3.4.106}$$

where we have rearranged the Lagrangian as usual into a piece with the same form and normalization as the original, written in terms of Q_i (containing the renormalized the quark fields q_i) and renormalized Wilson coefficients C_i. Ultraviolet divergences are now

however contained within the (2×2 matrix of) counterterms $\Delta_{ij} \equiv (Z_q^2 Z_{ij} - \delta_{ij})$, which we fix to cancel the $\mathcal{O}(\alpha_s)$ poles (in $\overline{\text{MS}}$).

Meanwhile, the divergent part of our explicit one-loop amplitude 3.4.105 had the structure:

$$\langle Q_i \rangle^{(0)}_{\text{1-loop}} = Z_{ij} \langle Q_j \rangle^{(0)}_{\text{tree}} \tag{3.4.107}$$

where Z_{ij} carries the $1/\bar{\epsilon}$ poles. Comparing this structure with that of matrix elements calculated using the renormalized Lagrangian 3.4.106, we can identify the choices of the parameters Z_q and Z^C which absorb these into the definitions of the rescaled C_i and q exactly as:

$$\begin{aligned} C_i^{(0)} \langle Q_i \rangle^{(0)}_{\text{1-loop}} = Z_q^2 Z^C_{ij} C_j \langle Q_i \rangle_{\text{1-loop}} &= Z_q^2 Z^C_{ij} C_j Z_{ik} \langle Q_k \rangle_{\text{tree}} = C_j \langle Q_j \rangle \\ &\implies Z_q^2 Z^C_{ij} Z_{ik} = \delta_{jk} \\ &\implies Z^C = (\bar{Z}^T)^{-1}, \end{aligned}$$

where we have factorized out the multiplicative divergences (which we associate with the quark wavefunction renormalization) and the additive ones (which we treat in the coefficient renormalization matrix Z^C) appropriately by writing $Z_{ik} \equiv Z_q^{-2} \bar{Z}_{ik}$. The structure of $\bar{Z}_{ij}$ can be read from the second line of 3.4.105 as:

$$\bar{Z}_{ij} = 1 + \frac{\alpha_s}{4\pi\bar{\epsilon}} \begin{pmatrix} 1 & -3 \\ -3 & 1 \end{pmatrix}$$

Where the values 1 and -3 echo the relative factors in the $SU(3)$ Fierz identity 3.2.23 which we used to express the operator structure falling out of our one-loop calculation in a basis of colour-singlet quark currents.

With the ultraviolet divergences removed, we can use the renormalization group to resum the leading logarithmic corrections $\alpha_s \times \log\left(\frac{\mu^2}{-p^2}\right)$ into the definition of running Wilson coefficients $C_i(\mu)$. Following the usual arguments, we demand that the bare Lagrangian and its parameters be independent of the renormalization scale μ. For our bare Wilson coefficient, we get the condition:

$$\begin{aligned} &\frac{d}{d(\log\mu)}(C_i^{(0)}) = \frac{d}{d(\log\mu)}(Z^C_{ij} C_j) = 0. \\ &\implies Z^C_{ij} \frac{d}{d(\log\mu)}(C_j) + (\frac{d}{d(\log\mu)} Z^C_{ij}) C_j = 0 \end{aligned}$$

$$\implies \frac{d}{d(\log\mu)}(C_j) = -(Z^C)^{-1}_{ki}\left(\frac{d}{d(\log\mu)}Z^C_{ij}\right)(C_j) \equiv \gamma_{kj}C_j$$

Where γ_{ij} is called the anomalous dimension matrix. We can read this from our matrix $\bar{Z} = (Z^T_C)^{-1}$. At $\mathcal{O}(\alpha_s)$ this is:

$$\gamma_{ij} = \frac{\alpha_s}{4\pi}\begin{pmatrix} -2 & 6 \\ 6 & -2 \end{pmatrix} \tag{3.4.108}$$

Where we have used $\frac{d}{d\log\mu}\alpha_s = -2\epsilon\alpha_s + \mathcal{O}(\alpha^2)$. The differential equation governing the running of the Wilson coefficients C_1 and C_2 is now parametrized by a matrix. We say then that C_1 and C_2 mix under the renormalization group. The solution to this equation then takes the form:

$$C_i(\mu) = U_{ij}(\mu,\mu')C_j(\mu')\,, \tag{3.4.109}$$

such that the effective Wilson coefficient C_i seen at the scale μ corresponds to a linear combination of each of the C_j into which C_i mixes at another scale μ'. Suppose that we fix a matching condition, by equating matrix elements in the full and effective theories such as $C_1(\mu = m_W) = 1, C_2(\mu = m_W) = 0$. We would now like to use our effective field theory to describe a lower energy process with, say, a typical energy scale around the bottom quark mass, so we'd like to use matrix elements for which $\mu' = \mathcal{O}(m_b)$. The renormalization group tells us that we can do this for free by using the couplings $C_1(m_b)$ and $C_2(m_b)$. However, this is really a linear combination $C_i(m_b) = U_{ij}(m_b, m_W)\,C_j(m_W)$, such that *even if we fix* $C_2 = 0$ *at the high scale*, it will acquire a finite value when we use calculations appropriate to the energy scale we're interested in.

When we are unaware of what the high energy theory is (particularly the mass M at which we can integrate out the heavy state), this means that the values we ascribe to Wilson coefficients from low-energy measurements correspond to some mixture of those which actually reproduce the behaviour of this state when we calculate matrix elements appropriate to an experiment at $\sqrt{s} = M$. Given γ_{ij}, and some initial conditions by which we fix $C_i(M)$, we can determine the appropriate linear combination of coefficients $C_i(\sqrt{s}_{\text{LHC}})$ that we would see at our collider.

In our example in Fermi theory (constructed to describe the weak interactions of light fermions), we chose to use Fierz identities to express the operator structure appearing in our one-loop matrix element as a linear combination of the two four-fermion

operators Q_1 and Q_2. In the SMEFT, we explicitly construct a set operators using the full set of Standard Model degrees of freedom. We have seen that a basis of 59 operators can parametrize each possible effective interaction these can experience at dimension six. Thus, in this case γ_{ij} is (in a given basis) a 59×59 matrix. We have also encountered the correspondingly large number of interrelations between operators which follow, for example, from the nine equations of motion. As such, the number of degenerate structures which might appear at loop level is far more considerable. Consequently, even with explicit knowledge of its one-loop anomalous dimension matrix (now known in the Warsaw basis [40, 50, 51]), it is non-trivial to translate this information over to another pragmatic or physically motivated choice of operator basis.

Hopefully by this point we have established that calculations in effective field theories are plagued with extensive subtleties. For this reason, they have so far resisted the same level of automation enjoyed by renormalizable models. Central to this has been the degree of arbitrariness in how a set of independent operators can be chosen. In principle however, the identities which give rise to these redundancies are well-understood.

3.4.2 General Improvements to the Symbolic Manipulation of Operators

We will now describe ongoing work towards supplementing FeynRules with an automated framework for performing conversions between sets of operators in the SMEFT. This will be presented in a future publication, and takes the form of a modular extension to the main package. The main functionality we aim to add will be:

- Given any operator Q, determine its classification, mass dimension, gauge invariance and hermiticity. If it carries flavour indices $Q \equiv Q_{\{p_i\}}$, determine the correct structure for its matrix of Wilson coefficients automatically (as in the example 3.2.57).
- Through application of Fierz, integration-by-parts, and equation of motion identities, calculate the possible ways of expressing any Q in terms of linear combinations of other operators; $Q = C'_i Q'_i = C''_j Q''_j \ldots$
- Given a reference basis of linearly independent dimension-six operators $\{Q_i^B\}$, determine the decomposition of any other (set of) operator(s) onto this, i.e. $\mathcal{L} = C_i Q_i \to C_j^B Q_j^B$.

- Given an input Lagrangian $\mathcal{L}(\{Q_i\})$, determine whether the set $\{Q_i\}$ is linearly independent, and if not, identify the redundant linear combinations.

We will again use the Warsaw set [14] as a reference point at dimension six, while noting that - with the exception of the absent $\mathcal{O}(\Lambda^{-2})$ terms in the equations of motion 3.2.41-3.2.49 - much of the relevant machinery extends to operators of higher mass dimension.

Since FeynRules manipulates expressions directly at the level of the Lagrangian, the discussion can be framed through direct analogy with analytic expressions written in terms of operators. Each of features described henceforth is new, and presented here are only those which are functional and at a stage of approximate completion.

FeynRules is perhaps unsurprisingly designed with the extraction of Feynman rules from a Lagrangian as a priority. While this is useful for the calculation of matrix elements, this means that the its machinery predominantly manipulates objects written directly in terms of fields, rather than gauge invariant operators. Consequently, expressions representing Lagrangian level objects such as covariant derivatives and field strength tensors are interpreted immediately in terms of their explicit definitions in this form, i.e.:

$$\begin{aligned}(D_\mu q)^{\alpha j} &\to \left(\partial_\mu + i g_s T^A_{\alpha\beta} G^A_\mu + i g_2 \tau^I_{jk} W^I_\mu + i g_1 Y_q B_\mu\right) q^{\beta k},\\ G^A_{\mu\nu} &\to \partial_\mu G^A_\nu - \partial_\nu G^A_\mu - g_s f^{ABC} G^B_\mu G^C_\nu,\end{aligned}$$

For this reason, expressions built from the symbolic objects representing the fundamental quantities are not directly aware of all of their own properties. Requirements such as hermiticity are not imposed, while gauge invariance is confirmed by checking the conservation of quantum numbers at the level of the extracted vertices, rather than being identified through a structural understanding of the Lagrangian. Hence operators built from these which, for example, carry a symmetry in their indices do not reflect this as expressions.

In order to unambiguously perform algebraic operations which map effective operators onto related linear combinations while ensuring that the resulting expressions possess the correct properties, an extra layer of structure at the Lagrangian level must be established. We also have to fix a convention for expressing individual operators in a unique way. The baseline functionality implemented to accomplish this can be summarized as:

- Operators built from objects which possess a symmetry in (any of) their indices reflect this. For example, $Q \equiv \varepsilon_{IJK}(\varphi^\dagger\tau^I\varphi)(\varphi^\dagger\tau^J\varphi)(\varphi^\dagger\tau^K\varphi) = 0$ by the antisymmetry of ε_{IJK} and because each of the $SU(2)$ triplets are identical. Likewise, the order in which indices appear within symmetric and antisymmetric tensors is always fixed to a canonical choice, accompanied by the appropriate signature, i.e. $f^{ACB} \equiv -f^{ABC}$. Two operators are considered the same if their field content and relative index structure is identical.

- When encountering a situation in which a symmetry in an operator's indices means that it is in disguise and actually belongs to another classification, this is recognized and corrected for automatically. For example, in writing down $Q' \equiv (\bar{q}\sigma^{\mu\nu}d)(D_\mu D_\nu\varphi)$ which naively belongs to the $\psi^2\varphi D^2$ classification, the antisymmetry of the Lorentz indices in $\sigma^{\mu\nu}$ projects out the antisymmetric part of the covariant derivatives; $(D_\mu D_\nu)\varphi \to \frac{1}{2}[D_\mu, D_\nu]\varphi \equiv -i\frac{1}{2}Y_\varphi g_1 B_{\mu\nu}\varphi - \frac{1}{2}g_2 W^I_{\mu\nu}\tau^I\varphi$. Thus this operator doesn't, for example, generate vertices sensitive to the momentum of the Higgs, and it is expressed as: $Q' = C_1Q_1 + C_2Q_2 =\subset \psi^2X\varphi = -i\frac{1}{2}Y_\varphi g_1(\bar{q}\sigma^{\mu\nu}d)\varphi B_{\mu\nu} + \frac{1}{2}g_2(\bar{q}\sigma^{\mu\nu}\tau^I d)\varphi W^I_{\mu\nu}$.

- Gauge invariance is ensured symbolically by requiring that the fields constituting each operator carry indices which are contracted to form an overall singlet under the SM gauge group $\boldsymbol{\mathcal{G}}_{SM}$.

- Hermiticity is ensured symbolically by comparing each operator to its hermitian conjugate. For any $\mathcal{L}$ containing an operator $Q \neq Q^\dagger$, the presence of $Q^\dagger$ is always ensured by adding it if it were not present.

- Wilson coefficients C_i are allocated with properties appropriate to the operator they accompany. These are equipped with mass dimensions, real and imaginary parts and number of flavour indices inferred directly from the properties of Q_i.

- Dirac matrix structures are decomposed automatically onto the basis 3.2.26 wherever applicable, with the appropriate coefficients calculated using gamma matrix trace identities according to 3.2.30. For example, the current-current operator encountered in the one-loop QCD corrections to the Fermi interaction carrying the vertex structure $(\gamma^\nu\gamma^\lambda\gamma^\mu)_{\bar{\psi}_1\psi_2} \otimes (\gamma_\nu\gamma_\lambda\gamma_\mu)_{\bar{\psi}_3\psi_4}$ is automatically converted to the form $16\,(\gamma^\mu)_{\bar{\psi}_1\psi_2} \otimes (\gamma_\mu)_{\bar{\psi}_3\psi_4}$.

With these conventions in place, a given operator Lagrangian is written unambiguously, and the prerequisites of gauge invariance and hermiticity are enforced.

3.4.3 Applying Operator Identities

To distinguish the roles of each of the identities discussed in establishing redundant linear combinations, we can factorize a given operator Q schematically as:

$$Q(\{\Phi\}) \equiv [SU(2)] \times [SU(3)] \times [\Gamma] \times (\{D\} \cdot \{\Phi\}) \ ,$$

Where the factors $[SU(N)]$ stand in for the colour and weak isospin matrices with indices in the configuration in which they appear, while $[\Gamma]$ contains the analogous Dirac matrices appearing in any fermion billinears. Any covariant derivatives are contained within $\{D\}$, which is implicitly understood to associate each of these (if any) with the field on which it acts, hence the suggestive writing as a dot product. The field content alone is represented by $\{\Phi\}$.

Written in this way, applying the Fierz identities for weak isospin (3.2.22), colour (3.2.23), or spin (3.2.33) amounts to rewriting the corresponding matrices within the factors $[SU(2)]$, $[SU(3)]$ or $[\Gamma]$ respectively, while leaving the remaining factors intact. Similarly, using the integration-by-parts relations exchanges the arrangement of covariant derivatives specified by $\{D\}$ in favour of a linear combination of the other arrangements which occur in the total derivative, as described in section . Rewriting an operator in terms of those related to it through the equations of motion (3.2.41-3.2.49) will in general modify each of these factors, as these identities relate operators with different field contents to each other.

To illustrate this decomposition explicitly, we can write a few dimension-six operators in this form, leaving flavour indices suppressed:

$$\begin{aligned}
Q_{u\varphi} &\equiv (\varphi^\dagger\varphi)(\bar{q}u\widetilde{\varphi}) \to [\delta_{ij}\delta_{kl}]_{SU(2)} \times [\delta_{ab}]_{SU(3)} \times [\delta_{s_1s_2}]_{\text{spin}} \times \{\varphi_i^\dagger,\, \varphi_j,\, \bar{q}_{s_1}^{k\,a},\, u_{s_2}^b,\, \widetilde{\varphi}_l\} \\
Q_2 &\equiv (\bar{l}\sigma^{\mu\nu}D_\mu e)D_\nu\varphi \to [\delta_{ij}]_{SU(2)} \times [\delta_{s_1s_2}]_{\text{spin}} \times [\sigma^{\mu\nu}_{s_1s_2}]_{\text{spin}} \times \left(\{1,\, D_\mu,\, D_\nu\} \cdot \{\bar{l}^i_{s_1},\, e_{s_2},\, \varphi_j\}\right) \\
Q_{qd}^{(8)} &\equiv (\bar{q}\gamma_\mu T^A q)(\bar{d}\gamma^\mu T^A d) \to [\delta_{ij}]_{SU(2)} \times [T_{ab}T_{cd}]_{SU(3)} \times [\gamma_{s_1s_2}\gamma_{s_3s_4}]_{\text{spin}} \times \{\bar{q}^{i\,a}_{s_1},\, q^{j\,b}_{s_2},\, \bar{d}^c_{s_3},\, d^d_{s_4}\}
\end{aligned}$$

Here, the individual factors which may be re-expressed to generate redundant linear combinations using Fierz and integration-by-parts identities are highlighted in red and blue. By factorizing operators internally this way, the possible transformations which can be applied to each is determined automatically, enabling these to be carried out in accordance with any algorithm which specifies the operator content of a basis. In this example, $Q_{u\varphi}$ and $Q_{qd}^{(8)}$ are operators belong to the Warsaw set 3.3. The operator content

of a target basis B can be specified, such that when applying a transformation to an operator $Q \notin B$ produces a linear combination which includes one element $Q_B \in B$, i.e. $Q \to C'Q' + C^B Q^B$, Q_B meets the criteria for being in the desired form, and Q' does not.

Given one complete basis of operators and a general implementation of each of the operator identities discussed, we can in principle transform any dimension-six Lagrangian by applying these repeatedly until every Q is written in the form $C_i^B Q_i^{B*}$.

We now summarize the implementation of each operator identity in turn. These are applied directly to operator expressions, and return the associated redundant linear combinations.

Fierz Identities

The application of the Fierz identities (3.2.22), (3.2.23), and (3.2.33) is the simplest transformation we can perform, the practical applications of which we have already encountered. For an operator which qualifies - i.e. one with an arrangement in which fields are contracted between two $SU(N)$ or Dirac matrices, these can be applied individually or in combination to redirect the indices carried by the fields as desired. Using the example of $Q_{qd}^{(8)}$ above, we could sequentially transform this as:

$$\begin{aligned}
Q_{qd}^{(8)} = \quad & [\delta_{ij}]_{SU(2)} \times [T_{ab}T_{cd}]_{SU(3)} \times & & [\gamma_{s_1 s_2}\gamma_{s_3 s_4}]_{\text{spin}} \times \{\bar{q}_{s_1}^{i\,a},\, q_{s_2}^{j\,b},\, \bar{d}_{s_3}^{c},\, d_{s_4}^{d}\} \\
\overset{(3.2.23)}{\to} \quad & [\delta_{ij}]_{SU(2)} \times [\frac{1}{2}\,\delta_{ad}\,\delta_{cb} - \frac{1}{6}\,\delta_{ab}\,\delta_{cd}]_{SU(3)} \times & & [\gamma_{s_1 s_2}\gamma_{s_3 s_4}]_{\text{spin}} \times \{\bar{q}_{s_1}^{i\,a},\, q_{s_2}^{j\,b},\, \bar{d}_{s_3}^{c},\, d_{s_4}^{d}\} \\
\overset{(3.2.36)}{\to} \quad & [\delta_{ij}]_{SU(2)} \times [\frac{1}{2}\,\delta_{ad}\,\delta_{cb} - \frac{1}{6}\,\delta_{ab}\,\delta_{cd}]_{SU(3)} \times & & [-2\,\delta_{s_1 s_4}\delta_{s_3 s_2}]_{\text{spin}} \times \{\bar{q}_{s_1}^{i\,a},\, q_{s_2}^{j\,b},\, \bar{d}_{s_3}^{c},\, d_{s_4}^{d}\}
\end{aligned}$$

Where the colour indices are suppressed in the first operator since the billinears are each colour singlets. In doing this, we have re-expressed $Q_{qd}^{(8)}$ in a different basis of operators, as:

$$Q_{qd}^{(8)} = C_1' Q_1' + C_2' Q_2' = -(\bar{q}d)(\bar{d}q) + \frac{1}{3}(\bar{q}_a d_b)(\bar{d}_b q_a).$$

The generalization to the case of more than two $SU(N)$ or Dirac matrices is included, although this is only relevant to mapping out the redundancies of operators of mass dimension eight and higher. The maximum number of distinct $SU(N)$ matrices which can arise at dimension-eight is four, corresponding to eight φ fields carrying indices in

*The full automation of this process - i.e. setting up conditions such that the appropriate identities are selected and applied recursively until this is satisfied - is a feature still under development.

the fundamental representation of $SU(2)$. In this case, when an operator possesses a structure such as:

$$Q_{\text{D8}} = [\tau_{ij}\tau_{kl}\tau_{mn}\tau_{op}]_{SU(2)} \times (\dots)$$

The Fierz identities can be used to re-express the desired pairwise combination(s) of the matrices τ.

Integration-by-Parts Identities

Using the above example of the operator Q_2, integration-by-parts identities are implemented by replacing the configuration of covariant derivative factors appropriately. We had:

$$Q_2 = (\bar{l}\sigma^{\mu\nu}D_\mu e)D_\nu\varphi = [\delta_{ij}]_{SU(2)} \times [\delta_{s_1s_2}]_{\text{spin}} \times [\sigma^{\mu\nu}_{s_1s_2}]_{\text{spin}} \times \left(\{1,\, D_\mu,\, D_\nu\} \bullet \{\bar{l}^i_{s_1},\, e_{s_2},\, \varphi_j\}\right)$$

Since there are two covariant derivatives, there are two redundant linear combinations which are identified. There associated with $D_\mu\mathcal{O}^\mu = 0$ and $D_\nu\mathcal{O}^\nu = 0$ respectively, where $\mathcal{O}^{\mu_i}$ represents the operator with D_{μ_i} removed, as discussed in section 3.4.3. These translate into our schematic language in each case as:

$$\begin{aligned} D_\mu\mathcal{O}^\mu &= D_\mu\left((\bar{l}\sigma^{\mu\nu}e)D_\nu\varphi\right) = 0 \\ &\implies [\dots] \times (\{D_\mu,\, 1,\, D_\nu\} + \{1,\, D_\mu,\, D_\nu\} + \{1,\, 1,\, D_\mu D_\nu\}) \bullet \{\bar{l}^i_{s_1},\, e_{s_2},\, \varphi_j\} = 0, \\ &\text{And:} \\ D_\nu\mathcal{O}^\nu &= D_\nu\left((\bar{l}\sigma^{\mu\nu}D_\mu e)\varphi\right) = 0 \\ &\implies [\dots] \times (\{D_\nu,\, D_\mu,\, 1\} + \{1,\, D_\nu D_\mu,\, 1\} + \{1,\, D_\mu,\, D_\nu\}) \bullet \{\bar{l}^i_{s_1},\, e_{s_2},\, \varphi_j\} = 0. \end{aligned}$$

Where the matrices contracting field indices are understood to sit in the factors $[\dots]$*. Identifying the related linear combinations can then be accomplished by making the replacements:

$$\begin{aligned} \{1,\, D_\mu,\, D_\nu\} &\to -\left(\{D_\mu,\, 1,\, D_\nu\} + \{1,\, 1,\, D_\mu D_\nu\}\right) \\ \{1,\, D_\mu,\, D_\nu\} &\to -\left(\{D_\nu,\, D_\mu,\, 1\} + \{1,\, D_\nu D_\mu,\, 1\}\right), \end{aligned}$$

*This is just a convoluted way of expressing the Leibniz rule; $\frac{d}{dx}(fgh) = \frac{df}{dx}gh + f\frac{dg}{dx}h + fg\frac{dh}{dx}$.

So that we can re-express Q_2 in two ways:

$$\begin{aligned} Q_2 &= -(D_\mu \bar{l}\sigma^{\mu\nu} e) D_\nu \varphi - (\bar{l}\sigma^{\mu\nu} e) D_\mu D_\nu \varphi \\ &= -(D_\nu \bar{l}\sigma^{\mu\nu} D_\mu e)\varphi - (\bar{l}\sigma^{\mu\nu} D_\nu D_\mu e)\varphi \end{aligned}$$

Note that in each case, the redundant linear combinations contain the structures $\sigma^{\mu\nu} D_\mu D_\nu \varphi$ and $\sigma^{\mu\nu} D_\mu D_\nu e$ respectively. As was mentioned, these are further simplified automatically by the antisymmetry of the Lorentz indices. This dictates $(D_\mu D_\nu)\varphi \to \frac{1}{2}[D_\mu, D_\nu] \propto X_{\mu\nu}$. These are replaced by the appropriate field strength tensors based on the hypercharges and gauge indices carried by φ and e. In the language of [14], this moves these operators to lower classification, in both cases:

$$\boxed{\psi^2 \varphi D^2} \to \boxed{\psi^2 \varphi D^2} + \boxed{\psi^2 X \varphi}$$

The implementation of integration-by-parts identities in this way extends automatically to operators of higher mass dimension.

Equation of Motion Identities

Using the Standard Model Euler-Lagrange equations 3.2.41-3.2.49 to identify related operators is - from an implementation standpoint - the most complex case. For our example we'll need the equation of motion for the gluon, which is repeated here for convenience:

$$(D^\rho G_{\rho\mu})^A - g_s \left(\bar{q}\gamma_\mu T^A q \;+\; \bar{u}\gamma_\mu T^A u \;+\; \bar{d}\gamma_\mu T^A d\right) = 0$$

We will once again take $Q_{qd}^{(8)}$ as our demonstration operator*, which we re-express with two choices of highlighting:

$$\begin{aligned} Q_{qd}^{(8)} \equiv (\bar{q}\gamma_\mu T^A q)(\bar{d}\gamma^\mu T^A d) \quad &\to [\delta_{ij}]_{SU(2)} \times [T_{ab} T_{cd}]_{SU(3)} \times [\gamma_{s_1 s_2} \gamma_{s_3 s_4}]_{\text{spin}} \times \{\bar{q}_{s_1}^{i\,a},\, q_{s_2}^{j\,b},\, \bar{d}_{s_3}^{c},\, d_{s_4}^{d}\} \\ &\equiv [\delta_{ij}]_{SU(2)} \times [T_{ab} T_{cd}]_{SU(3)} \times [\gamma_{s_1 s_2} \gamma_{s_3 s_4}]_{\text{spin}} \times \{\bar{q}_{s_1}^{i\,a},\, q_{s_2}^{j\,b},\, \bar{d}_{s_3}^{c},\, d_{s_4}^{d}\} \end{aligned}$$

Where the pieces highlighted in purple collectively coincide with terms in the gluon equation of motion. This is identified by testing the operator for the specific structures which occur therein, in this case for each of the colour-octet, flavour-diagonal quark currents. Since there are two currents which satisfy this, $Q_{qd}^{(8)}$ can be re-expressed in two

*Here it is understood that each quark billinear is diagonal in flavour.

ways. Only the highlighted components are then replaced, according to the appropriate rearrangements:

$$\bar{d}\gamma_\mu T^A d \to \frac{1}{g_s} D^\rho G^A_{\rho\mu} - \bar{q}\gamma_\mu T^A q - \bar{u}\gamma_\mu T^A u\,,$$
$$\bar{q}\gamma_\mu T^A q \to \frac{1}{g_s} D^\rho G^A_{\rho\mu} - \bar{u}\gamma_\mu T^A u - \bar{d}\gamma_\mu T^A d$$

The linear combinations are then just:

$$\begin{aligned} Q^{(8)}_{qd} &= \frac{1}{g_s}(\bar{q}\gamma_\mu T^A q) D^\rho G^A_{\rho\mu} - (\bar{q}\gamma_\mu T^A q)(\bar{q}\gamma_\mu T^A q) - (\bar{q}\gamma_\mu T^A q)(\bar{u}\gamma_\mu T^A u) \\ &= \frac{1}{g_s}(\bar{d}\gamma^\mu T^A d) D^\rho G^A_{\rho\mu} - (\bar{d}\gamma^\mu T^A d)(\bar{u}\gamma_\mu T^A u) - (\bar{d}\gamma^\mu T^A d)(\bar{d}\gamma_\mu T^A d) \end{aligned}$$

In this case, the operator contained two fermion currents which appeared in the Euler-Lagrange equation for the gluon. Generally, a given operator is tested for the presence of any structures coinciding with those in any one of the nine equations of motion. We started with the Warsaw operator $Q^{(8)}_{qd} \in \boxed{\psi^4}$, and a central ingredient in establishing this basis was the requirement that the operators therein belong to the lowest possible classifications. This was achieved by using the equations of motion to rewrite operators in terms of those containing fewer covariant derivatives. This amounts to making the replacement $(D^\rho G_{\rho\mu})^A \to$ (colour currents) whenever possible and never the converse, with a directly analogous statement holding for the remaining eight equations. By using them as in the way we have in this example, we can reverse the 'reduction' procedure, and generate operators in higher classifications if they suit our purposes.

Testing operators for the presence of structures which appear in the equations of motion is usually fairly transparent, as in the above example. The exception to this is operators which contain covariant derivatives within fermion billinears. Recall that, as part of our conventions, any spinor product with a complicated Dirac structure (such as $\sigma^{\mu\nu}\sigma^{\rho\kappa}$, or - as in our one-loop example - $\gamma^\mu\gamma^\nu\gamma^\rho$) was automatically decomposed onto a linear combination of billinears expressed in the usual basis $\Gamma^A \equiv \{\mathbb{I}, \gamma_5, \gamma^\mu, \gamma^\mu\gamma_5, \sigma^{\mu\nu}\}$. Since the fermion equations of motion (3.2.41)-(3.2.45) permit replacements of the form $i\not{D}\psi \equiv \gamma^\mu D_\mu \psi \to (\ldots)$, if we aspire to automatically identify and determine redundant structures we must be able to robustly test whether the Dirac matrix structure can be re-expressed in this form.

To this end, we automate and generalize the prescription established in Section 6 of Ref. [14]. We can look first at a simple example. For a general fermion current making

up one part of a gauge-invariant operator Q, we could encounter something like:

$$Q \equiv (\bar{\psi}_1 \sigma^{\mu\nu} D_\nu \psi_2)\mathcal{O}_\mu \,,$$

Where $\mathcal{O}_\mu$ denotes the rest of the operator. Because we are concerned with the space-time degrees of freedom alone, structure reflecting the representations of the fields in the gauge groups is suppressed. In this simple example, we need to identify that $D_\nu\psi_2$ appears without the associated γ^ν necessary to render this redundant with other operators through the equations of motion. Once this condition has been established, we can re-express the tensor current $\sigma^{\mu\nu} \in \{\Gamma^A\}$ back into a product of gamma matrices using the identity $\sigma^{\mu\nu} = i(\gamma^\mu\gamma^\nu - g^{\mu\nu}\mathbb{I})$. We then have a linear combination:

$$Q = i(\bar{\psi}_1 \gamma^\mu \not{D}\psi_2)\mathcal{O}_\mu - i(\bar{\psi}_1 D^\mu \psi_2)\mathcal{O}_\mu \,,$$

Where the equation of motion for ψ_2 can be used directly on the first operator.

In more complicated cases we would like to be able to determine exactly how we should apply identities to establish definitively whether or not we can reproduce something which occurs in the equations of motion. To do this automatically we need a robust procedure based only on the structure of the operator presented to us. This is accomplished generally by identifying the arrangement of Dirac matrices which occur in an operator with the same field content and arrangement of gauge indices which *is* reducible using the EoM. The spin matrices of this can then be decomposed onto the basis $\{\Gamma^A\}$, and if this decomposition contains the structure present in our original operator, we can re-express it accordingly to get our EoM reducible linear combination. For example, consider something like:

$$Q \equiv (D_\mu\bar{\psi}_1\gamma_\rho D_\nu\bar{\psi}_2)\mathcal{O}^{\mu\nu\rho} = (D_\mu\bar{\psi}_1\gamma^\rho D_\nu\bar{\psi}_2)g^{\mu\alpha}g^{\nu\beta}\mathcal{O}_{\alpha\beta\rho} \,,$$

Again, $\mathcal{O}$ is everything outwith our fermion billinear. We've highlighted in purple the structures carrying Lorentz indices which we want to check can be written in a form which gives us $\not{D}\psi$. Meanwhile, the redundant linear combinations arising from applying the equations of motion for ψ_1 and ψ_2 respectively come from the structures:

$$(D_\mu\bar{\psi}_1\gamma^\mu\sigma^{\rho\alpha}D_\nu\bar{\psi}_2)g^{\nu\beta}\mathcal{O}_{\alpha\beta\rho} \qquad \text{and} \qquad (D_\mu\bar{\psi}_1\sigma^{\rho\beta}\gamma^\nu D_\nu\bar{\psi}_2)g^{\mu\alpha}\mathcal{O}_{\alpha\beta\rho} \,.$$

We calculate the decomposition of the desirable form onto $\{\Gamma^A\}$, as:

$$\gamma^\mu\sigma^{\rho\alpha} = -i\gamma^\rho g^{\mu\alpha} + i\gamma^\alpha g^{\mu\rho} - \epsilon^{\alpha\mu\rho\kappa}\gamma_\kappa\gamma_5$$
$$\sigma^{\rho\beta}\gamma^\nu = i\gamma^\rho g^{\nu\beta} - i\gamma^\beta g^{\nu\rho} - \epsilon^{\beta\nu\rho\kappa}\gamma_\kappa\gamma_5\,,$$

where it is confirmed that we can indeed massage our fermion billinear into a form which contains a redundancy through the equations of motion. This is then performed in each of the two possible ways, giving us our pair of linear combinations:

$$\begin{aligned} Q &= i(\not{D}\bar{\psi}_1\sigma^{\rho\alpha}D_\nu\bar{\psi}_2)\mathcal{O}^{\alpha\nu\rho} - (D_\mu\bar{\psi}_1\gamma_\alpha D_\nu\bar{\psi}_2)\mathcal{O}^{\alpha\nu\mu} + i(D_\mu\bar{\psi}_1\gamma_\kappa\gamma_5 D_\nu\bar{\psi}_2)\epsilon^{\alpha\mu\rho\kappa}\mathcal{O}_{\alpha\nu\rho} \\ &= -i(D_\mu\bar{\psi}_1\sigma_{\rho\beta}\not{D}\bar{\psi}_2)\mathcal{O}_{\mu\beta\rho} + (D_\mu\bar{\psi}_1\gamma_\beta D_\nu\bar{\psi}_2)\mathcal{O}^{\mu\beta\nu} - i(D_\mu\bar{\psi}_1\gamma_\kappa\gamma_5 D_\nu\bar{\psi}_2)\epsilon^{\beta\nu\rho\kappa}\mathcal{O}_{\mu\beta\rho} \end{aligned}$$

In this way, we have a concrete prescription for establishing the linear combinations through which fermionic current operators can be related to those in different classifications, and the gamma matrix algebra is performed automatically. This procedure is also not restricted to dimension six.

Functionality in Development

We have demonstrated thus far that the application of operator identities in the SMEFT (at least at dimension-six) can be incorporated into the FeynRules framework. Determining which of these can be used in a given context is a task which is automated by subjecting operators to pattern recognition. The application of each of the permissible transformations to a given operator is achieved by making the appropriate structural replacements in accordance with clearly defined rules. We also outlined functionality to decompose and re-express tensor structures in a purposeful way without manual input.

The current task is now automating the directed application of the operator identities in such a way that any given set is decomposed onto a specified basis. This amounts to constructing a recursive algorithm which selects and applies operator identities intelligently, using the equations of motion to move between classifications. To facilitate doing this in general, we can first aim to emulate the decision-making procedure used to derive the Warsaw basis, which enshrined the requirement that classifications be lowered wherever possible. Work in this direction is currently underway.

3.5 Outlook

In this chapter we have described and explored the SMEFT Lagrangian, with an emphasis on dimension-six operators. We have established how operators are individually structured and how they can be related to each other, and given some examples of simplifying assumptions which reduce the number of these which need to be considered.

We saw that the inclusion of the Warsaw basis of higher-dimensional operators necessitated sweeping parameter redefinitions throughout the Standard Model Lagrangian, and that these can be accounted for in a FeynRules model which we can interface to event generators.

In our example of operator mixing, we saw how radiative corrections to higher dimensional operators can, in general, induce local terms associated with other operators. As a consequence of this, the evolution of Wilson coefficients under the renormalization group is encoded by a matrix, such that a fixed coefficient $C_i(\mu)$ at the scale μ corresponds to a linear combination of several coefficients at a different scale μ'. In this context, the radiatively generated operators which appear do not respect our choice of operator basis, and we must reduce them back into a desired form using operator identities on a case-by-case basis*.

It was shown that identifying these redundancies and applying operator identities is achievable at the Lagrangian level within FeynRules, and that the necessary machinery to identify redundant linear combinations can be automated. A natural next step is to extend this framework into something which can translate between generic bases by systematically transforming operators symbolically. This would alleviate the inherently labour-intensive procedure of doing this by hand on a case-by-case basis, and serve as an important ingredient in the automation of higher order calculations.

*No pun intended.

Chapter 4

Constraining Dimension Six Operators in Top Quark Production

Resonance searches during runs I and II of the LHC have so far failed to shed light on the physics responsible for Electroweak symmetry breaking, a description of which is imperative for the theoretical consistency of the SM. The prediction of new states around the TeV scale is a generic feature of models aiming to address this mystery, and continually higher experimental limits set on their masses cast doubts on the explanations so far conceived. While a significant mass gap between the Electroweak scale and that of new physics is disconcerting - for both our immediate discovery prospects and hopes to resolve the hierarchy problem, such a scenario - where $\Lambda_{NP} \gg v$ - is ideal for applying EFT methods.

The ascension of the SMEFT in recent years - plausibly a natural response to this lack of discoveries - has seen the fragmented, ad-hoc model-independent approaches of old replaced by a universal language. This paradigm shift away from ambiguous constructions - such as the parametrisation of deviations in cross section measurements with simple 'signal strength' ratios, or in general differential observables with 'anomalous couplings' - is a welcome development arguably following from our failure to observe new states. From a phenomenological perspective, the ability to match higher-dimensional operators to UV completions in a well-defined way, their natural contribution to differential observables, and their consistency with higher-order perturbative calculations has made EFT the model-independent tool of choice.

Next to studying the scalar boson itself, our most promising windows into the physics behind EWSB are the SM degrees of freedom which couple most strongly to the Higgs field. The top quark, with its $\mathcal{O}(1)$ Yukawa coupling and central role in establishing

the hierarchy problem, is then a natural candidate for close scrutiny. The top thus plays an important part in most prominent UV-complete models. In supersymmetric extensions to the SM, the quantum corrections of the stop quark to the Higgs mass parameter cancel those of the top, the dominant factor toward eliminating the need for fine-tuning (see, e.g. [60, 61]). In composite Higgs theories [62, 63], the size of y_t is indicative of the strength of its interaction with new states in the strongly coupled sector. Likewise in models with warped extra dimensions [64, 65], the top preferentially couples to Kaluza-Klein modes propagating in the 5D bulk.

The modifications to Higgs boson phenomenology predicted by BSM scenarios have inspired widespread application of EFT methods to constraining NP in the Higgs sector [66–83]. However, these investigations are currently hindered by the relatively small statistics collected in the observed Higgs production channels.

In contrast to this, the direct production of tops by the QCD interaction and the relative manageability of the associated final states have led to an abundance of data from the LHC and TeVatron. Model-independent studies into the possibility of detecting new physics in the top sector have thus been a complementary agenda in which the SMEFT has featured prominently [84–93]. While these have produced constraints on dimension-six Wilson Coefficients, so far only limited subsets of all possible operators which modify top phenomenology have been considered at a given time. Such an approach is justified whenever the physics application is specialized to processes sensitive only to particular coupling structures, such as in parametrizing FCNCs [87, 88] or in investigating contributions of the top to precision electroweak observables [86, 94].

The wealth of measurements of the main top quark production modes motivates the desire for a tool with which plentiful statistics can confront the most general set of dimension-six operators in the SMEFT simultaneously. This was realized in [2], where we performed the first global fit of all relevant Wilson Coefficients to the full available set of suitable differential and inclusive measurements of top pair and single top quark production. In [3], this was expanded upon to incorporate both new datasets from the 8 and 13 TeV LHC and additional observables.

4.1 Top Quark Observables in the SMEFT

The leading modifications of dimension-six operators to SM phenomenology at $\mathcal{O}(\Lambda^{-2})$ arise through the interference of Feynman diagrams containing a single dimension-six operator insertion from $\mathcal{L}^{(6)}$ with those originating from $\mathcal{L}^{(4)}_{\text{SM}}$. In an expansion of the matrix element $\mathcal{M}$ in the dimension-six couplings C this takes the form:

$$|\mathcal{M}_{\text{tot}}|^2 = |\mathcal{M}_{\text{SM}}|^2 + 2\Re\mathfrak{e}\ \{\mathcal{M}_{\text{SM}}\mathcal{M}^*_{D6}\} + |\mathcal{M}_{D6}|^2 + \mathcal{O}(\Lambda^{-4}),$$

where the third term, representing the squared contribution of the set of dimension-six diagrams, is itself formally $\mathcal{O}(\Lambda^{-4})$. As these terms enter at the same order in Λ^{-1} as the interference with the SM of operators belonging to $\mathcal{L}^{(8)}$*, they are usually discarded. Provided a given Wilson Coefficient C is small, such a truncation is typically valid and the squared dimension-six terms are numerically subleading.

However, in cases where the interference of a dimension-six operator with the SM is zero (e.g. when it possesses an orthogonal colour structure to the SM QCD process) or suppressed (e.g. by light fermion masses which appear when operator vertices containing right-handed fields intefere with left-handed weak interaction) this is no longer strictly true. In such a scenario, the dominant contributions to the observable of interest come from both $|\mathcal{M}_{D6}|^2$ and $\mathcal{M}_{\text{SM}}\mathcal{M}^*_{D8}$, the latter of which is unknown in general. In the absence of explicit structural arguments for why interfering dimension-eight terms must be subdominant to $|\mathcal{M}_{D6}|^2$†, a fixed-order approach should abandon such operators in the analysis. In general, it is also not possible to exclude the possibility of anomalously large dimension-eight coefficients without making model-dependent assumptions. A comprehensive discussion exploring how these scenarios can arise from UV-complete models was given in [56].

We generally expect the contributions of higher-dimensional operators to a given observable to vary over the phase space of the final state particles. The contribution to the total cross section σ from the interference terms in a $2 \to n$ reaction will take the usual form:

$$d\sigma_{2\to n} = \frac{(2\pi)^4}{2\sqrt{\lambda(s, m_1^2, m_2^2)}} \times \overline{\mathcal{M}^2}_{int} \times d\Pi_n, \tag{4.1.1}$$

*That is - those that belong to the explicitly neglected terms $\mathcal{O}(\Lambda^{-4})$. A complete operator basis at mass dimension eight is yet to be determined, however recent efforts (see, e.g. [95]) have mapped out the schematic field content and number of Wilson Coefficients of each classification.

†We will encounter one example of this in $gg \to t\bar{t}$ production.

where $\overline{\mathcal{M}^2}_{int} \equiv 2\,\Re\mathfrak{e}\,(\overline{\mathcal{M}^*_{SM}\mathcal{M}_{D6}})$ is the $\mathcal{O}(\Lambda^{-2})$ part of the squared probability amplitude averaged appropriately over spin/polarization and gauge degrees of freedom. $\overline{\mathcal{M}^2}_{int}$ is dimensionless through its dependence on the kinematic invariants and the (fixed) scale Λ^{-2} carried by the Wilson Coefficients. Then, the cross section for a final state f described by any dimensionful kinematic invariant k_f^2 (e.g. the transverse momentum p_T^2, or invariant mass m_f^2) scales as $d\sigma \propto k_f^2/\Lambda^2$. Consequently, deviations from the Standard Model will be most pronounced in harder reactions. Of course, this scaling behaviour is only physical within the range of EFT's validity $\sqrt{s} \ll \Lambda$, and at larger momentum transfers higher order terms in the EFT expansion become more important.

Recently a lot of progress has been made in extending the dimension six-extended SM to higher perturbative orders in the SM couplings [40, 50, 51, 96–106]. As with radiative corrections in the renormalizable SM, the one-loop effects of dimension-six operators are formally suppressed by $\mathcal{O}(g_{SM}^2/16\pi^2)$. Generally then, these will be subleading when compared with the tree-level dimension-six contributions. It is well known, however, that NLO QCD corrections to particular SM processes (such as in top pair production, with an overall k-factor of $\approx 50\%$) can be $\mathcal{O}(1)$. Although there is no reason to assume that similarly large k-factors might apply to the SMEFT, the calculation of these is less essential than in the SM, where radiative corrections are essential to obtain an accurate description of a physical process within the experimental uncertainties. Current consistency of the renormalizable SM alone with experimental data makes precise signal modelling less pressing until we observe *some* non-resonant effect with statistical significance. QCD corrections to four fermion operators included via renormalization group equations are typically of the order of 15%, depending on the resolved phase space [102]. Hereon we suppress the argument μ when referring to Wilson Coefficients $C_i(\mu)$, noting that these should be understood as being evaluated at the scale $\mu \sim m_t$, and as such correspond to a linear combination of the same coefficients evaluated at the high scale $C_i(\Lambda)$.

As pointed out in Ref. [107], NLO effects can also become important in electroweak precision data fits. Similarly, four-fermion operators entering at the one-loop level to the Higgs decays $h \to b\bar{b}$ and $h \to \tau^+\tau^-$ can be effectively constrained by measurements of these processes, as recently pointed out in [106].

In top physics, we encounter the following subset of effective operators at leading order, expressed in the 'Warsaw basis' [54]:*

$$
\begin{aligned}
Q_{qq}^{(1)} &= (\bar{q}\gamma_\mu q)(\bar{q}\gamma^\mu q) & Q_{uW} &= (\bar{q}\sigma^{\mu\nu}\tau^I u)\tilde{\varphi}W^I_{\mu\nu} & Q_{\varphi q}^{(3)} &= i(\varphi^\dagger \overleftrightarrow{D}^I_\mu \varphi)(\bar{q}\gamma^\mu\tau^I q)\\
Q_{qq}^{(3)} &= (\bar{q}\gamma_\mu\tau^I q)(\bar{q}\gamma^\mu\tau^I q) & Q_{uG} &= (\bar{q}\sigma^{\mu\nu}T^A u)\tilde{\varphi}G^A_{\mu\nu} & Q_{\varphi q}^{(1)} &= i(\varphi^\dagger \overleftrightarrow{D}_\mu \varphi)(\bar{q}\gamma^\mu q)\\
Q_{uu} &= (\bar{u}\gamma_\mu u)(\bar{u}\gamma^\mu u) & Q_G &= f_{ABC}G^{A\nu}_\mu G^{B\lambda}_\nu G^{C\mu}_\lambda & Q_{uB} &= (\bar{q}\sigma^{\mu\nu}u)\tilde{\varphi}B_{\mu\nu}\\
Q_{qu}^{(8)} &= (\bar{q}\gamma_\mu T^A q)(\bar{u}\gamma^\mu T^A u) & Q_{\tilde{G}} &= f_{ABC}\tilde{G}^{A\nu}_\mu G^{B\lambda}_\nu G^{C\mu}_\lambda & Q_{\varphi u} &= (\varphi^\dagger i\overleftrightarrow{D}_\mu \varphi)(\bar{u}\gamma^\mu u)\\
Q_{qd}^{(8)} &= (\bar{q}\gamma_\mu T^A q)(\bar{d}\gamma^\mu T^A d) & Q_{\varphi G} &= (\varphi^\dagger\varphi)G^A_{\mu\nu}G^{A\mu\nu} & Q_{\varphi\tilde{G}} &= (\varphi^\dagger\varphi)\tilde{G}^A_{\mu\nu}G^{A\mu\nu}\\
Q_{ud}^{(8)} &= (\bar{u}\gamma_\mu T^A u)(\bar{d}\gamma^\mu T^A d)\,. & & & & & (4.1.2)
\end{aligned}
$$

To demonstrate the wide applicability of the EFT approach, we can observe that these contain the low-energy effects of several BSM scenarios. For example, $Q_{\varphi q}^{(3)}$ is generated by integrating out sfermions in the MSSM [111], $Q_{\text{xx}}^{(8)}$ appear in models with heavy axigluons [112], while Q_{uG} appears in composite top scenarios [52].

The non self-hermitian operators O_{uW}, O_{uG} and O_{uB} may have complex coefficients which, along with $O_{\tilde{G}}$ and $O_{\varphi\tilde{G}}$, lead to $\mathcal{CP}$-violating effects. These do not contribute to Standard Model spin-averaged cross-sections, though they are in principle sensitive to polarimetric observables such as spin correlations [113]†, and should therefore be treated as independent operators. However, currently available measurements that would be sensitive to these effects have been extracted by making model-specific assumptions that preclude their usage in our fit, e.g. by assuming that the tops are produced with either SM-like spin correlation or no spin correlation at all, as in Refs. [119, 120]. Currently there is no evidence for $\mathcal{CP}$-violation in the top sector beyond the minimal flavor violation assumption.

With these caveats, a total of 14 constrainable $\mathcal{CP}$-even dimension-six operators contribute to top quark production and decay at leading order in the SMEFT.

Parton-level theory predictions were first obtained for each process by interfacing the FeynRules [34] model file for the SMEFT via UFO [11] to MadGraph/MadEvent [11, 121]. Herein, the minimal set of global parameter and field redefinitions necessary to restore canonical normalisation and mass-diagonal states to the Lagrangian were included as discussed in section 3.3. In the case of strong top pair production the

*Given the simplicity of how it captures modifications to SM fermion couplings, this basis is well-suited to top EFT. For basis choices of interest in Higgs physics, see e.g. Refs. [48, 49, 108–110]

†For recent analyses focusing on the tWb vertex, for instance, see Refs. [114–118]

resulting rescalings of e.g. the strong gauge coupling:

$$g_s \to g_s \left(1 + v^2 C_{\varphi G}\right) \equiv \bar{g}_s, \tag{4.1.3}$$

have no physical consequences for our analysis*.

As MadGraph generates the full squared matrix elements (i.e. including the $\mathcal{O}(\Lambda^{-4})$ terms from $|\mathcal{M}_{D6}|^2$), the validity of the assumption that interference terms represent the leading effect can be checked on a process-by-process basis. To this end, the dependence on the dimension-six Wilson Coefficients was verified explicitly by calculating the interference terms using the FeynArts [57] and FormCalc [58] interface, and cross-checking these with previous explicit calculations [91] in the obsolete operator basis of Ref. [47].

To verify the model implementation produces the expected event shapes, illustrative differential cross section distributions for each of the considered partonic subprocesses in top pair and single top production were produced by implementing simple parton-level analyses in ROOT [122]. To check the relative numerical importance of $|\mathcal{M}_{\text{int}}|^2$ and $|\mathcal{M}_{D6}|^2$ in each channel, reference events were generated where each Wilson Coefficient carried the (unphysically low) scale $\Lambda' = \frac{1}{a}\Lambda$ (such that, for the chosen value $a = 100$, the cross section is entirely dominated by $|\mathcal{M}_{D6}|^2$). These were then used to subtract the $|\mathcal{M}_{D6}|^2$ contributions from each bin of the $d\sigma/d(cos\theta)$ distributions†.

$|\mathcal{M}_{D6}|^2$ terms are kept in the final MadGraph samples that were used in the fit. Along with representing the numerically leading SMEFT contribution at the squared matrix element level in some special cases, retaining these prevents the appearance of spurious negative cross sections in regions of phase space where $|\mathcal{M}_{SM}|^2$ is small and $|\mathcal{M}_{\text{int}}|^2 < 0$. Furthermore, it has been shown that retaining contributions from $|\mathcal{M}_{D6}|^2$ is necessary when fitting to data to ensure that the χ^2 has a local minimum [56, 81].

4.1.1 Top Pair Production

By far the most abundant source of data in top physics is from the production of top pairs. The $\mathcal{CP}$-even dimension-six operators that interfere with the Standard Model

*i.e. these shifts affect the definition of couplings in $\mathcal{L}^{(6)}$ relative to in the renormalizable $\mathcal{L}_{\text{SM}}$, and produce no measurable effect. Given an independent knowledge of the value of $C_{\varphi G}$, one could however make some statement about the magnitude of the unshifted g_s.

†Schematically, with $\sigma_{\text{full}} = \sigma_{\text{SM}} + a^2\Lambda^{-2}\sigma_{\text{int}} + a^4\Lambda^{-4}\sigma_{\text{sq}}$, we can plot $\sigma_{a=1} - \sigma_{\text{SM}} = \Lambda^{-2}\sigma_{\text{int}} + \Lambda^{-4}\sigma_{\text{sq}}$ and $(\sigma_{a=1} - 100^4\sigma_{a=100}) - \sigma_{\text{SM}} \simeq \Lambda^{-2}\sigma_{\text{int}}$.

amplitude are:

$$\begin{aligned}\mathcal{L}_{D6} \supset\; & C_{uG}(\bar{q}\sigma^{\mu\nu}T^A u)\tilde{\varphi}G^A_{\mu\nu} \;+\; C_G f_{ABC}G^{A\nu}_{\mu}G^{B\lambda}_{\nu}G^{C\mu}_{\lambda} \;+\; C_{\varphi G}(\varphi^\dagger\varphi)G^A_{\mu\nu}G^{A\mu\nu} \\ & +\; C^{(1)}_{qq}(\bar{q}\gamma_\mu q)(\bar{q}\gamma^\mu q) \;+\; C^{(3)}_{qq}(\bar{q}\gamma_\mu \tau^I q)(\bar{q}\gamma^\mu \tau^I q) + C_{uu}(\bar{u}\gamma_\mu u)(\bar{u}\gamma^\mu u) \\ & +\; C^{(8)}_{qu}(\bar{q}\gamma_\mu T^A q)(\bar{u}\gamma^\mu T^A u) \;+\; C^{(8)}_{qd}(\bar{q}\gamma_\mu T^A q)(\bar{d}\gamma^\mu T^A d) \;+\; C^{(8)}_{ud}(\bar{u}\gamma_\mu T^A u)(\bar{d}\gamma^\mu T^A d)\,.\end{aligned}$$

The $2 \to 2$ production of top antitop pairs $t\bar{t}$ proceeds in QCD through the two distinct partonic channels: quark-antiquark annihilation $q\bar{q} \to t\bar{t}$, and gluon fusion $gg \to t\bar{t}$.

$\bar{q}q \to \bar{t}t$ Production

Quark-antiquark annihilation is the smaller of the two $t\bar{t}$ production modes at the LHC, owing to the relative dominance of the gluon at small x over the valence u and d quarks in the proton PDFs. With only one s-channel diagram comprising the leading order QCD mechanism in the SM, the interfering operators in the SMEFT for $d\bar{d}, u\bar{u} \to t\bar{t}$ are flavour-diagonal modifications to the qqg vertex, and four-fermion contact interactions. The relevant operators are then Q_{uG} and $\{Q^{(1)}_{qq}, Q^{(3)}_{qq}, Q_{uu}, Q^{(8)}_{qu}, Q^{(8)}_{qd}, Q^{(8)}_{ud}\}$ respectively. We can safely neglect the contribution of the first generation flavour arrangement Q^{11}_{uG},

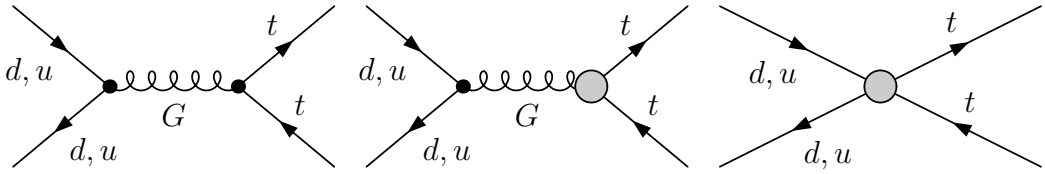

Figure 4.1: *Feynman diagrams for $\bar{q}q \to t\bar{t}$ production. The shaded circles represent qqg and $qqqq$ vertices arising from dimension-six operator insertions.*

as this operator is a direct mixing of the left- and right- chiral u quark fields, and so contributes terms proportional to the up-quark mass m_u. The spin and colour averaged interference terms are:

$$\begin{aligned}\overline{\mathcal{M}^2}_{int}(u\bar{u} \to t\bar{t}) = \;& \Re\mathfrak{e}\, C_{\substack{uG\\33}}\frac{32\bar{g}_s^3 v_T m_t}{9\sqrt{2}} + \left(C^{(1)}_{\substack{qq\\1331}} + C_{\substack{uu\\1331}} + C^{(3)}_{\substack{qq\\1331}}\right)\frac{\bar{g}_s^2}{18s}(3m_t^4 - m_t^2(t+3u) + u^2) \\ & + \left(C^{(8)}_{\substack{qu\\1133}} + C^{(8)}_{\substack{qu\\3311}}\right)\frac{\bar{g}_s^2}{36s}(3m_t^4 - m_t^2(3t+u) + t^2) \\ \overline{\mathcal{M}^2}_{int}(d\bar{d} \to t\bar{t}) = \;& \Re\mathfrak{e}\, C_{\substack{uG\\33}}\frac{32\bar{g}_s^3 v_T m_t}{9\sqrt{2}} + \left(C^{(3)}_{\substack{qq\\1331}} + \tfrac{1}{4}C^{(8)}_{\substack{ud\\3311}}\right)\frac{\bar{g}_s^2}{9s}(3m_t^4 - m_t^2(t+3u) + u^2)\end{aligned}$$

$$+\left(C^{(8)}_{\substack{qu\\1133}}+C^{(8)}_{\substack{qd\\3311}}\right)\frac{\bar{g}_s^2}{36s}(3m_t^4-m_t^2(3t+u)+t^2)$$

Since QCD treats L and R chiralities on equal footing, the six four-quark operators interfere with the SM amplitude to produce terms dependent only on two linear combinations of four-fermion Wilson Coefficients. For each of the $u\bar{u}$ and $d\bar{d}$ initial states, these arise from operators in which identical ($\bar{L}L\bar{L}L$, $\bar{R}R\bar{R}R$) and opposite ($\bar{L}L\bar{R}R, \bar{R}R\bar{L}L$) arrangements of the chiral d and u-quark field currents appear respectively. In the spirit of the notation of Ref. [91], which first characterised these dimension-six contributions in the overcomplete basis of [47], we denote these:

$$\begin{aligned}
C_u^1 &= C^{(1)}_{\substack{qq\\1331}}+C_{\substack{uu\\1331}}+C^{(3)}_{\substack{qq\\1331}}\\
C_u^2 &= C^{(8)}_{\substack{qu\\1133}}+C^{(8)}_{\substack{qu\\3311}}\\
C_d^1 &= C^{(3)}_{\substack{qq\\1331}}+\tfrac{1}{4}C^{(8)}_{\substack{ud\\3311}}\\
C_d^2 &= C^{(8)}_{\substack{qu\\1133}}+C^{(8)}_{\substack{qd\\3311}}.
\end{aligned}$$

It is these four that are constrainable in a dimension-six analysis. In Fig. 4.2, we can see that even for a large $s/\Lambda^2 = (4m_t)^2/\text{TeV} \simeq 0.5$, the interference term is the dominant contribution from the EFT. The analagous C_d distributions are identical, as their interference carries the same kinematic dependence.

The real part of $Q_{\substack{uG\\33}}$, the 'chromomagnetic dipole moment operator', enters in both the $q\bar{q}$ and gg channels through the gtt vertex. We can note that the single s-channel topology restricts this operator to the production vertex for the final state $t\bar{t}$ pair. Since $Q_{\substack{uG\\33}}$ directly couples left and right-chiral top quark fields, while QCD is chirality-diagonal, the interference of the two diagrams carries no dependence on the $t\bar{t}$ kinematics. We expect the same dependency for the squared contribution of this operator so that the interference is dominant, since no dependency on the top kinematics can arise. In Fig. 4.3, we can again confirm this: for $s/\Lambda^2 = (4m_t)^2/\text{TeV} \simeq 0.5$, truncating at the interference term is a very good approximation. The analagous $d\bar{d}$ distributions are identical, as the operator insertion modifies the gtt vertex*.

*Here, and in the case of Q_G, the analytic curves are visibly enhanced by a small rescaling factor above the MadGraph events. The analytic differential cross sections were superimposed using the value of α_s at the Z boson mass, whereas MadGraph uses a dynamic scale choice based on the m_T of the final states [123]. Hence for t-quark production in general, $\alpha_s(m_Z) > \alpha_s(m_T^t)$.

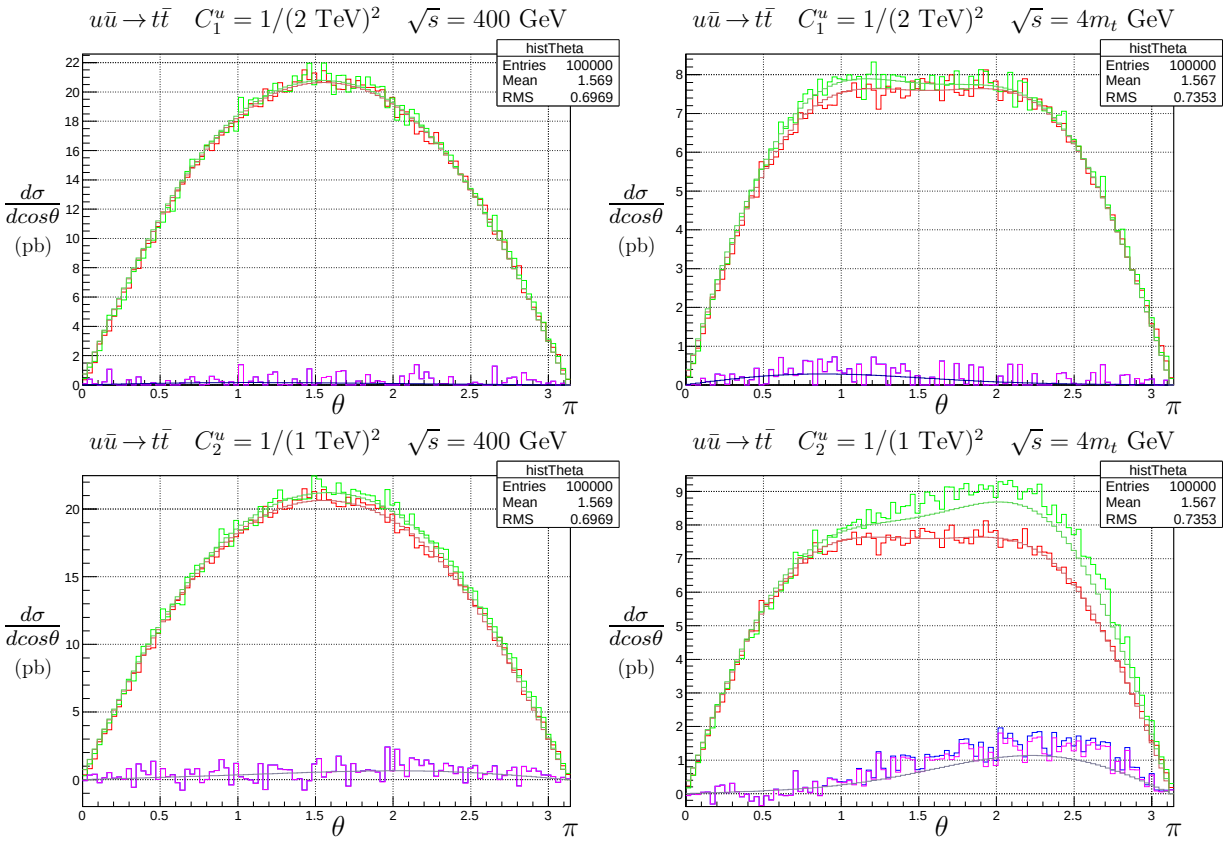

Figure 4.2: *Example parton level $d\sigma/dcos\theta$ distributions for the two independent linear combinations of operators controlled by C_u^1 and C_u^2 for $\sqrt{s} = 400\,GeV$ (left) and $\sqrt{s} = 4m_t \simeq 692\,GeV$ (right). Histograms show* MadGraph *events corresponding to $|\mathcal{M}_{SM}|^2$, $|\mathcal{M}_{int}|^2$, $|\mathcal{M}_{int}|^2 + |\mathcal{M}_{D6}|^2$ and $|\mathcal{M}_{tot}|^2$, while the solid lines are analytic checks for $|\mathcal{M}_{SM}|^2$, $|\mathcal{M}_{int}|^2$, and $|\mathcal{M}_{SM}|^2 + |\mathcal{M}_{int}|^2$.*

$gg \to \bar{t}t$ Channel

Gluon fusion is the dominant $t\bar{t}$ production channel at the LHC, (accounting for over 90% of the cross section at 14 TeV) since the low-x gluon luminosity dwarfs that of the valence quarks. While the SM production contains more topologies than $q\bar{q}$, the interfering dimension-six operators can only modify the ggg and $(g)gtt$ vertices, or couple these to an s-channel colour singlet. Fewer gauge-invariant operators then arise, and these are $\{Q_G, Q_{uG}^{33}, Q_{\varphi G}\}$. The spin and colour averaged interference terms are:

$$\overline{\mathcal{M}^2}_{int}(gg \to t\bar{t}) = \Re\mathfrak{e}\, C_{\substack{uG \\ 33}} \frac{\bar{g}_s^3 v_T m_t (4s^2 - 9tu - 9m_t^2 s + 9m_t^4)}{3\sqrt{2}(m_t^2 - t)(m_t^2 - u)} + C_G \frac{9\,\bar{g}_s^3\, m_t^2 (t-u)^2}{8\,(m_t^2 - t)(m_t^2 - u)}$$
$$- C_{\varphi G} \frac{\bar{g}_s^2\, m_t^2\, s^2 (s - 4m_t^2)}{8(s - m_h^2)(t - m_t^2)(u - m_t^2)}$$

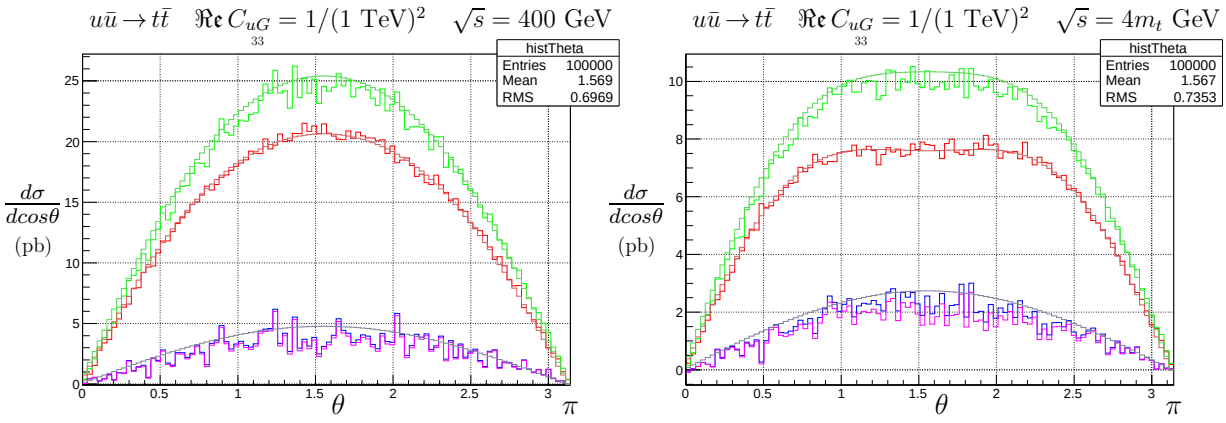

Figure 4.3: *Example parton level $d\sigma/dcos\theta$ distributions for $\Re\mathfrak{e}\, Q_{uG}^{33}$ for $\sqrt{s} = 400\,GeV$ (left) and $\sqrt{s} = 4m_t \simeq 692\,GeV$ (right). Histograms show* MadGraph *events corresponding to $|\mathcal{M}_{SM}|^2$, $|\mathcal{M}_{int}|^2$, $|\mathcal{M}_{int}|^2 + |\mathcal{M}_{D6}|^2$ and $|\mathcal{M}_{tot}|^2$, while the solid lines are analytic checks for $|\mathcal{M}_{SM}|^2$, $|\mathcal{M}_{int}|^2$, and $|\mathcal{M}_{SM}|^2 + |\mathcal{M}_{int}|^2$.*

The operator $O_{\varphi G}$ cannot be bounded by top pair production alone, since the branching

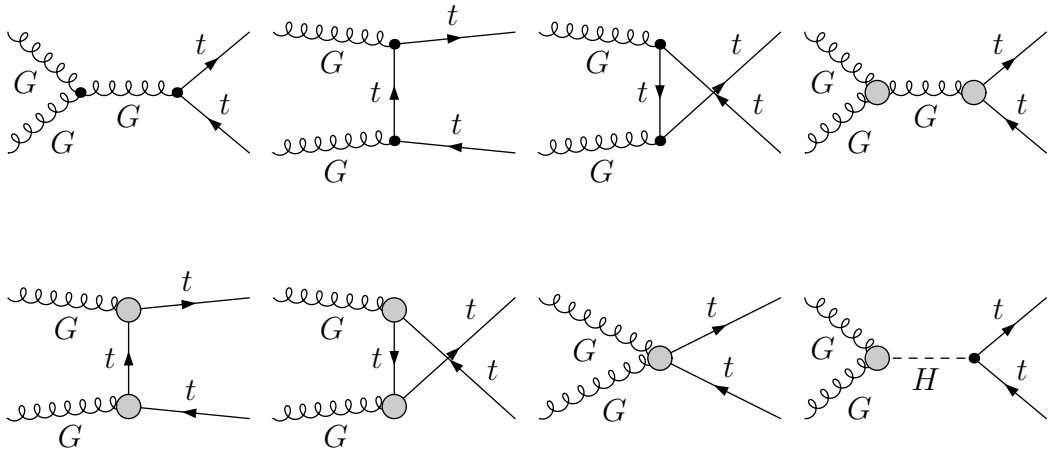

Figure 4.4: *Feynman diagrams for $gg \to t\bar{t}$ production. Shaded circles represent each possible operator insertion at the ggg, ggH and gtt vertices (for a maximum of one per diagram) of Q_G, $Q_{\varphi G}$ and Q_{uG}^{33} respectively.*

ratio to a $t\bar{t}$ pair for a 125 GeV Higgs is practically zero *, therefore we do not consider it here. For a recent constraint from Higgs physics see e.g. Ref. [76, 78, 82, 83]. In Fig. 4.5, we confirm this assertion numerically.

The purely gluonic operator Q_G (which, in contrast to 'top-philic' operators contributes to any QCD process dependent on the gluon-self coupling) is known to con-

*i.e. the presence of an s-channel Higgs propagator $(s - m_h^2)^{-1}$ heavily suppresses this channel, given the distance between m_h and the $t\bar{t}$ threshold.

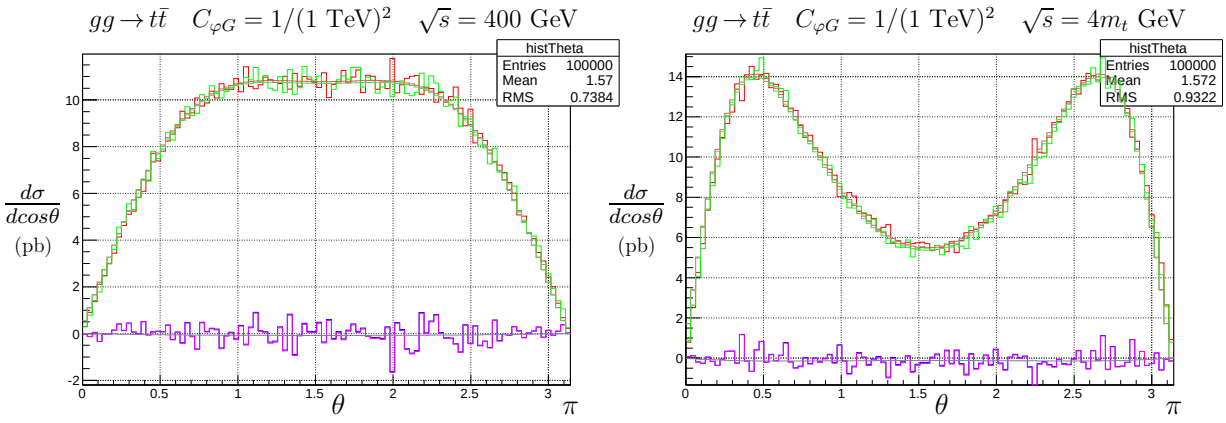

Figure 4.5: *Example parton level $d\sigma/dcos\theta$ distributions for $Q_{\varphi G}$ for $\sqrt{s} = 400\,GeV$ (left) and $\sqrt{s} = 4m_t \simeq 692\,GeV$ (right). Histograms show* MadGraph *events corresponding to $|\mathcal{M}_{SM}|^2$, $2\Re\mathfrak{e}\,\mathcal{M}_{SM}\mathcal{M}^*_{D6}$, $|\mathcal{M}_{D6}|^2$ and $|\mathcal{M}_{tot}|^2$, while the solid lines are analytic checks for $|\mathcal{M}_{SM}|^2$, $2\Re\mathfrak{e}\,\mathcal{M}_{SM}\mathcal{M}^*_{D6}$, and $|\mathcal{M}_{SM+int}|^2$.*

tribute mainly though its square term, rather than its interference with the SM. The interference of gluonic amplitudes featuring ggg vertices from a Q_G insertion with the corresponding SM QCD amplitudes was shown to be zero by merit of their orthogonal helicity structures [124]. We can verify this by noticing the net interference of the single Q_G diagram with the SM channels carries an overall proportionality factor of m_t^2.

Since this contribution would be zero for massless quarks, Q_G's $\mathcal{O}(\Lambda^{-2})$ effect must originate from the massive top propagator which couples to both gluon helicities. This mass suppression clearly will not apply to the coherent $\mathcal{O}(\Lambda^{-4})$ product of s-channel Q_G topologies with themselves. It was verified in an explicit calculation [125] that, taking advantage of the fact that pure gauge-boson operators are relatively simple to construct explicitly at a given mass dimension, $|\mathcal{M}_{D6}|^2$ indeed carries a quadratic dependence on $\hat{s}, \hat{t}$ and $\hat{u}$ which dominates the linear scaling experienced by all interfering dimension-eight operators. Then although both of these are $\mathcal{O}(\Lambda^{-4})$, the former is numerically dominant. In Fig. 4.6 we verify that $|\mathcal{M}_{D6}|^2$ is the leading effect even for small values of C_G such that $s/\Lambda^2 = (400\text{GeV})^2/(1\text{TeV})^2 = 0.16$.

Fig. 4.7 exhibits $Q_{\underset{33}{uG}}$ in the gg channel. In contrast to the $q\bar{q}$ channel, the additional Feynman topologies permit operator insertions coupling the final states to virtual t and u-channel tops and the scattering gluons. This lifts the restriction that the interference be directly proportional to the part of the matrix element contracting the $t\bar{t}$ pair of opposite chiralities, and we see that this process resultantly scales with the top kinematics. Consequently, the squared term need not conform to the same behaviour as was argued

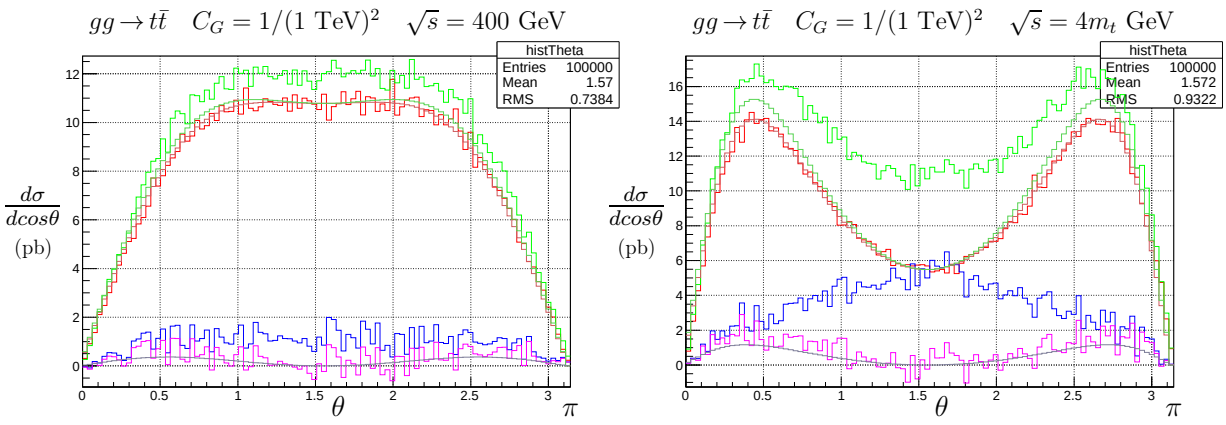

Figure 4.6: *Example parton level $d\sigma/dcos\theta$ distributions for Q_G for $\sqrt{s} = 400\,GeV$ (left) and $\sqrt{s} = 4m_t \simeq 692\,GeV$ (right). Histograms show* MadGraph *events corresponding to $|\mathcal{M}_{SM}|^2$, $|\mathcal{M}_{int}|^2$, $|\mathcal{M}_{int}|^2 + |\mathcal{M}_{D6}|^2$ and $|\mathcal{M}_{tot}|^2$, while the solid lines are analytic checks for $|\mathcal{M}_{SM}|^2$, $|\mathcal{M}_{int}|^2$, and $|\mathcal{M}_{SM}|^2 + |\mathcal{M}_{int}|^2$.*

in the $q\bar{q}$ production channel. We verify this in Fig. 4.7, where we see $|\mathcal{M}_{D6}|^2$ begin to become a significant contribution to the cross section for $s/\Lambda^2 \simeq 0.5$.

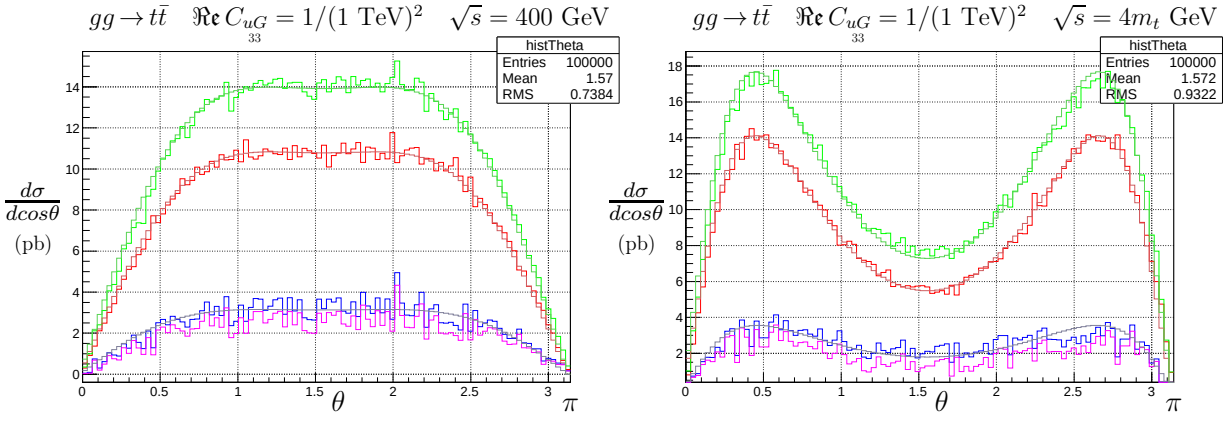

Figure 4.7: *Example parton level $d\sigma/dcos\theta$ distributions for $\Re\mathfrak{e}\, Q_{uG}^{33}$ for $\sqrt{s} = 400\,GeV$ (left) and $\sqrt{s} = 4m_t \simeq 692\,GeV$ (right). Histograms show* MadGraph *events corresponding to $|\mathcal{M}_{SM}|^2$, $|\mathcal{M}_{int}|^2$, $|\mathcal{M}_{int}|^2 + |\mathcal{M}_{D6}|^2$ and $|\mathcal{M}_{tot}|^2$, while the solid lines are analytic checks for $|\mathcal{M}_{SM}|^2$, $|\mathcal{M}_{int}|^2$, and $|\mathcal{M}_{SM}|^2 + |\mathcal{M}_{int}|^2$.*

4.1.2 Single Top Quark Production

The next most abundant source of top quark data is from single top production. In our fit we will consider production in the t and s channels, and omit Wt-associated

production. Though measurements of the latter process have been published, they are not suitable for inclusion in a fit involving parton level theory predictions. As is well-known, Wt production interferes with top pair production at NLO and beyond in a five-flavour scheme [126–128], or at LO in a four-flavour one. Its separation from top pair production is then a delicate issue, discussed in detail in Refs. [129–132]. We thus choose to postpone the inclusion of Wt production to a future study, going beyond parton level. The interfering dimension-six operators are:

$$\begin{aligned}\mathcal{L}_{D6} \supset\; & C_{uW}(\bar{q}\sigma^{\mu\nu}\tau^I u)\,\tilde{\varphi}\,W^I_{\mu\nu} \;+\; C^{(3)}_{\varphi q} i(\varphi^\dagger \overleftrightarrow{D}^I_\mu \varphi)(\bar{q}\gamma^\mu\tau^I q) \\ & +\; C_{\varphi ud}(\varphi^\dagger \overleftrightarrow{D}_\mu \varphi)(\bar{u}\gamma^\mu d) \;+\; C_{dW}(\bar{q}\sigma^{\mu\nu}\tau^I d)\,\tilde{\varphi}\,W^I_{\mu\nu} \\ & +\; C^{(3)}_{qq}(\bar{q}\gamma_\mu\tau^I q)(\bar{q}\gamma^\mu\tau^I q) + C^{(1)}_{qq}(\bar{q}\gamma_\mu q)(\bar{q}\gamma^\mu q) \;+\; C^{(1)}_{qu}(\bar{q}\gamma_\mu q)(\bar{u}\gamma^\mu u)\,.\end{aligned}$$

As in top pair production there are several simplifications which reduce this operator set. The right-chiral down quark fields appearing in Q_{dW} and $Q_{\varphi ud}$ cause these operators' interference with the left-chiral SM weak interaction to be proportional to the relevant down-type quark mass. For example, an operator insertion of $Q^{33}_{\varphi ud}$ will always contract with the SM Wtb-vertex to form a term of order $m_b\, m_t\, C^{33}_{\varphi ud}/\Lambda^2$. Since m_b is much less than both $\hat{s}$ and the other dimensionful parameters that appear, v and m_t, we may choose to neglect these operators. By the same rationale we neglect $Q^{(1)}_{qu}$ as its contribution to observables is $\mathcal{O}(m_u)$.

s-Channel $u\bar{d} \to t\bar{b}$ Production

$u\bar{d} \to t\bar{b}$ production of single top quarks proceeds in the SM through the s-channel exchange of a virtual W-boson. The interference with dimension-six operators takes

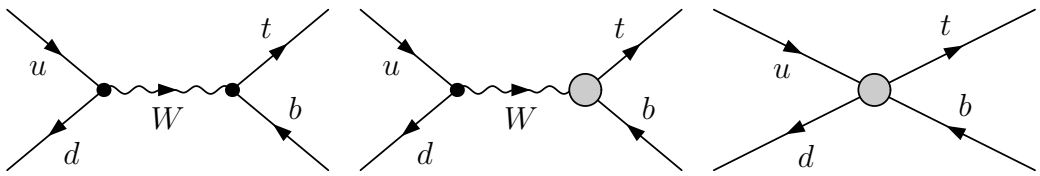

Figure 4.8: *Feynman diagrams for s-channel single top quark production. Shaded circles represent operator insertions of $Q^{(3)}_{\varphi q}$ or $\mathfrak{Re}\,Q_{uW}$ at the Wtb vertex, and one of the operators $Q^{(3)1133}_{qq}$, $Q^{(1)1331}_{qq}$ or $Q^{(3)1331}_{qq}$ for the four-fermion contact interactions.*

the form:

$$\overline{\mathcal{M}^2}_{int}\,(u\bar{d}\to t\bar{b}) = \; C^{(3)}_{\substack{\varphi q\\33}}\frac{\bar{g}_2^3 V_{tb}|V_{ud}|^2 v_T^2 u(u-m_t^2)}{4(s-m_W^2)^2} - \Re\mathfrak{e}\, C_{\substack{uW\\33}}\frac{\sqrt{2}\bar{g}_2^2 V_{tb}|V_{ud}|^2 m_t m_W su}{(s-m_W^2)^2}$$
$$+\left(C_{qq}^{(3)1133}+\tfrac{1}{6}(C_{qq}^{(1)1331}-C_{qq}^{(3)1331})\right)V_{tb}V_{ud}\frac{9\bar{g}_2^2 u(u-m_t^2)}{8(s-m_W^2)}$$

Interference with the exclusively left-chiral weak interaction leads to just one contributing linear combination of four-fermion Wilson Coefficients:

$$C_t = C^{(3)}_{\substack{qq\\1133}} + \tfrac{1}{6}(C^{(1)}_{\substack{qq\\1331}} - C^{(3)}_{\substack{qq\\1331}})$$

Single top production is thus sensitive to the three independent Wilson Coefficients C_{uW}, $C^{(3)}_{\substack{\varphi q\\33}}$ and C_t. After EWSB, the term proportional to v_T^2 in the operator $Q^{(3)}_{\substack{\varphi q\\33}}$ is structurally identical to the SM fermion weak interaction term. As was noted in Ref. [91], this amounts in single top production to a pure rescaling of the SM Wtb vertex by a factor $(1+v_T^2 C^{(3)}_{\substack{\varphi q\\33}})$, with no effect on event shapes. In Fig. 4.9, we confirm that the contribution of this operator is a net rescaling of the SM distribution, and $|\mathcal{M}_{D6}|^2$ terms are negligible.

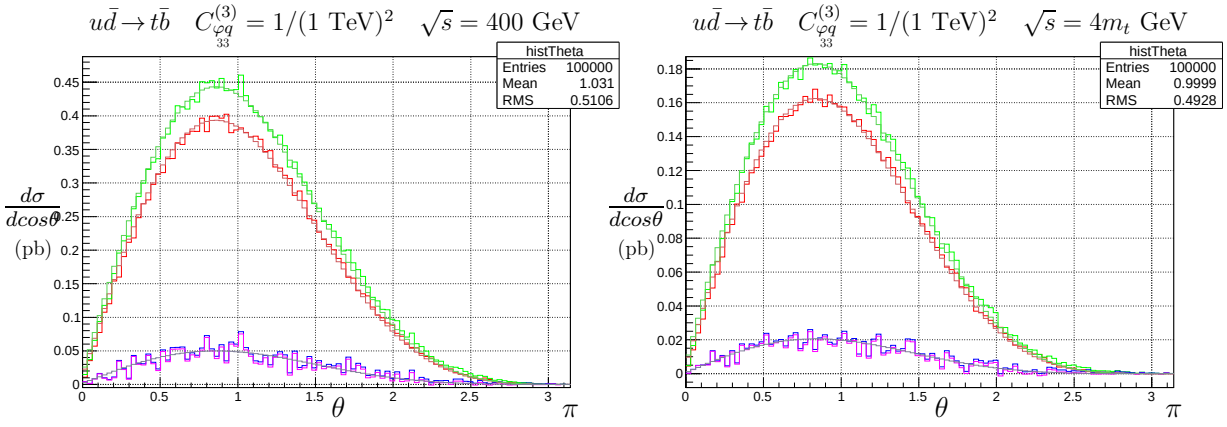

Figure 4.9: *Example parton level $d\sigma/dcos\theta$ distributions for $Q^{(3)}_{\substack{\varphi q\\33}}$ for $\sqrt{s} = 400\,GeV$ (left) and $\sqrt{s} = 4m_t \simeq 692\,GeV$ (right). Histograms show* MadGraph *events corresponding to $|\mathcal{M}_{SM}|^2$, $|\mathcal{M}_{int}|^2$, $|\mathcal{M}_{int}|^2 + |\mathcal{M}_{D6}|^2$ and $|\mathcal{M}_{tot}|^2$, while the solid lines are analytic checks for $|\mathcal{M}_{SM}|^2$, $|\mathcal{M}_{int}|^2$, and $|\mathcal{M}_{SM}|^2 + |\mathcal{M}_{int}|^2$.*

Suppression by the W-boson virtuality $(s-m_W^2)$ in s-channel production - along with contributing to the small contribution of this channel to SM single top production at the LHC - drastically increases sensitivity to four-fermion operators. Since these are contact interactions without no dependence on a W-propagator, for highly off-shell Ws

(i.e. when $s \gg m_W^2$) their matrix elements are relatively enhanced. The absence of one (both) of these factors causes the interference (squared contribution) to dominate the SM production mechanism even for small values of C_t, and likewise the contribution from $|\mathcal{M}_{D6}|^2$ to overwhelm that of the interference. In Fig. 4.10 we see this behaviour directly*, and truncating at $\mathcal{O}(\Lambda^{-2})$ is a poor approximation of four-fermion operators' signatures in this channel. However, $\mathcal{O}(\Lambda^{-4})$ contributions arising from interference of dimension-eight operators with the SM must again carry a suppression by the W-virtuality. In the absence of a hierarchy in the BSM theory producing a scenario where $C_{D8} \gg C_{D6}$, $|\mathcal{M}_{D6}|^2$ should then be the most numerically significant effect.

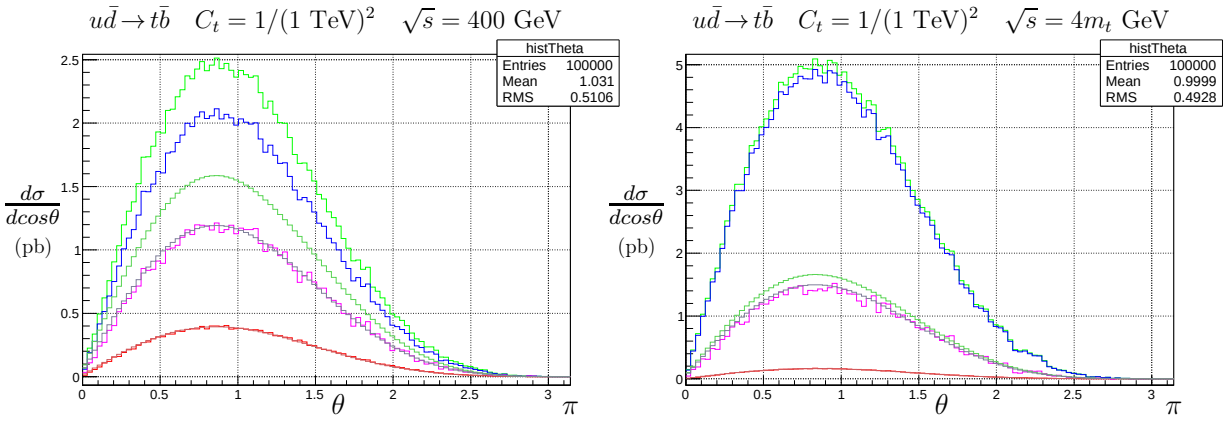

Figure 4.10: *Example parton level $d\sigma/dcos\theta$ distributions for the linear combinations of operators four-fermion operators controlled by C_t for $\sqrt{s} = 400\,GeV$ (left) and $\sqrt{s} = 4m_t \simeq 692\,GeV$ (right). Histograms show* MadGraph *events corresponding to $|\mathcal{M}_{SM}|^2$, $|\mathcal{M}_{int}|^2$, $|\mathcal{M}_{int}|^2 + |\mathcal{M}_{D6}|^2$ and $|\mathcal{M}_{tot}|^2$, while the solid lines are analytic checks for $|\mathcal{M}_{SM}|^2$, $|\mathcal{M}_{int}|^2$, and $|\mathcal{M}_{SM}|^2 + |\mathcal{M}_{int}|^2$.*

Finally in this channel we have the operator $\Re\mathfrak{e}\, Q_{uW}^{33}$, an electroweak analogue to the chromomagnetic operator $\Re\mathfrak{e}\, Q_{uG}^{33}$. In contrast to the behaviour of its gluonic cousin in $gg \to t\bar{t}$ production, the longitudinal component of the massive W-boson propagator allows the interference term of this operator to scale with the momentum flowing through the s-channel diagram†, producing a stronger kinematic scaling than in the pure SM contribution. We see the result in Fig. 4.11, where the dimension-six contribution is already of the same order as the SM for the lower illustrative centre of mass energy chosen $s/\Lambda^2 = (400\text{GeV})^2/(1\text{TeV})^2 = 0.16$. For $s/\Lambda^2 \simeq 0.5$, we can see $|\mathcal{M}_{D6}|^2$ then

*Note that the green histograms and curves correspond to the full squared matrix elements including quadratic terms, and the SM plus interference respectively. Thus a mismatch between these corresponds to a large squared contribution.

†Q_{uW}^{33} produces a vertex carrying a factor of $(k_1 + k_2)^\mu$ (from the W-boson field strength tensor $\partial_\mu W_\nu - (\mu \leftrightarrow \nu)$), where k_1 and k_2 are the four momenta of the scattering quarks.

becomes larger than the interference, as its squared contribution can carry two powers of s from the modified Wtb vertex*.

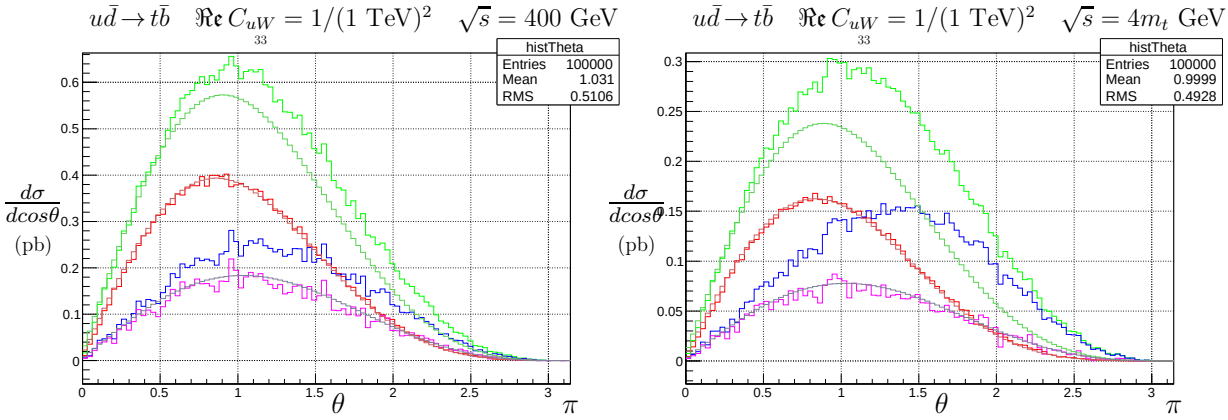

Figure 4.11: *Example parton level $d\sigma/dcos\theta$ distributions for $\Re\mathfrak{e}\, Q_{uW}^{33}$ for $\sqrt{s} = 400\,GeV$ (left) and $\sqrt{s} = 4m_t \simeq 692\,GeV$ (right). Histograms show* MadGraph *events corresponding to $|\mathcal{M}_{SM}|^2$, $|\mathcal{M}_{int}|^2$, $|\mathcal{M}_{int}|^2+|\mathcal{M}_{D6}|^2$ and $|\mathcal{M}_{tot}|^2$, while the solid lines are analytic checks for $|\mathcal{M}_{SM}|^2$, $|\mathcal{M}_{int}|^2$, and $|\mathcal{M}_{SM}|^2 + |\mathcal{M}_{int}|^2$.*

t-Channel $qb \to q't$ Production

Production of single top quarks in the t-channel is possible through the partonic sub-processes $u\bar{d} \to t\bar{b}$ and $ub \to dt$ in the SM. The contributing operators are the same as those in s-channel production. The interference terms take the form:

$$\begin{aligned}
\overline{\mathcal{M}^2}_{int}\,(ub \to dt) = \; & C_{\substack{\varphi q \\ 33}}^{(3)} \frac{\bar{g}_2^3 V_{tb}|V_{ud}|^2 v_T^2 s(s-m_t^2)}{4(t-m_W^2)^2} - \Re\mathfrak{e}\, C_{\substack{uW \\ 33}} \frac{\sqrt{2}\bar{g}_2^2 V_{tb}|V_{ud}|^2 m_t m_W st}{(t-m_W^2)^2} \\
& + \left(C_{qq}^{(3)1133} + \tfrac{1}{6}(C_{qq}^{(1)1331} - C_{qq}^{(3)1331})\right) V_{tb}V_{ud} \frac{9\bar{g}_2^2 s(s-m_t^2)}{8(t-m_W^2)} \\
\overline{\mathcal{M}^2}_{int}\,(\bar{d}b \to \bar{u}t) = \; & C_{\substack{\varphi q \\ 33}}^{(3)} \frac{\bar{g}_2^3 V_{tb}|V_{ud}|^2 v_T^2 u(u-m_t^2)}{4(t-m_W^2)^2} - \Re\mathfrak{e}\, C_{\substack{uW \\ 33}} \frac{\sqrt{2}\bar{g}_2^2 V_{tb}|V_{ud}|^2 m_t m_W ut}{(t-m_W^2)^2} \\
& + \left(C_{qq}^{(3)1133} + \tfrac{1}{6}(C_{qq}^{(1)1331} - C_{qq}^{(3)1331})\right) V_{tb}V_{ud} \frac{9\bar{g}_2^2 u(u-m_t^2)}{8(t-m_W^2)}.
\end{aligned}$$

As with in s-channel production, $Q_{\substack{\varphi q \\ 33}}^{(3)}$ contributes only through a rescaling of the SM cross section, and truncating $|\mathcal{M}_{D6}|^2$ is well-justified. This is illustrated in Fig. 4.13.

*However, the cross section for production of a single top quark in the s-channel mechanism is (at the matrix element level) heavily suppressed by the W virtuality at LHC energies, while $\Re\mathfrak{e}\, Q_{uW}^{33}$ also contributes both t-channel production, and to top quark decay.

The analagous distributions for the process $\bar{d}b \to \bar{u}t$ obtained by interchanging the u and d quarks behave similarly.

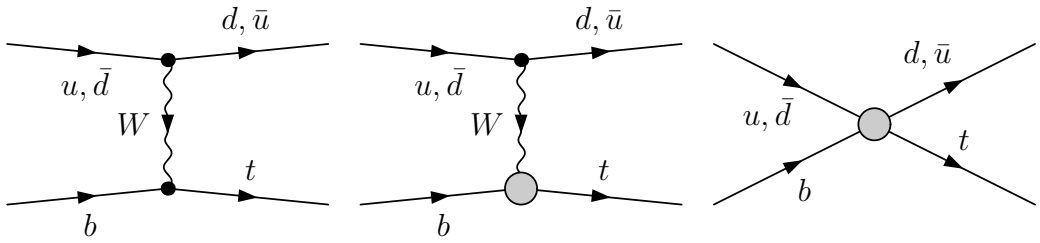

Figure 4.12: *Feynman diagrams for t-channel single top quark production. Shaded circles represent operator insertions of $Q^{(3)}_{\varphi q}$ or $\Re\mathfrak{e}\, Q_{uW}$ at the Wtb vertex, and one of the operators $Q^{(3)1133}_{qq}$, $Q^{(1)1331}_{qq}$ or $Q^{(3)1331}_{qq}$ for the four-fermion contact interactions.*

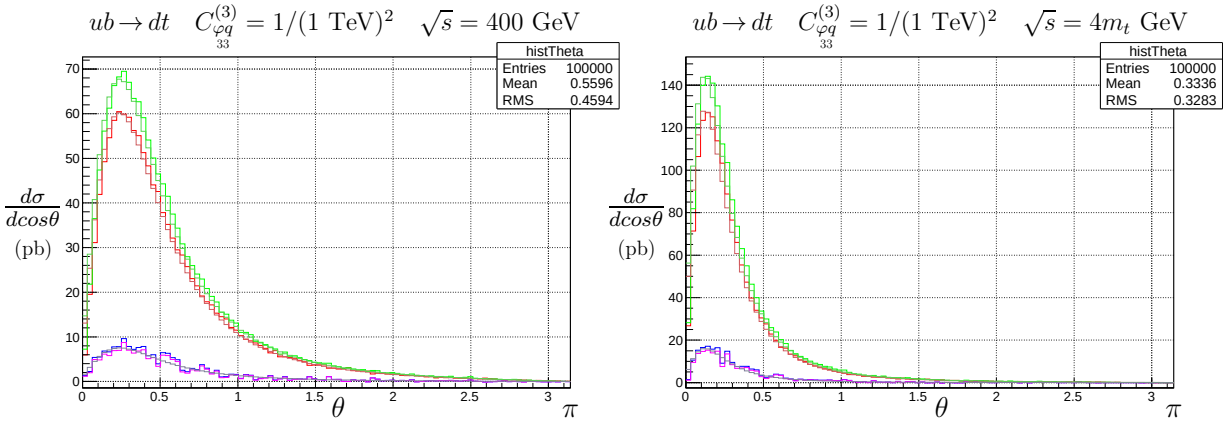

Figure 4.13: *Example parton level $d\sigma/dcos\theta$ distributions for $Q^{(3)}_{\varphi q}$ for $\sqrt{s} = 400\,GeV$ (left) and $\sqrt{s} = 4m_t \simeq 692\,GeV$ (right). Histograms show* MadGraph *events corresponding to $|\mathcal{M}_{SM}|^2$, $|\mathcal{M}_{int}|^2$, $|\mathcal{M}_{int}|^2 + |\mathcal{M}_{D6}|^2$ and $|\mathcal{M}_{tot}|^2$, while the solid lines are analytic checks for $|\mathcal{M}_{SM}|^2$, $|\mathcal{M}_{int}|^2$, and $|\mathcal{M}_{SM}|^2 + |\mathcal{M}_{int}|^2$.*

With the presence of the W-boson now in the t-channel, the suppression of the cross section by factors of $1/(s - m_W^2)$ is no longer present, and consequently four-fermion contact interactions no longer dominate the SM production mechanism. In Fig. 4.14, we can confirm this - these operators' leading contribution comes from their interference with the SM t-channel mode diagram.

For $\Re\mathfrak{e}\, Q^{33}_{uW}$, the interference with the SM is now proportional to the momentum in the t-channel W-boson propagator, while this contribution to the cross section peaks for $t = m_W^2$. In Fig. 4.15, we can see the result - the enhancement to the cross section is negligible compared to the SM production mechanism which doesn't carry this dependence.

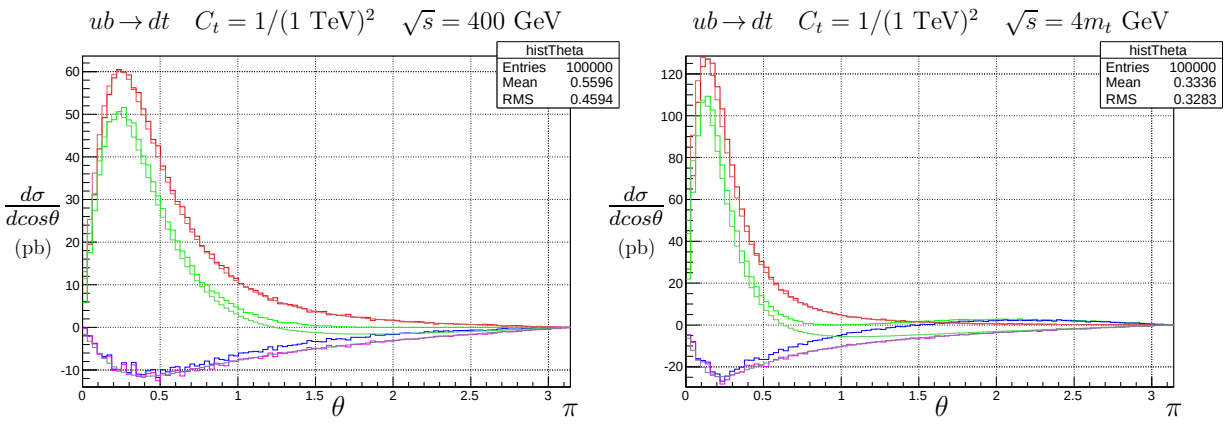

Figure 4.14: *Example parton level $d\sigma/dcos\theta$ distributions for the linear combinations of operators four-fermion operators controlled by C_t for $\sqrt{s} = 400\,GeV$ (left) and $\sqrt{s} = 4m_t \simeq 692\,GeV$ (right). Histograms show* MadGraph *events corresponding to $|\mathcal{M}_{SM}|^2$, $|\mathcal{M}_{int}|^2$, $|\mathcal{M}_{int}|^2 + |\mathcal{M}_{D6}|^2$ and $|\mathcal{M}_{tot}|^2$, while the solid lines are analytic checks for $|\mathcal{M}_{SM}|^2$, $|\mathcal{M}_{int}|^2$, and $|\mathcal{M}_{SM}|^2 + |\mathcal{M}_{int}|^2$.*

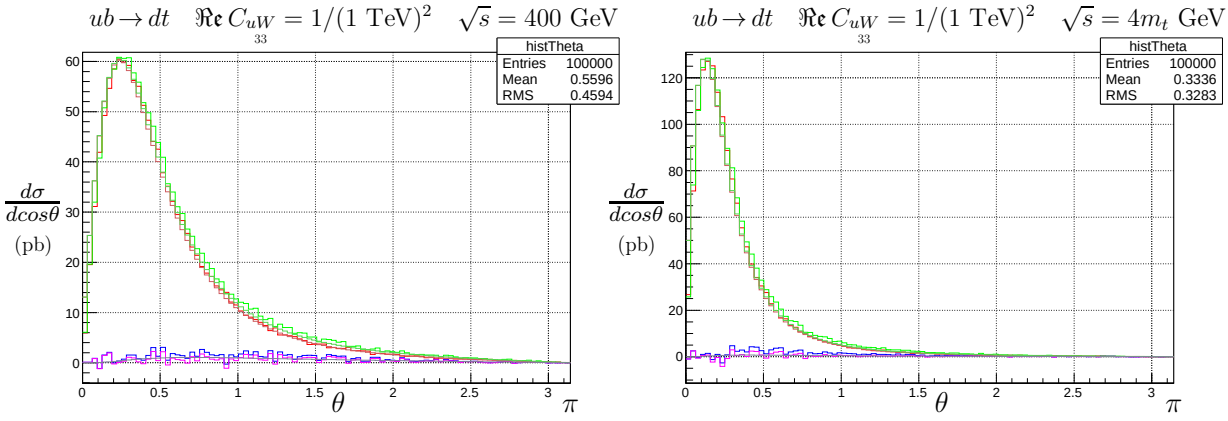

Figure 4.15: *Example parton level $d\sigma/dcos\theta$ distributions for $\Re\mathfrak{e}\, Q_{uW}^{33}$ for $\sqrt{s} = 400\,GeV$ (left) and $\sqrt{s} = 4m_t \simeq 692\,GeV$ (right). Histograms show* MadGraph *events corresponding to $|\mathcal{M}_{SM}|^2$, $|\mathcal{M}_{int}|^2$, $|\mathcal{M}_{int}|^2 + |\mathcal{M}_{D6}|^2$ and $|\mathcal{M}_{tot}|^2$, while the solid lines are analytic checks for $|\mathcal{M}_{SM}|^2$, $|\mathcal{M}_{int}|^2$, and $|\mathcal{M}_{SM}|^2 + |\mathcal{M}_{int}|^2$.*

4.1.3 $q\bar{q}$, $gg \to t\bar{t}Z/\gamma$ Associated Production

Alongside top pair and single top production, first measurements have been reported [133–135] of top pair production in association with a photon and with a Z boson ($t\bar{t}\gamma$ and $t\bar{t}Z$)*. In contrast to the tbW vertex which is accessible through both single top produc-

*Early measurements of top pair production in association with a W has also been reported by ATLAS and CMS, but the experimental errors are too large to say anything meaningful about new physics therein; the measured cross-sections are still consistent with zero.

tion and top quark decay, the neutral ttZ and $tt\gamma$ couplings have been far less thoroughly explored experimentally. Through a combination of factors including high production thesholds (for the massive gauge bosons) and small branching fractions, the cross-section for these processes are considerably smaller, and statistical uncertainties currently dominate the quoted measurements.

Still, they are of interest because they are sensitive to a new set of operators not previously accessible, corresponding to enhanced top-gauge couplings (which are common characteristics of simple W' and Z models), and which allow contact to be made with electroweak observables. The operator set for $t\bar{t}Z$, for instance, contains the 6 top pair operators, plus the following:

$$\begin{aligned}\mathcal{L}_{D6} \supset\; & C_{uW}(\bar{q}\sigma^{\mu\nu}\tau^I u)\,\tilde{\varphi}\,W^I_{\mu\nu} + C_{uB}(\bar{q}\sigma^{\mu\nu}u)\,\tilde{\varphi}\,B_{\mu\nu} + C^{(3)}_{\varphi q} i(\varphi^\dagger \overleftrightarrow{D}^I_\mu \varphi)(\bar{q}\gamma^\mu\tau^I q) \\ & + C^{(1)}_{\varphi q} i(\varphi^\dagger \overleftrightarrow{D}_\mu \varphi)(\bar{q}\gamma^\mu q) + C_{\varphi u}(\varphi^\dagger i\overleftrightarrow{D}_\mu \varphi)(\bar{u}\gamma^\mu u)\,,\end{aligned} \tag{4.1.4}$$

where the operators Q^{33}_{uW} and $Q^{(3)}_{\substack{\varphi q \\ 33}}$ occur also in single top production.

The comparatively low number of individual $t\bar{t}V$ measurements and their relatively large uncertainties leads to these having little impact on a simultaneous global fit with top pair and single top production. For this reason, individual constraints will be presented on these operators for the moment, keeping in mind that the significantly increased production cross sections and corresponding differential measurements expected in LHC Run II will improve prospects in these channels. Prospects for isolating and constraining the ttV vertex operators using 13 TeV data and ratios of $t\bar{t}V/t\bar{t}$ observables were recently discussed in [136].

4.1.4 Decay observables

Interfering dimension-six operators also contribute to top quark decay observables. Since $V_{tb} \simeq 1$, tops decay nearly 100% of the time to a W-boson and b quark. The fraction of these events which decay to W-bosons with a given helicity: left-handed, right-handed or longitudinal helicity, can be expressed in terms of helicity fractions, which for leading

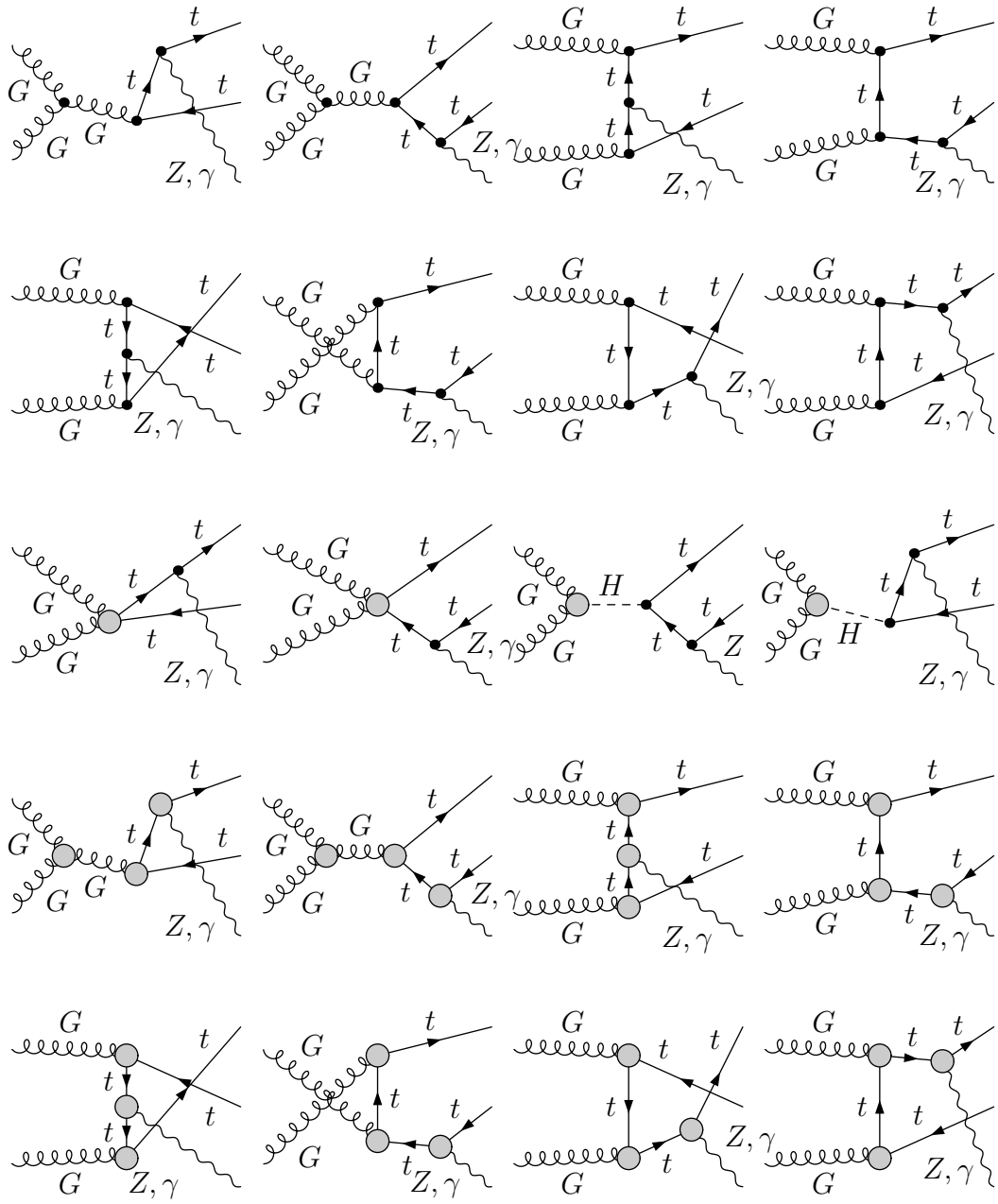

Figure 4.16: *Example Feynman diagrams for $gg \to t\bar{t}(Z/\gamma)$ production. In addition to the operators present in $gg \to t\bar{t}$, the shaded ttV vertices allow emissions of a Z/γ from insertions of the dimension-six operators $Q_{uB}^{33}, Q_{uW}^{33}, Q_{\varphi u}, Q_{\varphi q}^{(1)}$ and $Q_{\varphi q}^{(3)}$.*

order with a finite b-quark mass are:

$$
\begin{aligned}
F_0 &= \frac{(1-y^2)^2 - x^2(1+y^2)}{(1-y^2)^2 + x^2(1-2x^2+y^2)} \\
F_L &= \frac{x^2(1-x^2+y^2) + \sqrt{\lambda}}{(1-y^2)^2 + x^2(1-2x^2+y^2)} \\
F_R &= \frac{x^2(1-x^2+y^2) - \sqrt{\lambda}}{(1-y^2)^2 + x^2(1-2x^2+y^2)}
\end{aligned}
\tag{4.1.5}
$$

for the SM with $x = M_W/m_t$, $y = m_b/m_t$ and $\lambda = 1 + x^4 + y^4 - 2x^2y^2 - 2x^2 - 2y^2$. As noted in Ref. [91], measurements of these fractions can be translated into bounds on the operator $\Re\mathfrak{e}\, Q_{uW}^{33}$. The desirable feature of these quantities is that they are relatively stable against higher order corrections, so the associated scale uncertainties are small. The Standard Model NNLO estimates for these are: $\{F_0, F_L, F_R\} = \{0.687 \pm 0.005, 0.311 \pm 0.005, 0.0017 \pm 0.0001\}$ [137], i.e. the uncertainties are at the per mille level.

4.1.5 Charge Asymmetries

Asymmetries in the production of top quark pairs have received a lot of attention in recent years, particularly due to an apparent discrepancy between the Standard Model prediction for the so-called 'forward-backward' asymmetry A_{FB} in top pair production:

$$A_{\mathrm{FB}} = \frac{N(\Delta y > 0) - N(\Delta y < 0)}{N(\Delta y > 0) + N(\Delta y < 0)} \tag{4.1.6}$$

where $\Delta y = y_t - y_{\bar{t}}$, as measured at the TeVatron [138]. This discrepancy was most pronounced in the high invariant mass region, pointing to potential TeV-scale physics at play. However, recent work has cast doubts on its significance for two reasons: Firstly, an updated analysis with higher statistics [139] has slightly lowered the excess. Secondly, a full NNLO QCD calculation [140] of A_{FB} showed that, along with NLO QCD + electroweak calculations [141–143] the radiative corrections to A_{FB} are large. The current measurements are now consistent with the Standard Model within 2σ. Moreover, the DØ experiment reports [144] a high-invariant mass measurement *lower* than the SM prediction. From a new physics perspective, it is difficult to accommodate all of this information in a simple, uncontrived model without tension.

Still, in an effective field theory approach, deviations from the Standard Model prediction of A_{FB} take a very simple form. A non-zero asymmetry arises from the difference of four-quark operators:

$$A_{\mathrm{FB}} = ((2C_u^1 - C_u^2) + (4C_d^1 - C_d^2))\frac{3\hat{s}\beta}{64g_s^2\Lambda^2(3-\beta^2)}, \tag{4.1.7}$$

where $\beta = \sqrt{1 - s/4m_t^2}$ is the velocity of the $t\bar{t}$ system*. Combining this inclusive measurement with differential measurements such as $dA_{\rm FB}/dM_{t\bar{t}}$ allows simultaneous bounds to be extracted on all four of these operators.

Though the charge symmetric initial state of the LHC does not define a 'forward-backward' direction, a related charge asymmetry can be defined as:

$$A_C = \frac{N(\Delta|y| > 0) - N(\Delta|y| < 0)}{N(\Delta|y| > 0) + N(\Delta|y| < 0)} \tag{4.1.8}$$

making use of the fact that tops tend to be produced at larger rapidities than antitops. At the 13 TeV LHC and beyond, the predominance of the $gg \to t\bar{t}$ production channel (for which $A_C = 0$) will dilute $A_{\rm C}$, which arises from four-quark operators probed in $q\bar{q} \to t\bar{t}$ scattering.

4.1.6 NLO *k*-factors

The implementation of general NLO matrix elements for higher-dimensional operators into event generators is currently a work in progress. Recent advances in expanding the UFO format [148] to incorporate the necessary operator counterterms has led to the availability of models for limited processes, such as top FCNCs [149]†. As was discussed in Chapter 2, the ability to translate between different operator bases is essential for a general automated solution to this problem.

Consequently, we model NLO QCD corrections by including Standard Model K-factors (bin-by-bin for differential observables), where the NLO observables are calculated using MCFM [151], cross-checked with MC@NLO [152, 153]. These K-factors are used for arbitrary values of the Wilson coefficients, thus modelling NLO effects in the pure-SM contribution only. More specifically, this amounts to performing a simultaneous expansion of each observable in the strong coupling α_s and the (inverse) new physics scale Λ^{-1}, and neglecting terms $\sim\mathcal{O}(\alpha_S\Lambda^{-2})$. In the case of top pair total inclusive cross-sections, we use global K-factors from next-to-next-to leading order QCD with soft gluons resummed to next-to-next-to-leading logarithmic accuracy [154–158].

*Contributions to A_{FB} also arise from the normalisation of A_{FB} and the dimension-six squared term [145–147], which we keep, as discussed in sections 3.3 and 4.

†Currently, a general treatment of 'evanescent' four-fermion operators (for an introduction, see e.g. [150]) which arise in dimensional regularization must be automated to be able to obtain the finite parts of the matrix elements. Broadly speaking, the associated difficulties stem from the incompleteness of a given operator basis in d dimensions.

4.2 Fitting Framework

Our fitting procedure utilizes novel techniques developed in the context of Monte Carlo event generator tuning, as implemented in the PROFESSOR [159] framework. The first step is to construct an N-dimensional hypercube in the space of dimension six Wilson Coefficients, compute the K-factor reweighted observables at each point in the space, and then to fit an *interpolating function* $f(\mathbf{C})$ that parametrises the theory prediction as a function of the Wilson coefficients $\mathbf{C} = \{C_i\}$. The values of the operator coefficients are sampled logarithmically about the SM point $\{C_i\} = 0$ to avoid oversampling regions in which these are large. This can then be used to rapidly generate theory observables for arbitrary values of the coefficients. Motivated by the dependence of the total cross-section with a Wilson coefficient:

$$\sigma \sim \sigma_{\text{SM}} + C_i\sigma_{D6} + C_i^2\sigma_{D6^2}\,, \tag{4.2.9}$$

the fitting function is chosen to be a second-order or higher polynomial:

$$f_b(\{C_i\}) = \alpha_0^b + \sum_i \beta_i^b C_i + \sum_{i\leq j} \gamma_{i,j}^b C_i C_j + \dots\,. \tag{4.2.10}$$

In the absence of systematic uncertainties, each observable would exactly follow a second-order polynomial in the coefficients, and higher-order terms capture bin uncertainties which modify this. Observables such as asymmetries, or distributions normalised to the total cross section also invalidate this simple relation. The polynomial also serves as a useful check that the dimension-six approximation is valid. By comparing eq. (4.2.9) with eq. (4.2.10), we see that the terms quadratic in C_i are small provided that the coefficients in the interpolating function $\gamma_{i,j}$ are small. This is a more robust way to ensure validity of the dimension-six approximation than to assume a linear fit from the start.

In practice, to minimise the interpolation uncertainty, we use up to a 4th order polynomial in eq. (4.2.10), depending on the observable of interest. The performance of the interpolation method is shown in Figure 4.17, which depicts the fractional deviation of the polynomial fit from the explicit MC points used to constrain it. The central values and the sizes of the modelling uncertainties may both be parameterised with extremely similar performance, with 4th order performing best for both. The width of this residual mismodeling distribution being $\sim$3% for each of the value and error components is the motivation for a total 5% interpolation uncertainty to be included in the goodness of fit

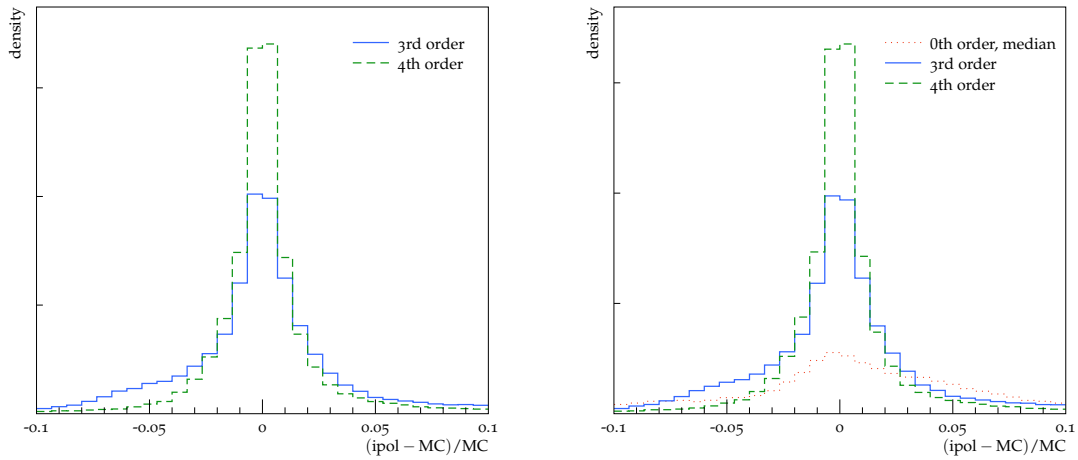

Figure 4.17: *Residuals distributions for interpolated observable values (left) and uncertainties (right), evaluated over all input MC runs and all observables. The 4th order polynomial parameterisation gives the best performance and the vast majority of entries are within 5% of the explicit MC value. The poor performance of a constant uncertainty assumption based on the median input uncertainty is evident – since all three lines have the same normalisation, the majority of residual mismodellings for the median approach are (far) outside the displayed 10% interval.*

of the interpolated MC polynomial $f(\mathbf{C})$ to the experimentally measured value E:

$$\chi^2(\mathbf{C}) = \sum_{\mathcal{O}} \sum_{i,j} \frac{(f_i(\mathbf{C}) - E_i)\rho_{i,j}(f_j(\mathbf{C}) - E_j)}{\sigma_i \sigma_j}\,, \tag{4.2.11}$$

where we sum over all observables $\mathcal{O}$ and all bins in that observable i. We include the correlation matrix $\rho_{i,j}$ where this is provided by the experiments, otherwise $\rho_{i,j} = \delta_{ij}$. The uncertainty on each bin is given by $\sigma_i = \sqrt{\sigma^2_{\text{th},i} + \sigma^2_{\text{exp},i}}$, i.e. we treat theory and experimental errors as uncorrelated. The parameterisation of the theory uncertainties is restricted to not become larger than in the training set, to ensure that polynomial blow-up of the uncertainty at the edges of the sampling range cannot produce a spuriously low χ^2 and disrupt the fit.

We hence have constructed a fast parameterisation of model goodness-of-fit as a function of the EFT operator coefficients. This may be used to produce χ^2 maps in slices or marginalised projections of the operator space, which are then transformed to confidence intervals on the coefficients C_i, defined by the regions for which

$$1 - \text{CL} \geq \int_{\chi^2(C_i)}^{\infty} f_k(x)dx\,, \tag{4.2.12}$$

where typically CL $\in \{0.68, 0.95, 0.99\}$ and $f_k(x)$ is the χ^2 distribution for k degrees of freedom, which we define as $k = N_{\text{measurements}} - N_{\text{coefficients}}$.

4.2.1 Treatment of uncertainties

The uncertainties entering our fit can be classed into three categories:

Experimental uncertainties: We generally have no control over these. In cases where statistical and systematic (and luminosity) errors are recorded separately, we add them in quadrature. Correlations between measurements are also an issue: the unfolding of measured distributions to parton-level introduces some correlation between neighbouring bins. If estimates of these effects have been provided in the experimental analysis, we use this information in the fit, if they are not, we assume zero correlation. However, we have checked that bin correlations have little effect on our numerical results.

There will also be correlations between apparently separate measurements. The multitude of different top pair production cross-section measurements will clearly be correlated due to overlapping event selection criteria and detector effects, etc. Without a full study of the correlations between different decay channels measured by the same experiment, these effects cannot be completely taken into account, but based on the negligible effects of the bin-by-bin correlations on our numerical results we can expect these effects to be small as well.

Theoretical uncertainties: These stem from the choice of parton distribution functions (PDFs), as well as neglected higher-order perturbative corrections. As is conventional, we model the latter by varying the renormalisation and factorisation scales independently in the range $\mu_0/2 \leq \mu_{\text{R,F}} \leq 2\mu_0$, where we use $\mu_0 = m_t$ as the default scale, and take the envelope as our uncertainty. For the PDF uncertainty, we follow the PDF4LHC recommendation [160] of using CT10 [161], MSTW [162] & NNPDF [163] NLO fits, each with associated scale uncertainties, then taking the full width of the scale+PDF envelope as our uncertainty estimate – i.e. we conservatively assume that scales and parton densities are 100% correlated. Unless otherwise stated, we take the top quark mass to be $m_t = 173.2 \pm 1.0$ GeV. We do not consider electroweak corrections. We also re-iterate that since the Wilson coefficients are evaluated at this scale $\mu \sim m_t$, an interpretation of these in the context of a given BSM model at $\mu \sim \Lambda$ should include their running and mixing under the renormalization group.

Interpolation error: The small error relating to the Monte Carlo interpolation (depicted in 4.17) is conservatively estimated to be 5%, as outlined in the previous section. This is subleading compared to the previous two categories.

Constraints are obtained in two ways, for ease of comparison with existing literature. Firstly, single operator coefficients are allowed to vary, with all others set to zero (the SM value). The χ^2 is then minimised using PyMinuit [164], and used to set confidence limits on the operator value. A second approach is to marginalise over the remaining operators, namely to construct the confidence limit for a given operator coefficient whilst allowing all other coefficients to vary.

4.2.2 Experimental Datasets

The experimental measurements used in the fit [133–135, 139, 144, 165–197] are included in Table 4.1. All these measurements are quoted in terms of 'parton-level' quantities; that is, top quarks and their direct decay products. Whilst it is possible to include particle-level observables, available measurements for these are far less abundant and they are beyond the scope of the present study.

The importance of including kinematic distributions is manifest here. For top pair production, for instance, we have a total of 195 measurements, 174 of which come from differential observables. This size of fit is unprecedented in top physics, which underlines the need for a systematic fitting approach, as provided by Professor. Indeed top pair production cross-sections make up the bulk of measurements that are used in the fit. Single top production cross-sections comprise the next dominant contribution. We also make use of data from charge asymmetries in top pair production, as well as inclusive measurements of top pair production in association with a photon or a Z ($t\bar{t}\gamma$ and $t\bar{t}Z$). Measurements of the top width Γ_{top} and W-boson helicity fractions constrain operators impacting the top decay.

4.3 Results

We explore each category of these measurement in turn, discussing the constraints obtained on the applicable operators from the datasets. We will restore the explicit factor of Λ^{-2} carried by each Wilson Coefficient (i.e. writing $C \to C/\Lambda^2$ so that the quantity C

Dataset	$\sqrt{s}$ (TeV)	Measurements	arXiv ref.	Dataset	$\sqrt{s}$ (TeV)	Measurements	arXiv ref.
Top pair production							
Total cross-sections:				Differential cross-sections:			
ATLAS	7	lepton+jets	1406.5375	ATLAS	7	$p_T(t), M_{t\bar{t}}, \lvert y_{t\bar{t}}\rvert$	1407.0371
ATLAS	7	dilepton	1202.4892	CDF	1.96	$M_{t\bar{t}}$	0903.2850
ATLAS	7	lepton+tau	1205.3067	CMS	7	$p_T(t), M_{t\bar{t}}, y_t, y_{t\bar{t}}$	1211.2220
ATLAS	7	lepton w/o b jets	1201.1889	CMS	8	$p_T(t), M_{t\bar{t}}, y_t, y_{t\bar{t}}$	1505.04480
ATLAS	7	lepton w/ b jets	1406.5375	DØ	1.96	$M_{t\bar{t}}, p_T(t), \lvert y_t\rvert$	1401.5785
ATLAS	7	tau+jets	1211.7205				
ATLAS	7	$t\bar{t}, Z\gamma, WW$	1407.0573	Charge asymmetries:			
ATLAS	8	dilepton	1202.4892	ATLAS	7	A_C (inclusive+$M_{t\bar{t}}, y_{t\bar{t}}$)	1311.6742
CMS	7	all hadronic	1302.0508	CMS	7	A_C (inclusive+$M_{t\bar{t}}, y_{t\bar{t}}$)	1402.3803
CMS	7	dilepton	1208.2761	CDF	1.96	A_{FB} (inclusive+$M_{t\bar{t}}, y_{t\bar{t}}$)	1211.1003
CMS	7	lepton+jets	1212.6682	DØ	1.96	A_{FB} (inclusive+$M_{t\bar{t}}, y_{t\bar{t}}$)	1405.0421
CMS	7	lepton+tau	1203.6810				
CMS	7	tau+jets	1301.5755	Top widths:			
CMS	8	dilepton	1312.7582	DØ	1.96	Γ_{top}	1308.4050
CDF + DØ	1.96	Combined world average	1309.7570	CDF	1.96	Γ_{top}	1201.4156
Single top production				W-boson helicity fractions:			
ATLAS	7	t-channel (differential)	1406.7844	ATLAS	7		1205.2484
CDF	1.96	s-channel (total)	1402.0484	CDF	1.96		1211.4523
CMS	7	t-channel (total)	1406.7844	CMS	7		1308.3879
CMS	8	t-channel (total)	1406.7844	DØ	1.96		1011.6549
DØ	1.96	s-channel (total)	0907.4259				
DØ	1.96	t-channel (total)	1105.2788				
Associated production				*Run II data*			
ATLAS	7	$t\bar{t}\gamma$	1502.00586	CMS	13	$t\bar{t}$ (dilepton)	1510.05302
ATLAS	8	$t\bar{t}Z$	1509.05276				
CMS	8	$t\bar{t}Z$	1406.7830				

Table 4.1: *The measurements entering our fit. Details of each are described in the text.*

is dimensionless), and express bounds on these in terms of the dimensionless quantities $\overline{C} \equiv C\, v^2/\Lambda^2$.

The importance of including measurements of the $t\bar{t}$ and single top quark differential distributions is illustrated in Fig 4.18, where we plot our NLO SM estimate for two top pair distributions with and without the dimension-six four-quark contribution from C_u^2.

Both are consistent with the data in the threshold region, which dominates the cross-section, but clear discrimination between SM and dimension-six effects is visible in the high $m_{t\bar{t}}$ / p_T^t regions, which simply originates from the scaling of the dimension-six effects with s/Λ^{2*}.

*One may worry that the inclusion of the final 'overflow' bin in the invariant mass distributions may invalidate the EFT approach. We have performed the global fit without these data points, and found that they have little effect on our constraints. This is due to the large experimental uncertainties

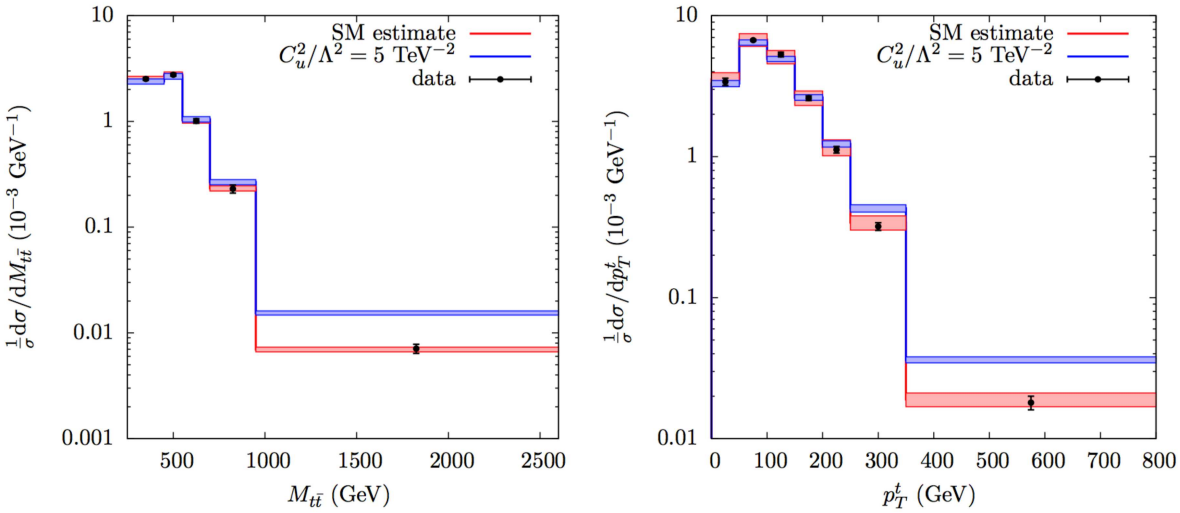

Figure 4.18: *Parton level differential distributions in top pair production, considering SM only (red) and the effects of the four-quark operator O_u^2, showing the enhancement in the tails of the distributions. Data taken from Ref. [185].*

The (individual and marginalized) 95% confidence limits obtained on the nine independent Wilson Coefficients affecting top pair and single top production are shown in Fig 4.19.

Given the lack of reported deviations in top quark measurements, it is unsurprising to see that all Wilson coefficients are consistent with zero within the 95% confidence intervals, and that the SM hypothesis is an excellent description of the data. As one would expect, marginalization over the nine-dimensional space of coefficients leads to weaker bounds on each C than the individual constraints obtained by presuming all others to be zero.

The bounds on operators contributing only to top pair production are typically stronger, consistent with the higher collected statistics in this channel. Constraints obtained on the four-fermion couplings $C_{u/d}^{1/2}$ are looser than their counterparts C_G and C_{uG}^{33}, in line with the expectation that $t\bar{t}$ events are predominantly gluon-fusion induced at the LHC. The coefficient of the so-called chromomagnetic moment operator Q_{uG} is the most tightly constrained in $t\bar{t}$ production, owing to its appearance in both the $q\bar{q}$ and gg channels, i.e. it benefits from both the $q\bar{q}$ dominated TeVatron and the gg dominated LHC measurements. As was discussed, the cross section enhancements from the operator Q_G are driven by the squared dimension six terms. Nonetheless, in the interests of

in this region, and the fact that these bins comprise less than 5% of the total degrees of freedom in our fit, so have little statistical pull.

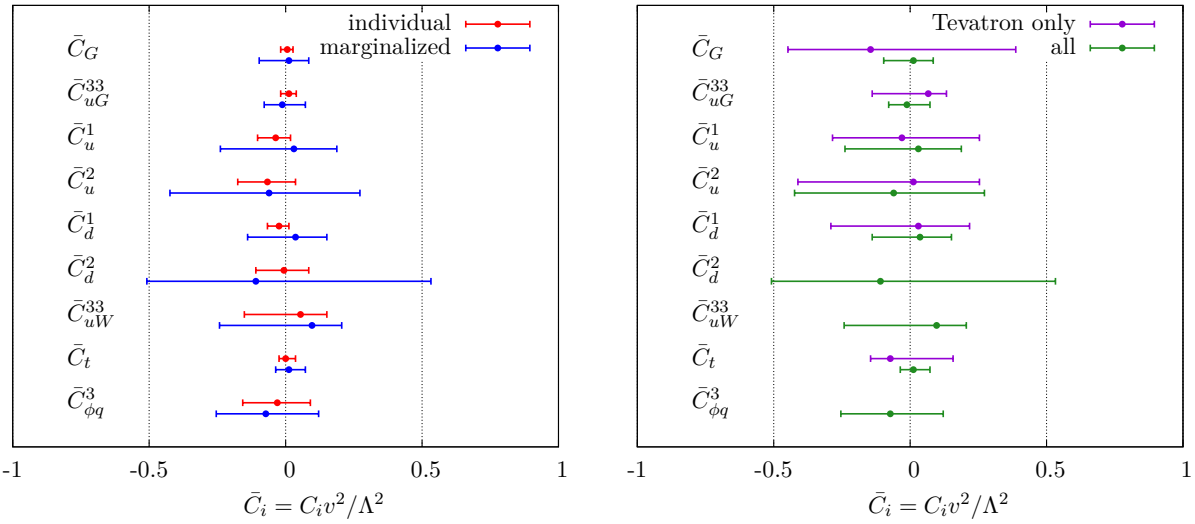

Figure 4.19: *Left: Individual (red) and marginalised (blue) 95% confidence intervals on dimension-six operators from top pair production and single top production (bottom three). Right: Marginalised 95 % bounds considering all data from LHC and Tevatron (green) vs Tevatron only (purple).*

generality, we choose to include this operator in our fit at this stage, noting that bounds on its Wilson coefficient should be interpreted with caution.*

For the four-quark operators, the stronger bounds are typically on the C_i^1-type. This originates simply from the choice of normalization of these linear combinations (as visible in their contribution to the squared matrix element in Section 4.1.1).

With the exception of C_t, which strongly modifies the single top production cross-section, the individual bounds on the operator coefficients from single top production are typically weaker. This originates from the larger experimental uncertainties on single top production, that stem from the multitude of different backgrounds that contaminate this process, particularly top pair production. For the TeVatron datasets this is particularly telling: the few measurements that have been made, with no differential distributions, combined with the large error bars on the available data, mean that two of the three operators are not constrained at dimension-six†. Still, as before, excellent agreement with the SM is observed.

*We have observed that excluding this operator actually tightens the bounds on the remaining ones, so choosing to keep it is the more conservative option.

†Our bounds on these two operators are of the same order, but wider, than a pre-LHC phenomenological study [89], owing to larger experimental errors than estimated there.

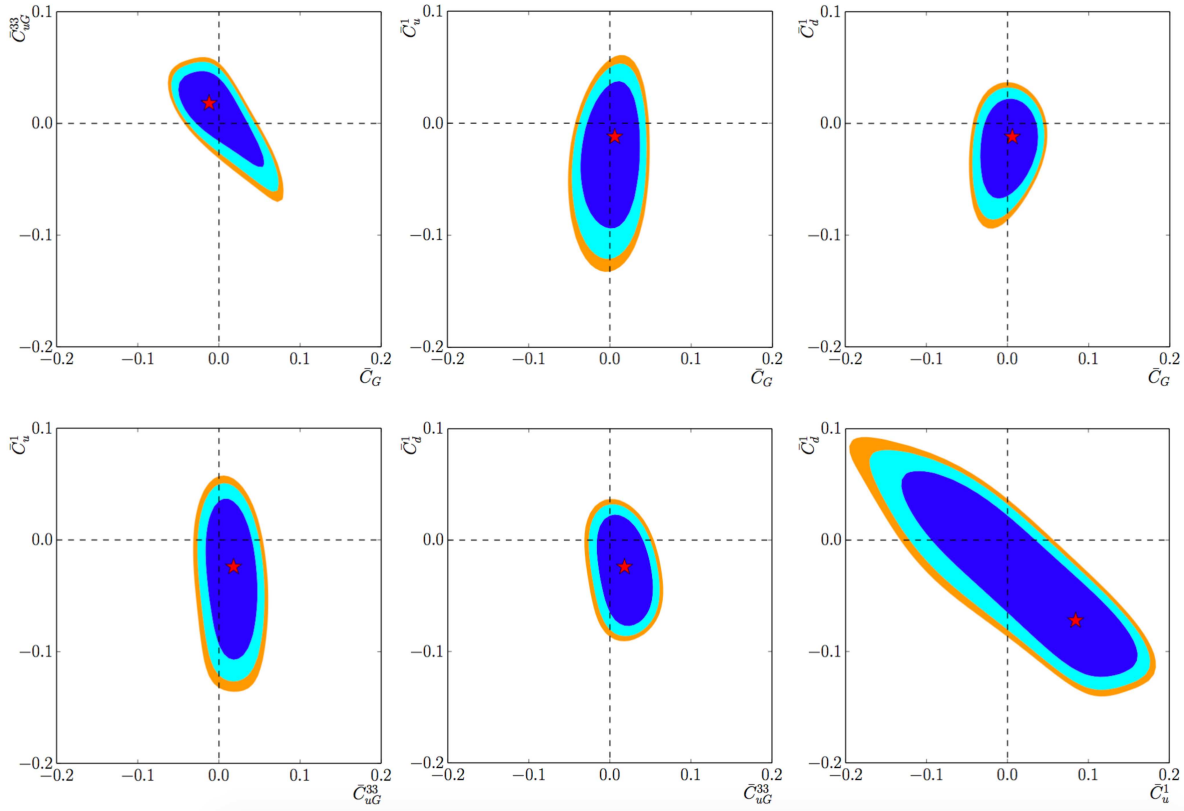

Figure 4.20: *68%, 95% and 99% confidence intervals for selected combinations of operators contributing to top pair production, with all remaining operators set to zero. The star marks the best fit point, indicating good agreement with the Standard Model. Here* $\bar{C}_i = C_i v^2/\Lambda^2$.

In addition to single-top production, Q_{uW} may be constrained by measurements of the distributions of the top quark's decay products. The matrix element for hadronic top quark decay $t \to Wb \to bqq'$, for instance, is equivalent to that for t-channel single top production via crossing symmetry, so decay observables provide complementary information on this operator.

Along with examining the marginalized and individual bounds obtained on each operator, we can also examine the correlation of constraints between pairs of operators. In Figure 4.20 we plot the allowed 68%, 95% and 99% confidence intervals for various pairs of operators, with all others set to zero, showing correlations between some coefficients. Most of these operators appear uncorrelated, though there is a strong correlation between C_u^1 and C_d^1, as their contribution to the squared matrix elements has the same form. In Figure 4.21, the stronger joint constraints on C_G vs C_u^1 obtained from including differential measurements make manifest the importance of utilizing all available cross-

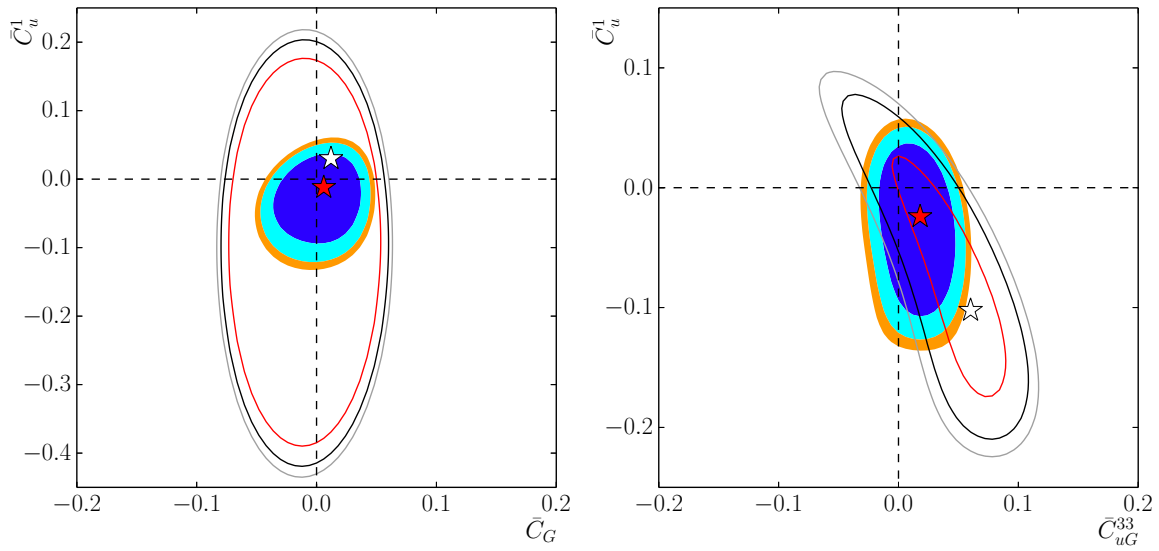

Figure 4.21: *Left: 68%, 95% and 99% confidence intervals on the operators C_G vs. C_u^1 , considering differential and total cross-sections (contours, red star), and total cross-sections only (lines, white star). Right: Limits on C_{uG}^{33} vs. C_u^1, considering both Tevatron and LHC data (contours) and Tevatron data only (lines).*

section information. It is also interesting to note the relative pull of measurements from the LHC and Tevatron, as illustrated in Figure 4.21. It is interesting to see that although Tevatron data are naively more sensitive to four-quark operators, after the LHC Run I and early into Run II, the LHC data size and probed energy transfers lead to comparably stronger constraints. In our fit this is highlighted by the simple fact that LHC data comprise more than 80% of the bins in our fit, so have a much larger pull. This stresses the importance of collecting large statistics as well as using sensitive discriminating observables.

Constraints on operators contributing to the associated production processes $t\bar{t}\gamma$ and $t\bar{t}Z$ as listed in eq. (4.1.4) are displayed in Figure 4.22. As was mentioned, these processes are also sensitive to the set of top pair operators. The bounds obtained on these operators from measurements of $t\bar{t}\gamma$ and $t\bar{t}Z$ production are thus much weaker than those obtained from top pair production due to much more abundant data available for $t\bar{t}$ production, so are not shown here. It is interesting to note that the individual constraints obtained on the operators shared with single top production are comparable from these channels, despite the relative paucity of measurements of associated production.

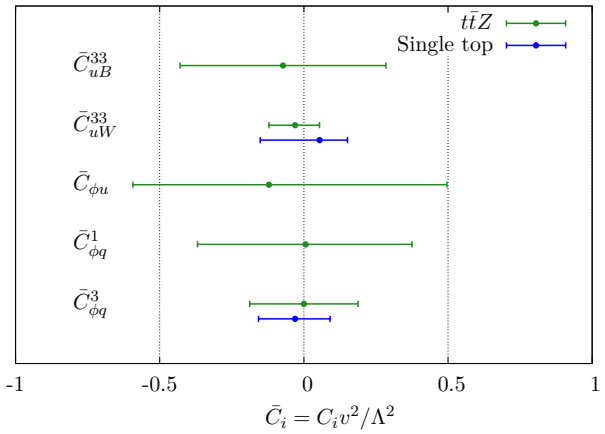

Figure 4.22: *Individual 95% confidence intervals for the operators of 4.1.4 from $t\bar{t}\gamma$ and $t\bar{t}Z$ production (green) and in the two cases where there is overlap, from single top measurements (blue).*

It is interesting to ask how the bound obtained on Q^{33}_{uW} from measurements of the W-boson helicity fractions F_i from the decay of top quarks compares with that obtained from single top production cross-section measurements. In Figure 4.23 we show the constraints obtained in each way. Although they are in excellent agreement with each other, cross-section information gives a slightly stronger bound, mainly due to the larger amount of data available, but also due to the large experimental uncertainties on F_i. Still, these measurements provide complementary information on the operator Q^{33}_{uW}, and combining both results in a stronger constraint than either alone, in line with expectations.

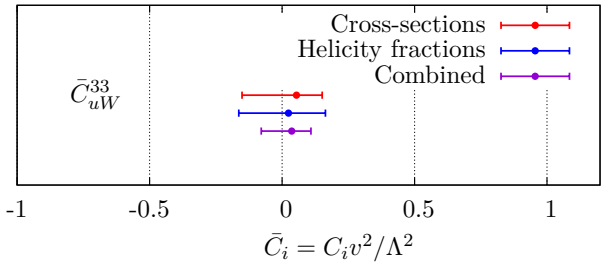

Figure 4.23: *95% bounds on the operator Q^{33}_{uW} obtained from data on top quark helicity fractions (blue) vs. single top production cross-sections (red), and both sets of measurements combined (purple).*

By taking advantage of both inclusive and differential measurements of the $t\bar{t}$ asymmetries $A_{\rm FB}$ and $A_{\rm C}$ from the TeVatron and LHC respectively, bounds can be obtained on the four linear combinations of four-quark operators $C^{1/2}_{u/d}$ complementary to those ex-

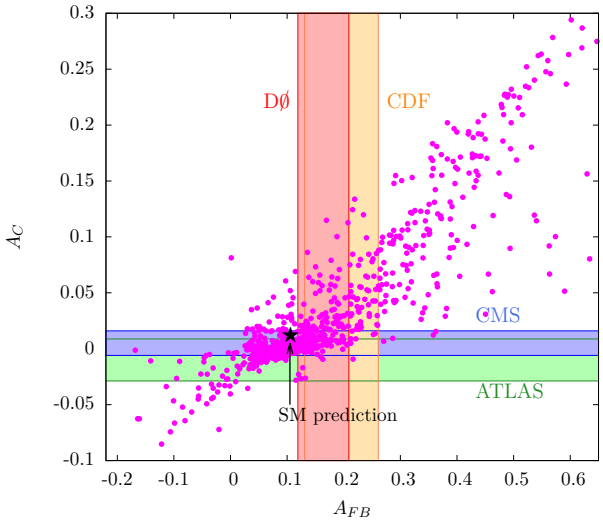

Figure 4.24: *Results of a 1000 point parameter space scan over -10 TeV $^{-2}$ $< C_{u,d}^{1,2}/\Lambda^2 <$ 10 TeV^{-2} overlaid with the most up to date measurements of $A_{\rm FB}$ and $A_{\rm C}$, showing clearly the correlation between them.*

tracted from cross section measurements.*. Again it's possible to (indirectly) investigate the complementarity between Tevatron and LHC constraints.

The most up-to-date SM prediction is $A_C = 0.0123 \pm 0.005$ [143] for $\sqrt{s} = 7$ TeV. The experimental status of these measurements is illustrated in Figure 4.24. The inclusive measurements of $A_{\rm FB}$ are consistent with the SM expectation, as are those of $A_{\rm C}$. The latter, owing to large statistical errors, are also consistent with zero, however, so this result is not particularly conclusive. Since these are different measurements, it is also possible to modify one without significantly impacting the other. Clearly they are correlated, as evidenced in Figure 4.24, where the most up to date measurements of $A_{\rm FB}$ and $A_{\rm C}$ are shown along with the results of a 1000 point parameter space scan over the four-quark operators. This highlights the correlation between the two observables: non-resonant new physics which causes a large $A_{\rm FB}$ will also cause a large $A_{\rm C}$, provided it generates a dimension-six operator at low energies.

We have used both inclusive measurements of the charge asymmetries $A_{\rm C}$ and $A_{\rm FB}$, and measurements as a function of the top pair invariant mass $M_{t\bar{t}}$ and rapidity difference $|y_{t\bar{t}}|$. In addition, ATLAS has published measurements of $A_{\rm C}$ with a longitudinal boost of the $t\bar{t}$ system: $\beta = (|p_t^z + p_{\bar{t}}^z|)/(E_t + E_{\bar{t}}) > 0.6$, which may enhance sensitivity to new physics contributions to $A_{\rm C}$, depending on the model [198].

*Contributions to A_{FB} also arise from the normalisation of A_{FB} and the dimension-six squared term [145–147], which are included in the MadGraph matrix elements.

Since $A_{\rm FB} = 0$ at leading-order in the SM, it is not possible to define a K-factor in the usual sense. Instead we take higher-order QCD effects into account by adding the NNLO QCD prediction to the dimension-six terms. In the case of $A_{\rm C}$, we normalise the small (but non-zero) LO QCD piece, to the NLO prediction, which has been calculated with a Monte Carlo and cross-checked with a dedicated NLO calculation [143].

The above asymmetries have been included in the global fit results presented in Figure 5.5. However, it is also interesting to see what constraints are obtained on the operators from asymmetry data alone. To this end, the 95% confidence intervals on the coefficients of the operators $O_{u,d}^{1,2}$ from purely charge asymmetry data are shown in Figure 4.25. Unsurprisingly, the bounds are much weaker than for cross-section measurements, with the O_i^2-type operators unconstrained by LHC data alone. Despite the small discrepancy between the measured $A_{\rm FB}$ and its SM value, this does not translate into a non-zero Wilson coefficient; as before, all operators are zero within the 95% confidence intervals.

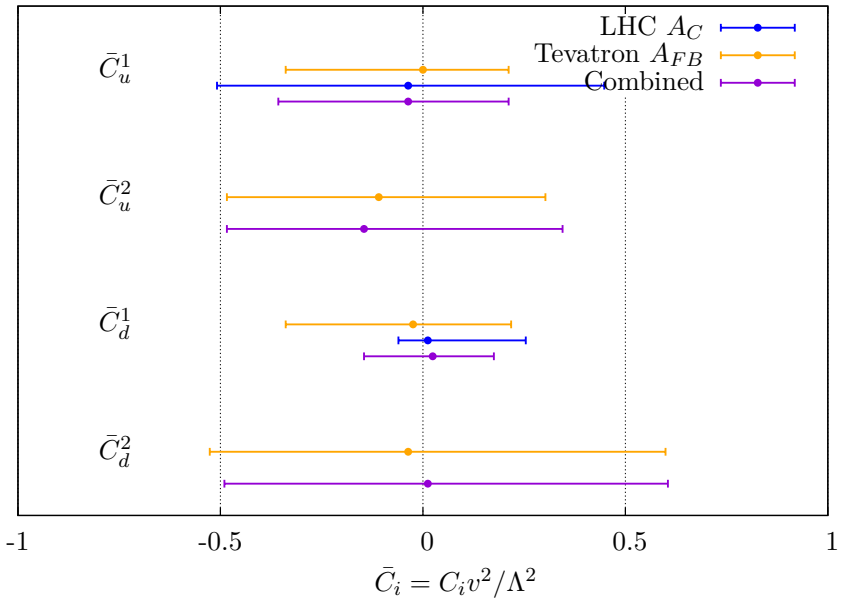

Figure 4.25: *Marginalised 95% confidence intervals on top pair four quark operators from charge asymmetries at the LHC and Tevatron.*

It's also possible to examine the quality of fit for different datasets. We quantify this by calculating the χ^2 per bin between the data and the global best fit point, as shown in Figure 4.27.

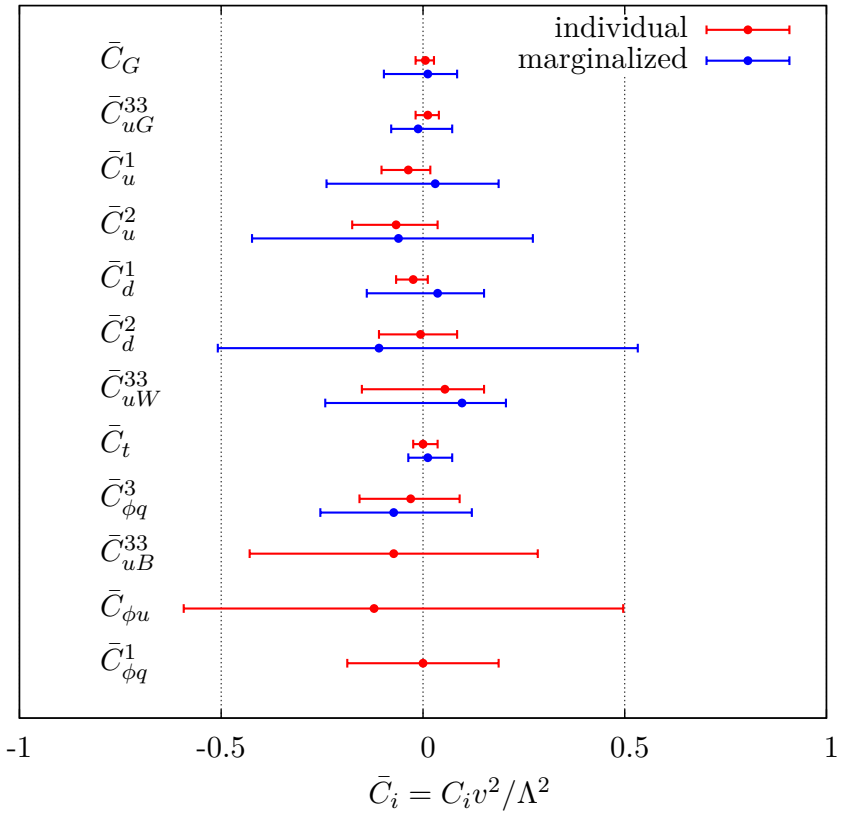

Figure 4.26: *95% confidence intervals for the dimension-six operators that we consider here, with all remaining operators set to zero (red) and marginalised over (blue). In cases where there are constraints on the same operator from different classes of measurement, the strongest limits are shown here. The lack of marginalised constraints for the final three operators is discussed in Section 4.1.3.*

Overall, excellent agreement is seen across the board, with no measurement in obvious tension with any other. The largest single contributors to the χ^2 come from the rapidity distributions in top pair production. It has been known for some time that these are quite poorly modelled with Monte Carlo generators, especially in the boosted regime. It is quite likely that this discrepancy stems from the QCD modelling of the event kinematics, rather than potential new physics. Moreover, in a fit with this many measurements, discrepancies of this magnitude are to be expected on purely statistical grounds.

At the level of total cross-sections, the vanishingly small contributions to the χ^2 stem from two factors: the $\mathcal{O}(10\%)$ measurement uncertainties, which are even larger in hadronic channels, and the large scale uncertainties from the large kinematic range that is integrated over to obtain the total rate. Single top production measurements are also in good agreement with the SM. The associated production processes $tt\gamma$ and ttZ, along

with the charge asymmetry measurements from the LHC, have a very small impact on the fit, owing to the large statistical uncertainties on the current measurements. For the former, this situation will improve in Run II, while the predominance of the gluon fusion channel in $t\bar{t}$ production will hinder prospects for measuring A_C. The forward-backward asymmetry measurements from CDF remain the most discrepant dataset used in the fit.

4.4 Matching to UV Models

As an illustration of the wide-ranging applicability of EFT techniques, we conclude by conducting some simple matching calculations in order to interpret our low-energy effective operator constraints in terms of some specific UV models, and estimate how these compare with corresponding direct searches.

4.4.1 Axigluon searches

Considering top pair production, one can imagine the four-fermion operators appearing in top pair production as being generated by integrating out a heavy s-channel resonance which interferes with the QCD $q\bar{q} \to t\bar{t}$ amplitude.

One particle that could generate such an interference is the so-called colouron, one postulated BSM state offering an explanation for the $t\bar{t}$ forward-backward asymmetry A_{FB}. These are massive colour-octet vector bosons arising in 'chiral colour' models with an extended strong sector, where the gauge group $SU(3)_{c1} \times SU(3)_{c2}$ is spontaneously broken by a non-linear sigma field to the diagonal subgroup $SU(3)_c$ of QCD (for an overview, see e.g. Ref [199]). Analagously to the photon and Z-boson after EWSB, the resulting spectrum includes the massless gluons, and massive colourons which may possess chiral couplings to the quarks. The QCD Lagrangian is replaced by:

$$\mathcal{L} = -\frac{1}{4} G_{1\mu\nu} G_1^{\mu\nu} - \frac{1}{4} G_{2\mu\nu} G_2^{\mu\nu} + \frac{f^2}{4} \, \mathrm{Tr} D_\mu \Sigma \, D^\mu \Sigma^\dagger + \mathcal{L}_{\text{quark}} + \mathcal{L}_{\text{g.f.}} \, .$$

Σ is the nonlinear sigma field transforming in the bi-fundamental representation of $SU(3)_{1c} \times SU(3)_{2c}$ which triggers the breaking to $SU(3)_c$,

$$\Sigma = \exp\left(\frac{2i\pi^a t^a}{f}\right) \, , \quad a = 1, \ldots, 8 \, ,$$

where π^a are the Nambu-Goldstone bosons "eaten" by the coloron, f is the corresponding "decay-constant", and t^a are the usual Gell-Mann matrices. The physical gluon and massive colouron fields G^a_μ and C^a_μ are related to $G^a_{1\,\mu}$ and $G^a_{2\,\mu}$ by a rotation through an angle θ_c, and the quark covariant derivative is supplemented by additional L and R chiral couplings to the colouron:

$$\mathcal{L}^C_{quarks} = \bar{q}^i \left[\not{C}^a t^a \left(g_L P_L + g_R P_R \right) \right] q_i \,, \quad \text{where} \quad g_L, g_R \in g_s \left\{ -\tan\theta_c, \cot\theta_c \right\}.$$

The axigluon is the name given to C^a_μ in the special case $\theta = \pi/4$, i.e. $g_L = -g_R = g_s$.

In the limit $s \ll M_A^2$, where M_A is the axigluon mass, the leading-order interference of an s-channel axigluon with the SM $q\bar{q} \to t\bar{t}$ process identifies the Wilson Coefficients:

$$\frac{C^1_u}{\Lambda^2} = \frac{g_s^2}{M_A^2}, \qquad \frac{C^1_d}{\Lambda^2} = \frac{5g_s^2}{4M_A^2}, \qquad \frac{C^2_u}{\Lambda^2} = \frac{C^2_d}{\Lambda^2} = \frac{2g_s^2}{M_A^2}$$

Substituting the marginalised constraints on the 4-quark operators, we find this translates into a lower bound on an axigluon mass. $M_A \gtrsim 1.4$ TeV at the 95% confidence level. Since this mass range coincides with the overflow bin of figure 4.18, this bound creates some tension with the validity of the EFT approach in the presence of resonances in the $t\bar{t}$ spectrum (for a general discussion see Ref. [102, 200, 201]); at this stage in the LHC programme indirect searches are not sensitive enough to compete with dedicated searches.

4.4.2 W' searches

Turning our attention to single top production, we consider the example of the operator $O^{(3)}_{qq}$ being generated by a heavy charged vector resonance (W') which interferes with the SM amplitude for s-channel single top production: $u\bar{d} \to W \to t\bar{b}$. The generic Lagrangian for such a particle, allowing for both left- and right-handed chiral couplings (see e.g. Ref. [202].), is:

$$\mathcal{L} = \frac{1}{2\sqrt{2}} V_{ij} g_{W'} \bar{q}_i \gamma_\mu (f^R_{ij}(1+\gamma^5) + f^L_{ij}(1-\gamma^5)) W^\mu q_j + h.c. \tag{4.4.13}$$

We consider the scenario where the W' coupling has the same magnitude as that of the W, $g_{W'} = g_2$. The leading contribution from interference with the SM must share

the same $(V-A)$ structure as the weak interaction, so $f^R = \mathcal{O}(\Lambda^{-4})$ can be neglected. The tree-level interference term for between the W and W' diagrams for $u\bar{d} \to t\bar{b}$ in the limit $s \ll M_W'^2$ then identifies:

$$\frac{C_{qq}^{(3)\,1133}}{\Lambda^2} = \frac{g^2}{4M_{W'}^2} \tag{4.4.14}$$

which, using our global constraint on C_t, translates into a bound $M_{W'} \gtrsim 1.2$ TeV.

These bounds are consistent with, but much weaker than, constraints from direct searches for dijet resonances from ATLAS [203, 204] and CMS [205], which report lower bounds of $\{M_A, M_{W'}\} > \{2.72, 3.32\}$ TeV and $\{M_A, M_{W'}\} > \{2.2, 3.6\}$ TeV respectively. It is unsurprising that these dedicated analyses obtain stronger limits, given the generality of this fit. Again this energy range is resolved in our fit, in principle invalidating the use of the dimension-six EFT approach to obtain constraints on this model. Nonetheless, these bounds provide an interesting comparison of our numerical results, whilst emphasising that for model-specific examples, direct searches for high-mass resonances provide stronger limits than general global fits.

4.5 Outlook

Despite the absence of any indication of non-resonant new physics so far, the level of agreement with the SM in such a large global fit is itself a testament to the consistency of different top quark measurements. While we await new data from Run II of the LHC, there are a number of possibilities to expand upon and improve the scope and accuracy of the TopFitter framework.

With the prospect of automated, fully NLO in QCD matrix elements for higher-dimensional operators on the horizon, we will be able to confront mounting datasets and narrowing experimental uncertainties expected over the lifetime of the LHC with more accurate signal modelling. Incorporating operator RGE running and mixing effects will be an essential ingredient in attempting to offer an interpretation of any promising deviations in terms of UV-complete models.

With the appearance in Run II of differential measurements of the $t\bar{t}(Z/\gamma)$ production channels with higher statistics, the number of Wilson Coefficients which can be simultaneously constrained in a global fit will increase. Coupled with our becoming

sensitive to additional operators which enter via loops at $\mathcal{O}(\alpha_s)$, this will necessitate the development of methods by which such a fit can be optimized to accommodate a larger parameter space.

The release of particle level top quark measurements from ATLAS and CMS will also bring new challenges and opportunities. Relaxing the SM-biased assumptions implicit in the 'unfolding' of the detector level final states back to partonic tops opens up sensitivity to probing operators entering into the top decay. While offering potential sensitivity to these effects across all production channels, the computationally intensive inclusion of parton showering and hadronization in the theoretical modelling must be met for this to be taken advantage of. The task of expanding the complexity and number of the accompanying analyses to include the reconstruction of the tops in each of the possible decay channels must then also be overcome.

Particle level datasets also open up the door to exploring more sophisticated observables. Angular asymmetries in the top decay products in particular are sensitive to $\mathcal{CP}$ violating effects of BSM origin, and measurements thereof allow constraints to be placed on the imaginary parts of dimension-six Wilson Coefficients which cannot be seen in cross section measurements.

Work in these directions is currently underway, and hopefully the top sector may surprise us yet.

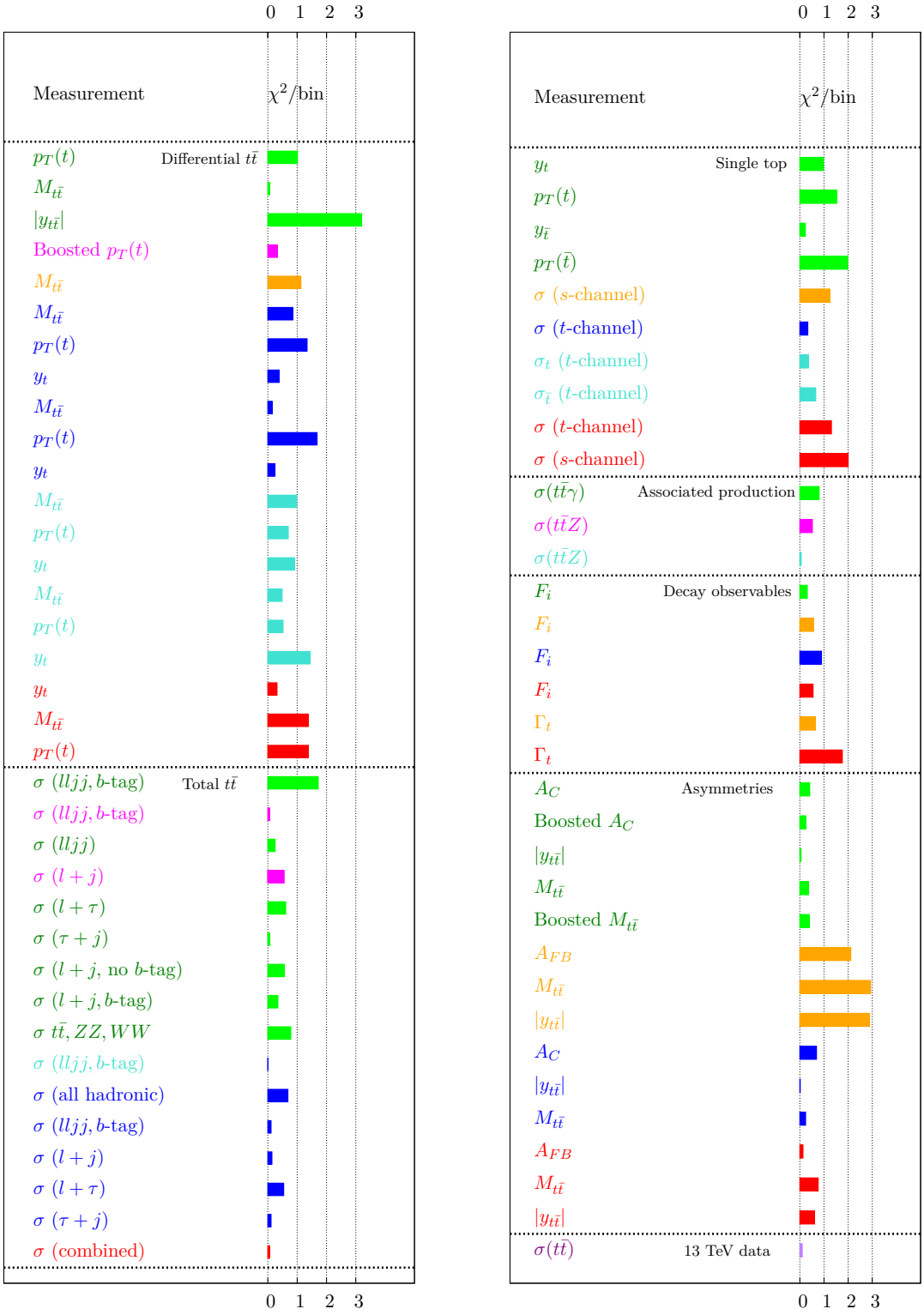

Figure 4.27: *χ^2 per bin between measurement and the interpolated best fit point, for measurements considered in this fit. Colours: Green: ATLAS 7 TeV, Magenta: ATLAS 8 TeV, Blue: CMS 7 TeV, Turquoise: CMS 8 TeV, Red: DØ, Orange: CDF, Purple: CMS 13 TeV.*

Chapter 5

Improving the Top EFT Fit with Boosted Reconstruction Techniques

Unfortunately, the constraints on non-standard behaviour in top quark physics extracted from the small integrated luminosity available from Run I of the LHC are rather weak. For limits set on effective operator coefficients to be useful, they must remain informative (i.e. accurately capture the leading low energy effects) when given a physical interpretation in a matching calculation to a given UV-complete model. Exclusion limits from $t\bar{t}$ resonance searches currently still permit (for some typical perturbative scenarios such as Z', W', or Kaluza-Klein gluon resonances [206–208]) the existence of states in the $M_{NP} \simeq \mathcal{O}(1\text{ TeV})$ region.

This is problematic for EFT, as interpreting a quoted constraint on a Wilson coefficient C/Λ^2 as a model specific statement about an underlying coupling g_* can imply a corresponding mass scale M_* that is resolved by measurements used in the fit [3, 56, 102]. To be compatible with corresponding resonance searches, we must then abandon any attempt to connect this model to the effective description, since our initial assumption $\Lambda = M_* \gg \sqrt{s}$ is no longer valid. The prospects for interpreting EFT constraints in a manner consistent with an inherently limited range of validity will be discussed in more detail in Section 5.4.1.

The increased luminosity in Run II, as well as the 'high luminosity' (HL) phase of the LHC (and in the long term, a potential proposed 100 TeV collider) will lead to a significant improvement of these currently loose constraints. The degree of improvement will depend on the relative importance of particular top channels and the impact of their associated experimental systematic uncertainties on the limit setting. Although we expect deviations from the SM to be most pronounced in scattering at large momentum

transfers where higher-dimensional operators' effects will be most apparent, the theoretical modelling as well as the experimental measurements tend to be less reliable in this regime than at low momentum transfers. With an aim to strengthening our ability to extract information on new physics manifesting in the production of top quarks with large transverse momenta, we conduct a study into the impact of employing dedicated analysis methods geared toward this kinematic regime.

5.1 The Impact of High p_T Final States

The reconstruction of high p_T top quarks demands the use of qualitatively different methods than their softer counterparts. Broadly speaking, the traditional approach to reconstructing top quarks from their decay products proceeds by first identifying separated jets and leptons in an event, then utilizing knowledge of their individual four-momenta to assemble these according to the combinations whose invariant masses most closely match that of the mother W-boson and t-quark. The extraction of jet masses relies on clustering algorithms, which combine together the packed energy deposits left by the jet constituents according to a distance metric in $\eta - \phi$ space in order to invert the successive QCD splitting of individual hard partons. In the presence of boosted final states where the top decay products are closely collimated, the interwoven jet profiles arising from the overlapping b-quark and (hadronic) W-boson decays render attempting to extract a naïve distinction in terms of individual partonic jets insufficient.

Figure 5.1: *Illustration of overlapping 'fat'jets containing concentrated information from the hadronic decay of a boosted top quark. Figure from [209].*

The identification of such tops and the determination of their kinematics falls to jet substructure algorithms (see e.g. [210]) which necessarily abandon attempting to reconstruct the individual top decay products in isolation. Rather, these are tailored specifically toward identifying small scale discriminating features within geometrically

large 'fat' jets comprised of concentrated information from intermingled splittings of partons known to originate from a hadronic top quark decay. Thus by design, they outperform a 'resolved' approach which, while providing good coverage of the low p_T region, suffer from poor statistical and systematic uncertainties in the tails of distributions where isolation criteria begin to fail. Tagging algorithms based on substructure are thus by nature subject to qualitatively different limitations which eliminate this disadvantage. This is pertinent for the future prospects of the global fit, where the incorporated differential measurements - predominantly from Run I - have so far relied on resolved analyses strategies. Furthermore, the availability of efficient tools for these phase space regions has the potential to mitigate the inherent limitation posed to NP searches by correspondingly small production cross sections.

While the available experimental measurements included in the global fit were quoted at the level of partonic tops, a phenomenological study utilizing jet substructure techniques requires, by definition, a hadron-level analysis.

The 'unfolded' measurements released by the experimental collaborations are typically presented at one of two levels. In both cases, datasets are corrected internally for detector effects and extrapolated from the measured 'fiducial' cross section to the full phase space. These distributions are then suitable for comparison with those obtained by reconstructing hadron-level final states simulated in a Monte Carlo event generator. However, as with the majority of measurements available to TopFitter, quantities at this level are often further simplified by incorporating an in-house reconstruction of the hard partons - in our case the $t\bar{t}$ pair. This precludes the possibility of a study employing jet substructure algorithms, since the reconstruction has already been performed on the experimental side.

In a global fit, these substantially ease the workflow by allowing like-for-like comparison of partonic quantities without the need for showering, hadronisation and detector simulation at each point in the parameter space. On the contrary, bypassing the inherent assumptions associated with unfolded distributions comes with the advantage of circumventing inherent biases towards SM-like shapes which arise from implicit input from Monte Carlo simulations. This procedure also introduces additional correlations between neighbouring bins, leading to a broadening of the χ^2 obtained from a fit of theory to data.

Despite the relative lack of suitable hadron-level datasets on which to operate, we can nonetheless account for these factors and utilize boosted top-tagging by working

with hadron-level pseudodata generated by a Monte Carlo simulation. The benefits of targeting final state objects with large transverse momenta are then twofold. Firstly, by making use of sophisticated reconstruction techniques for boosted objects, we isolate the region of phase space where the effects of heavy new degrees of freedom will be most pronounced, as illustrated in Fig. 5.2, and secondly, in doing so we necessarily avoid the model-dependence that fitting parton-level distributions to unfolded measurements suffers from.

It then warrants investigation how the combined effect of these factors influences the potential improvement of a global fit targeting the effective operators arising in top physics. We will again set our sights on $t\bar{t}$ production, which, with a cross section of around 900 pb [158, 211–213] at 13 TeV, is the most abundant source of hard tops. By filtering events according to criteria to distinguish boosted and resolved $t\bar{t}$ final states,

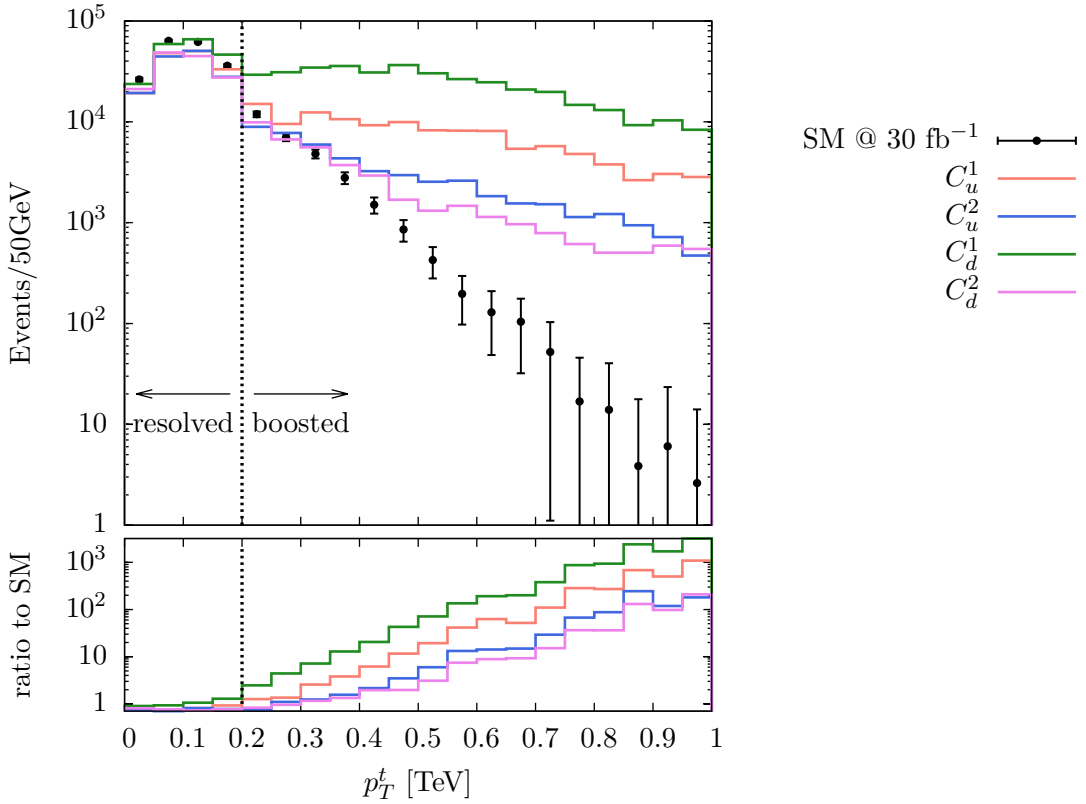

Figure 5.2: *Transverse momentum distributions for the reconstructed hadronic top quark candidate. The bars represent 30 fb^{-1} of pseudodata with $\sqrt{s}$ = 13 TeV constructed with the SM-only hypothesis, while the shaded curves include the effects of four-quark operators with Wilson coefficients $C_i = 10$ TeV^{-2} for illustrative purposes.*

Coefficient C_i	Operator $\mathcal{O}_i$
C_G	$f_{ABC}G_\mu^{A\nu}G_\nu^{B\lambda}G_\lambda^{C\mu}$
C_{uG}	$(\bar{q}\sigma^{\mu\nu}T^A u)\tilde{\varphi}G_{\mu\nu}^A$
C_{qq}^1	$(\bar{q}\gamma_\mu q)(\bar{q}\gamma^\mu q)$
C_{qq}^3	$(\bar{q}\gamma_\mu \tau^I q)(\bar{q}\gamma^\mu \tau^I q)$
C_{uu}	$(\bar{u}\gamma_\mu u)(\bar{u}\gamma^\mu u)$
C_{qu}^8	$(\bar{q}\gamma_\mu T^A q)(\bar{u}\gamma^\mu T^A u)$
C_{qd}^8	$(\bar{q}\gamma_\mu T^A q)(\bar{d}\gamma^\mu T^A d)$
C_{ud}^8	$(\bar{u}\gamma_\mu T^A u)(\bar{d}\gamma^\mu T^A d)$

Table 5.1: *Dimension-six operators affecting $t\bar{t}$ production. The lower six (ψ^4 class) operators contribute via the partonic subprocess $q\bar{q} \to t\bar{t}$ and interfere with the SM through the four linear combinations $C_{u,d}^{1,2}$ listed in section 4.1.1.*

the impact of performing a dedicated analysis on high p_T tops on our sensitivity to non-resonant new physics can be quantified.

The prospective gains from this selection will however be fundamentally limited by the associated low production rates, while boosted top tagging methods innately require the composite jets formed by final states in this phase space region to offer a performance advantage. We choose $p_T^t \geq 200$ GeV as a cutoff point for employing the boosted reconstruction, as the top tagging below this threshold suffers from large mistag rates and small efficiencies [210,214–219]. At 13 TeV and with this threshold in place, we find, for example, that 90% of the cross section comes from the resolved region $p_T^t < 200$ GeV. In light of these competing effects, we thus aim to quantify at what stage in the LHC programme, if at all, the increased sensitivity in this region can compensate for the relatively poor statistics.

5.2 Setup

As a starting point, we once again choose the 'Warsaw' Basis [54] of the SMEFT as our model-independent language and utilize the FeynRules [10] model implementation described in Chapter 3. This was interfaced via the UFO [11] format to MadEvent [220]. The operators relevant to top quark pair production at leading order in the dimension-six SMEFT are re-summarised for convenience in Tab. 5.1.

The generation of theory predictions proceeds as in TopFitter. Events are generated from the (LO in the SMEFT) matrix elements in MadEvent which sample the space of Wilson coefficients. Higher-order QCD corrections are included by re-weighting our distributions by the SM NLO QCD prediction with K-factors, as obtained from Mcfm [151] and cross-checked with Mc@Nlo [220]. Recently, full NNLO results for top quark pair production have become available in [158, 213, 221], we will comment on their potential for improving our results in Sec. 5.4.

We estimate scale uncertainties in the usual way: For the central value of the distributions we choose renormalisation and factorisation scales equal to the top quark mass $\mu_R = \mu_F = m_t$. Then we vary the scales independently over the range $m_t/2 < \mu_{R,F} < 2m_t$. PDF uncertainties are estimated by generating events with Ct14 [222], Mmht14 [223] and Nnpdf3.0 [224] as per the recommendations of the Pdf4Lhc working group for LHC run 2 [160], and we take the full scale+PDF envelope as our theory band. This defines an uncertainty on the differential K-factor which we propagate into each bin in our observable of interest, the hadronic top quark p_T spectrum. We treat theory uncertainties as uncorrelated with experimental systematics and take them to be fixed as a function of luminosity unless stated otherwise.

An interpolation-based parametrising function, as detailed in section 4.2, is invoked to supply theory predictions for each observable for arbitrary values of C_i. This takes the form of a fourth order polynomial in the coefficients $\{C_i\}$ for each bin b:

$$f_b(\{C_i\}) = \alpha_0^b + \sum_i \beta_i^b C_i + \sum_{i \leq j} \gamma_{i,j}^b C_{i,j} + \dots$$

Once f_b is constructed, all that remains is to define a goodness of fit function between theory and (pseudo-)data, and minimise it to obtain exclusion contours for $\{C_i\}$.

To benchmark the expected exclusion limits for each operator coefficient, we generate pseudodata for the SM hypothesis by showering a $\{C_i = 0\}$ sample in Herwig++ [225, 226] which, along with incorporating the decay of the $t\bar{t}$ pair, models initial and final state radiation, as well as hadronisation and the underlying event.

The reconstructed hadronic top p_T spectrum was obtained from a large MC event sample, which was reweighted to correspond to the relevant LHC integrated luminosity scenarios $\mathcal{L}$ and experimental statistical uncertainties (see Section 5.4). The statistical uncertainties associated with each bin for a given scenario were imposed by extracting the equivalent luminosity $\mathcal{L}_0$ of the pseudodata set generated with a known number of

events, and applying the Poisson counting error $1/\sqrt{N_{\mathcal{L}}}$ corresponding to the appropriate fraction of this. Systematics are then inserted by defining a flat percentage interval associated with each bin.

5.3 Analysis Strategy

We will restrict ourselves to the semileptonic top pair decay channel (as illustrated in Fig. 5.3) in which we can take advantage of boosted top-tagging methods on the hadronic top quark, while benefitting from a cleaner environment and comparable cross section relative to the all-hadronic decay mode.

Our analysis setup, as implemented in RIVET [227], is as follows:

We first require a single charged lepton with $p_T > 30$ GeV*, and find the E_T^{miss} vector which we require to have a magnitude > 30 GeV. The leptonic W-boson is then reconstructed from these by requiring transverse momentum conservation and imposing that $m_{l\nu}$ is equal to the on-shell W mass.

*We do not consider τ decays here to avoid the more involved reconstruction.

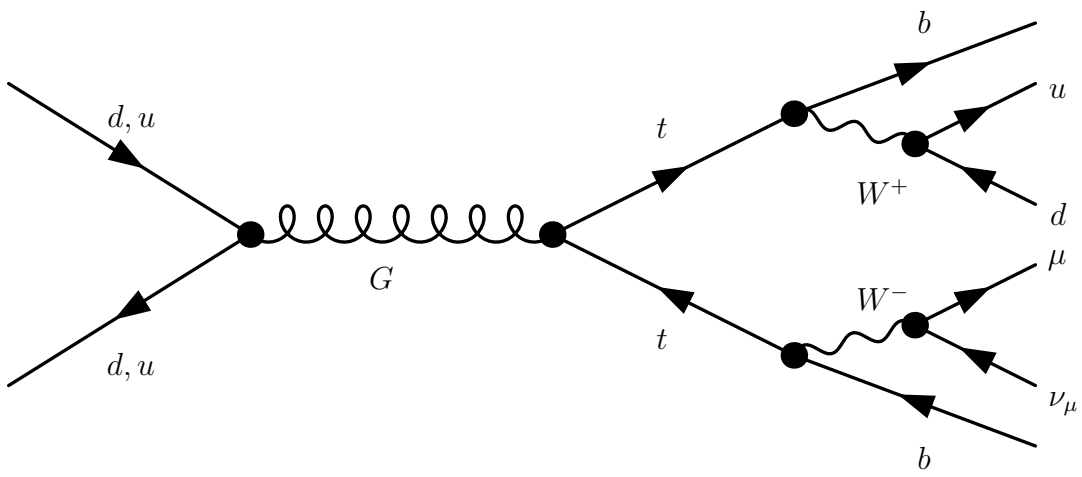

Figure 5.3: *Example Feynman diagram for $\bar{q}q \to t\bar{t}$ production in the semileptonic decay channel with $t \to bu\bar{d}$, $\bar{t} \to \bar{b}\mu\bar{\nu_\mu}$ in the SM. Operator insertions in the production of the $t\bar{t}$ pair are as in Fig. 4.1.*

Leptons	$p_T > 30$ GeV
	$\|\eta\| < 4.2$
Missing energy	$E_T^{\text{miss}} > 30$ GeV
Small jets	anti-k_T $R = 0.4$
	$p_T > 30$ GeV , $\|\eta\| < 2$
Fat jets	anti-k_T $R = 1.2$
	$p_T > 200$ GeV , $\|\eta\| < 2$
Resolved	≥ 4 small jets w/≥ 2 b-tags
Boosted	≥ 1 fat jet, ≥ 1 small jet w/ b-tag

Table 5.2: *Summary of the physics object definitions and event selection criteria in our hadron-level analysis.*

Jets are then clustered using the anti-k_T algorithm [228] using FastJet [229] in two separate groups with $R \equiv (\sqrt{\delta\eta^2 + \delta\phi^2}) = (0.4, 1.2)$ requiring $p_T > (30, 200)$ GeV respectively, and jets which overlap with the charged lepton are removed. The $R = 1.2$* fat jets are required to be within $|\eta| < 2$, and the $R = 0.4$ small jets are b-tagged within the same η range with an efficiency of 70% and fake rate of 1% [230].

If at least one fat jet and one b-tagged small jet which does not overlap with the leading fat jet exists, we perform a boosted top-tag of the leading fat jet using HEPTopTagger [214, 215, 231]. This iteratively inverts the original clustering of a fat jet j step-by-step into its constituents (i.e. $j \to j_1,\ j_2\ \ j_1 \to j_3, j_4, \ldots$), identifying hard substructure according to a '*mass drop*' requirement [232] $\max(m_1, m_2) < \mu_{\text{frac}}\, m_j$ (we use $\mu = 0.8$, the recommended tuning for this parameter). If this criterion is not satisfied in a given splitting, the lighter of j_1, j_2 is discarded, otherwise both are kept, and the procedure repeated on the surviving jet components. This preferentially retains splittings following from the decay of massive particles, rather than from soft QCD-mediated emissions. The declustering procedure terminates when a minimum subjet mass $m_i < 30$GeV is reached, ensuring further iteration will not reveal substructure from decaying heavy states.

From each possible triplet of the N_i 'substructure objects' j_i identified by this stage, a scale R_{filter} can then be inferred, corresponding to the angular separation between

*The angular separation between the decay products of a particle with mass m carrying transverse momentum p_T scales as $\Delta R \simeq 2m/p_T$, which together with parity with typical experimental criteria motivates this choice.

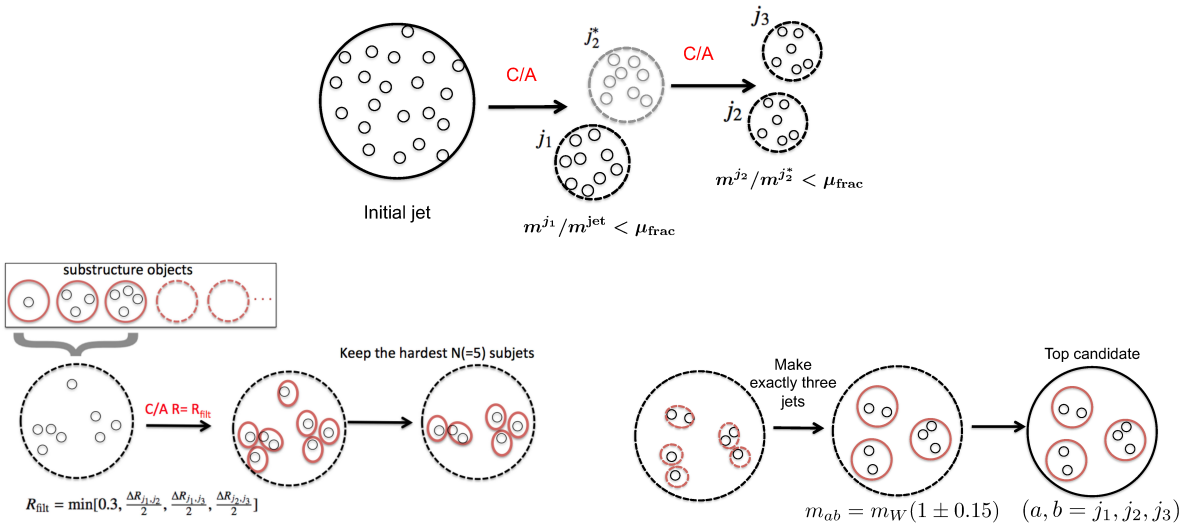

Figure 5.4: *Schematic diagram of the* HEPTopTagger *procedure. The mass-drop stage identifies heavy splittings and their associated angular separations, while discarding soft radiation. This is used to define a 'filtering' radius R_{filter}, with which the fat jet can be resolved at a smaller angular scale relevant to massive decays. Hard subjets are then clustered within R_{filter} in the potentially interesting areas of the fat jet, mitigating the impact of QCD contamination. These are required to have total invariant mass consistent with m_t, before being recombined into three jets whose kinematics most closely resemble those of a hadronic top decay. Image credit [233].*

the decay products of heavy states within the original jet. This is defined as $R_{\text{filter}} = \min(0.3, R_{ij})$, where R_{ij} is the minimum smallest angular distance between two substructures j_i and j_j in this triplet. The constituents of this choice of three j_i are then re-clustered into a number of subjets N_{sub} using the standard Cambridge-Aachen (C/A) algorithm [234] with this smaller radius parameter, resolving only promising areas of the original jet at this higher resolution. Hereby, most of the large area within the fat jet is discarded, minimizing the influence of unrelated QCD radiation on the top mass reconstruction. The hardest of these N_{sub} subjets (up to five, each satisfying $p_T > 30\text{GeV}$) must have a total invariant mass around that of the top, $m = m_t \pm 25\text{GeV}$. Once the top candidate subjets are chosen, these are re-clustered into three final jets corresponding to the d, u and b partons, and their invariant masses are finally required to fulfil criteria corresponding to the $t \to bW^+ \to bu\bar{d}$ decay kinematics [210]. If this is satisfied, this triplet of the j_i is a potential top quark candidate, and if several triplets must be considered (i.e. $N_i > 3$), that which has mass closest to m_t is selected.

The leptonic top candidate is then reconstructed using the leading, non-overlapping b-tagged small jet and the reconstructed leptonic W.

If no fat jet fulfilling all the criteria exists, we instead require at least 2 b-tagged small jets and 2 light small jets. If these exist we perform a resolved analysis by reconstructing the hadronic W-boson by finding the light small jet pair that best reconstructs the W mass, and reconstruct the top candidates by similarly finding the pairs of reconstructed W-boson and b-tagged small jet that best reconstruct the top mass.

Finally, regardless of the approach used, we require both top candidates to have $|m_{\text{cand}} - m_{\text{top}}| < 40$ GeV. If this requirement is fulfilled the event passes the analysis.

5.4 Results

Impact of experimental precision

We choose the three integrated luminosities $\mathcal{L} = \{30\ \text{fb}^{-1}, 300\ \text{fb}^{-1}, 3\ \text{ab}^{-1}\}$ and flat systematic uncertainties $\varepsilon_{\text{syst}} = \{10\%, 20\%\}$ as our experimental points of reference for both selections, motivated by typical estimates from existing analyses by ATLAS [235] and CMS [236].

All the bounds presented here are 'one-at-a-time', i.e. we do not marginalise over the full operator set. Our purpose here is to ascertain the relative improvements to the individual Wilson coefficient confidence intervals, rather than to present a global operator analysis.

In Fig. 5.5, we present 1-dimensional 95% confidence intervals on the operators considered for both selections using $\mathcal{L} = 30\ \text{fb}^{-1}$ and $\varepsilon_{\text{syst}} = 20\%$ as a first benchmark.

As a general rule, the increased sensitivity to the Wilson coefficients offered by the boosted selection is overpowered by the large statistical uncertainties in this region, and the combined limits are dominated by the resolved top quarks. The exception to this rule is the coefficient C_G from the operator $Q_G = f_{ABC} G^{\mu,A}_{\nu} G^{\nu,B}_{\lambda} G^{\lambda,C}_{\mu}$. As noted in section 4.1.1, the squared contribution from this operator's lone s-channel diagram* scales quadratically with all partonic mandelstam variables and carries a large prefactor [125]. High p_T final states thus give stronger bounds on this coefficient, even with comparatively fewer events.

*This has been shown to be the leading gluonic effect in the SMEFT, outshining all contributions from interfering dimension-eight operators [124].

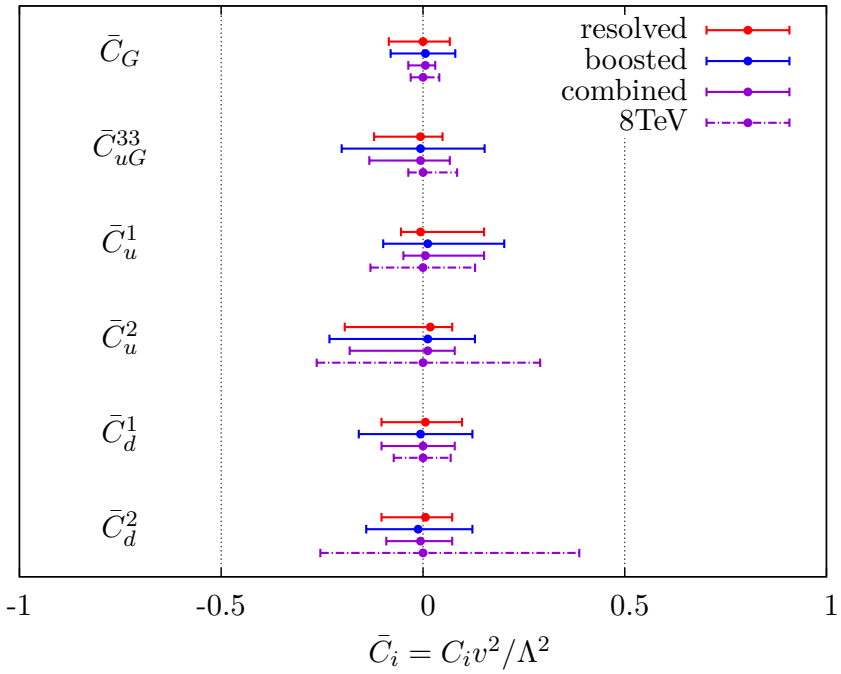

Figure 5.5: *Individual 95% bounds on the operators considered here, from the boosted analysis and the resolved fat jet analysis, and the combined constraint from both, assuming 20% systematics and 30 fb^{-1} of data. We also show existing constraints from unfolded 8 TeV p_T distributions published in [188] and [237], showing a considerable improvement even for a modest luminosity gain.*

With these constraints as a baseline, we can quantify by how much they can be improved upon given an enhancement to the experimental precision. The constraints are presented in Fig. 5.6 for different combinations of systematic and statistical uncertainties. We take the width of the 95% confidence interval in Fig. 5.5 as our normalisation (the green bars), and express the fractional improvements on the limits that can be achieved relative to this baseline, for each operator. The right bars (green, purple, blue) represent 20% systematic uncertainties with, respectively 30, 300 and 3 ab^{-1} of data. The left bars (yellow, orange, red) represent the same respective data sample sizes with a reduction to 10% systematic uncertainties.

Beginning with the resolved selection, we find that the limits on the coefficient C_G can be improved by 40% by going from 30 fb^{-1} to 300 fb^{-1}, and by a further 20% when the full LHC projected data sample is collected. Systematic uncertainties have a more modest effect on this operator: at 3 ab^{-1} the limit on C_G is only marginally improved by a 10% reduction in systematic uncertainty. This merely reflects that C_G mostly impacts

the high p_T tail, so it can only be improved upon in the threshold region by collecting enough data to overcome the lack of sensitivity.

For the chromomagnetic dipole operator Q_{uG}^{33}, improving the experimental systematics plays much more of role. A 10% improvement in systematics, coupled with an increase in statistics from 30 fb^{-1} to 300 fb^{-1} leads to stronger limits that maintaining current systematics and collecting a full 3 ab^{-1} of data. Similar conclusions apply for the four-quark operators, to varying degrees, i.e. reducing systematic uncertainties can provide comparable improvements to collecting much larger data samples.

For the boosted selection, the situation is quite different. For all the operators we consider, improving systematic uncertainties by 10% has virtually no effect on the improvement in the limits. This simply indicates that statistical uncertainties dominate the boosted region at 30 fb^{-1}. For C_G, at 300 fb^{-1} some improvement can be made if systematics are reduced, however we then see that systematic uncertainties saturate the sensitivity to C_G, i.e. there is no improvement to be made by collecting more data. For C_{uG}^{33}, a modest improvement can also be made both by reducing systematics by 10% and by increasing the dataset to 300 fb^{-1}. However, going beyond this, the improvement

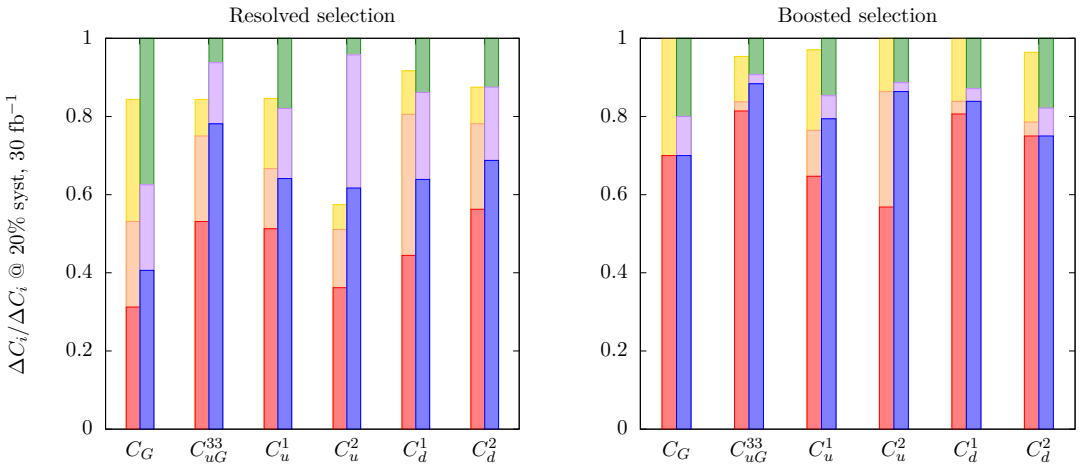

Figure 5.6: *Fractional improvement on the 95% confidence intervals for the operators considered here, with various combinations of luminosity and experimental systematics considered. We take the width of the 95% confidence limit obtained from 20 % systematic uncertainty and 30 fb^{-1} of data as a baseline (green bar), and normalise to this, i.e. we express constraints as a fractional improvement on this benchmark. The purple and blue bars represent respectively, 300 fb^{-1} and 3 ab^{-1} of data, also at 20% systematics, while the yellow, orange and red are the analogous data sample sizes for 10% systematics.*

is minute. The four-quark operators again follow this trend, although C_u^2 shows much more of an improvement when going from 300 fb^{-1} to 3 ab^{-1}.

The impact of theoretical uncertainties

The other key factor in the strength of our constraints is the uncertainties that arise from theoretical modelling. The scale and PDF variation procedure typically leads to uncertainties in the 10-15% range. Recently, fully differential K-factors for top pair production at NNLO QCD (i.e. to order $\mathcal{O}(\alpha_s^4)$) have become available, which have substantially reduced the scale uncertainties. The numbers quoted in Refs. [213, 238] are presently limited to the low to intermediate p_T^t range ($p_T^t < 400$ GeV) applicable to the TeVatron and 8 TeV LHC, as the phase space integration for boosted tops poses a numerical challenge. However, if similar theoretical precision can be achieved for the 13 TeV calculation and used in the boosted regime, it is worthwhile to ask what impact such an improvement could have on the constraints.

We put this question on a firm footing by showing in Fig. 5.7 the 2D exclusion contours for the coefficients C_G and C_{uG}^{33}, as obtained from combining the boosted and resolved limits, at fixed luminosity and experimental systematics, first using our NLO

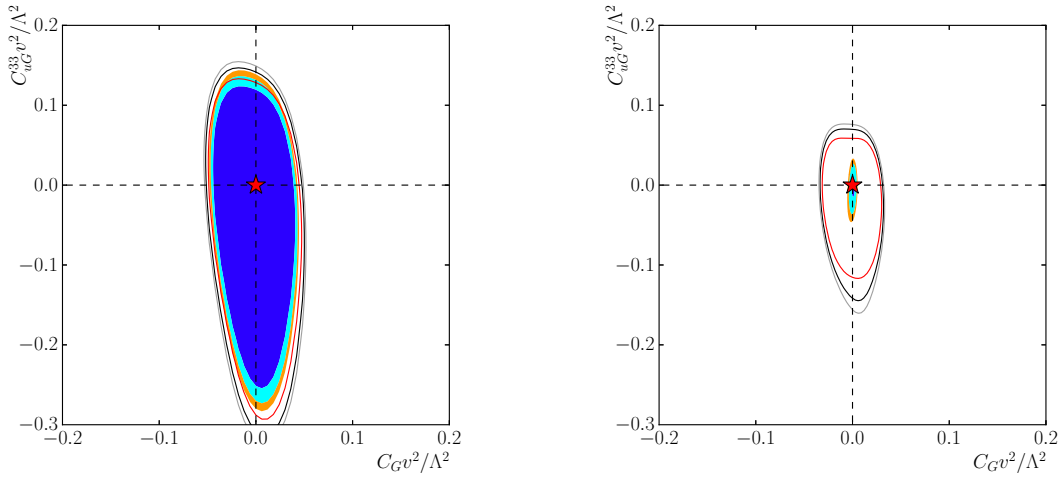

Figure 5.7: *Left: 68%, 95% and 99% confidence intervals for C_G and C_{uG}^{33}, the lines are obtained using experimental (20% systematics and 30 fb^{-1} of data) uncertainties along with theoretical uncertainties, the filled contours using only experimental uncertainties. Right: the same plot, but using 10% systematics and 3 ab^{-1} of data, showing the much stronger impact of theory uncertainties in these circumstances.*

theory uncertainty, and also using *no theory uncertainty at all*. For 30 fb^{-1} the improvement is limited, indicating that at this stage in the LHC programme the main goal should be to first improve experimental reconstruction of the top quark pair final state. However, at 3 ab^{-1} the improvement is substantial, indicating that it will also become necessary to improve the theoretical modelling of this process if the LHC is to extend its kinematic reach for non-resonant new physics.

In addition to SM theoretical uncertainties, there are uncertainties relating to missing higher-order terms in the EFT expansion. Uncertainties due to to loop corrections and renormalisation-group flow of the operators Q_i are important for measurements at LEP-level precision [81,239] where electroweak effects are also resolved. However, at the LHC we find them to be numerically insignificant compared to the sources of uncertainty that we study in detail here. In addition, there is also a possibility of significant effects due to interfering dimension-8 operators, for example due to the presence of the structures in Table. 5.1 carrying additional covariant derivatives. A proper consideration of these effects is left as a future direction of study.

5.4.1 Interpreting constraints

Utilizing EFT to catalogue and set limits on the permissible low-energy footprints of unspecified physics, while a self-consistent procedure, inherently stops short of offering unambiguous information on new states. To serve as a true bridge between the Standard Model and heavy degrees of freedom, one must at some point ascribe to Wilson coefficients an interpretation with a degree of model specificity.

In between stating raw constraints on C/Λ^2 and interpreting them explicitly in terms of UV-complete model parameters, one can gain some insight by viewing these through the lens of varying *general* assumptions about the underlying physics. In this sense, definitive statements about the mass spectrum of specific states and their couplings obtained by explicit matching - e.g. those sketched for axigluon and W' scenarios in section 4.4 - can be abstractified into relationships between the sizes of generic NP couplings g_* and potential resonance masses M_*. Relatively speaking, any intuition acquired from this exercise is low-hanging fruit, as by construction no dedicated BSM calculation need be invoked.

Consider, for example, the simple case where perturbative UV physics is characterised by a single coupling g_* and a unique mass scale M_*. Such a scenario could arise from

integrating out a heavy, narrow resonance. The leading contribution to the dimension-six Wilson coefficient then comes from the simple tree-level matching condition (as exemplified in Fermi's interaction) i.e.:

$$\frac{C_i}{\Lambda^2} = \frac{g_*^2}{M_*^2} \tag{5.4.1}$$

Constraints on the quantity C_i/Λ^2 then correspond to allowed regions in the g_*-M_* plane,

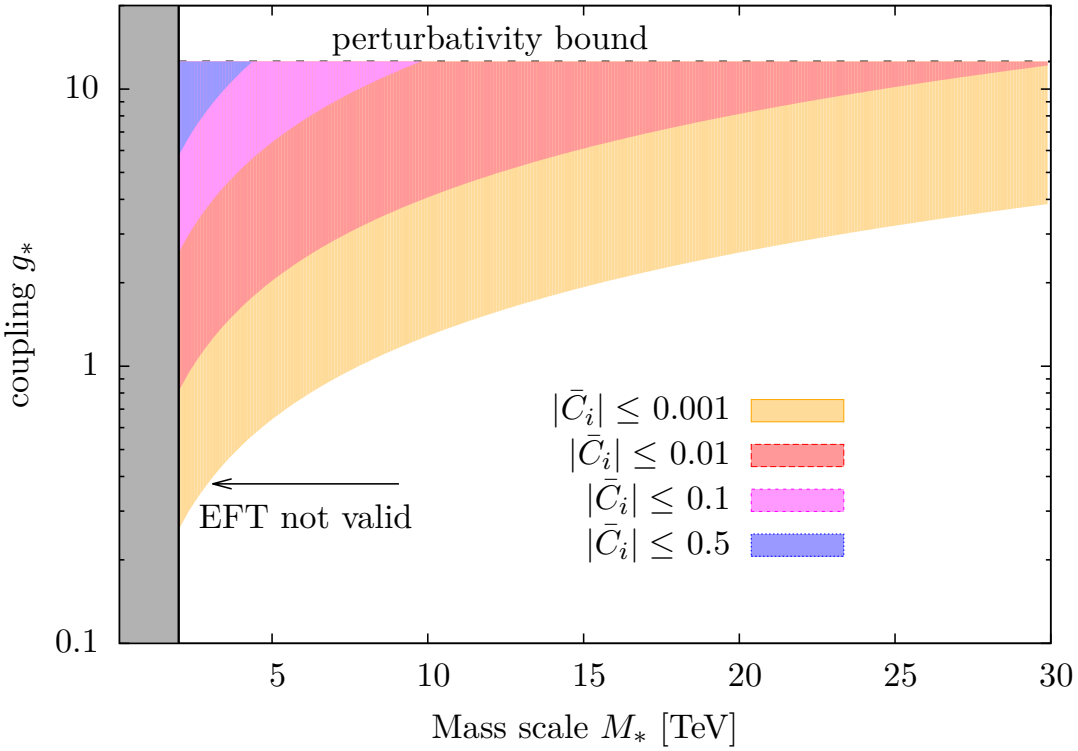

Figure 5.8: *Areas in the new coupling-BSM mass scale plane (see also [102]), resulting from our fit coverage. Coloured areas are constrained in perturbative UV completions at a scale M_*, subject to the boundary condition Eq. (5.4.1). The shaded grey area corresponds to mass scales $M_* < m_{t\bar{t}}^{max}$ probed by the pseudo-data of our fit.*

with each particular value tracing a line of constant g_*/M_*. In Fig. 5.8 we sketch these regions on a logarithmic scale for illustrative choices of C_i, representing a continuum of possible such BSM scenarios.

In order for the EFT description of a given mass region to be valid, we must not resolve it in our measurement. Fortunately, a natural boundary which enshrines this condition emerges from the data in the form of the maximum $t\bar{t}$ invariant mass probed. Imposing the requirement $M_* > m_{t\bar{t}}^{\max}$ ensures that we avoid ascribing an interpretation

to C_i/Λ^2 in the region of the g_*-M_* plane below the production threshold of the heavy state. Therefore we impose a hard cut at $m_{t\bar{t}} = 2$ TeV, obtained from the maximum $t\bar{t}$ invariant mass probed in our SM pseudodata.

By a similarly general argument, one natural partitioning of the coupling g_* into two distinct regions can be imposed by knowledge of the behaviour of perturbation theory. At a given mass scale in the region of EFT's validity $M_* > m_{t\bar{t}}^{\max}$, a weaker constraint on C_i/Λ^2 informs us on the limited region of the g_*-M_* plane corresponding to a larger NP coupling g_*. Here, the convergence of the EFT expansion is slower, since loop diagrams in the BSM theory which produce factors of $g_*^2/(4\pi)^2$ will be more important. Including these diagrams in matching to an EFT will then generate operators of dimension-eight and beyond carrying larger Wilson coefficients, rendering a description in terms of an operator series truncated at $\mathcal{O}(\Lambda^{-2})$ less reliable. The limiting case is represented by the *perturbativity bound* $g_* \simeq 4\pi$ in 5.8, beyond which the low-energy Wilson coefficients are no longer calculable in a perturbative expansion in g_*, as the BSM theory is strongly coupled.

We see that for large Wilson coefficients $\bar{C}_i \gtrsim 0.5$ only a very small window of parameter space may be constrained, but the weak limits push the underlying coupling to such large values that loop corrections are likely to invalidate the simple relation of Eq. (5.4.1), making it hard to trust these limits. However, at 3 ab^{-1}, our projected constraints are typically $\bar{C}_i \lesssim 0.01$, therefore, even for moderate values of the coupling g_*, our constraints are able to indirectly probe mass scales much higher than the kinematic reach of the LHC.

5.5 Conclusions

A crucial question that remains after the first results from LHC Run I is how far a global fit from direct search results will improve with higher statistics and larger kinematic coverage. For representative experimental scenarios and carrying out a dedicated analysis at values of momentum transfer $p_T^t \geq 200$ GeV where top-tagging becomes relevant, we can arrive at the following conclusions:

By making use of jet-substructure algorithms to reconstruct boosted top quarks arising from $t\bar{t}$ production, we see that these are a sensitive probe of new interactions which induce a modified trilinear gluon coupling through Q_G. The resulting stronger

combined limits support the assertion that differential distributions are key in breaking degenerate directions in a global fit, by capturing sensitivity in the phenomenologically pertinent phase space regions for particular operators. The remaining operators' (of Table 5.1) weaker scaling with p_T leads to relatively looser bounds than are obtained from the resolved analysis, and the combined limits yield little significant improvement.

The boosted selection is generally saturated by large statistical uncertainties for the typical expected integrated luminosity of Run II. This renders improvements in the associated systematic uncertainties less important relative to the resolved selection, where a similar improvement in experimental precision produces more stringent constraints. Similar observations have been made for boosted Higgs final states [240] and are supported by the fact that the overflow bins in run 1 analyses provide little statistical pull [3]. Thus while boosted analyses are highly efficient tools in searches for resonant new degrees of freedom [206–208, 241], we observe that similar conclusions do not hold for non-resonant signatures where the states responsible fall outside the kinematic coverage of the boosted selection.

In contrast, for a fully resolved analysis targeting tops with $p_T \lesssim 200\text{GeV}$, the sensitivity to new physics-induced deviations is more of a trade-off between weaker distinguishability from the SM and more plentiful data, and collecting more statistics or improving systematics offers comparable benefits.

Theoretical uncertainties that are inherent to our approach are not the limiting factors of the described analysis in the forseeable future, but will become relevant when statistical uncertainties become negligible at very large integrated luminosity.

Under these circumstances, medium p_T range configurations which maximise new physics deviation relative to statistical and experimental as well as theoretical uncertainty are the driving force in setting limits on operators whose effects are dominated by interference with the SM amplitude in the top sector. Given the relative dominance of statistical uncertainties in the boosted region, we can infer that abandoning the boosted analysis for the resolved one beyond $p_T^t \geq 200$ GeV will not affect our results significantly. The most informative phase space region is already accessed with fully resolved techniques, and improved systematic uncertainties in this regime would lead to a significant strengthening of constraints.

Chapter 6

Conclusions

In this thesis we have discussed aspects of Effective Field Theory and its application to searches for physics beyond the Standard Model on the current frontier of high energy physics. We introduced the Standard Model of particle physics as a gauge theory with spontaneously broken symmetry, and described aspects of perturbative Quantum Field Theory, the fundamental forces and the origin of mass. In doing so we explored the role and generation of scales in QFTs using the example of QCD, and made a connection between mass scales and operator dimension. Following on from this we demonstrated the physical context in which Effective Field Theory emerges as a tool with which to parametrize generic non-resonant new physics, and motivated the application of this to the Standard Model in the scenario in which a large separation exists between the Electroweak scale and the masses of new states. In exploring the current paradigm of the SMEFT (with an emphasis on the dimension-six operators), we identified and discussed solutions to the problem of operator redundancies, and the subtleties arising in interpreting the Lagrangian in the Electroweak broken phase. We demonstrated that the task of treating an extensive set of generic higher-dimensional operators was well-suited to applying modern model-building applications based on symbolic manipulation, for which we utilized the FeynRules package. Work to extend this framework was detailed to facilitate conversions between bases of dimension-six operators, and applications were motivated in the context of facilitating higher order perturbative calculations in the future. In the process we explored an example of calculating radiative corrections to effective field theories, and encountered the novel behaviour of operator mixing, discussing its ramifications on interpreting measurements of Wilson coefficients. Through this, we saw that a correct interpretation of any promising constraints on the parameters of the SMEFT will also depend crucially on an understanding of quantum corrections to effective operators.

In summarizing applications in top quark phenomenology at the LHC, we discussed the role of dimension-six operators in top pair and single top production, verifying our model implementation by exploring the features of simulated observables and interpreting the origins of these in light of the structure of the effective operators present. We described the TopFitter framework, in which we performed a global fit of the dimension-six Wilson coefficients to differential top quark measurements from the LHC and TeVatron, finding good agreement with the SM hypothesis so far from datasets collected from Run I of the LHC. While the datasets included herein failed to offer compelling evidence for non-resonant new physics in the top sector, the self-consistency of the constraints obtained vindicated our proof-of-principle that large-scale EFT fits to diverse experimental measurements is a promising avenue to pursue to search for model-independent discrepancies from the SM. After interpreting the constraints obtained and supplying some example matching calculations to compare with direct resonance searches, we discussed some future directions of work through which current limits could be improved, particularly the inclusion of higher-order corrections, of measurements of associated production channels in Run II, and the use of particle-level datasets to probe BSM physics modifying the decay of the top.

Using the example of a phenomenological study into prospects for improving current limits on Wilson coefficients, we also investigated the projected change to constraints over time in a Run II environment, in which a higher proportion of boosted top quarks offers an opportunity to examine a particularly sensitive region of phase space. Herein we saw that the characteristic scaling behaviour with energy exhibited by theories with nonrenormalizable interactions competed with lower statistics and larger theoretical uncertainties in this regime. We demonstrated that the drawbacks of traditional top reconstruction methods can be overcome by employing jet substructure algorithms to reconstruct top quarks produced with large transverse momenta, and understood the spectrum of relative improvements seen using pseudodata to the behaviour of individual operators and to the proton PDFs at the LHC. Looking to the future, we quantified the connection between the strength of experimental bounds and the validity range of EFT when utilized in matching calculations, establishing that the utility of the effective description will increase such that a broader spectrum of UV completions will be consistently constrained once larger datasets are accumulated. We identified a crossover point in which theoretical uncertainties will become important, reinforcing the need for greater precision in future EFT calculations and providing further motivation for the development of automated frameworks for higher-order calculations in the SMEFT.

Colophon

This thesis was made in LaTeX 2_ε using the "hepthesis" class [242].

Bibliography

[1] C. Englert, K. Nordstrom, L. Moore, and M. Russell, "Giving top quark effective operators a boost," *Phys. Lett.* **B763** (2016) 9–15, arXiv:1607.04304 [hep-ph].

[2] A. Buckley, C. Englert, J. Ferrando, D. J. Miller, L. Moore, M. Russell, and C. D. White, "Global fit of top quark effective theory to data," *Phys. Rev.* **D92** no. 9, (2015) 091501, arXiv:1506.08845 [hep-ph].

[3] A. Buckley, C. Englert, J. Ferrando, D. J. Miller, L. Moore, M. Russell, and C. D. White, "Constraining top quark effective theory in the LHC Run II era," arXiv:1512.03360 [hep-ph].

[4] **ATLAS Collaboration** Collaboration, G. Aad *et al.*, "Observation of a new particle in the search for the Standard Model Higgs boson with the ATLAS detector at the LHC," *Phys.Lett.* **B716** (2012) 1–29, arXiv:1207.7214 [hep-ex].

[5] "Atlas luminosity public results run 2." https://twiki.cern.ch/twiki/bin/view/AtlasPublic/LuminosityPublicResultsRun2#Lum
Accessed: 2016-09-06.

[6] G. Buchalla, A. J. Buras, and M. E. Lautenbacher, "Weak decays beyond leading logarithms," *Rev. Mod. Phys.* **68** (1996) 1125–1144, arXiv:hep-ph/9512380 [hep-ph].

[7] S. Scherer, "Introduction to chiral perturbation theory," *Adv. Nucl. Phys.* **27** (2003) 277, arXiv:hep-ph/0210398 [hep-ph].

[8] T. Becher, A. Broggio, and A. Ferroglia, *Introduction to Soft-Collinear Effective Theory*, vol. 896. Springer, 2015. arXiv:1410.1892 [hep-ph]. https://inspirehep.net/record/1320996/files/arXiv:1410.1892.pdf.

[9] T. Mannel, "Review of heavy quark effective theory," in *Heavy quarks at fixed target. Proceedings, Workshop, St. Goar, Germany, October 3-6, 1996*, pp. 107–129. 1996. arXiv:hep-ph/9611411 [hep-ph].

[10] A. Alloul, N. D. Christensen, C. Degrande, C. Duhr, and B. Fuks, "FeynRules 2.0 - A complete toolbox for tree-level phenomenology," *Comput. Phys. Commun.* **185** (2014) 2250–2300, arXiv:1310.1921 [hep-ph].

[11] C. Degrande, C. Duhr, B. Fuks, D. Grellscheid, O. Mattelaer, *et al.*, "UFO - The Universal FeynRules Output," *Comput.Phys.Commun.* **183** (2012) 1201–1214, arXiv:1108.2040 [hep-ph].

[12] M. E. Peskin and D. V. Schroeder, *An introduction to quantum field theory*. Advanced book program. Westview Press Reading (Mass.), Boulder (Colo.), 1995. http://opac.inria.fr/record=b1131978. Autre tirage : 1997.

[13] M. Dine, "TASI lectures on the strong CP problem," in *Flavor physics for the millennium. Proceedings, Theoretical Advanced Study Institute in elementary particle physics, TASI 2000, Boulder, USA, June 4-30, 2000*, pp. 349–369. 2000. arXiv:hep-ph/0011376 [hep-ph]. http://alice.cern.ch/format/showfull?sysnb=2232477.

[14] B. Grzadkowski, M. Iskrzynski, M. Misiak, and J. Rosiek, "Dimension-Six Terms in the Standard Model Lagrangian," *JHEP* **1010** (2010) 085, arXiv:1008.4884 [hep-ph].

[15] L. Faddeev and V. Popov, "Feynman diagrams for the yang-mills field," *Physics Letters B* **25** no. 1, (1967) 29 – 30. http://www.sciencedirect.com/science/article/pii/0370269367900676.

[16] F. Englert and R. Brout, "Broken symmetry and the mass of gauge vector mesons," *Phys. Rev. Lett.* **13** (Aug, 1964) 321–323. http://link.aps.org/doi/10.1103/PhysRevLett.13.321.

[17] P. W. Higgs, "Broken symmetries and the masses of gauge bosons," *Phys. Rev. Lett.* **13** (Oct, 1964) 508–509. http://link.aps.org/doi/10.1103/PhysRevLett.13.508.

[18] J. Goldstone, "Field theories with « superconductor » solutions," *Il Nuovo Cimento (1955-1965)* **19** no. 1, (1961) 154–164. http://dx.doi.org/10.1007/BF02812722.

[19] N. Cabibbo, "Unitary symmetry and leptonic decays," *Phys. Rev. Lett.* **10** (Jun, 1963) 531–533. http://link.aps.org/doi/10.1103/PhysRevLett.10.531.

[20] C. Grosche, "An Introduction into the Feynman path integral," arXiv:hep-th/9302097 [hep-th].

[21] J. Schwinger, "On Quantum-Electrodynamics and the Magnetic Moment of the Electron," *Physical Review* **73** (Feb., 1948) 416–417.

[22] C. G. Callan, "Broken scale invariance in scalar field theory," *Phys. Rev. D* **2** (Oct, 1970) 1541–1547. http://link.aps.org/doi/10.1103/PhysRevD.2.1541.

[23] D. J. Gross and F. Wilczek, "Ultraviolet behavior of non-abelian gauge theories," *Phys. Rev. Lett.* **30** (Jun, 1973) 1343–1346. http://link.aps.org/doi/10.1103/PhysRevLett.30.1343.

[24] H. D. Politzer, "Reliable Perturbative Results for Strong Interactions?," *Phys. Rev. Lett.* **30** (1973) 1346–1349.

[25] M. Schmelling, "Status of the strong coupling constant," in *High energy physics: Proceedings, 28th International Conference, ICHEP'96, Warsaw, Poland, July 25-31, 1996. Vol. 1, 2*, pp. 91–102. 1996. arXiv:hep-ex/9701002 [hep-ex].

[26] T. Appelquist and J. Carazzone, "Infrared Singularities and Massive Fields," *Phys. Rev.* **D11** (1975) 2856.

[27] S. Coleman and E. Weinberg, "Radiative corrections as the origin of spontaneous symmetry breaking," *Phys. Rev. D* **7** (Mar, 1973) 1888–1910. http://link.aps.org/doi/10.1103/PhysRevD.7.1888.

[28] R. Alonso, E. E. Jenkins, and A. V. Manohar, "Geometry of the Scalar Sector," *JHEP* **08** (2016) 101, arXiv:1605.03602 [hep-ph].

[29] R. Contino, "The Higgs as a Composite Nambu-Goldstone Boson," in *Physics of the large and the small, TASI 09, proceedings of the Theoretical Advanced Study Institute in Elementary Particle Physics, Boulder, Colorado, USA, 1-26 June 2009*, pp. 235–306. 2011. arXiv:1005.4269 [hep-ph]. https://inspirehep.net/record/856065/files/arXiv:1005.4269.pdf.

[30] R. Alonso, I. Brivio, B. Gavela, L. Merlo, and S. Rigolin, "Sigma Decomposition,"

JHEP **12** (2014) 034, arXiv:1409.1589 [hep-ph].

[31] I. M. Hierro, L. Merlo, and S. Rigolin, "Sigma Decomposition: The CP-Odd Lagrangian," *JHEP* **04** (2016) 016, arXiv:1510.07899 [hep-ph].

[32] A. Kobach, "Baryon Number, Lepton Number, and Operator Dimension in the Standard Model," *Phys. Lett.* **B758** (2016) 455–457, arXiv:1604.05726 [hep-ph].

[33] S. Weinberg, "Phenomemological lagrangians," *Physica* **96A** (1979) 327.

[34] N. D. Christensen and C. Duhr, "FeynRules - Feynman rules made easy," *Comput.Phys.Commun.* **180** (2009) 1614–1641, arXiv:0806.4194 [hep-ph].

[35] K. Nakamura and P. D. Group, "Review of particle physics," *Journal of Physics G: Nuclear and Particle Physics* **37** no. 7A, (2010) 075021. http://stacks.iop.org/0954-3899/37/i=7A/a=075021.

[36] **SLD Electroweak Group, DELPHI, LEP, ALEPH, SLD Heavy Flavour Group, OPAL, LEP Electroweak Working Group, L3** Collaboration, "A Combination of preliminary electroweak measurements and constraints on the standard model," arXiv:hep-ex/0412015 [hep-ex].

[37] G. D'Ambrosio, G. Giudice, G. Isidori, and A. Strumia, "Minimal flavor violation: An Effective field theory approach," *Nucl.Phys.* **B645** (2002) 155–187, arXiv:hep-ph/0207036 [hep-ph].

[38] Z. Han and W. Skiba, "Effective theory analysis of precision electroweak data," *Phys. Rev.* **D71** (2005) 075009, arXiv:hep-ph/0412166 [hep-ph].

[39] M. Schmaltz and D. Tucker-Smith, "Little Higgs review," *Ann. Rev. Nucl. Part. Sci.* **55** (2005) 229–270, arXiv:hep-ph/0502182 [hep-ph].

[40] R. Alonso, E. E. Jenkins, A. V. Manohar, and M. Trott, "Renormalization Group Evolution of the Standard Model Dimension Six Operators III: Gauge Coupling Dependence and Phenomenology," *JHEP* **04** (2014) 159, arXiv:1312.2014 [hep-ph].

[41] W. Buchmuller and D. Wyler *Nucl. Phys.* **B268** (1986) 621.

[42] M. Fierz, "Zur fermischen theorie des β-zerfalls,"

Zeitschrift für Physik **104** no. 7, (1937) 553–565. http://dx.doi.org/10.1007/BF01330070.

[43] J. F. Nieves and P. B. Pal, "Generalized Fierz identities," *Am. J. Phys.* **72** (2004) 1100–1108, arXiv:hep-ph/0306087 [hep-ph].

[44] C. C. Nishi, "Simple derivation of general Fierz-like identities," *Am. J. Phys.* **73** (2005) 1160–1163, arXiv:hep-ph/0412245 [hep-ph].

[45] Y. Takahashi, "The Fierz identities," in *Progress in Quantum Field Theory*, H. Ezawa and S. Kamefuchi, eds., p. 121. 1986.

[46] H. D. Politzer, "Power Corrections at Short Distances," *Nucl. Phys.* **B172** (1980) 349–382.

[47] W. Buchmuller and D. Wyler, "Effective Lagrangian Analysis of New Interactions and Flavor Conservation," *Nucl. Phys.* **B268** (1986) 621–653.

[48] G. F. Giudice, C. Grojean, A. Pomarol, and R. Rattazzi, "The Strongly-Interacting Light Higgs," *JHEP* **06** (2007) 045, arXiv:hep-ph/0703164 [hep-ph].

[49] R. Contino, M. Ghezzi, C. Grojean, M. Muhlleitner, and M. Spira, "Effective Lagrangian for a light Higgs-like scalar," arXiv:1303.3876 [hep-ph].

[50] E. E. Jenkins, A. V. Manohar, and M. Trott, "Renormalization Group Evolution of the Standard Model Dimension Six Operators I: Formalism and lambda Dependence," *JHEP* **10** (2013) 087, arXiv:1308.2627 [hep-ph].

[51] E. E. Jenkins, A. V. Manohar, and M. Trott, "Renormalization Group Evolution of the Standard Model Dimension Six Operators II: Yukawa Dependence," *JHEP* **01** (2014) 035, arXiv:1310.4838 [hep-ph].

[52] C. Englert, D. Goncalves, and M. Spannowsky, "Nonstandard top substructure," *Phys.Rev.* **D89** no. 7, (2014) 074038, arXiv:1401.1502 [hep-ph].

[53] C. Englert, A. Freitas, M. Spira, and P. M. Zerwas, "Constraining the Intrinsic Structure of Top-Quarks," *Phys.Lett.* **B721** (2013) 261–268, 1210.2570.

[54] B. Grzadkowski, M. Iskrzynski, M. Misiak, and J. Rosiek, "Dimension-Six Terms in the Standard Model Lagrangian," *JHEP* **10** (2010) 085, arXiv:1008.4884 [hep-ph].

[55] C. Degrande, "A basis of dimension-eight operators for anomalous neutral triple gauge boson interactions," *JHEP* **02** (2014) 101, arXiv:1308.6323 [hep-ph].

[56] R. Contino, A. Falkowski, F. Goertz, C. Grojean, and F. Riva, "On the Validity of the Effective Field Theory Approach to SM Precision Tests," arXiv:1604.06444 [hep-ph].

[57] T. Hahn, "Generating Feynman diagrams and amplitudes with FeynArts 3," *Comput.Phys.Commun.* **140** (2001) 418–431, arXiv:hep-ph/0012260 [hep-ph].

[58] T. Hahn and M. Perez-Victoria, "Automatized one loop calculations in four-dimensions and D-dimensions," *Comput. Phys. Commun.* **118** (1999) 153–165, arXiv:hep-ph/9807565 [hep-ph].

[59] V. Shtabovenko, "FeynCalc 9," in *17th International workshop on Advanced Computing and Analysis Techniques in physics research (ACAT 2016) Valparaiso, Chile, January 18-22, 2016*. 2016. arXiv:1604.06709 [hep-ph]. https://inspirehep.net/record/1451651/files/arXiv:1604.06709.pdf.

[60] H. P. Nilles, "Supersymmetry, Supergravity and Particle Physics," *Phys.Rept.* **110** (1984) 1–162.

[61] H. E. Haber and G. L. Kane, "The Search for Supersymmetry: Probing Physics Beyond the Standard Model," *Phys.Rept.* **117** (1985) 75–263.

[62] R. Contino, Y. Nomura, and A. Pomarol, "Higgs as a holographic pseudoGoldstone boson," *Nucl.Phys.* **B671** (2003) 148–174, arXiv:hep-ph/0306259 [hep-ph].

[63] K. Agashe, R. Contino, and A. Pomarol, "The Minimal composite Higgs model," *Nucl.Phys.* **B719** (2005) 165–187, arXiv:hep-ph/0412089 [hep-ph].

[64] N. Arkani-Hamed and M. Schmaltz, "Hierarchies without symmetries from extra dimensions," *Phys.Rev.* **D61** (2000) 033005, arXiv:hep-ph/9903417 [hep-ph].

[65] T. Gherghetta and A. Pomarol, "Bulk fields and supersymmetry in a slice of AdS," *Nucl.Phys.* **B586** (2000) 141–162, arXiv:hep-ph/0003129 [hep-ph].

[66] A. Azatov, R. Contino, and J. Galloway, "Model-Independent Bounds on a Light Higgs," *JHEP* **04** (2012) 127, arXiv:1202.3415 [hep-ph]. [Erratum: JHEP04,140(2013)].

[67] J. R. Espinosa, C. Grojean, M. Muhlleitner, and M. Trott, "First Glimpses at Higgs' face," *JHEP* **12** (2012) 045, arXiv:1207.1717 [hep-ph].

[68] T. Plehn and M. Rauch, "Higgs Couplings after the Discovery," *Europhys. Lett.* **100** (2012) 11002, arXiv:1207.6108 [hep-ph].

[69] D. Carmi, A. Falkowski, E. Kuflik, T. Volansky, and J. Zupan, "Higgs After the Discovery: A Status Report," *JHEP* **10** (2012) 196, arXiv:1207.1718 [hep-ph].

[70] M. E. Peskin, "Comparison of LHC and ILC Capabilities for Higgs Boson Coupling Measurements," arXiv:1207.2516 [hep-ph].

[71] B. Dumont, S. Fichet, and G. von Gersdorff, "A Bayesian view of the Higgs sector with higher dimensional operators," *JHEP* **07** (2013) 065, arXiv:1304.3369 [hep-ph].

[72] A. Djouadi and G. Moreau, "The couplings of the Higgs boson and its CP properties from fits of the signal strengths and their ratios at the 7+8 TeV LHC," *Eur. Phys. J.* **C73** no. 9, (2013) 2512, arXiv:1303.6591 [hep-ph].

[73] D. Lopez-Val, T. Plehn, and M. Rauch, "Measuring extended Higgs sectors as a consistent free couplings model," *JHEP* **10** (2013) 134, arXiv:1308.1979 [hep-ph].

[74] C. Englert, A. Freitas, M. M. Muehlleitner, T. Plehn, M. Rauch, M. Spira, and K. Walz, "Precision Measurements of Higgs Couplings: Implications for New Physics Scales," *J. Phys.* **G41** (2014) 113001, arXiv:1403.7191 [hep-ph].

[75] J. Ellis, V. Sanz, and T. You, "Complete Higgs Sector Constraints on Dimension-6 Operators," *JHEP* **07** (2014) 036, arXiv:1404.3667 [hep-ph].

[76] J. Ellis, V. Sanz, and T. You, "The Effective Standard Model after LHC Run I," *JHEP* **1503** (2015) 157, arXiv:1410.7703 [hep-ph].

[77] A. Falkowski and F. Riva, "Model-independent precision constraints on dimension-6 operators," *JHEP* **02** (2015) 039, arXiv:1411.0669 [hep-ph].

[78] T. Corbett, O. J. P. Eboli, D. Goncalves, J. Gonzalez-Fraile, T. Plehn, and M. Rauch, "The Higgs Legacy of the LHC Run I," *JHEP* **08** (2015) 156, arXiv:1505.05516 [hep-ph].

[79] G. Buchalla, O. Cata, A. Celis, and C. Krause, "Fitting Higgs Data with Nonlinear Effective Theory," arXiv:1511.00988 [hep-ph].

[80] **ATLAS** Collaboration, G. Aad *et al.*, "Constraints on non-Standard Model Higgs boson interactions in an effective field theory using differential cross sections measured in the $H \to \gamma\gamma$ decay channel at $\sqrt{s} = 8$ TeV with the ATLAS detector," arXiv:1508.02507 [hep-ex].

[81] L. Berthier and M. Trott, "Consistent constraints on the Standard Model Effective Field Theory," arXiv:1508.05060 [hep-ph].

[82] A. Falkowski, M. Gonzalez-Alonso, A. Greljo, and D. Marzocca, "Global constraints on anomalous triple gauge couplings in effective field theory approach," arXiv:1508.00581 [hep-ph].

[83] C. Englert, R. Kogler, H. Schulz, and M. Spannowsky, "Higgs coupling measurements at the LHC," arXiv:1511.05170 [hep-ph].

[84] S. Davidson, M. L. Mangano, S. Perries, and V. Sordini, "Lepton Flavour Violating top decays at the LHC," *Eur. Phys. J.* **C75** no. 9, (2015) 450, arXiv:1507.07163 [hep-ph].

[85] S. Jung, P. Ko, Y. W. Yoon, and C. Yu, "Renormalization group-induced phenomena of top pairs from four-quark effective operators," *JHEP* **08** (2014) 120, arXiv:1406.4570 [hep-ph].

[86] J. de Blas, M. Chala, and J. Santiago, "Renormalization Group Constraints on New Top Interactions from Electroweak Precision Data," *JHEP* **09** (2015) 189, arXiv:1507.00757 [hep-ph].

[87] R. R. Aguilar, A. O. Bouzas, and F. Larios, "Limits on the anomalous Wtq couplings," arXiv:1509.06431 [hep-ph].

[88] G. Durieux, F. Maltoni, and C. Zhang, "Global approach to top-quark flavor-changing interactions," *Phys. Rev.* **D91** no. 7, (2015) 074017, arXiv:1412.7166 [hep-ph].

[89] Q.-H. Cao, J. Wudka, and C. P. Yuan, "Search for new physics via single top production at the LHC," *Phys. Lett.* **B658** (2007) 50–56, arXiv:0704.2809 [hep-ph].

[90] C. Degrande, J.-M. Gerard, C. Grojean, F. Maltoni, and G. Servant,

"Non-resonant New Physics in Top Pair Production at Hadron Colliders," *JHEP* **1103** (2011) 125, arXiv:1010.6304 [hep-ph].

[91] C. Zhang and S. Willenbrock, "Effective-Field-Theory Approach to Top-Quark Production and Decay," *Phys. Rev.* **D83** (2011) 034006, arXiv:1008.3869 [hep-ph].

[92] N. Greiner, S. Willenbrock, and C. Zhang, "Effective Field Theory for Nonstandard Top Quark Couplings," *Phys. Lett.* **B704** (2011) 218–222, arXiv:1104.3122 [hep-ph].

[93] C. Degrande, N. Greiner, W. Kilian, O. Mattelaer, H. Mebane, T. Stelzer, S. Willenbrock, and C. Zhang, "Effective Field Theory: A Modern Approach to Anomalous Couplings," *Annals Phys.* **335** (2013) 21–32, arXiv:1205.4231 [hep-ph].

[94] N. Greiner, S. Willenbrock, and C. Zhang, "Constraints on non-standard top quark couplings," *Phys. Rev.* **D86** (2012) 014024, hep-ph/1201.6670.

[95] L. Lehman and A. Martin, "Low-derivative operators of the Standard Model effective field theory via Hilbert series methods," *JHEP* **02** (2016) 081, arXiv:1510.00372 [hep-ph].

[96] G. Passarino, "NLO Inspired Effective Lagrangians for Higgs Physics," *Nucl. Phys.* (2013) 416–458, arXiv:1209.5538 [hep-ph].

[97] H. Mebane, N. Greiner, C. Zhang, and S. Willenbrock, "Constraints on Electroweak Effective Operators at One Loop," *Phys.Rev.* **D88** no. 1, (2013) 015028, 1306.3380.

[98] E. E. Jenkins, A. V. Manohar, and M. Trott, "Naive Dimensional Analysis Counting of Gauge Theory Amplitudes and Anomalous Dimensions," *Phys. Lett.* **B726** (2013) 697–702, arXiv:1309.0819 [hep-ph].

[99] C. Hartmann and M. Trott, "On one-loop corrections in the standard model effective field theory; the $\Gamma(h \to \gamma\,\gamma)$ case," *JHEP* **07** (2015) 151, arXiv:1505.02646 [hep-ph].

[100] M. Ghezzi, R. Gomez-Ambrosio, G. Passarino, and S. Uccirati, "NLO Higgs effective field theory and kappa-framework," *JHEP* **07** (2015) 175, arXiv:1505.03706 [hep-ph].

[101] C. Zhang and F. Maltoni, "Top-quark decay into Higgs boson and a light quark at next-to-leading order in QCD," *Phys. Rev.* **D88** (2013) 054005, arXiv:1305.7386 [hep-ph].

[102] C. Englert and M. Spannowsky, "Effective Theories and Measurements at Colliders," *Phys. Lett.* **B740** (2015) 8–15, arXiv:1408.5147 [hep-ph].

[103] C. Hartmann and M. Trott, "Higgs decay to two photons at one-loop in the SMEFT," arXiv:1507.03568 [hep-ph].

[104] C. Cheung and C.-H. Shen, "Nonrenormalization Theorems without Supersymmetry," *Phys. Rev. Lett.* **115** no. 7, (2015) 071601, arXiv:1505.01844 [hep-ph].

[105] A. Drozd, J. Ellis, J. Quevillon, and T. You, "The Universal One-Loop Effective Action," arXiv:1512.03003 [hep-ph].

[106] R. Gauld, B. D. Pecjak, and D. J. Scott, "One-loop corrections to $h \to b\bar{b}$ and $h \to \tau\bar{\tau}$ decays in the Standard Model Dimension-6 EFT: four-fermion operators and the large-m_t limit," arXiv:1512.02508 [hep-ph].

[107] L. Berthier and M. Trott, "Towards consistent Electroweak Precision Data constraints in the SMEFT," *JHEP* **05** (2015) 024, arXiv:1502.02570 [hep-ph].

[108] R. S. Gupta, A. Pomarol, and F. Riva, "BSM Primary Effects," *Phys. Rev.* **D91** no. 3, (2015) 035001, arXiv:1405.0181 [hep-ph].

[109] E. Masso, "An Effective Guide to Beyond the Standard Model Physics," *JHEP* **10** (2014) 128, arXiv:1406.6376 [hep-ph].

[110] A. Pomarol, "Higgs Physics," in *2014 European School of High-Energy Physics (ESHEP 2014) Garderen, The Netherlands, June 18-July 1, 2014*. 2014. arXiv:1412.4410 [hep-ph].

[111] R. Huo, "Effective Field Theory of Integrating out Sfermions in the MSSM: Complete One-Loop Analysis," arXiv:1509.05942 [hep-ph].

[112] M. Cvetic, J. Halverson, and P. Langacker, "Ultraviolet Completions of Axigluon Models and Their Phenomenological Consequences," *JHEP* **11** (2012) 064, arXiv:1209.2741 [hep-ph].

[113] T. Han and Y. Li, "Genuine CP-odd Observables at the LHC,"

Phys.Lett. **B683** (2010) 278–281, arXiv:0911.2933 [hep-ph].

[114] C.-R. Chen, F. Larios, and C. P. Yuan, "General analysis of single top production and W helicity in top decay," *Phys. Lett.* **B631** (2005) 126–132, arXiv:hep-ph/0503040 [hep-ph]. [AIP Conf. Proc.792,591(2005)].

[115] J. A. Aguilar-Saavedra, "Single top quark production at LHC with anomalous Wtb couplings," *Nucl. Phys.* **B804** (2008) 160–192, arXiv:0803.3810 [hep-ph].

[116] J. A. Aguilar-Saavedra and J. Bernabeu, "W polarisation beyond helicity fractions in top quark decays," *Nucl. Phys.* **B840** (2010) 349–378, arXiv:1005.5382 [hep-ph].

[117] J. A. Aguilar-Saavedra, N. F. Castro, and A. Onofre, "Constraints on the Wtb vertex from early LHC data," *Phys. Rev.* **D83** (2011) 117301, arXiv:1105.0117 [hep-ph].

[118] C. Bernardo, N. F. Castro, M. C. N. Fiolhais, H. Gonçalves, A. G. C. Guerra, *et al.*, "Studying the Wtb vertex structure using recent LHC results," *Phys.Rev.* **D90** no. 11, (2014) 113007, arXiv:1408.7063 [hep-ph].

[119] **CMS Collaboration** Collaboration, S. Chatrchyan *et al.*, "Measurements of $t\bar{t}$ spin correlations and top-quark polarization using dilepton final states in pp collisions at $\sqrt{s} = 7$ TeV," *Phys.Rev.Lett.* **112** (2014) 182001, arXiv:1311.3924 [hep-ex].

[120] **ATLAS** Collaboration, G. Aad *et al.*, "Measurements of spin correlation in top-antitop quark events from proton-proton collisions at $\sqrt{s} = 7$ TeV using the ATLAS detector," *Phys. Rev.* **D90** no. 11, (2014) 112016, arXiv:1407.4314 [hep-ex].

[121] J. Alwall, M. Herquet, F. Maltoni, O. Mattelaer, and T. Stelzer, "MadGraph 5 : Going Beyond," *JHEP* **1106** (2011) 128, arXiv:1106.0522 [hep-ph].

[122] R. Brun and F. Rademakers, "ROOT: An object oriented data analysis framework," *Nucl.Instrum.Meth.* **A389** (1997) 81–86.

[123] "MadGraph Wiki what are the default dynamic factorization and renormalization scales in madevent?." https://cp3.irmp.ucl.ac.be/projects/madgraph/wiki/FAQ-General-13.

Accessed: 2016-10-18.

[124] E. Simmons, "Dimension-6 gluon operators as probes of new physics," *Physics Letters B* **226** no. 1, (1989) 132 – 136. http://www.sciencedirect.com/science/article/pii/0370269389903018.

[125] P. L. Cho and E. H. Simmons, "Searching for G3 in $t\bar{t}$ production," *Phys. Rev.* **D51** (1995) 2360–2370, arXiv:hep-ph/9408206 [hep-ph].

[126] S. Zhu, "Next-to-leading order QCD corrections to bg –> tW- at CERN large hadron collider," arXiv:hep-ph/0109269 [hep-ph].

[127] J. M. Campbell and F. Tramontano, "Next-to-leading order corrections to Wt production and decay," *Nucl.Phys.* **B726** (2005) 109–130, arXiv:hep-ph/0506289 [hep-ph].

[128] Q.-H. Cao, "Demonstration of One Cutoff Phase Space Slicing Method: Next-to-Leading Order QCD Corrections to the tW Associated Production in Hadron Collision," arXiv:0801.1539 [hep-ph].

[129] S. Frixione, E. Laenen, P. Motylinski, B. R. Webber, and C. D. White, "Single-top hadroproduction in association with a W boson," *JHEP* **0807** (2008) 029, arXiv:0805.3067 [hep-ph].

[130] C. D. White, S. Frixione, E. Laenen, and F. Maltoni, "Isolating Wt production at the LHC," *JHEP* **0911** (2009) 074, arXiv:0908.0631 [hep-ph].

[131] N. Kauer and D. Zeppenfeld, "Finite width effects in top quark production at hadron colliders," *Phys.Rev.* **D65** (2002) 014021, arXiv:hep-ph/0107181 [hep-ph].

[132] B. P. Kersevan and I. Hinchliffe, "A Consistent prescription for the production involving massive quarks in hadron collisions," *JHEP* **09** (2006) 033, arXiv:hep-ph/0603068 [hep-ph].

[133] **ATLAS** Collaboration, G. Aad *et al.*, "Observation of top-quark pair production in association with a photon and measurement of the $t\bar{t}\gamma$ production cross section in pp collisions at $\sqrt{s} = 7$ TeV using the ATLAS detector," *Phys. Rev.* **D91** no. 7, (2015) 072007, arXiv:1502.00586 [hep-ex].

[134] **ATLAS** Collaboration, G. Aad *et al.*, "Measurement of the $t\bar{t}W$ and $t\bar{t}Z$ production cross sections in pp collisions at $\sqrt{s} = 8$ TeV with the ATLAS

detector," arXiv:1509.05276 [hep-ex].

[135] **CMS** Collaboration, V. Khachatryan *et al.*, "Measurement of top quark-antiquark pair production in association with a W or Z boson in pp collisions at $\sqrt{s} = 8$ TeV," *Eur. Phys. J.* **C74** no. 9, (2014) 3060, arXiv:1406.7830 [hep-ex].

[136] M. Schulze and Y. Soreq, "Pinning down electroweak dipole operators of the top quark," *Eur. Phys. J.* **C76** no. 8, (2016) 466, arXiv:1603.08911 [hep-ph].

[137] A. Czarnecki, J. G. Korner, and J. H. Piclum, "Helicity fractions of W bosons from top quark decays at NNLO in QCD," *Phys. Rev.* **D81** (2010) 111503, arXiv:1005.2625 [hep-ph].

[138] **CDF** Collaboration, T. Aaltonen *et al.*, "Evidence for a Mass Dependent Forward-Backward Asymmetry in Top Quark Pair Production," *Phys. Rev.* **D83** (2011) 112003, arXiv:1101.0034 [hep-ex].

[139] **CDF Collaboration** Collaboration, T. Aaltonen *et al.*, "Measurement of the top quark forward-backward production asymmetry and its dependence on event kinematic properties," *Phys.Rev.* **D87** no. 9, (2013) 092002, arXiv:1211.1003 [hep-ex].

[140] M. Czakon, P. Fiedler, and A. Mitov, "Resolving the Tevatron Top Quark Forward-Backward Asymmetry Puzzle: Fully Differential Next-to-Next-to-Leading-Order Calculation," *Phys. Rev. Lett.* **115** no. 5, (2015) 052001, arXiv:1411.3007 [hep-ph].

[141] W. Hollik and D. Pagani, "The electroweak contribution to the top quark forward-backward asymmetry at the Tevatron," *Phys. Rev.* **D84** (2011) 093003, arXiv:1107.2606 [hep-ph].

[142] J. H. Kuhn and G. Rodrigo, "Charge asymmetries of top quarks at hadron colliders revisited," *JHEP* **01** (2012) 063, arXiv:1109.6830 [hep-ph].

[143] W. Bernreuther and Z.-G. Si, "Top quark and leptonic charge asymmetries for the Tevatron and LHC," *Phys. Rev.* **D86** (2012) 034026, arXiv:1205.6580 [hep-ph].

[144] **D0 Collaboration** Collaboration, V. M. Abazov *et al.*, "Measurement of the forward-backward asymmetry in top quark-antiquark production in ppbar

collisions using the lepton+jets channel," *Phys.Rev.* **D90** no. 7, (2014) 072011, arXiv:1405.0421 [hep-ex].

[145] M. Bauer, F. Goertz, U. Haisch, T. Pfoh, and S. Westhoff, "Top-Quark Forward-Backward Asymmetry in Randall-Sundrum Models Beyond the Leading Order," *JHEP* **11** (2010) 039, arXiv:1008.0742 [hep-ph].

[146] J. A. Aguilar-Saavedra and M. Perez-Victoria, "Probing the Tevatron t tbar asymmetry at LHC," *JHEP* **05** (2011) 034, arXiv:1103.2765 [hep-ph].

[147] C. Delaunay, O. Gedalia, Y. Hochberg, G. Perez, and Y. Soreq, "Implications of the CDF $t\bar{t}$ Forward-Backward Asymmetry for Hard Top Physics," *JHEP* **08** (2011) 031, arXiv:1103.2297 [hep-ph].

[148] C. Degrande, "Automatic evaluation of UV and R2 terms for beyond the Standard Model Lagrangians: a proof-of-principle," *Comput. Phys. Commun.* **197** (2015) 239–262, arXiv:1406.3030 [hep-ph].

[149] C. Degrande, F. Maltoni, J. Wang, and C. Zhang, "Automatic computations at next-to-leading order in QCD for top-quark flavor-changing neutral processes," *Phys. Rev.* **D91** (2015) 034024, arXiv:1412.5594 [hep-ph].

[150] S. Herrlich and U. Nierste, "Evanescent operators, scheme dependences and double insertions," *Nucl. Phys.* **B455** (1995) 39–58, arXiv:hep-ph/9412375 [hep-ph].

[151] J. M. Campbell and R. Ellis, "MCFM for the Tevatron and the LHC," *Nucl.Phys.Proc.Suppl.* **205-206** (2010) 10–15, arXiv:1007.3492 [hep-ph].

[152] S. Frixione and B. R. Webber, "Matching NLO QCD computations and parton shower simulations," *JHEP* **06** (2002) 029, arXiv:hep-ph/0204244 [hep-ph].

[153] S. Frixione, F. Stoeckli, P. Torrielli, B. R. Webber, and C. D. White, "The MCaNLO 4.0 Event Generator," arXiv:1010.0819 [hep-ph].

[154] M. Beneke, P. Falgari, S. Klein, and C. Schwinn, "Hadronic top-quark pair production with NNLL threshold resummation," *Nucl.Phys.* **B855** (2012) 695–741, arXiv:1109.1536 [hep-ph].

[155] M. Cacciari, M. Czakon, M. Mangano, A. Mitov, and P. Nason, "Top-pair production at hadron colliders with next-to-next-to-leading logarithmic soft-gluon resummation," *Phys.Lett.* **B710** (2012) 612–622, arXiv:1111.5869 [hep-ph].

[156] M. Czakon and A. Mitov, "Top++: A Program for the Calculation of the Top-Pair Cross-Section at Hadron Colliders," *Comput.Phys.Commun.* **185** (2014) 2930, arXiv:1112.5675 [hep-ph].

[157] P. Bärnreuther, M. Czakon, and A. Mitov, "Percent Level Precision Physics at the Tevatron: First Genuine NNLO QCD Corrections to $q\bar{q} \to t\bar{t} + X$," *Phys.Rev.Lett.* **109** (2012) 132001, arXiv:1204.5201 [hep-ph].

[158] M. Czakon, P. Fiedler, and A. Mitov, "Total Top-Quark Pair-Production Cross Section at Hadron Colliders Through $O(\frac{4}{S})$," *Phys.Rev.Lett.* **110** (2013) 252004, arXiv:1303.6254 [hep-ph].

[159] A. Buckley, H. Hoeth, H. Lacker, H. Schulz, and J. E. von Seggern, "Systematic event generator tuning for the LHC," *Eur.Phys.J.* **C65** (2010) 331–357, arXiv:0907.2973 [hep-ph].

[160] J. Butterworth *et al.*, "PDF4LHC recommendations for LHC Run II," arXiv:1510.03865 [hep-ph].

[161] P. M. Nadolsky, H.-L. Lai, Q.-H. Cao, J. Huston, J. Pumplin, *et al.*, "Implications of CTEQ global analysis for collider observables," *Phys.Rev.* **D78** (2008) 013004, arXiv:0802.0007 [hep-ph].

[162] A. Martin, W. Stirling, R. Thorne, and G. Watt, "Parton distributions for the LHC," *Eur.Phys.J.* **C63** (2009) 189–285, arXiv:0901.0002 [hep-ph].

[163] R. D. Ball, L. Del Debbio, S. Forte, A. Guffanti, J. I. Latorre, *et al.*, "A first unbiased global NLO determination of parton distributions and their uncertainties," *Nucl.Phys.* **B838** (2010) 136–206, arXiv:1002.4407 [hep-ph].

[164] F. James and M. Roos, "Minuit: A System for Function Minimization and Analysis of the Parameter Errors and Correlations," *Comput.Phys.Commun.* **10** (1975) 343–367.

[165] **ATLAS Collaboration** Collaboration, G. Aad *et al.*, "Measurement of the $t\bar{t}$ production cross-section using $e\mu$ events with b-tagged jets in pp collisions at $\sqrt{s} = 7$ and 8 TeV with the ATLAS detector," *Eur.Phys.J.* **C74** no. 10, (2014) 3109, arXiv:1406.5375 [hep-ex].

[166] **ATLAS** Collaboration, G. Aad *et al.*, "Measurement of the cross section for top-quark pair production in pp collisions at $\sqrt{s} = 7$ TeV with the ATLAS

detector using final states with two high-pt leptons," *JHEP* **05** (2012) 059, arXiv:1202.4892 [hep-ex].

[167] **ATLAS** Collaboration, G. Aad *et al.*, "Measurement of the top quark pair cross section with ATLAS in pp collisions at $\sqrt{s} = 7$ TeV using final states with an electron or a muon and a hadronically decaying τ lepton," *Phys. Lett.* **B717** (2012) 89–108, arXiv:1205.2067 [hep-ex].

[168] **ATLAS** Collaboration, G. Aad *et al.*, "Measurement of the top quark pair production cross-section with ATLAS in the single lepton channel," *Phys. Lett.* **B711** (2012) 244–263, arXiv:1201.1889 [hep-ex].

[169] **ATLAS** Collaboration, G. Aad *et al.*, "Measurement of the ttbar production cross section in the tau+jets channel using the ATLAS detector," *Eur. Phys. J.* **C73** no. 3, (2013) 2328, arXiv:1211.7205 [hep-ex].

[170] **ATLAS** Collaboration, G. Aad *et al.*, "Simultaneous measurements of the $t\bar{t}$, W^+W^-, and $Z/\gamma^* \to \tau\tau$ production cross-sections in pp collisions at $\sqrt{s} = 7$ TeV with the ATLAS detector," *Phys. Rev.* **D91** no. 5, (2015) 052005, arXiv:1407.0573 [hep-ex].

[171] **ATLAS** Collaboration, G. Aad *et al.*, "Measurement of the top pair production cross section in 8 TeV proton-proton collisions using kinematic information in the lepton+jets final state with ATLAS," *Phys. Rev.* **D91** no. 11, (2015) 112013, arXiv:1504.04251 [hep-ex].

[172] **CMS** Collaboration, S. Chatrchyan *et al.*, "Measurement of the $t\bar{t}$ production cross section in the all-jet final state in pp collisions at $\sqrt{s} = 7$ TeV," *JHEP* **05** (2013) 065, arXiv:1302.0508 [hep-ex].

[173] **CMS** Collaboration, S. Chatrchyan *et al.*, "Measurement of the $t\bar{t}$ production cross section in the dilepton channel in pp collisions at $\sqrt{s} = 7$ TeV," *JHEP* **11** (2012) 067, arXiv:1208.2671 [hep-ex].

[174] **CMS** Collaboration, S. Chatrchyan *et al.*, "Measurement of the $t\bar{t}$ production cross section in pp collisions at $\sqrt{s} = 7$ TeV with lepton + jets final states," *Phys. Lett.* **B720** (2013) 83–104, arXiv:1212.6682.

[175] **CMS** Collaboration, S. Chatrchyan *et al.*, "Measurement of the top quark pair production cross section in pp collisions at $\sqrt{s} = 7$ TeV in dilepton final states containing a τ," *Phys. Rev.* **D85** (2012) 112007, arXiv:1203.6810 [hep-ex].

[176] **CMS** Collaboration, S. Chatrchyan *et al.*, "Measurement of the top-antitop production cross section in the tau+jets channel in pp collisions at sqrt(s) = 7 TeV," *Eur. Phys. J.* **C73** no. 4, (2013) 2386, arXiv:1301.5755 [hep-ex].

[177] **CMS** Collaboration, S. Chatrchyan *et al.*, "Measurement of the $t\bar{t}$ production cross section in the dilepton channel in pp collisions at $\sqrt{s} = 8$ TeV," *JHEP* **02** (2014) 024, arXiv:1312.7582 [hep-ex]. [Erratum: JHEP02,102(2014)].

[178] **CMS** Collaboration, V. Khachatryan *et al.*, "Measurement of the top quark pair production cross section in proton-proton collisions at $\sqrt{s} = 13$ TeV," arXiv:1510.05302 [hep-ex].

[179] **CDF, D0** Collaboration, T. A. Aaltonen *et al.*, "Combination of measurements of the top-quark pair production cross section from the Tevatron Collider," *Phys. Rev.* **D89** no. 7, (2014) 072001, arXiv:1309.7570 [hep-ex].

[180] **ATLAS Collaboration** Collaboration, G. Aad *et al.*, "Comprehensive measurements of t-channel single top-quark production cross sections at $\sqrt{s} = 7$ TeV with the ATLAS detector," arXiv:1406.7844 [hep-ex].

[181] **CDF Collaboration** Collaboration, T. A. Aaltonen *et al.*, "Evidence for s-channel Single-Top-Quark Production in Events with one Charged Lepton and two Jets at CDF," *Phys.Rev.Lett.* **112** (2014) 231804, arXiv:1402.0484 [hep-ex].

[182] **CMS Collaboration** Collaboration, V. Khachatryan *et al.*, "Measurement of the t-channel single-top-quark production cross section and of the $| V_{tb} |$ CKM matrix element in pp collisions at $\sqrt{s}$= 8 TeV," *JHEP* **1406** (2014) 090, arXiv:1403.7366 [hep-ex].

[183] **D0** Collaboration, V. M. Abazov *et al.*, "Measurement of the t-channel single top quark production cross section," *Phys. Lett.* **B682** (2010) 363–369, arXiv:0907.4259 [hep-ex].

[184] **D0** Collaboration, V. M. Abazov *et al.*, "Model-independent measurement of t-channel single top quark production in $p\bar{p}$ collisions at $\sqrt{s} = 1.96$ TeV," *Phys. Lett.* **B705** (2011) 313–319, arXiv:1105.2788 [hep-ex].

[185] **ATLAS Collaboration** Collaboration, G. Aad *et al.*, "Measurements of normalized differential cross-sections for $t\bar{t}$ production in pp collisions at $\sqrt{s}$=7

TeV using the ATLAS detector," *Phys.Rev.* **D90** (2014) 072004, arXiv:1407.0371 [hep-ex].

[186] **CDF Collaboration** Collaboration, T. Aaltonen *et al.*, "First Measurement of the t anti-t Differential Cross Section d sigma/dM(t anti-t) in p anti-p Collisions at s**(1/2)=1.96-TeV," *Phys.Rev.Lett.* **102** (2009) 222003, arXiv:0903.2850 [hep-ex].

[187] **CMS Collaboration** Collaboration, S. Chatrchyan *et al.*, "Measurement of differential top-quark pair production cross sections in pp colisions at $\sqrt{s} = 7$ TeV," *Eur.Phys.J.* **C73** (2013) 2339, arXiv:1211.2220 [hep-ex].

[188] **CMS** Collaboration, V. Khachatryan *et al.*, "Measurement of the Differential Cross Section for Top Quark Pair Production in pp Collisions at $\sqrt{s} = 8$ TeV," arXiv:1505.04480 [hep-ex].

[189] **D0 Collaboration** Collaboration, V. M. Abazov *et al.*, "Measurement of differential $t\bar{t}$ production cross sections in $p\bar{p}$ collisions," *Phys.Rev.* **D90** (2014) 092006, arXiv:1401.5785 [hep-ex].

[190] **ATLAS Collaboration** Collaboration, G. Aad *et al.*, "Measurement of the top quark pair production charge asymmetry in proton-proton collisions at $\sqrt{s} = 7$ TeV using the ATLAS detector," *JHEP* **1402** (2014) 107, arXiv:1311.6724 [hep-ex].

[191] **CMS Collaboration** Collaboration, S. Chatrchyan *et al.*, "Measurements of the $t\bar{t}$ charge asymmetry using the dilepton decay channel in pp collisions at $\sqrt{s} = 7$ TeV," *JHEP* **1404** (2014) 191, arXiv:1402.3803 [hep-ex].

[192] **CDF** Collaboration, T. A. Aaltonen *et al.*, "Direct Measurement of the Total Decay Width of the Top Quark," *Phys. Rev. Lett.* **111** no. 20, (2013) 202001, arXiv:1308.4050 [hep-ex].

[193] **D0** Collaboration, V. M. Abazov *et al.*, "An Improved determination of the width of the top quark," *Phys. Rev.* **D85** (2012) 091104, arXiv:1201.4156 [hep-ex].

[194] **ATLAS** Collaboration, G. Aad *et al.*, "Measurement of the W boson polarization in top quark decays with the ATLAS detector," *JHEP* **06** (2012) 088, arXiv:1205.2484 [hep-ex].

[195] **CDF** Collaboration, T. Aaltonen *et al.*, "Measurement of W-Boson Polarization

in Top-quark Decay using the Full CDF Run II Data Set,"
Phys. Rev. **D87** no. 3, (2013) 031104, arXiv:1211.4523 [hep-ex].

[196] **CMS** Collaboration, S. Chatrchyan *et al.*, "Measurement of the W-boson helicity in top-quark decays from $t\bar{t}$ production in lepton+jets events in pp collisions at $\sqrt{s} = 7$ TeV," *JHEP* **10** (2013) 167, arXiv:1308.3879 [hep-ex].

[197] **D0** Collaboration, V. M. Abazov *et al.*, "Measurement of the W boson helicity in top quark decays using 5.4 fb^{-1} of $p\bar{p}$ collision data,"
Phys. Rev. **D83** (2011) 032009, arXiv:1011.6549 [hep-ex].

[198] J. A. Aguilar-Saavedra, A. Juste, and F. Rubbo, "Boosting the $t\bar{t}$ charge asymmetry," *Phys. Lett.* **B707** (2012) 92–98, arXiv:1109.3710 [hep-ph].

[199] R. S. Chivukula, A. Farzinnia, E. H. Simmons, and R. Foadi, "Production of Massive Color-Octet Vector Bosons at Next-to-Leading Order,"
Phys. Rev. **D85** (2012) 054005, arXiv:1111.7261 [hep-ph].

[200] J. Brehmer, A. Freitas, D. Lopez-Val, and T. Plehn, "Pushing Higgs Effective Theory to its Limits," arXiv:1510.03443 [hep-ph].

[201] G. Isidori and M. Trott, "Higgs form factors in Associated Production,"
JHEP **02** (2014) 082, arXiv:1307.4051 [hep-ph].

[202] E. Boos, V. Bunichev, L. Dudko, and M. Perfilov, "Interference between W' and W in single-top quark production processes," *Phys. Lett.* **B655** (2007) 245–250, arXiv:hep-ph/0610080 [hep-ph].

[203] **ATLAS** Collaboration, G. Aad *et al.*, "Search for New Physics in the Dijet Mass Distribution using 1 fb^{-1} of pp Collision Data at $\sqrt{s}$ =7 TeV collected by the ATLAS Detector," *Phys. Lett.* **B708** (2012) 37–54, arXiv:1108.6311 [hep-ex].

[204] **ATLAS** Collaboration, G. Aad *et al.*, "Search for new phenomena in the dijet mass distribution using $p - p$ collision data at $\sqrt{s} = 8$ TeV with the ATLAS detector," *Phys. Rev.* **D91** no. 5, (2015) 052007, arXiv:1407.1376 [hep-ex].

[205] **CMS** Collaboration, V. Khachatryan *et al.*, "Search for resonances and quantum black holes using dijet mass spectra in proton-proton collisions at $\sqrt{s} = 8$ TeV,"
Phys. Rev. **D91** no. 5, (2015) 052009, arXiv:1501.04198 [hep-ex].

[206] **ATLAS** Collaboration, G. Aad *et al.*, "Search for resonant top plus jet production in $t\bar{t}$ + jets events with the ATLAS detector in pp collisions at

$\sqrt{s} = 7$ TeV," *Phys. Rev.* **D86** (2012) 091103, arXiv:1209.6593 [hep-ex].

[207] **ATLAS** Collaboration, G. Aad *et al.*, "Search for resonances decaying into top-quark pairs using fully hadronic decays in pp collisions with ATLAS at $\sqrt{s} = 7$ TeV," *JHEP* **01** (2013) 116, arXiv:1211.2202 [hep-ex].

[208] **CMS** Collaboration, S. Chatrchyan *et al.*, "Search for Z ' resonances decaying to $t\bar{t}$ in dilepton+jets final states in pp collisions at $\sqrt{s} = 7$ TeV," *Phys. Rev.* **D87** no. 7, (2013) 072002, arXiv:1211.3338 [hep-ex].

[209] "Universität Hamburg research activities - boosted topologies." https://www.emmynoethercms.uni-hamburg.de/en/research.html. Accessed: 2016-10-11.

[210] T. Plehn and M. Spannowsky, "Top Tagging," *J. Phys.* **G39** (2012) 083001, arXiv:1112.4441 [hep-ph].

[211] S. Moch and P. Uwer, "Theoretical status and prospects for top-quark pair production at hadron colliders," *Phys. Rev.* **D78** (2008) 034003, arXiv:0804.1476 [hep-ph].

[212] M. Aliev, H. Lacker, U. Langenfeld, S. Moch, P. Uwer, and M. Wiedermann, "HATHOR: HAdronic Top and Heavy quarks crOss section calculatoR," *Comput. Phys. Commun.* **182** (2011) 1034–1046, arXiv:1007.1327 [hep-ph].

[213] M. Czakon, P. Fiedler, D. Heymes, and A. Mitov, "NNLO QCD predictions for fully-differential top-quark pair production at the Tevatron," *JHEP* **05** (2016) 034, arXiv:1601.05375 [hep-ph].

[214] T. Plehn, G. P. Salam, and M. Spannowsky, "Fat Jets for a Light Higgs," *Phys. Rev. Lett.* **104** (2010) 111801, arXiv:0910.5472 [hep-ph].

[215] T. Plehn, M. Spannowsky, M. Takeuchi, and D. Zerwas, "Stop Reconstruction with Tagged Tops," *JHEP* **10** (2010) 078, arXiv:1006.2833 [hep-ph].

[216] A. Altheimer *et al.*, "Boosted objects and jet substructure at the LHC. Report of BOOST2012, held at IFIC Valencia, 23rd-27th of July 2012," *Eur. Phys. J.* **C74** no. 3, (2014) 2792, arXiv:1311.2708 [hep-ex].

[217] S. Schaetzel and M. Spannowsky, "Tagging highly boosted top quarks," *Phys. Rev.* **D89** no. 1, (2014) 014007, arXiv:1308.0540 [hep-ph].

[218] T. Plehn, M. Spannowsky, and M. Takeuchi, "How to Improve Top Tagging," *Phys. Rev.* **D85** (2012) 034029, arXiv:1111.5034 [hep-ph].

[219] M. Backovic, O. Gabizon, J. Juknevich, G. Perez, and Y. Soreq, "Measuring boosted tops in semi-leptonic $t\bar{t}$ events for the standard model and beyond," *JHEP* **04** (2014) 176, arXiv:1311.2962 [hep-ph].

[220] J. Alwall, R. Frederix, S. Frixione, V. Hirschi, F. Maltoni, O. Mattelaer, H. S. Shao, T. Stelzer, P. Torrielli, and M. Zaro, "The automated computation of tree-level and next-to-leading order differential cross sections, and their matching to parton shower simulations," *JHEP* **07** (2014) 079, arXiv:1405.0301 [hep-ph].

[221] S. Moch, P. Uwer, and A. Vogt, "On top-pair hadro-production at next-to-next-to-leading order," *Phys. Lett.* **B714** (2012) 48–54, arXiv:1203.6282 [hep-ph].

[222] S. Dulat, T.-J. Hou, J. Gao, M. Guzzi, J. Huston, P. Nadolsky, J. Pumplin, C. Schmidt, D. Stump, and C. P. Yuan, "New parton distribution functions from a global analysis of quantum chromodynamics," *Phys. Rev.* **D93** no. 3, (2016) 033006, arXiv:1506.07443 [hep-ph].

[223] L. A. Harland-Lang, A. D. Martin, P. Motylinski, and R. S. Thorne, "Parton distributions in the LHC era: MMHT 2014 PDFs," *Eur. Phys. J.* **C75** no. 5, (2015) 204, arXiv:1412.3989 [hep-ph].

[224] **NNPDF** Collaboration, R. D. Ball *et al.*, "Parton distributions for the LHC Run II," *JHEP* **04** (2015) 040, arXiv:1410.8849 [hep-ph].

[225] M. Bahr, S. Gieseke, M. Gigg, D. Grellscheid, K. Hamilton, *et al.*, "Herwig++ Physics and Manual," *Eur.Phys.J.* **C58** (2008) 639–707, arXiv:0803.0883 [hep-ph].

[226] J. Bellm *et al.*, "Herwig 7.0/Herwig++ 3.0 release note," *Eur. Phys. J.* **C76** no. 4, (2016) 196, arXiv:1512.01178 [hep-ph].

[227] A. Buckley, J. Butterworth, L. Lonnblad, D. Grellscheid, H. Hoeth, *et al.*, "Rivet user manual," *Comput.Phys.Commun.* **184** (2013) 2803–2819, arXiv:1003.0694 [hep-ph].

[228] M. Cacciari, G. P. Salam, and G. Soyez, "The Anti-k(t) jet clustering algorithm,"

JHEP **0804** (2008) 063, arXiv:0802.1189 [hep-ph].

[229] M. Cacciari, G. P. Salam, and G. Soyez, "FastJet User Manual," *Eur.Phys.J.* **C72** (2012) 1896, arXiv:1111.6097 [hep-ph].

[230] **ATLAS** Collaboration, G. Aad *et al.*, "Measurement of the b-tag Efficiency in a Sample of Jets Containing Muons with 5 fb1 of Data from the ATLAS Detector,".

[231] G. Kasieczka, T. Plehn, T. Schell, T. Strebler, and G. P. Salam, "Resonance Searches with an Updated Top Tagger," *JHEP* **06** (2015) 203, arXiv:1503.05921 [hep-ph].

[232] J. M. Butterworth, A. R. Davison, M. Rubin, and G. P. Salam, "Jet substructure as a new higgs-search channel at the large hadron collider," *Phys. Rev. Lett.* **100** (Jun, 2008) 242001. http://link.aps.org/doi/10.1103/PhysRevLett.100.242001.

[233] **ATLAS** Collaboration, G. Aad *et al.*, "Performance of jet substructure techniques for large-R jets in proton-proton collisions at $\sqrt{s} = 7$ TeV using the ATLAS detector," *JHEP* **09** (2013) 076, arXiv:1306.4945 [hep-ex].

[234] Y. L. Dokshitzer, G. D. Leder, S. Moretti, and B. R. Webber, "Better jet clustering algorithms," *JHEP* **08** (1997) 001, arXiv:hep-ph/9707323 [hep-ph].

[235] **ATLAS** Collaboration, G. Aad *et al.*, "Measurement of the differential cross-section of highly boosted top quarks as a function of their transverse momentum in $\sqrt{s} = 8$ TeV proton-proton collisions using the ATLAS detector," *Phys. Rev.* **D93** no. 3, (2016) 032009, arXiv:1510.03818 [hep-ex].

[236] **CMS** Collaboration, V. Khachatryan *et al.*, "Measurement of the integrated and differential t-tbar production cross sections for high-pt top quarks in pp collisions at $\sqrt{s} = 8$ TeV," arXiv:1605.00116 [hep-ex].

[237] **ATLAS** Collaboration, G. Aad *et al.*, "Measurements of top-quark pair differential cross-sections in the lepton+jets channel in pp collisions at $\sqrt{s} = 8$ TeV using the ATLAS detector," arXiv:1511.04716 [hep-ex].

[238] M. Czakon, D. Heymes, and A. Mitov, "High-precision differential predictions for top-quark pairs at the LHC," *Phys. Rev. Lett.* **116** no. 8, (2016) 082003, arXiv:1511.00549 [hep-ph].

[239] L. Berthier, M. Bjørn, and M. Trott, "Incorporating doubly resonant $W^{\pm}$ data

in a global fit of SMEFT parameters to lift flat directions,"
arXiv:1606.06693 [hep-ph].

[240] J. M. Butterworth, I. Ochoa, and T. Scanlon, "Boosted Higgs $\to b\bar{b}$ in vector-boson associated production at 14 TeV,"
Eur. Phys. J. **C75** no. 8, (2015) 366, arXiv:1506.04973 [hep-ph].

[241] K. Joshi, A. D. Pilkington, and M. Spannowsky, "The dependency of boosted tagging algorithms on the event colour structure,"
Phys. Rev. **D86** (2012) 114016, arXiv:1207.6066 [hep-ph].

[242] A. Buckley, "The hepthesis LaTeX class.".

List of figures

List of tables